ANALYSIS OF THE EFFECT OF CLIMATE CHANGE IMPACTS ON FLOODS IN KELANI RIVER BASIN, SRI LANKA

S.P.S.P. Kulathunga

(179239C)

Degree of Master of Science

Department of Civil Engineering

University of Moratuwa
Sri Lanka

June 2023

ANALYSIS OF THE EFFECT OF CLIMATE CHANGE IMPACTS ON FLOODS IN KELANI RIVER BASIN, SRI LANKA

S.P.S.P. Kulathunga

(179239C)

Supervised by

Prof. R. L. H. L. Rajapakse

Degree of Master of Science
Water Resources Engineering and Management

Thesis submitted in partial fulfillment of the requirements for the degree Master of Science in Water Resources Engineering and Management

UNESCO Madanjeet Singh Centre for
South Asia Water Management (UMCSAWM)

Department of Civil Engineering
University of Moratuwa
Sri Lanka

June 2023

DECLARATION OF THE CANDIDATE AND SUPERVISOR

"I declare that this is my own work, and this thesis/dissertation does not incorporate without acknowledgement any material previously submitted for a Degree or Diploma in any other University or institute of higher learning and to the best of my knowledge and belief it does not contain any material previously published or written by another person except where the acknowledgement is made in the text".

Also, I hereby grant to University of Moratuwa the non-exclusive right to reproduce and distribute my thesis/dissertation, in whole or in part in print, electronic or other medium. I retain the right to use this content in whole or part in future works (such as articles or books).

30/06/2023

Date

S.P.S.P. Kulathunga

Thesis submitted in partial fulfillment of the requirements for the degree of Master of Engineering in Water Resources Engineering and Management

The above candidate has carried out research for the Master's Thesis/Dissertation under my supervision.

2023-06-30

Date

Prof. R. L. H. L. Rajapakse

ABSTRACT

Analysis of the Effect of Climate Change Impacts on Floods in Kelani River Basin, Sri Lanka

Sri Lanka is highly vulnerable to climate change impacts, including rising land and sea temperatures, changing precipitation patterns, more extreme weather events, and sea-level rise. Notably, climate change has been observed to increase flood frequency, expand flood areas, and intensify flood damages. Previous research in Sri Lanka has mainly focused on rainfall estimation using weather models and examining climate change scenarios. This study aims to improve flood forecasting by analyzing climate change-induced changes in rainfall depths from Intensity-Duration-Frequency (IDF) curves and considering design sea levels. The objective is to gain insights into future flood characteristics, specifically the projected increases in discharges and water levels.

The HEC-HMS Hydrological modelling tool was selected for the hydrological modelling of the entire Kelani Basin, while the HEC-RAS model was used for flood modelling in the Lower Kelani Basin which is downstream from Glencourse. HEC-HMS simulating discharges from rainfall inputs that served as boundary conditions for the HEC-RAS model. The verified models are utilized to simulate the 50-year design rainfall dataset lasting 3 days, incorporating published IDF equations from selected rain gauge locations along with the calibrated models. Rainfall depth multipliers of 1.100, 1.122, and 1.140 were applied to the design rainfall dataset for the RCP4.5, RCP6.0, and RCP8.5 projections, respectively. Simulations also considered sea-level rise values of 0.47 m, 0.48 m, and 0.63 m corresponding to the respective climate change projection scenarios.

Calibration and validation of the three HEC-HMS models (Kelani Upper, Kelani Middle, and Kelani Lower) and the HEC-RAS Flood model for Lower Kelani (downstream to Glencourse) Basin were successfully calibrated using 2016 May and validated using 2017 May flood event data. The Nash Efficiency values during calibration were 0.79, 0.95, and 0.85 for the Kelani Upper, Kelani Middle, and Kelani Lower models, respectively. During validation, the Nash Efficiency values were 0.87, 0.85, and 0.25, respectively. The calibration Nash Efficiency values for the HEC-RAS model were 0.57, 0.56, and 0.52, and the validation Nash Efficiency values were 0.80, 0.57, and 0.53 for the respective models considering Hanwella Discharges, Hanwella Water Levels and Nagalagama Street Water levels, respectively.

The research concluded that, under climate change projections, the Glencourse Peak Discharge is projected to increase by approximately 13.3% to 16.2%. Similarly, at Hanwella, the peak discharge is expected to increase by approximately 6.4% to 8.8%, while the maximum water level is anticipated to rise by approximately 3.1% to 4.2%. Moreover, the maximum water level at Nagalagama Street is likely to experience an increase of around 16.2% to 21.7% under climate change projections.

Keywords: Design Rainfall, HEC-HMS, HEC-RAS, Hourly Data, IDF

DEDICATION

This thesis work is dedicated to my wife Champika, and my two sons Ihansa, and Mihinsa who have been a constant source of support and encouragement during the challenges of academic commitments and life. I am truly thankful for having you in my life. This work is also dedicated to my parents, Nimal and Ranjani, who have always loved me unconditionally and whose good examples have taught me to work hard for the things that I aspire to achieve.

ACKNOWLEDGEMENT

I would like to express my sincere gratitude to my research supervisor, Prof. R.L.H.L Rajapakse for the continuous support extended for this research and case study, for his patience, motivation and guidance. Without his dedicated supervision and continued guidance, this thesis would not have been a success. I am really grateful to him for spending his valuable time with me towards completing this research.

I wish to convey my sincere gratitude to the overall course director, Senior Professor N.T.S. Wijesekera for extending all necessary help to achieve success in the program. His kindness to provide me with all the guidance, help and support amidst his busy schedule and sincere and consistent encouragement are greatly appreciated.

I would also like to thank Late Shri Madanjeet Singh, the Founder of SAF-Madanjeet Singh Foundation (MSF), the South Asia Foundation (SAF) and the University of Moratuwa for enabling me to join this study towards a Master's Degree of Water Resource Engineering and Management, at UNESCO Madanjeet Singh Centre for South Asia Water Management (UMCSAWM), Department of Civil Engineering, University of Moratuwa, Sri Lanka.

My gratitude is also extended to all Department staff and all Centre staff including Mr. Wajira Kumarasinghe, Mr. Samantha Ranaweera, Ms. Vinu and Ms. Janani who gave me support to carry out the studies successfully within the university and their encouragement are greatly appreciated.

Finally, I would like to express my very profound gratitude to my parents, my wife and my two sons and my friends for providing unfailing support and continuous encouragement throughout this research work.

TABLE OF CONTENT

LIST OF FIGURES

LIST OF TABLES

LIST OF ABBREVIATIONS

1D	One Dimensional
2D	Two Dimensional
ALOS	Advanced Land Observing Satellite
AMC	Antecedent Moisture Condition
ANN	Artificial Neural Network
ASTER	Advanced Spaceborne Thermal Emission and Reflection Radiometer
BIMSTEC	Bay of Bengal Initiative for Multi-Sectoral Technical and Economic Cooperation
CanESM2	Canadian Earth System Model, version 2
CC	Climate Change
CHIRPS	Climate Hazards Group Infrared Precipitation with Station Data
CMIP	Coupled Model Inter-Comparison Project
CN	Curve Number
CO2	Carbon Dioxide
CRIP	Climate Resilient Improvement Project
CS	Cross Section
DEM	Digital Elevation Model
DHI	Danish Hydraulic Institute
DIAS	Data Integration and Analysis System
GCM	General Circulation Models
GIS	Geographic information system
HadCM3	Hadley Centre Coupled Model version 3
HEC	Hydrological Engineering Center
HMS	Hydrological Modelling System
ID	Irrigation Department
IDF	Intensity Duration Frequency
IPCC	Intergovernmental Panel on Climate Change
iRIC	International River Interface Cooperative
ITCZ	Intertropical Convergence Zone
LiDAR	Light Detection and Ranging
MCM	Million Cubic Meters
MSL	Mean Sea Level
NASA	National Aeronautics and Space Administration
NEX-GDDP	NASA Earth Exchange Global Daily Downscaled Climate Projections
NSE	Nash-Sutcliffe model efficiency
PALSAR	Phased Array type L-band Synthetic Aperture Radar
PPM	Parts Per Million
R^2	Coefficient of Determination
RAS	River Analysis System
RCM	Regional Climate Model
RCP	Representative Concentration Pathway
RF	Rainfall
RRI	Rainfall-Runoff-Inundation
SCS	Soil Conservation Service
SD	Survey Department

SDSM	Statistical Downscaling Model
SDSM	Statistical Downscaling Model
SHER	Similar Hydrologic Element Response
SPI	Standard Precipitation Index
SRTM	Shuttle Radar Topography Mission
UH	Unit Hydrograph
UK	United Kingdom
UNFCCC	United Nations Framework Convention on Climate Change
WEB-RRI	Water Energy Budget-based Rainfall-Runoff-Inundation model
WL	Water Level
WRF	Weather Research and Forecasting
Yr.	Year

CHAPTER 1

1 INTRODUCTION

1.1 General

1.1.1 Climate Change Definition

Climate Change, as defined by the Intergovernmental Panel on Climate Change (IPCC) is a significant and persistent variation in the climate's average condition or variability, lasting for decades or longer (IPCC, 2007). It can result from natural internal or external processes, as well as human-induced changes in atmospheric composition and land usage (Premalal, 2009; O'Brien et al., 2006). However, human activities have accelerated climate change by disrupting the Earth's balance through interactions like fossil fuel burning, livestock emissions, and deforestation as well, which generate more greenhouse gases into the atmosphere and exceed sustainable limits.

Since 1900, global temperatures have increased by approximately 0.6°C, with scientific consensus attributing most of this increase due to the aforementioned human interactions intensifying the greenhouse effect and warming the planet (Mullan et al., 2005). Without action to decrease greenhouse gas emissions, global Climate Change is projected to raise atmospheric temperatures from 1.4°C to 5.8°C at the end of the century. This temperature increase will have implications for flooding, as warmer air can hold more moisture, leading to increased rainfall and more intense rainfall systems (Mullan et al., 2005).

1.1.2 Effects Due to Climate Change

Climate change has far-reaching impacts on various sectors, including water resources, agriculture, ecosystems, human health, and coastal zones (UNFCCC, 2013). While global warming is undeniable (IPCC, 2014) understanding and predicting its effects on geo-hydrological hazards like floods, landslides, and droughts remain challenging. To address this, it is crucial to investigate how climate variables and their variations influence these hazards, especially flooding.

The Fourth Assessment Report by the Intergovernmental Panel on Climate Change (IPCC, 2007) provided valuable insights into the previously uncertain aspects of climate change. Over the past century, atmospheric CO_2 concentrations decreased from 278 parts per million (ppm) compared with pre-industrial times to 379 ppm in 2005, resulting in a mean global temperature increase of 0.74°C. Scientists

acknowledge this as the most notable and rapid warming trend in the history of our planet, with the warming rate accelerating last 25 years. The baseline data reveals that 11 out of the 12 were recorded as the hottest years within the last 12 years. Projections outlined in IPCC (2007) indicate that global warming will persist and intensify throughout the 21st century, with estimates suggesting a potential temperature rise of 3°C by 2100. Even with greenhouse gas emission reductions, the Globe will be warming continuously with projections ranging from a minimum of 1.8°C to a maximum of 4°C increase in global mean temperatures by 2100 (UNFCCC, 2013).

1.1.3 Climate Change Impacts on Natural Disasters

Global warming leads to alterations in the disaster category, frequency, as well intensity of extreme events such that tropical cyclones, flooding, droughts, and heavy rainfall events (IPCC, 2007). Observable changes have already been witnessed, including more frequent and intense heatwaves and heavy rainfall events. As a result, climate change will exert extensive effects on the environment, social and economic sectors, and relevant fields. Water scarcity and flooding are likely consequences of shifting rainfall patterns. Glacier melting contributes to floods and soil erosion. Rising temperatures disrupt crop growing seasons, impacting food security. Changes in disease vectors' distribution, influenced by temperature shifts, increase the risk of diseases like malaria and dengue fever. Rising temperatures also pose a significant threat to biodiversity, with up to 30% of habitats and species at risk of extinction resulting from a 2°C temperature increase. Particularly the coral reefs, boreal forests, and Mediterranean and mountain habitats are vulnerable. Additionally, the rise in sea levels heightens the vulnerability of coastlines to storm surges, inundation depth and extents, and wave damage, mainly small islands as well the delta regions with lower elevations. The extreme events increasing has profound implications for health, lives, and associated environmental and economic consequences (UNFCCC, 2013).

1.1.4 Climate Change Impacts on Flooding

Januriyadi et al. (2018) studied natural disasters including floods, which resulted in finding that floods have become more frequent and making a severe threat to human lives. Floods are the most severe natural disasters, causing extensive damage to both people and property (Tanaka et al., 2019; Teng et al., 2017). Floods have been a recurring hazard throughout history, affecting societies worldwide and continue to have a significant impact on every inhabited continent today (Papaioannou et al., 2016; Teng et al., 2017). The vulnerability of communities and infrastructure to flooding has been exacerbated by climate change and rapid urbanization (Wagenaar et al., 2019; Erena & Worku, 2018).

Climate change is expected to worsen land degradation processes, leading to more intense rainfall, flooding, and droughts (Iturbide et al., 2020). Surface water flooding arises when the drainage system becomes overwhelmed by precipitation, hindering the effective removal of excess water (Yu et al.,

2016). The vulnerability of communities and infrastructure to flooding impacts is rising because of demographic changes, land use changes, and economics in flooding areas (Alahacoon et al., 2016). Floods are now considered a common and more frequent natural hazard worldwide, with extreme weather events becoming more severe due to climate change (Komolafe et al., 2018a; Siddiqui et al., 2018).

1.2 Flood Characteristics of Sri Lanka and Kelani River Basin

Sri Lanka, located in the tropical region, is prone to frequent flooding, resulting in to ranked as the eleventh in the world, based on average annual flood exposure, higher population density and economic activities in flood-prone areas (Alahacoon & Edirisinghe, 2021). Flooding in Sri Lanka is primarily caused by excessive rainfall in monsoon periods (Fowze et al., 2008). The country experiences maximum rainfall in May and September months, resulting from convective cell thunderstorms because Sri Lanka is located in the Inter Tropical Convergence Zone. Monsoons and tropical cyclones mostly initiated from Bengal Bay provide heavy rainfall in October and November, while the westerly winds cause orographic rainfall from June to September in the hilly regions (Vuillaume et al., 2018). These rainfall patterns result in recurrent floods, with approximately 60% of rainfall occurring during these periods (De Silva et al., 2012; Alahacoon & Edirisinghe, 2021). The topography of Sri Lanka plays a significant role in the concentration and timing of rainfall, which can lead to rapid flood events (Vuillaume et al., 2018). Flood simulations in Sri Lanka typically focus on the downstream areas of river basins, where urban areas are most vulnerable to flooding, while the upstream areas serve as the inflow to downstream regions (Komolafe et al., 2019).

The Kelani River basin, which originated from central hilly areas of Sri Lanka and flows towards the sea, is highly susceptible to floods. The downstream region of the Kelani River basin, encompassing the Colombo suburbs, is often subjected to severe flooding as a result of intense rainfall in the upper basin (De Silva et al., 2012). Colombo, which operates as the commercial capital of the country and a coastal city, is highly influenced by the Kelani River due to its economic and social importance (Moufar & Perera, 2018). The Kelani River basin has a history of flooding, with significant events occurring in 1989, 1992, 2005, 2008, and 2010, causing severe damage to properties (Komolafe et al., 2019; Wagenaar et al., 2019). In recent years, floods in May 2016 and May 2017 further highlighted the destructive impact of climate change, particularly in Colombo City (Dammalage & Jayasinghe, 2019; Disaster Management Center, 2017; Disaster Management Center, 2016).

1.3 Climate Change Impacts on Flooding in Sri Lanka

The impact of climate change on flooding in Sri Lanka is evident in various aspects such as increased flood frequency, expanded flood extent, and intensified flood damages (Kay et al., 2011). Understanding the potential changes in flooding patterns is challenging due to uncertainties in climate predictions and

the complex responses of different flooding mechanisms. A comprehensive analysis of rainfall-induced flood risk during the end of the 20th to early 21st centuries reveals a significant rise in economic losses attributed to the growing exposure of vulnerable assets. However, attributing trends in rain-generated peak stream flow to anthropogenic climate change over the past few decades has proven difficult. Nonetheless, climate models project a frequency increase and heavy rainfall intensifying, which is likely to contribute to localized precipitation-driven floodings such as flash floods and urban flooding (Kundzewicz et al., 2013).

Considering sea-level rise, estimated for the 2080s, the affected people count by the flooding induced by storm surge will be more than five times higher compared to a reference scenario without sea-level rise. Many of these individuals will face annual or even more frequent flooding, highlighting the need for significant measures such as increased protection and migration. Finally, the low-lying populated deltas in the southern Mediterranean, Africa, and South and Southeast Asia regions are most vulnerable to this kind of flooding. However, the small islands located in the Caribbean, Indian Ocean islands, and the Pacific Ocean are expected to experience the most substantial increase in flood risk (Klein & Nicholls, 1999).

1.4 Importance of Proposed Study

Climate change is common and has wide-ranging effects on various fields, such that water resources, agriculture as well food security, ecosystems and biodiversity, the health sector, and coastal regions. As an island state, Sri Lanka is particularly vulnerable to all the identified impacts of climate change, including rising temperatures on land and sea surface, precipitation changes as patterns and amounts, increasing frequency of extreme climate events, and sea level rise. Regarding flooding, climate change has been identified as causing an increase in flood frequency, expanding flood extent, and intensifying flood damages.

Research conducted in Sri Lanka has focused on exploring rainfall estimation using weather forecasting models and examining climate change projections. The objective of the research is to develop forecasts for future floods by examining changes in rainfall intensity (IDF) resulting from climate change.

1.5 Problem Statement

The problem addressed in this study is the necessity of integrating the climate change impacts into hydrological and flood modelling in a simplified manner. Climate change is a widely recognized natural phenomenon that has negative consequences for flooding. It is crucial to develop an accessible methodology that effectively incorporates these climate change impacts into hydrological modelling and flood forecasting. This integration is vital to improve our understanding of flood rescue operations and facilitate the development of efficient flood mitigation infrastructure. Accurately predicting future flood

characteristics, such as flood discharges, flood levels, and the extent of flood inundation, while considering climate change projections, is essential in addressing this problem.

1.6 Overall Objective

The Overall Objective of this study is to identify and quantify the effects of climate change on flood characteristics in the Kelani River Basin. Specifically, to determine the magnitude of changes in discharge increasing and water levels increasing at specific locations due to climate change impacts.

1.7 Specific Objectives

For the achieving of Overall Objective, the specific objectives are well defined as follows;

- Identification of Past Flood events of Kelani River Basin and Data collection such that Rainfalls, Discharges, Water Levels and Flood Maps.
- Development of Hydrological and Flood Models, Model Calibration and Validation.
- Incorporation of climate change impacts (scenarios) and model simulations for statistical flood events.
- Forecast the climate change impacts on Kelani Floods such that increasing Discharges and Water Levels.

1.8 Scope and Limitation of the Study

This research focuses on forecasting simulated flood outputs for hypothetical statistical design rainfall events in the Kelani Basin. These designed rainfall events are constructed as per the Rainfall Intensity Duration Frequency (IDF) curve. climate change projections are incorporated into the IDF relationships, as well as the design of sea levels. The study aims to provide insights into future flood characteristics, particularly the increase in discharges and water levels.

CHAPTER 2

2 LITERATURE REVIEW

2.1 Climate Change Studies

2.1.1 Climate Change Impacts on South Asia

The climate change impacts on the South Asian region were examined by Zheng et al. (2018). The study was undertaken to forecast future climate patterns and runoff using the RCP8.5 scenarios. To achieve this, climate change data from 42 CMIP5 GCMs were incorporated. Hydrological models were employed to project runoff at 0.5° grids, with future climate projections generated through scaling the historical climate data. The outcomes of the modelling demonstrate that, except the far north-east region and far north-west region, are anticipated to undergo amplified runoff in the future. The median projection suggests a mean annual runoff increase of 20–30% in the Indian sub-continent spanning 2046 to 2075, compared to the period from 1976 to 2005. The runoff change is primarily caused by precipitation changing, influenced by higher temperatures and potential evaporation.

Additionally, Pattnayak et al. (2017) assessed the impact of climate change on the Bay of Bengal Initiative for Multi-Sectoral Technical and Economic Cooperation (BIMSTEC), which consist of countries Bangladesh, Bhutan, India, Myanmar, Nepal, Sri Lanka, and Thailand. This study utilized the fifth phase of the Climate Model Inter-comparison Project (CMIP5) models to forecast climate scenarios for the BIMSTEC countries from 1901 to 2100, using the Representative Concentration Pathways (RCPs) 4.5 and 8.5. The analysis covered a historical period of 105 years and a projected period of 95 years. The results revealed that four out of six models indicate a decreasing trend in rainfall over India, Thailand, and Myanmar, while Bangladesh, Bhutan, Nepal, and Sri Lanka depict a rising trend in two RCP scenarios. Regarding temperature, all models indicate a rising trend across BIMSTEC countries for two scenarios, although the rising rate is lower in Sri Lanka compared to other countries. The rate of change in rainfall and temperature is comparatively higher in RCP8.5 than in RCP4.5 for BIMSTEC countries. Based on a comparison of inter-models underscores the presence of uncertainties within the CMIP5 model projections (Zheng et al., 2018; Pattnayak et al., 2017).

2.1.2 Climate Change Effects on Sri Lanka

The climate change impact on soil moisture deficits and water resources in Sri Lanka was studied by De Silva (2006). The study collected the data for climate change specifically for Sri Lanka generated by the

UK Hadley Centre for Climate Prediction and Research model (HadCM3), focusing on published IPCC SRES projections for the 2050s. The findings of the study indicated a minor rise in the annual average rainfall, primarily attributed to an augmentation in southwest monsoon rainfalls. Conversely, a decline in rainfall was observed during the northeast monsoon. Additionally, the study showed that the annual average temperature will increase, and these changes, associated with alternative climatic considerations, will significantly increase the maximum annual soil moisture deficit located in the dry zone. Furthermore, De Silva, (2007) expanded the study by analysing the HadCM3 dataset for two scenarios: one with high population and carbon dioxide concentrations (A2) and one with lesser impacts (B2). The results showed that the mean annual rainfall over Sri Lanka is forecasted to increase by 14% for the A2 scenario and in 5% for the B2 scenario, while the rainfall decrease in the dry zone is predicted. The predicted annual runoff in the A2 scenario for the 2050s is expected as decreasing by 10% compared with the baseline period (1961-1990), however, in the wet zone, a significant increase is predicted, leading towards floods and landslides.

Another study conducted by Muthuwaththa and Liyanage (2013) focused on future rainfall distribution changes based on agro-ecological regions of Sri Lanka. The baseline period for comparison was selected from 1970 to 2000, and downscaled climate change prediction grids using the HadCM3 dataset for 2050 were used. The study showed that out of 147 stations, 76 exhibited trends of decrease trends in annual rainfall, while 71 showed increasing trends. In the wet zone, 36 out of 76 stations indicated a decrease. Within the intermediate zone, 17 stations displayed upward trends, while the dry zone exhibited increasing trends in 34 stations. The mean annual rainfall spanning the baseline duration was recorded as 2094 mm/year, and the projected value for the year 2050 is estimated to be 2249 mm/year, indicating a notable 7% increase. The baseline period was compared with 2050, resulting that some dry zone areas may obtain mean annual rainfall of beyond 1750mm, potentially leading to their classification and inclusion in the intermediate zone.

Manawadu and Fernando (2008) analysed spatial and temporal trends in rainfall throughout the four rainy seasons in Sri Lanka, covering the period from 1961 to 2002. The research revealed a decline in the frequency of rainy days at the majority of meteorological stations, except the Nuwara Eliya station. Furthermore, the study highlighted a reduction in the extent of the wet zone, as indicated by the shrinking of the 2000 mm isohyet. Notably, watersheds in the northern region exhibited an upward trend in water volume, while those in the southern region displayed a decline.

Zubair and Agalawatte (2014) examined Sri Lanka related climate change forecasts using data generated by Coupled Model Inter-comparison Project (CMIP5). The study focused on future climate projections for the period 2040-2070, considering RCP8.5. The examination of outputs from 20 General Circulation Models (GCMs) indicated a consistent prediction of around a 2°C increase in both minimum and maximum temperature throughout the year. Regarding rainfall, the majority of GCMs expected an annual rainfall increase of around 0.5 mm/day. Rainfall throughout the months of September, October,

and, November was projected to a high increment, while a decrement was predicted during February and March. However, the uncertainty associated with rainfall predictions based on the GCM outputs was observed to be high.

Darshika and Jayawardene (2017) compared observed data from 1975-2005 with NASA Earth Exchange Global Daily Downscaled Projections (NEX-GDDP) from the climate models of GCM 6. The study found that the NEX-GDDP downscaled models accurately captured the annual cycle and Sri Lankan spatial rainfall pattern. Future climate projections using the NEX-GDDP data indicated a negative annual rainfall irregularity in north-eastern regions and a positive anomaly in south-western regions in the 2020-2040 time period under the RCP 4.5. Southwest monsoon rainfall anomaly was predicted to increase under both RCP 4.5 and 8.5. The northeast monsoon rainfall anomaly showed a negative trend in the short term and a positive in the longer durations under the RCP 8.5. The rainfall irregularity in the first inter-monsoon showed variation depending on the emission scenario and time frame, and the second inter-monsoon rainfall anomaly exhibited a similar pattern to the first inter-monsoon.

Patabendige et al. (2016) evaluated the potential effect of climate change on the annual and seasonal runoff in 49 river basins of Sri Lanka for the near future period of 2021-2050. They used a distributed hydrological model and statistically downscaled Global Climate Models (GCMs) selected for three RCPs projections. The study indicated a high probability of increased annual runoff shortly, with the mean annual runoff predicted to increase from 6% to 15.5% as per selected river basin as well applied climate change. The study also revealed a consensus for increased runoff during the southwest and second inter-monsoon seasons.

2.1.3 Climate Change Effect on Kelani River Basin

Niroshinie et al. (2011) conducted a study focusing on extreme flooding scenarios in Colombo because of climate change observations in the Kelani River basin. The researchers used Global Circulation Model (GCM) data with different extreme rainfall scenarios and developed flood inundation models for Colombo. The study found that upcoming dangerous rainfall trials in Colombo would continue similar to historical data, although upstream stations showed higher values. The increase in extreme events was estimated to be 1.5-2.5 percent with the preferred model (CSIROMk2), but with the average of several GCMs, a reduction was observed. However, the upstream areas showed an increase of more than 20% in extreme events with CSIRO-Mk2 model data.

De Silva et al. (2012) analysed possible extreme rainfall and generated flood inundation in the lower Kelani basin. Authors used Coarse grid atmospheric parameters from Global Climate Model (GCM) models considering different emission scenarios such that A2 and B2 downscaled to the local scale using a Statistical Downscaling Model (SDSM). The study found that under the A2 scenario, the 50-year. and 100-year. return period daily rainfall as 244 mm and 268 mm respectively in the lower basin. Under the

B2 scenario, the corresponding values were 227 mm and 248 mm, respectively. For the 50-year ,3-day rainfall was applied to, 415 mm for A2 and 393 mm for B2, and the 100-year return period values were 456 mm for A2 and 432 mm for B2 in the upper basin. The study suggested implementing approaches to decrease the flood-induced damages in the lower Kelani basin in response to anticipated climate change effects.

Dissanayaka and Rajapakse (2019) evaluated longstanding performance and trends of climate extremes established by past temperature and precipitation observations. They simulated and forecasted using downscaled temperature and precipitation outputs since the Canadian Earth System Model (CanESM2), and the HEC-HMS for the Upper Kelani Basin. The study assessed different concentration pathways (RCP2.6, RCP4.5, and RCP8.5) for climate projections in the 2020s, 2050s, and 2080s. The authors found rising temperature and precipitation extremes alongside a decrease in annual mean rainfall in the basin. They recommended using GCMs instead of RCMs to assess the river basin, considering monthly, seasonal, and annual variations of the climatology.

Wijekoon and Rajapakse (2022) examined the climate elasticity of runoff in the Kalu River basin and Kelani River basins, specifically focusing on the Hanwella sub-basin of the Kelani River in the wet zone of Sri Lanka. The researchers utilized the HEC-HMS hydrological model to assess the elasticity of rainfall and evaporation in existing climate conditions and synthetic climate change circumstances. The outcomes indicated that climate change could cause a change in runoff ranging from -49% to 23% for Kelani as per selected synthetic climate change scenarios anticipated for 2016-2035, compared to the baseline period of 1986-2005, considering predicted precipitation and evaporation.

Punsara and Rajapakse (2021) investigated the forthcoming Kelani River streamflow fluctuations induced by climate change using a synthetic climate scenario for Norwood and Deraniyagala sub-basins. The researchers utilized the Standard Precipitation Index (SPI) to recognize meteorological drought circumstances. The study found a 1% change in rainfall such that a 0.75% and 1.00% streamflow discharge change in the Norwood and Deraniyagala sub-basins, respectively.

Komolafe et al. (2018) analysed flood prediction in the Kelani Basin using bias-corrected precipitation data from the Japanese Meteorological Research Institute's Regional Climate Model (RCM). They simulated present and upcoming climate scenarios and a theoretical forthcoming climate prediction with a 1% increase in high rainfall trials. The study integrated forecasted extreme flood hazards with flood depth-damage functions to estimate possible damages using a spatially distributed model. The outcomes showed a slight decrease in anticipated upcoming flows and flood damages compared with the present conditions. However, the theoretical projection showed a 1.2% escalation in possible damages in the forthcoming climate compared to the present climate.

2.2 Model Studies Regarding Kelani River Basin

2.2.1 Hydrological Modelling of Kelani River

Several studies have focused on hydrologic modelling and flood simulation considering the Kelani River basin. De Silva et al. (2014) conducted a case study using the HEC-HMS. They calibrated the model parameters using a very high rainfall event that occurred in 2005 November and validated the model using other high rainfall events in 2008 and 2010. Event-based modelling employed the Green and Ampt infiltration loss method, while continuous modelling employed a five-layer soil moisture accounting loss method. Direct runoff was simulated using the Clark unit hydrograph method and base flow was simulated using the recession base flow method. The study reported Nash efficiency as 0.91 for event simulations as well 0.88 for continuous simulations.

Gunathilake et al. (2019) developed a flood-simulating application for the Seethawaka Ganga using the HEC-HMS. They tested different combinations of direct runoff, precipitation loss methods, base flow methods, and routing methods. The Soil Conservation Service Curve Number (SCS CN) method and non-linear Boussinesq method combined with the Clark unit hydrograph, Muskingum, and lag methods performed well in the simulations.

Senadhinatha (2020) utilized digital elevation models and GIS applications to generate stream features in the Nagalagama Street sub-catchment. They formulated an HEC-HMS rainfall-runoff simulation model using the delineated basin data, meteorological data, and calculated streamflow data. The model was calibrated and validated using the SCS CN method and Unit Hydrograph method. The study reported a relatively strong model performance with Nash Coefficients of 0.80 and 0.89 respectively for calibration and validation. The coefficient of determination (R^2) was 0.83 for calibration and 0.90 for validation. The study demonstrated that an increase in the number of rainy days led to a 50% to 100% runoff increase while rainfall decreased by 85% to 90% compared with the tenth rainy day to the first rainy day.

Rajkumar et al. (2021) researched flood assessment using the Kelani River basin as the basin up to the Hanwella gauging employing the HEC-HMS. They evaluated several goodness-of-fit techniques such as Nash-Sutcliffe, percent error in peak, per cent error in time to peak, and percent error in discharge volume. The study considered flood hydrograph simulation and utilized the Clark, SCS, and Snyder unit hydrograph models. Model calibration and validation were performed consuming hourly rainfall and runoff data from multiple rainfall events. The study concluded that the Clark model was the most suitable for flood modelling in the Kelani River basin.

2.2.2 Flood Modelling of Kelani River

Nanseer and Rajkumar (2006) conducted a study on the Kelani Ganga floods, focusing on two aspects the sand mining impact and the proposal of Kelani Conservation Barrage as a mitigation action for

salinity intrusion. Researchers used a one-dimensional hydrodynamic model, DHI-MIKE11, to assess the feasibility of the barrage. The research carried out from 1990 to 1992, concluded that while the riverbed lowering is an impact on low and medium discharges while there was no significant effect on high flood flows. Fowze et al. (2008) conducted a similar study using the HEC-RAS software and the HECGeoRAS utility in the ArcView environment. They modelled the Lower Kelani Basin, downstream of Glencourse, and used calibrated data from the 1989 flood event to simulate and generate flood hazard maps. The study indicated that the study area would experience flood encroachments of 60, 77, and 94 km^2 for events with return periods of 10, 20, and 50 years, respectively.

Bandara et al. (2022) focused on a specific section of the Kelani River from Glencourse to Hanwella. They utilized the DHI-MIKE11 application and calibrated the model using the 2016 May flood event. The study demonstrated that assimilating discharge observations effectively updated the model and improved flood hydrograph predictions at Hanwella, using both MIKE 11 and real-time data from flood events. Alahacoon et al. (2016) used 13 satellite images, including microwave and optical datasets, to generate flood situation maps daily for the May 2016 flood event in the Kelani Basin. The study combined multi-temporal and multi-satellite remotely sensed data to identify and generate rapid response maps of the victim regions. The authors suggested that resulted in maps will be utilized for post-disaster relief policy and damage valuation.

Dushyantha and Ptuhina (2020) implemented the extreme value theory to assess the water level risks at three gauging stations along the Kelani Ganga namely Glencourse, Hanwella, and Nagalagama Street. The study showed that the risk of water level exceeding certain thresholds was highest at the Hanwella station, with a 10-year risk of 0.809 for reaching 7.12m and a 10-year risk of 0.893 for reaching 9.6m. The Glencourse station had a 10-year risk of 0.643 for reaching 19.7 m. De Silva et al. (2012) analysed flows during floods and flood inundation below Hanwella using the two-dimensional (2D) flood simulation model namely FLO-2D with a 250m resolution. They estimated the inflow at Hanwella using the HEC-HMS model for upcoming extreme events. The models were verified for several flood events between 2005 and 2010, and forecasted flood inundation regions under future Climatic Change projections were identified.

Komolafe et al. (2018) generated discharge data for the upper Kelani Basin using the Similar Hydrologic Element Response (SHER) model. They also used the Flo-2D model with a 250 m resolution for the lower Kelani Basin, calibrating it with the 2010 May flood event. The study showed that the Flo-2D model could estimate flood inundation parameters and provided reasonably accurate results compared to observed flood maps. Siriwardena et al. (2021) assessed the flood effects of the Ambathale Salinity barrage during the 2016 May and 2017 May flood occasions utilizing a hydrodynamic 1D-2D model constructed with Flood Modeller and TUFLOW software. The study revealed a head loss of 0.5 m and a backwater consequence of approximately 10 km upstream during the 2016 event. Recommendations

were made to adjust the barrage's top level or relocate the water intake to mitigate the influence on the community throughout the flooding.

Samarasinghe et al. (2021) and Samarasinghe et al. (2022) compared the applicability of 1D and 2D hydrodynamic models which HEC-RAS coupled with HEC-HMS rainfall-runoff model in the Lower Kelani Basin. The study simulated 2016 and 2018 flood events and evaluated their accuracy against observed flood maps and satellite-generated inundation maps. The combined 1D/2D HEC-RAS flood model outperformed compared to fully 2D model in forecasting flows and inundation, making it the preferred model for predicting flood characteristics in the Kelani River basin. Suja and Rajapaksa (2020) addressed the lack of LiDAR data in Sri Lanka by evaluating alternative topographic data sources. They assessed the accuracy of flood models constructed based on freely available topographic data sets, such as SRTM and ASTER, having resolutions of 30 m and 90 m. The study used the Nays2D flood solver software developed by the International River Interface Cooperative (iRIC) to model the Lower Kelani River basin (downstream of Hanwella). The results showed that even 90 m resolution LiDAR data sources produced more accurate results than the 30 m resolution SRTM and ASTER data sources. Sudeshika and Rajapakse (2021) examined the influence of various Digital Elevation Models (DEM) produces on a Rainfall-Runoff-Inundation (RRI) hydrological model in the Lower Kelani Basin. They conducted a comparative analysis of the performance of DEMs with equal resolution, including SRTM, ASTER, HydroSHEDS, and ALOS PALSAR. They aimed to assess how different DEM products influenced the accuracy and effectiveness of the hydrological model. The study, focusing on the 2016 May flood event, demonstrated that the RRI model consuming SRTM and ALOS PALSAR achieved well considering both flood inundation and water level simulations for the study area.

In conclusion, these studies provide valuable insights into the Kelani River basin's flood dynamics, including factors such as sand mining, conservation barrages, hydrodynamic modelling, satellite-based mapping, water level risks, and the accuracy of data sources and modelling methodologies.

2.2.3 Climate Change Projection for Rainfall in Kelani River Basin

In a study conducted by Dorji et al. (2017), future climate projections for Colombo were estimated using two different methods such that conventional Statistical Downscaling Models (SDSM) and training an Artificial Neural Network (ANN), especially using the Time Delayed Neural Network (TDNN). The study provided future projections of an increase in average temperature and Rainfall for different climate Change pathways for 20's (2011–2040), 50's (2041–2070) and 80's (2071–2099), as compared with the current period of 1961–1990. Furthermore, according to the projections obtained from SDSM and TDNN models, under the RCP 8.5 scenario, the average annual temperature in Colombo is expected to increase by 2.83°C and 3.03°C, respectively. Additionally, the projections indicate that annual rainfall is projected to increase by 33% and 63% based on SDSM and TDNN models, respectively.

Additionally, the Climate Resilient Improvement Project (CRIP) funded by the World Bank, specifically the Kelani Basin Improvement Project, has recently conducted climate projections for the Kelani River basin. The CRIP (2019) has provided the Rainfall depth increasing factors for Pessimistic, Average and Optimistic scenarios for selected return periods such that 2-year, 5-year, 10-year, 25-year, 100-year and 200-year based on different climate model outputs. These findings were considered the most recent and updated climate projections for the Kelani River basin.

These studies, along with the research conducted by Dorji et al. (2017) and the CRIP (2019) climate projections, provide valuable insights into the future climate projections for the Kelani River basins in Sri Lanka. They contribute very important insights into the possible climate change impacts on water resources and help in developing climate-resilient strategies for water management in the region.

2.3 Studies on Other River Basins of Sri Lanka

Shantha and Jayasundara (2005) conducted a study to evaluate the annual rainfall pattern of the Mahaweli basin. Their findings indicated a significant reduction in annual rainfall over the past century, attributed to both local and global-scale climate changes. The upper watershed area of Mahaweli experienced a 39.12% decrease in rainfall during this period, and the declining trend is expected to continue with a projected reduction of 16.6% over the next 21 years. In a study by Herath et al. (2015), the future climate trends of the Mahaweli basin were investigated using the Statistical Downscaling Model (SDSM) and measured point rainfall data from ten rain gauges located in the basin. They employed the Hadley Centre Coupled Model, Version 3 (HadCM3) defined by the IPCC. The outcomes presented that under the high emission situation (A2), an increasing trend in total annual rainfall, maximum annual rainfall, and annual averaged daily rainfall was obtained. However, under the low emission scenario (B2), these parameters exhibited decreasing trends, although the recorded decreases were not statistically significant.

Selvarajah et al. (2021) conducted a study to investigate the climate change impacts of hydro-meteorological characteristics of the Mahaweli basin. They employed the Data Integration and Analysis System (DIAS) of Japan, and the Water Energy Budget-based Rainfall-Runoff-Inundation model (WEB-RRI) for analysing. The study focused on the RCP8.5 projection and utilized four Global Climate Models (GCMs). The findings indicated that the average temperature will increase by 1.1°C over the next 20 years spanning from 2026 to 2045, the basin is projected to receive more extreme rainfall, intense flood disasters, and increased water inflow. The range of increase in rainfall would be between 204 and 476 mm/year, while the inflow would increase by 11 m^3/s to 57 m^3/s. The study also highlighted an increase in socio-economic damage due to flood inundation. However, there was uncertainty regarding future meteorological and hydrological droughts.

Nandalal and Ratnayake (2010) developed a rainfall-runoff model for the Kalu River basin using the HEC-HMS lumped conceptual hydrologic model. The model was verified using four past flood events

data collected from three river gauging. The study compared flood peaks, time to peak, and the Nash efficiency, and found that the HEC-HMS software was suitable for modelling the Kalu-Ganga River basin. Additionally, they observed that the sub-basins amount employed to construct the model had no significant impact on flood prediction due to rainfall. Zubair and Agalawatte (2014) assessed the sensitivity using the runoff of Kalu Ganga to a 2°C rise in global average temperature using the HBV-Light hydrological model and scenario data from seven general circulation models (GCMs). They found substantial differences among the GCMs in consequence rainfall, leading to uncertainty in mean annual runoff changes. Monthly runoff exhibited a consistent direction of change only in June, suggesting a potential alteration in the hydrological regime of the Kalu Ganga basin due to climate change.

Sirisena et al. (2021) studied the projected deviations in hydrology as well as the sediment transport in the Kalu River Basin, Sri Lanka, driven by climate change. They used bias-corrected climate projections utilizing three high-resolution local climate models that RegCM4-MIROC5, MPI-M-MPIESM-MR, and NCC-NORESM1-M derived and applied to verified hydrological models. The simulations for two upcoming periods as mid-century: 2046-2065, and end of the century: 2081-2099 under RCPs 2.6 and 8.5 indicated amplified annual river discharges in 67-87% and sediment loads in128-145% by the end of the century under the RCP 8.5 scenario.

Rathnayake et al. (2010) utilized the Weather Research and Forecasting (WRF) weather model combined with HEC-HMS to predict rainfall in the Nilwala River Basin. They investigated the impacts of different physics options in the WRF model, including microphysics systems, cumulus systems, land surface systems, long and shortwave systems, and boundary layer systems, on rainfall forecasts. Chathuranika et al. (2022) evaluated the climate change impact on river discharges in the Upper Nilwala River Basin (UNRB). The researchers utilized bias-corrected rainfall data from three Regional Climate Models (RCMs) and integrated them into the HEC-HMS model. The RCP 4.5 and RCP 8.5 were selected and the study's findings revealed that for future periods, both RCP scenarios indicated a rise in annual precipitation and streamflow.

Halwatura and Najim (2013) verified the HEC-HMS model for the Attanagalu Oya basin. They employed three different calibration methods, including the SCS CN, the Snyder unit hydrograph method, and the Clark unit hydrograph method, and concluded that the Snyder unit hydrograph method performed better. They also recommended using the linear reservoir method for base flow estimation to improve accuracy. Anuruddhika et al. (2022) used HEC-HMS and HEC-RAS tools for flood modelling for Attanagalu Oya. They employed the Holt-Winters' time series projecting method to estimate climate data for HEC-HMS inputs and determined the HEC-HMS and HEC-RAS are suitable for flood modelling and forecasting future flood-prone areas. Kamran and Rajapakse (2018) studied the effect of watershed subdivisions on the model performance in the Badalgama watershed within the Maha Oya Basin. They used continuous simulation by HEC-HMS and evaluated the impacts of antecedent moisture condition (AMC) events on model performance. The study showed that the accuracy of the model

decreased with an increase in watershed subdivisions. They also found that the model's accuracy improved when using AMC-III as compared to AMC-II.

Herath and Wijesekera (2021) developed an HEC-HMS model for the Giriulla Watershed in the Maha Oya Basin and achieved good accuracy in streamflow simulation. The model can be used with approximately 75% - 80% overall accuracy for water resources management activities. Madhushankha and Wijesekera (2021) used HEC-HMS hydrological model to simulate daily streamflow in the Baddegama watershed. They calibrated and validated the model using different components, including simple canopy, initial deficit and constant loss, SCS direct runoff, and recession base flow. The model demonstrated good performance in flood management and water resource estimation. A case study was conducted by Sampath et al. (2015) to analyze continuous Hydrological modelling in a specific area of the Deduru Oya basin. The study specifically examined inter-basin diversions and storage irrigation schemes using the HEC-HMS model. Mahenthiran and Rajapakse (2021) investigated the impending impacts of climate change on two dry zone basins namely Kirindi Oya and Maduru Oya, employing the HEC-HMS hydrological model. They verified the model using data from different periods and employed various objective functions. The study demonstrated the practicality of HEC-HMS in low-flow analysis.

2.4 Rainfall Trend in Sri Lanka

Several studies have examined rainfall trends in different regions of Sri Lanka and their implications for climate change. Herath and Ratnayake (2004) analysed 30-years of rainfall data from 60 rain gauges in the central hilly area of Sri Lanka. They identified mixed results, with the 1st inter-monsoon period (March-April) showing the maximum reduction in rainfall. The study observed a decreasing trend in the rainy day’s amount but an increasing trend in rain intensity. Furthermore, the study used multifractal analysis to examine changes in rain intensity-frequency relations, revealing a reduction in inter-monsoon rainfall and smaller intensities and return periods for extreme events.

Jayawardene et al. (2005) studied annual rainfall trends in Sri Lanka over 100-years using records from 15 meteorological stations. They found a statistically remarkable rising trend of 3.15 mm/year in Colombo but decreasing trends of 4.87 mm/year in Nuwara Eliya and 2.88 mm/year in Kandy. The study also highlighted steeper downward trends in recent decades, particularly observing the major downward trend of 11.16 mm/year in Batticaloa.

Dammalage and Jayasinghe (2019) analysed daily rainfall totals for Sri Lanka's main agro-climatic zones from 1976 to 2006. They found a solid impact of El Niño and La Niña phases on rainfall distribution. Positive connections with Pacific sea-surface temperatures were observed during the northeast monsoon, while negative associations were found at other periods.

Naveendrakumar et al. (2018) examined historical rainfall trends averages and extremes across Sri Lanka from 1961 to 2015 using daily rainfall data from 20 stations. The study presented a major reduction in wet days during May, potentially due to a late southwest monsoon.

Alahacoon and Edirisinghe (2021) examined the spatial variability of rainfall trends in Sri Lanka utilizing the data from 1989 to 2019 using CHIRPS rainfall data. They found a significant increase in annual rainfall across all climatic zones, with the wet zone experiencing the highest escalation and the semi-arid zone the lowest. The study also forecasted an amplified risk of floods in the southern and western provinces and severe droughts in the eastern and south-eastern districts during the north-eastern monsoon.

Abeysingha (2022) conducted a review of 15 recent publications on rainfall trends in Sri Lanka. The review highlighted an increasing tendency of rainfall throughout the country, particularly in the eastern segment. The study also emphasized upward trends in the first inter-monsoon and northeast monsoon rainfall patterns across Sri Lanka.

2.5 Objective Functions for Model Performance Evaluation

2.5.1 Objective Functions

The objective function is a crucial component used to assess the accuracy of a model in matching its results with reality. Green and Stephenson (2009) examined 21 model performance evaluators and suggested ones such as Percent Error in Peak (PEP), Percent Error in Volume (PEV), Sum of Square Residual (SSR), Sum of Absolute Residual (SAR), and Coefficient of Efficiency (CE) or Nash-Sutcliffe Their study revealed that different criteria may weigh certain aspects of disagreement concerning simulated output and measured data differently. The choice of objective function depends on the modelling objective, whether it be flood control, water resource planning, or management. Calibration will be performed manually or through auto-run methods. Manual calibration depends on the user's awareness of the basin's physical properties and capability in modelling (Chunderlik & Simonovic, 2004).

The widely used Nash-Sutcliffe efficiency (E) is a consistent figure for evaluating the goodness of fit of hydrologic referring Refer to the study by Moriasi et al. (2007) and Ritter and Muñoz-Carpena (2013) established that an NSE value greater than 0.65 indicates an acceptable hydrologic model, while values below 0.65 yield unsatisfactory results. However, the Nash-Sutcliffe efficiency may lead to overestimation for peak flows and underestimation for low flows (Krause, et al., 2005). The coefficient of determination (R^2) is not a strong form-based evaluator used to estimate the statistical properties of model residuals between simulated and measured data (Guinot, et al., 2011). Mean absolute error, as described by Willmott et al. (1985), indicates the average magnitude of model accuracy. Mean squared

error (MSE), proposed by Green and Stephenson (1986), is widely used in model calibration. It serves as a distance-based objective function, measuring the deviation between model-simulated and measured data. This function is particularly useful in emphasizing special runoff components such as flood and base flow. The deviations of model simulated and measured data will be increased by user-defined weights in the distance-based objective function. The World Meteorological Organization (1982) evaluated theoretical models employed in operational hydrological predicting and recommended kind of objective functions. Wijesekera and Abeynayake (2003) analysed and resulted that the Mean Ratio of Absolute Error (MRAE) as the variance between simulated and observed flow.

2.5.2 Selection of Objective Functions

Legates and McCabe (1999) identified a drawback of NSE and MSE, as it squares the variance between model simulations and observations. To address this, the researchers offered a new objective function that allows users to choose the power of the error themselves. Gupta et al. (2009) explained that NSE is estimated by deducting the ratio of MSE to the variance of the observation from one, making it no dimensions and ranging from minus infinity to one in concept. Krause et al. (2005) emphasized that MAE will be used for a balance consideration of high and low flows, while Wu and Liu (2014) stated that MAE does not emphasize either high or low values. The World Meteorological Organization (1982) highlighted that the MRAE objective function hinge on the characteristics of the measured flow dataset and may not enable easy comparison when there are large and small peaks. Additionally, the average of measured flow may not accurately reflect the true mean value of the flow series. Wijesekera (2000) and Jayadeera (2016) argued that the Mean Ratio of Absolute Error (MRAE) well reflects the difference between measured and simulated flows at each data point, as it explains the difference concerning the specific data point of observation. Therefore, MRAE is more suitable for water resources management.

In the evaluation of the HEC-HMS model, De Silva et al. (2014) utilized the Nash-Sutcliffe efficiency. Similarly, Senadhinata (2020) used Nash-Sutcliffe Coefficients and the coefficient of determination (R^2) to evaluate the HEC-HMS model. Rajkumar et al. (2021) employed the Nash-Sutcliffe model efficiency, per cent error in peak, per cent error in time to peak, and per cent error in discharge volume as goodness-of-fit criteria for HEC-HMS. In the present study, the Nash-Sutcliffe Coefficients and the R^2 were selected to evaluate simulated discharges and water levels with the observed dataset.

CHAPTER 3

3 METHODOLOGY

3.1 Study Area

The study took place on the Kelani River, which is the fourth-longest river in Sri Lanka, stretching over 192 km and covering a basin area of 2,292 km^2. It lies between latitudes 6° 50' N to 7° 30' N and longitudes 79° 45' E to 80° 15' E. Originating from Adams Peak in the central hilly area, the Kelani River flows through steep slopes before transitioning into a gentle mid-range slope and eventually reaching the flat coastal plain. Its final destination is the Indian Ocean at Colombo. The river passes through six districts namely Kegalle, Gampaha, Colombo, Nuwara-Eliya, Kalutara, and Rathnapura while spanning three provinces namely Sabaragamuwa, Western, and Central.

The Kelani River basin is of great importance as a water source for Sri Lanka's capital, Colombo, and its surrounding areas. The land use in the basin is primarily dominated by tea, rubber, and coconut cultivation, while paddy fields are also present in the lower elevations. This river basin plays a critical role in Sri Lanka's social, economic, and environmental aspects, supporting a population of over three million people. Additionally, many industries rely on its resources.

The elevation within the basin varies from 0 to 2,524 meters above Mean Sea Level (MSL). On average, the Kelani catchment receives about 3,450 mm of rainfall annually. This rainfall leads to peak flows ranging from 800 to 1,500 m^3/s downstream, and the annual discharge volume is estimated to be approximately 7,860 million cubic meters (MCM). The majority of the rainfall occurs during the

southwest monsoon and the second inter-monsoon due to the topographical location. As a result, the lower part of the Kelani catchment is prone to frequent flash floods during these periods.

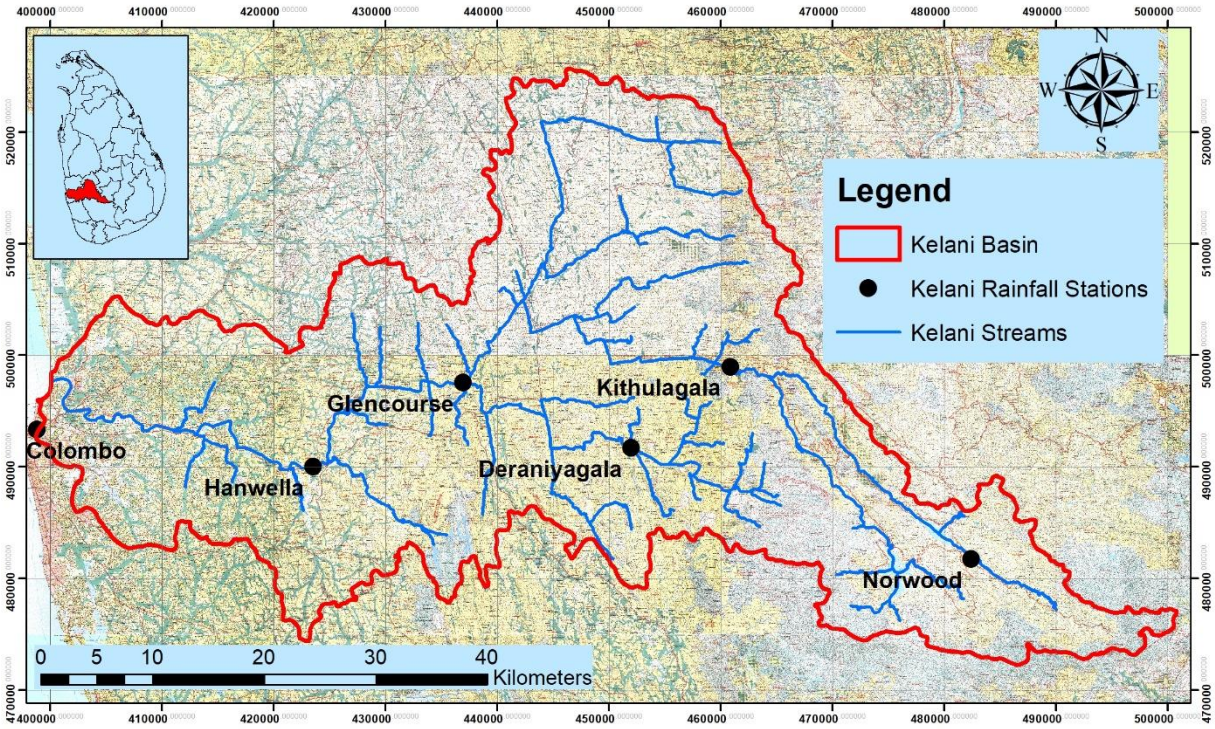

Figure 3-1:Study Area

3.2 Methodology Development

In Chapter 1, the research initially identified the problem and developed a problem statement. The overall objective was defined, and specific objectives were identified to achieve it. A literature survey was conducted to collect relevant literature and create a catalogue. The surveyed literature was carefully studied to extract data, adopt theories and methodologies, and critically evaluate the sources. This process led to the development of the research methodology.

The research methodology consisted of three components such that hydrological modelling, flood modelling, and incorporation of climate change projections with Hydrological and Flood modelling. To support these components, meteorological data, hydrometric data, topographic data, soil data, and land use data were collected from various organizations, considering their availability and selecting appropriate temporal and spatial resolutions. Chapter 4 provides more detailed information about the data collection process. The collected data underwent relevant data-checking procedures, and input files were prepared accordingly for the models.

During the study, the Kelani Basin was divided into two parts: Upper Kelani Basin, which encompasses the upstream portion until the Glencourse Water Level Gauging station, and the Lower Kelani Basin, which extends from the Glencourse station to the sea outfall. The Upper Kelani Basin was modelled as a hydrological model using the HEC-HMS tool to determine the Kelani River discharge at Glencourse.

The Lower Kelani Basin was predominantly modelled as a flood model using the HEC-RAS tool. The discharge generated by HEC-HMS (from the Kelani Upper model) served as the upper boundary condition for the flood model. Additionally, the catchment runoff generation for the Lower Kelani Basin was modelled separately by HEC-HMS, and the output was distributed along the Kelani River in the flood model. This interdependent model setup was utilized for all flood simulations presented in the study.

3.2.1 Hydrological Modelling

The literature review in Chapter 2 revealed that the HEC-HMS software was commonly used for hydrological modelling in the Kelani Basin. De Silva et al. (2014) employed HEC-HMS for modelling the Kelani Basin, while Gunathilake et al. (2019) developed a flood-simulating application for the Seethawaka Ganga using the same software. Senadhinatha (2020) utilized HEC-HMS for hydrological modelling of the Nagalagama Street sub-catchment, and Rajkumar et al. (2021) conducted flood assessment in the Kelani River basin up to the Hanwella gauging station, also employing HEC-HMS. Additionally, Samarasinghe et al. (2021) and Samarasinghe et al. (2022) utilized the HEC-HMS rainfall-runoff model in the Lower Kelani Basin during their studies.

The present study utilized the HEC-HMS tool for hydrological modelling. HEC-HMS, which stands for Hydrologic Engineering Centre's Hydrologic Modelling System, is a widely used and powerful tool for simulating hydrological processes in watershed systems, specifically for predicting surface water runoff. The HEC-HMS software is a highly advanced tool that is freely available and relatively easy to learn. It provides ample learning materials to assist users in understanding its functionality. One of its notable advantages is the convenience it offers in incorporating input data, as it seamlessly supports GIS and Tabular data outputs. Moreover, extracting time series results from the software is straightforward and efficient The model in HEC-HMS consists of several main components: The Basin model, the Meteorological model, Control specification, and Time-Series data for model development.

The Basin model represents the physical catchment and includes various hydrological elements such as sources, sub-basins, reaches, junctions, sinks, reservoirs, and diversions. These elements are used to model sub-basins, river tributaries, and junction inflows. The tool incorporates GIS capabilities, allowing for sub-catchment delineation, resulting in reaches and junctions. It also allows for the importation of predefined sub-basins and reaches. Different mathematical models are available within HEC-HMS for determining losses, excess transformation, and base flow addition for sub-basin elements. Various river routing methods are available for stream routing in reach elements.

The Meteorological Model is used to define precipitation data, offering different methods for inputting precipitation. The Time Series Data Manager is used for inserting gauge data such as precipitation gauges, discharge gauges, and stage gauges, which consist of time series data. In the HEC-HMS setup, time series data is coupled with the aforementioned data managers, linking precipitation gauges to the

Meteorological Model and discharge gauges to either sources or junctions as needed. The Control Specification is used to define the simulation duration and time interval. Computational methods and simulation run and optimization trial methods are available for analysis. Detailed results outputs are generated after computation, including the Global summary, calibration summary, and graphical and tabulated results for each element. The Global Summary includes peak discharge, time to peak, and volume, while the calibration summary includes objective function values such as Root Mean Square Error, standard deviation, Nash Sutcliffe coefficient, Percent Bias value, and Coefficient of Determination.

For hydrological modelling of the Kelani basin, it was divided into three parts as Figure 3-2, resulting in the development of three HEC-HMS models: Kelani Upper, Kelani Middle, and Kelani Lower. The Kelani Upper model represents the sub-basin element responsible for generating Glencourse Discharge. The Kelani Middle model consists of one sub-basin element for modelling the catchment discharge from Glencourse to Hanwella, one reach element for modelling the Kelani river portion from Glencourse to Hanwella, one source element for adding Glencourse inflow, and one junction element to combine the reach and sub-basin elements. This junction element generates the river discharge at Hanwella. Similarly, the Kelani Lower model follows the same structure as the Kelani Middle model, with one sub-basin element for modelling the catchment discharge from Hanwella to the Sea Outfall, one reach element for modelling the Kelani river portion from Hanwella to the Sea, one source element for adding Hanwella inflow, and one junction element to combine the reach and sub-basin elements. The aforementioned junction element generates the river discharge at the sea outfall.

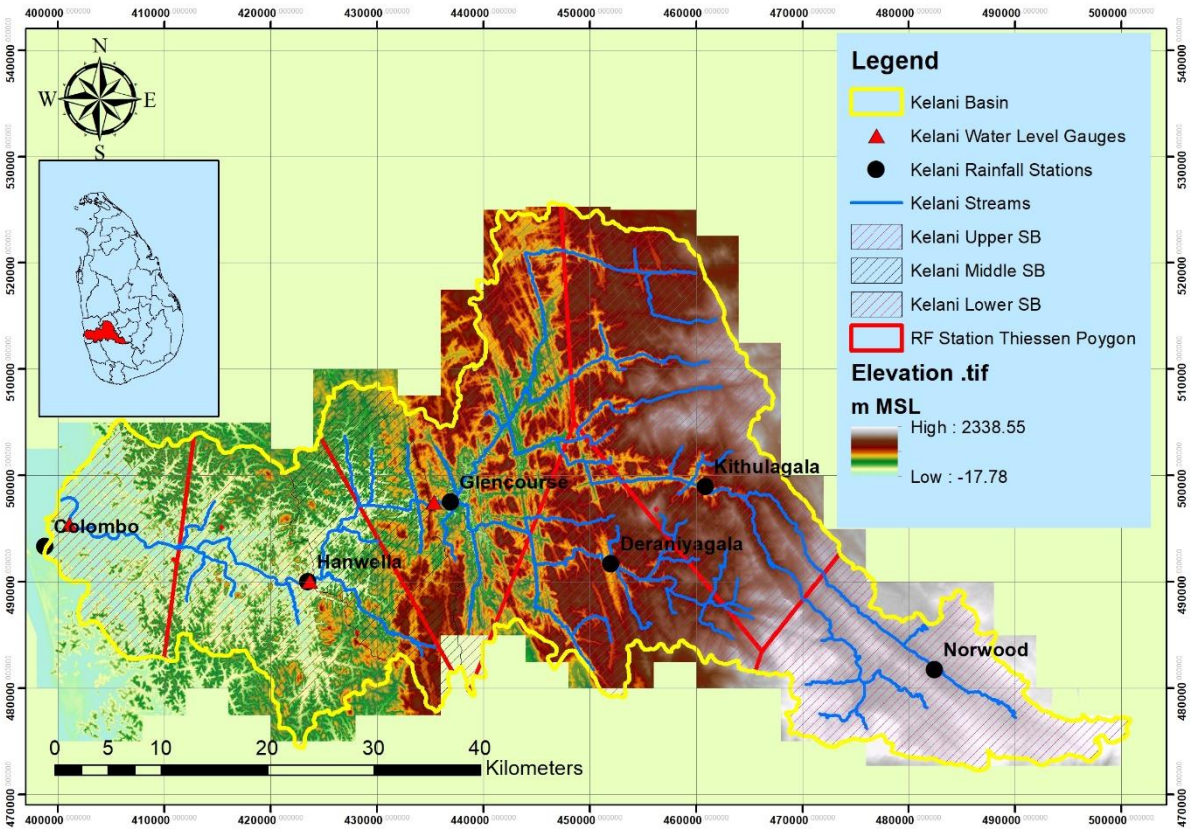

Figure 3-2:Kelani Basin Elevation Map with Rain Gauges, River Gauges and Sub-Basins

In their study, De Silva et al. (2014) employed the Clark unit hydrograph method to simulate direct runoff, while the recession base flow method was utilized for simulating base flow. Gunathilake et al. (2019) found that the SCS Curve Number (SCS CN) method, Clark unit hydrograph, Muskingum, and lag methods yielded satisfactory results in their simulations. Similarly, Senadhinatha (2020) achieved good performance in model calibration and validation by employing the SCS Curve Number method. Rajkumar et al. (2021) compared flood hydrograph simulations using the Clark Unit Hydrograph method, SCS CN, and Snyder unit hydrograph models and concluded that the Clark Unit Hydrograph method was the most suitable for flood modeling. Halwatura and Najim (2013) utilized the HEC-HMS model for the Attanagalu Oya basin, employing the SCS CN, Snyder unit hydrograph method, and Clark unit hydrograph method. In another study by Madhushankha and Wijesekera (2021), the HEC-HMS hydrological model was used to simulate daily streamflow in the Baddegama watershed, incorporating various components such as simple canopy, initial deficit and constant loss, SCS direct runoff, and recession base flow. Based on these findings, the SCS CN method was recommended for the Loss method, the Clark Unit Hydrograph method for the transform method in subbasin elements, and the recession method for baseflow modeling in subbasin elements. The Muskingum method was selected for the modeling of Reach elements, taking into account the literature recommendations.

The loss method for all sub-basin elements in this study is defined as the Soil Conservation Service (SCS) Curve Number (CN) method. This method is employed to estimate the runoff amount resulting

from rainfall in a specific area. It takes into account factors such as soil type, land use, and land cover by assigning a curve number that represents the potential for infiltration and runoff. This curve number is then utilized in an equation to calculate the volume of runoff. The mathematical equations are presented in Equation 3-1 to Equation 3-4.

$$P_e = \frac{(P - I_a)^2}{P - I_a + S} \quad 3\text{-}1$$

$$I_a = 0.2S \quad 3\text{-}2$$

$$P_e = \frac{(P - 0.2S)^2}{P + 0.8S} \quad 3\text{-}3$$

$$S = \frac{1000}{CN} - 10 \quad 3\text{-}4$$

Here, P_e - Excess Rainfall (Direct Run-off), P - Total Rainfall, I_e - Initial Abstraction, P - Potential Maximum Retention and *CN* - Curve Number.

The HEC-HMS tool incorporates three parameters for the SCS Curve Number method, namely Initial Abstraction, Curve Number, and Impervious, which are utilized for modelling precipitation loss.

For the Transform method of all sub-basin elements, the Clark Unit Hydrograph method is employed. This hydrological technique is used to estimate the flow rate and volume of surface runoff in a watershed. It involves creating a hypothetical, time-varying hydrograph based on the precipitation input and characteristics of the watershed. The method utilizes a linear reservoir model to account for the storage and release of water within the basin. By applying the convolution principle, the resulting unit hydrograph is convolved with the actual precipitation input, resulting in the runoff hydrograph. Within the HEC-HMS tool, two parameters, namely Time of Concentration and Storage coefficient, are used to model the transformation of excess rainfall volume into the hydrograph.

The SCS lag equation (1973) is used to calculate the Time of concentration as presented in Equation 3-5 and Equation 3-6.

$$l_c = \frac{100L^{08}[\left(\frac{1000}{CN}\right) - 9]^{0.7}}{1900S^{0.5}} \quad 3\text{-}5$$

$$t_c = 1.67\, l_c \quad 3\text{-}6$$

Here, l_c - Lag Time (min), L - Longest Flow path (ft) , CN - SCS Curve Number, S - Average Watershed Slope (%) and t_c - Time of Concentration (min).

Storage coefficient is determined by Equation 3-7;

$$t_c + R = 142.2A^{0.081}s^{0.539} \quad 3\text{-}7$$

where t_c - Time of Concentration (min), R - Storage Coefficient (Hr), A - Drainage Area (km^2) and s - Channel Slope (m/km).

The base flow method for all sub-basin elements in this study is defined as the Recession method, which includes the parameters of Initial Discharge, Recession Constant, and Ratio to Peak in the HEC-HMS tool.

As for the reach elements in all HEC-HMS models, the Muskingum Method is used as the routing option. This routing model employs a simple finite difference approximation of the continuity equation. Storage in the reach is represented by the combination of prism storage and wedge storage. Prism storage corresponds to the volume defined by a steady-flow water surface profile, while wedge storage accounts for the additional volume under the flood wave's profile. The main parameter of the Muskingum method, namely Muskingum *K*, is estimated by Equation 3-8 and Equation 3-9 and Muskingum *X* is estimated using Equation 3-10.

$$K = \frac{L}{V_\omega} \quad 3\text{-}8$$

$$V_\omega = \frac{1}{B}\frac{dQ}{dy} \quad 3\text{-}9$$

Here, K - Muskingum K, L - Channel Length, V_ω - Flood Wave Velocity, B - Top width of Water Surface and dQ/dy - Slope of the discharge rating curve;

$$X = \frac{1}{2}\left(1 - \frac{Q_0}{BS_0c\Delta_x}\right) \quad 3\text{-}10$$

where X - Muskingum X, Q_0 - Reference flow from Inflow Hydrograph, B - Top width of flow area, S_0 - Friction slope or Bed Slope, c - Flood wave speed and Δ_x - Length of reach.

3.2.1.1 Parameter Sensitivity Analysis

Conducting parameter sensitivity analysis is an important aspect of utilizing HEC-HMS. This analysis involves assessing the impact of different input parameters on the model output. By systematically varying these parameters, we can identify the most influential ones and gain insights into the behaviour of the hydrologic system. This information is valuable for refining model calibration and enhancing the accuracy of hydrologic predictions.

In this study, the sensitivity analysis was performed using hourly rainfall and discharge data from the 2016 May flood event, specifically from May 15th to May 23rd. The Kelani Upper model was utilized for the parameter sensitivity analysis of the sub-basin element. A Thiessen weighted single rainfall was developed based on observed rainfall gauge data and incorporated into the Kelani Upper model. The observed discharge at Glencourse served as the observed data at the outfall. The parameters of the sub-basin elements were evaluated using specific formulas, and parameter ranges were established for the sensitivity analysis.

For the parameter sensitivity analysis of the reach element, the Kelani Middle model, which includes both the reach element and source element, was utilized. The observed discharge at Glencourse was set as the inflow boundary condition, and the observed discharge at Hanwella was set as the outflow boundary condition. Parameter values for the reach elements were assumed based on the literature, and parameter ranges were determined accordingly.

During the simulations, one parameter was varied while keeping the other parameters constant. The resulting outputs were plotted against the changing parameter values. Peak discharges were analysed to assess the effect on the maximum discharge, and calibration objective functions such as Nash Sutcliffe efficiency and coefficient of determination (R^2) were plotted to evaluate the overall performance in comparison to observed and simulated time series. Additionally, time series discharge outputs were plotted alongside observed time series to assess the overall behaviour.

The Nash Sutcliffe efficiency (E) was used as a measure of performance. It is defined as one minus the sum of the absolute squared differences between the simulated and observed values, normalized by the variance of the observed values during the selected simulation period. The calculation of Nash Sutcliffe efficiency is calculated by Equation 3-11;

$$E = 1 - \frac{\sum_{i=1}^{n}(O_i - P_i)^2}{\sum_{i=1}^{n}(O_i - \bar{O})^2} \qquad 3\text{-}11$$

where E - Nash Sutcliffe efficiency, O_i - Observed Values, P_i - Simulated Value and $\bar{O}$ - Average of Observation.

The Coefficient of determination (R^2) is defined as the squared value of the coefficient of correlation according to Bravais Pearson. It is calculated by using the Equation 3-12;

$$R^2 = \left(\frac{\sum_{i=1}^{n}(O_i - \overline{O})(P_i - \overline{P})}{\sqrt{\sum_{i=1}^{n}(O_i - \overline{O})^2}\sqrt{\sum_{i=1}^{n}(P_i - \overline{P})^2}}\right)^2 \quad 3\text{-}12$$

where O_i - Observed Values and P_i - Simulated Value.

3.2.1.2 Model Calibration and Validation

The calibration event used for the study was the May 2016 flood, which can be considered as an almost 50-year flood event. On the other hand, the May 2017 flood event, which served as the validation event, had a slightly lower magnitude compared to the 50-year design flood event used for climate change analysis. These two events were selected as the most recent applicable flood events based on data availability and similarity in magnitude.

The parameter sensitivity analysis helped identify the most sensitive parameters, which were crucial for model calibration. Each of the three HEC-HMS models developed in this study underwent calibration for the 2016 May flood event, using observed rainfall and discharge data. The same model setup used for the parameter sensitivity analysis was employed for the calibration of the Kelani Upper model. The complete model setup of the Kelani Middle, including the Sub-Basin and Junction elements, and the complete setup of the Kelani Lower model were used for their respective calibrations.

During the calibration of the Kelani Lower model, the Nagalagama Street stage gauge, located close to the sea outfall, was assumed to have the same discharge as the sea outfall during the calibration process.

The optimization trial computation option available in the HEC-HMS tool was utilized for the initial model calibration. It provided suggestions for optimized model parameter values and the corresponding Nash-Sutcliffe efficiency. The objective function used was the Peak Weighted Root Mean Square Error. This approach involved systematically optimizing the model by adjusting parameter values based on the suggested values, Nash-Sutcliffe efficiency, and visual observations of graphs. Initially, the optimization trials focused on the most sensitive parameters while keeping the others fixed. Eventually, all parameters were considered in the optimization process. Once the optimal model calibration was achieved through the optimization trial process, manual model calibration was performed using the optimized parameters with the Simulation run option available in HEC-HMS. Visual observation of graphs, along with the Nash Sutcliffe efficiency and Coefficient of determination (R^2), were employed for the model calibration process.

For the model validation process, the 2017 May flood event from the 24th to the 29th of May was selected. Hourly rainfall and discharge data were used for this purpose. The calibrated models of Kelani Upper, Kelani Middle, and Kelani Lower were simulated using the data from the 2017 May event. The assigned rainfall and discharge data were used to evaluate the Nash Sutcliffe efficiency and Coefficient of determination (R^2). It was crucial to ensure that the objective functions fell within a satisfactory range to consider the model as validated. Once the models were successfully validated, they were deemed suitable for simulating hypothetical events and forecasting future discharge patterns. These validated models provide a reliable basis for predicting future discharges and analysing their potential impact.

3.2.1.3 Model Simulation for Statistical Rainfall Event

The validated HEC-HMS models were used to simulate a hypothetical flood event that was statistically developed to forecast future flood scenarios. For this study, a 50-year return period design flood event was selected. Intensity Duration Frequency (IDF) curves were utilized to determine the design rainfall for a 3-day duration with a 1-hour intensity using the alternative block method. To generate the rainfall for each sub-basin of the Kelani Upper, Kelani Middle, and Kelani Lower models, the Thiessen polygon technique was applied. Additionally, an Areal Reduction Factor was employed to adjust the rainfall depths for each sub-basin. The models were then simulated for a period of 5 days, and the time series discharge outputs for each sub-basin were extracted to serve as inputs for the flood model. These inputs are essential for analysing the potential impact of the hypothetical flood event and understanding its characteristics.

3.2.1.4 Model Simulation with Climate Change Projections

The validated HEC-HIS models, which were previously used for the statistical rainfall event, were utilized for conducting simulations of climate change projections without altering the model parameters. These simulations took into account the adjustment of rainfall depths based on climate change projections, as referenced in the relevant literature. The Thiessen weighted 50-year return period balanced storm, along with the application of an aerial reduction factor, was multiplied by the climate change Projection factor. These adjusted rainfall values were then employed in the HEC-HMS model simulations, similar to the previous statistical rainfall event simulations. The resulting time series discharge outputs for each sub-basin were extracted to serve as inputs for the flood model. This analysis enabled an assessment of the potential impacts of climate change on the hydrological system and aided in understanding how future climate scenarios may affect the studied area.

3.2.2 Flood Modelling

In a previous study on the Kelani River basin, Fowze et al. (2008) utilized the HEC-RAS software and the HECGeoRAS utility within the ArcView environment to model the Lower Kelani Basin downstream of Glencourse. Additionally, Samarasinghe et al. (2021) and Samarasinghe et al. (2022) compared the suitability of 1D and 2D hydrodynamic models by coupling HEC-RAS with the HEC-HMS rainfall-

runoff model in the Lower Kelani Basin. Gunasekera (2008) also employed HEC-RAS to model the potential flood areas in the Kelani River, resulting in flood depth and extent maps for various return periods. They further identified flood management and flood-disaster mitigation strategies. In another study by Anuruddhika et al. (2022) on different river basins, HEC-HMS and HEC-RAS tools were used for flood modelling of the Attanagalu Oya. The study concluded that HEC-HMS and HEC-RAS are suitable for flood modelling and forecasting future flood-prone areas in the basin.

Different flood modelling approaches have been employed for the Kelani River. Nanseer and Rajkumar (2006) and Bandara et al. (2022) utilized DHI-MIKE11, while De Silva et al. (2012) used the FLO-2D tool. Siriwardena et al. (2021) constructed a hydrodynamic 1D-2D model using Flood Modeller and TUFLOW software. Suja and Rajapakse (2020) utilized the Nays2D flood solver. It is important to note that, except for Nays2D, these tools are commercial software and not freely available.

In contrast, HEC-RAS software offers several advantages. It is a sophisticated tool that is freely available, and there are abundant learning materials to facilitate its use. Incorporating input data is straightforward as it supports GIS and tabular data outputs, allowing for the easy extraction of time series results. One distinguishing feature of HEC-RAS is its utilization of a Sub-Grid technique, which involves applying a separate computational grid based on catchment topography in addition to the terrain grid. This technique helps manage simulation time, which is a significant benefit. Overall, HEC-RAS stands out as an accessible and powerful option for flood modelling in the Kelani River, offering valuable capabilities and ease of use compared to other 2D flood models.

The lower basin, located downstream of the Glencourse gauging station, was chosen for flood modelling due to its flat topography and frequent occurrence of flooding. For this purpose, the Hydrological Engineers Centre River Analysis Model (HEC-RAS) was employed as a fully two-dimensional (2D) model. HEC-RAS's fully 2D modelling capabilities enable engineers to simulate complex river hydraulics by considering the variations in water flow and depth across the entire cross-section of the river. This powerful software tool can analyse floodplains, levee breaches, dam breaks, and other hydraulic structures, providing essential insights for floodplain management and infrastructure planning. By utilizing HEC-RAS's 2D modelling, engineers gain a comprehensive and efficient means to assess intricate river hydraulics and evaluate the impact of hydraulic structures on the overall river system.

The HEC-RAS modelling system consists of user-friendly components known as editors, including the geometric data editor, hydrologic data editor, hydraulic analysis engine, output processor, and mapping interface. The geometric data editor allows users to define the river channel's geometry, incorporating cross-sections, bridges, culverts, and other hydraulic structures. It also facilitates the specification of river reach lengths and slopes. The hydrologic data editor is responsible for defining the flow boundary conditions, such as flow rates, water surface elevations, and flow durations. The hydraulic analysis engine utilizes geometric and hydrologic data to perform hydraulic calculations, generating water surface elevations, water velocities, and other hydraulic parameters for each cross-section along the river

reach. The output processor generates graphical and tabular reports presenting the hydraulic results for each cross-section and the entire river reach. Additionally, the mapping interface allows for the visualization of hydraulic results on maps and aerial photographs, as well as the exportation of results to GIS software.

The HEC-RAS 2D model is specifically designed to simulate and model intricate floodplains where one-dimensional (1D) flow analysis alone may not provide accurate results. This 2D unsteady flow, varying with time and across two spatial dimensions, adheres to the principles of conservation of mass (continuity) and momentum. Mathematically, the continuity equation for the 2D unsteady flow is expressed as Equation 3-13;

$$\frac{\partial H}{\partial t} + \frac{\partial (hu)}{\partial x} + \frac{\partial (hv)}{\partial y} = 0 \qquad 3\text{-}13$$

where H - Water Surface Elevation (m), h - Water Depth (m), u - Depth averaged velocity in X axis and v - Depth averaged velocity in Y axis.

To calculate the conservation of momentum in the HEC-RAS 2D model, Newton's second law of motion is employed. This fundamental law states that the total forces acting on an element are equal to the rate of change of momentum. The equation considers various factors such as gravitational force, eddy viscosity, friction, and the Coriolis effect. However, in the 2D model, the Coriolis effect and eddy viscosity terms are often disregarded due to the size of the river basin and the unavailability of necessary parameters to calibrate the eddy viscosity coefficient. Therefore, the modified full momentum equations for the x and y directions can be expressed in Equation 3-14 and Equation 3-15, respectively;

$$\frac{\partial u}{\partial t} + u\frac{\partial u}{\partial x} + v\frac{\partial u}{\partial y} + g\frac{\partial H}{\partial x} + \frac{gn^2|u|}{R^{4/3}}u = 0 \qquad 3\text{-}14$$

$$\frac{\partial v}{\partial t} + u\frac{\partial v}{\partial x} + v\frac{\partial v}{\partial y} + g\frac{\partial H}{\partial y} + \frac{gn^2|u|}{R^{4/3}}v = 0 \qquad 3\text{-}15$$

where g - Gravitational Acceleration (m/s^2), n - Manning's Roughness Coefficient and R - Wetted Perimeter (m).

To enhance computational efficiency and mitigate numerical instabilities, the HEC-RAS 2D unsteady flow Saint-Venant equations, also known as shallow water equations, are commonly simplified using the diffusive wave approximation. However, it is important to note that these simplifications are only valid under certain flow conditions. When dealing with tidal influences in rivers, it is advisable to employ the full momentum equations instead of relying on simplified versions.

As mentioned earlier, the Kelani Glen-Lower Flood model was developed for the downstream sub-basin from Glencourse, covering the Kelani River and floodplain, utilizing the HEC-RAS tool. The physical geometry of the model was constructed using the RAS-Mapper tool, which incorporates GIS capabilities. The Kelani flood model was designed with SLD99 National Coordinate system projections to ensure accurate alignment with other GIS data.

To initiate model development, a 2 m resolution (main) and 30 m resolution Digital Elevation Model (DEM) were employed, with terrain data integrated into the model. However, the provided DEM did not include Kelani River Bathymetry. Thus, the bathymetry of the Kelani River was established using measured cross-section data, and a separate 2 m DEM was created for it, utilizing 1D river geometry and the provided cross-sections. These three DEMs were merged to generate a comprehensive terrain model incorporating Kelani River Bathymetry, which was then used for simulations.

This study utilized cross-section (CS) data that were measured in 2001 from Hanwella to the Sea outfall, as well as Glencourse to Hanwella CS data measured in 2016, to model the underwater topographic profile of the river. It is important to acknowledge that the river sections are subject to changes caused by activities such as sand mining, soil erosion, and man-made rehabilitations, all of which directly impact the river's flood levels. However, these changes in cross-sections were not taken into account during the study, and it was assumed that the underwater river profile remained constant over time.

The 2D flow area was defined as the entire Glen-Lower sub-basin, employing a mesh grid resolution of 100 m. For the Kelani River, a refinement region with a mesh grid resolution of 30 m was defined, incorporating flow separation lines, bunds, and roads as Breaklines. The Land Cover layer, providing Manning's roughness values, was developed using a Land use map with 10 m resolution grids. Appropriate Manning's roughness n values were assigned based on land use categories using the attribute table of the Land Cover Layer.

The Flow data file was created to include the inflow boundary at Glencourse, lateral inflows from the Kelani Middle Sub-basin, lateral inflows from the Kelani Lower Sub-basin, and the water level boundary condition at the Sea Outfall. The output discharge from the Kelani Upper model in HEC-HMS was utilized as the inflow boundary at Glencourse, and the output discharges from the Kelani Middle and Kelani Lower models were used to represent lateral inflows. The water level boundary condition was defined as the sea level data series at sea outfall.

3.2.2.1 Flood Model Parameter Sensitivity Analysis

For the Flood model parameter sensitivity analysis, observed data from the 2016 May Flood event, spanning from May 15th to May 23rd, was utilized. The observed flow at Glencourse served as the inflow data, while lateral flows were not considered. The parameter sensitivity analysis focused on the friction slope at the outfall in the flow model and Manning's n roughness values in the Land Cover Data. To determine the parameter ranges, initial values were estimated, and the model was simulated by altering

one parameter at a time while keeping the others constant. The simulated discharge at Hanwella and the simulated water level at Nagalagama Street were extracted and compared with their corresponding observed data series. The performance of each parameter sensitivity was evaluated through visual graphical observation, as well as the calculation of Nash-Sutcliffe efficiency and coefficient of determination (R^2).

These evaluations provided insights into the impact of individual parameters on the model's performance. By systematically varying the parameters and analysing the resulting simulations, the most influential parameters could be identified. This information would guide the refinement of the model calibration process, improving the accuracy of future hydrological predictions.

3.2.2.2 Flood Model Calibration and Validation

The observed data from the 2016 May Flood event, covering the period from May 15th to May 23rd, was utilized for calibrating the Flood Model. The Kelani Glen-Lower Flood model was developed using various input data sources. The observed Glencourse discharge was used to define the inflow boundary condition. The HEC-HMS output discharges were incorporated to represent the lateral flows. Additionally, the observed sea levels at the sea outfall were considered in the model development process.

Furthermore, the observed data series from the 2017 May Flood event, spanning from May 24th to May 29th, was employed for model validation. By comparing the simulated results of the Flood Model with the observed data from both the calibration and validation events, the accuracy and reliability of the model can be evaluated and verified. This iterative process of calibration and validation helps ensure that the Flood Model accurately captures the dynamics of the Kelani Glen-Lower area during flood events.

3.3 Methodology Flow Chart

The methodology employed in this study to achieve both the overall objective and specific objectives, as described in Section 3.2, was followed throughout the research. A visual representation of the methodology was represented in Figure 3-3, which depicts the methodology flow chart. This flow chart outlines the step-by-step process undertaken in this study to ensure a structured and systematic approach towards achieving the desired outcomes. By adhering to this methodology, the study aims to provide reliable and comprehensive results in accordance with the research objectives.

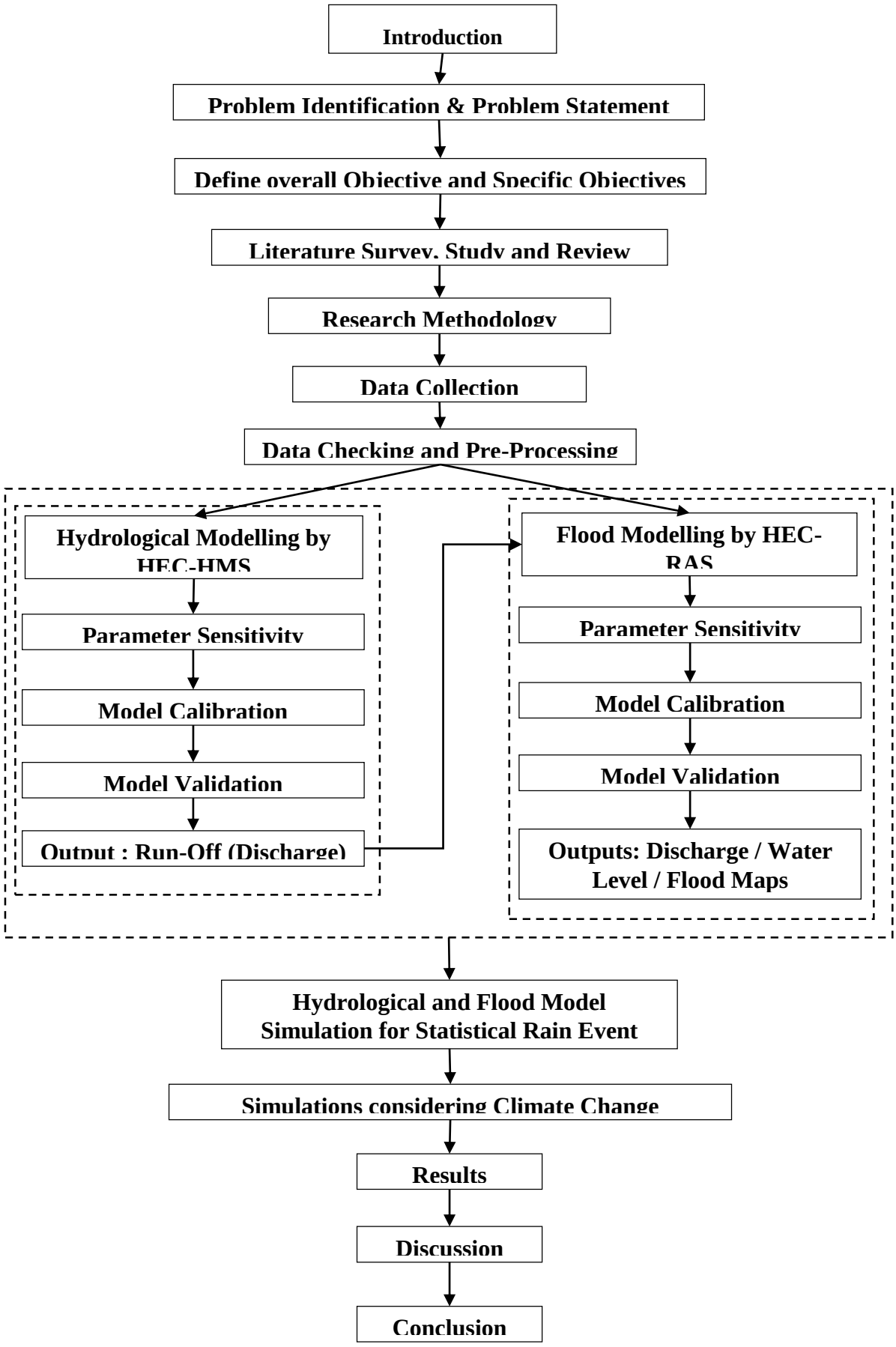

Figure 3-3: Methodology Flowchart

CHAPTER 4

4 DATA CHECKING AND ANALYSIS

4.1 Data Collection

To develop the hydrological models, flood models, hypothetical simulation models, and climate change projection models, various types of data were collected. These included hydrological data, meteorological data, topographical data, and flood-related data. A summary of the collected data can be found in Table 4.1, which provides an overview of the different types of data sources utilized in the study.

Table 4-1: Data Sources and Resolutions

Type of Data	Data Resolution / Data Extent	Source	Period/Year	Category
Digital Elevation Model (DEM) – 2 m	Kelani Basin	Department of Survey	2016	Topographical
Digital Elevation Model (DEM) – 30 m	Sri Lanka	Shuttle Radar and Transmission Mission (SRTM)	2007	Topographical
Kelani River Cross Section Data	Lower Kelani Basin downstream to Glencourse	Department of Irrigation	2016	Topographical
		Lanka Hydraulic Institute	2001	
Rainfall	Hourly	Department of Irrigation Department of Meteorological	2016 May 15th to 23rd 2017 May 24th to 29th	Meteorological
Discharge	Hourly	Department of Irrigation	2016 May 15th to 23rd 2017 May 24th to 29th	Hydrological

Type of Data	Data Resolution / Data Extent	Source	Period/Year	Category
Water Level	Hourly	Department of Irrigation	2016 May 15th to 23rd 2017 May 24th to 29th	Hydrological
Flood Maps	Lower Kelani Basin downstream to Glencourse	Department of Irrigation Department of Survey	2016 May and 2017 May	Hydrological
IDF Data	Kelani Basin	Department of Irrigation	Published in 2019 and 2022	Meteorological
Land Use	1:50 000	Department of Survey	2002	Topographical
Soil Map	Sri Lanka	Department of Survey	1988	Topographical
Topographic Maps	1:50 000	Department of Survey	2002	Topographical

4.2 Data and Data Checking

4.2.1 Topographical Data

Topographic data is information about the elevation of the Earth's surface. It can be represented in a variety of ways, including contour lines, digital elevation models (DEMs), and shaded relief maps. For this study, Digital elevation models (DEM) were used to represent the elevation.

4.2.1.1 Digital Elevation Model

DEMs are digital representations of the Earth's surface. They are created by collecting elevation data from a variety of sources, such as ground surveys, satellite imagery, and LiDAR (light detection and ranging) data.

Digital Elevation Model (DEM) – 2 m

The 2 m resolution digital elevation model (DEM) for the Kelani River Basin is used primarily for sub-catchment delineation, slope calculation, and 2D flood modelling. This data has been checked against the contours of 1:50,000 topographic maps and verified.

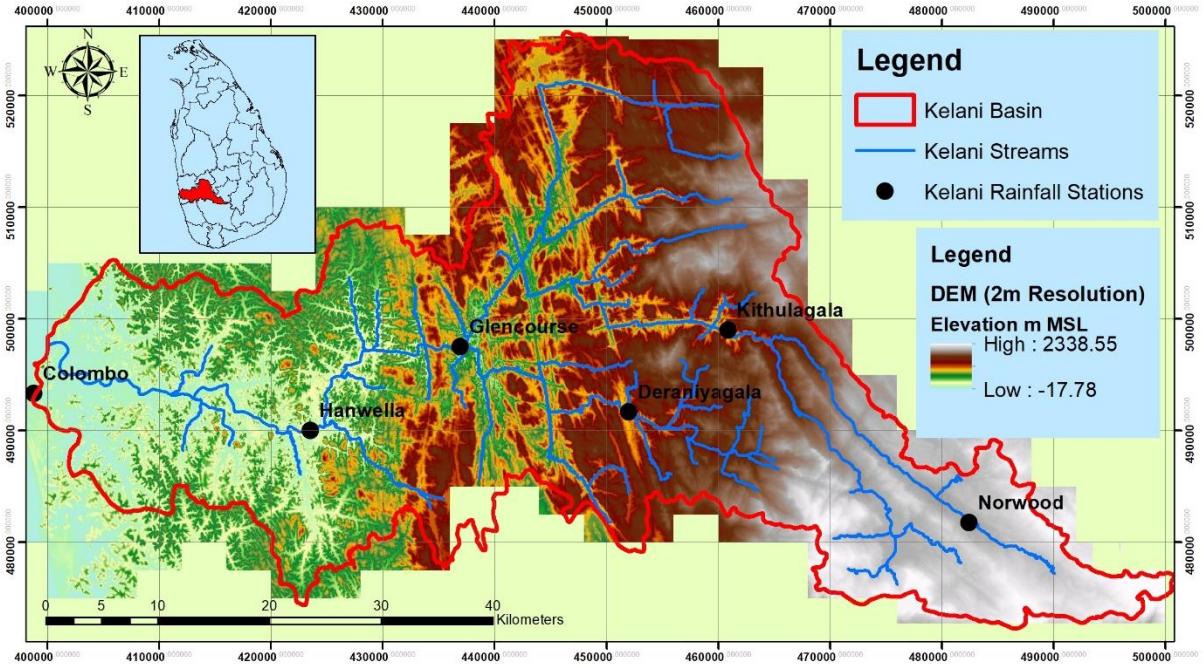

Figure 4-1:Digital Elevation Model (DEM) of 2m Resolution

Digital Elevation Model (DEM) – 30 m

The 2 m resolution digital elevation model (DEM) does not fully cover the Kelani Basin. Therefore, the Shuttle Radar Topography Mission (SRTM) 30 m DEM is used to fill in the missing areas. This data has also been checked against the contours of 1:50,000 topographic maps and verified.

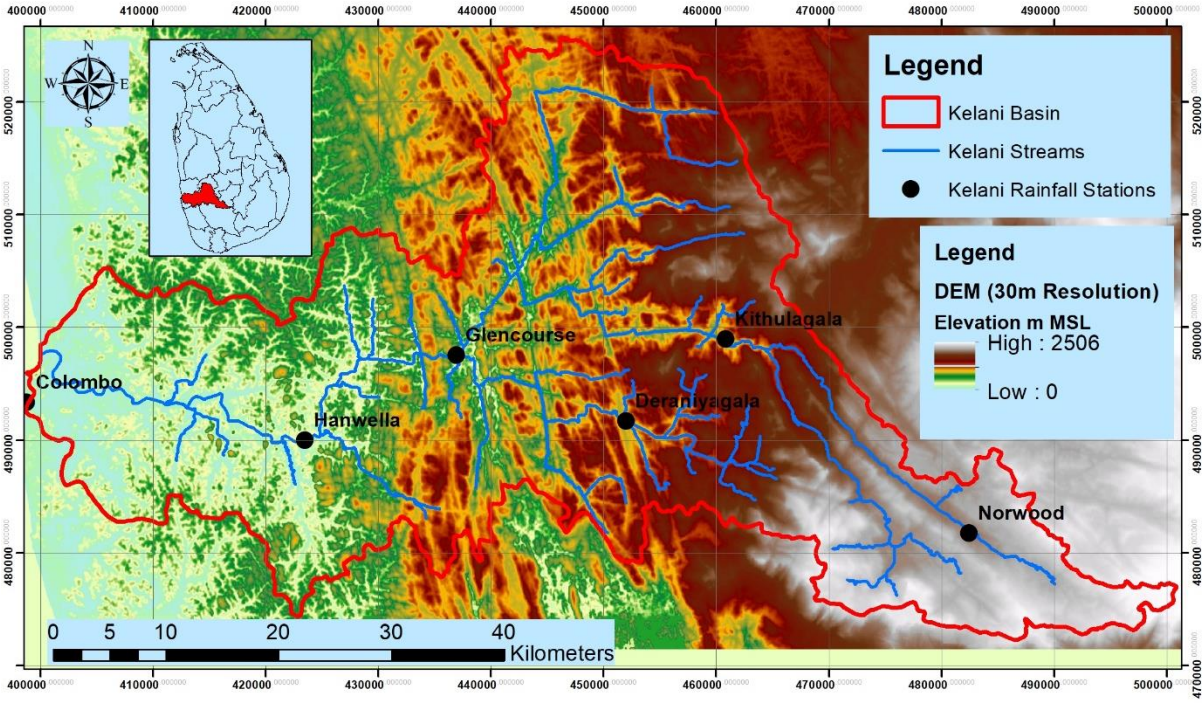

Figure 4-2::SRTM Digital Elevation Model (DEM) of 30 m Resolution

4.2.1.2 Kelani River Cross Section Data

River cross section data is a type of topographic data that represents the shape of a river's cross section. It is typically collected by taking measurements of the river's width, depth, and slope at a series of points along the river's course. This data can be used to model the river's flow, sediment transport, and erosion.

Cross Section Locations

Cross sections of the Kelani River were collected from Hanwella to the sea at 500 m intervals in 2001, and from Glencourse to Hanwella at section change locations in 2016. This data was used to build a river bathymetry terrain for 2D flood modelling.

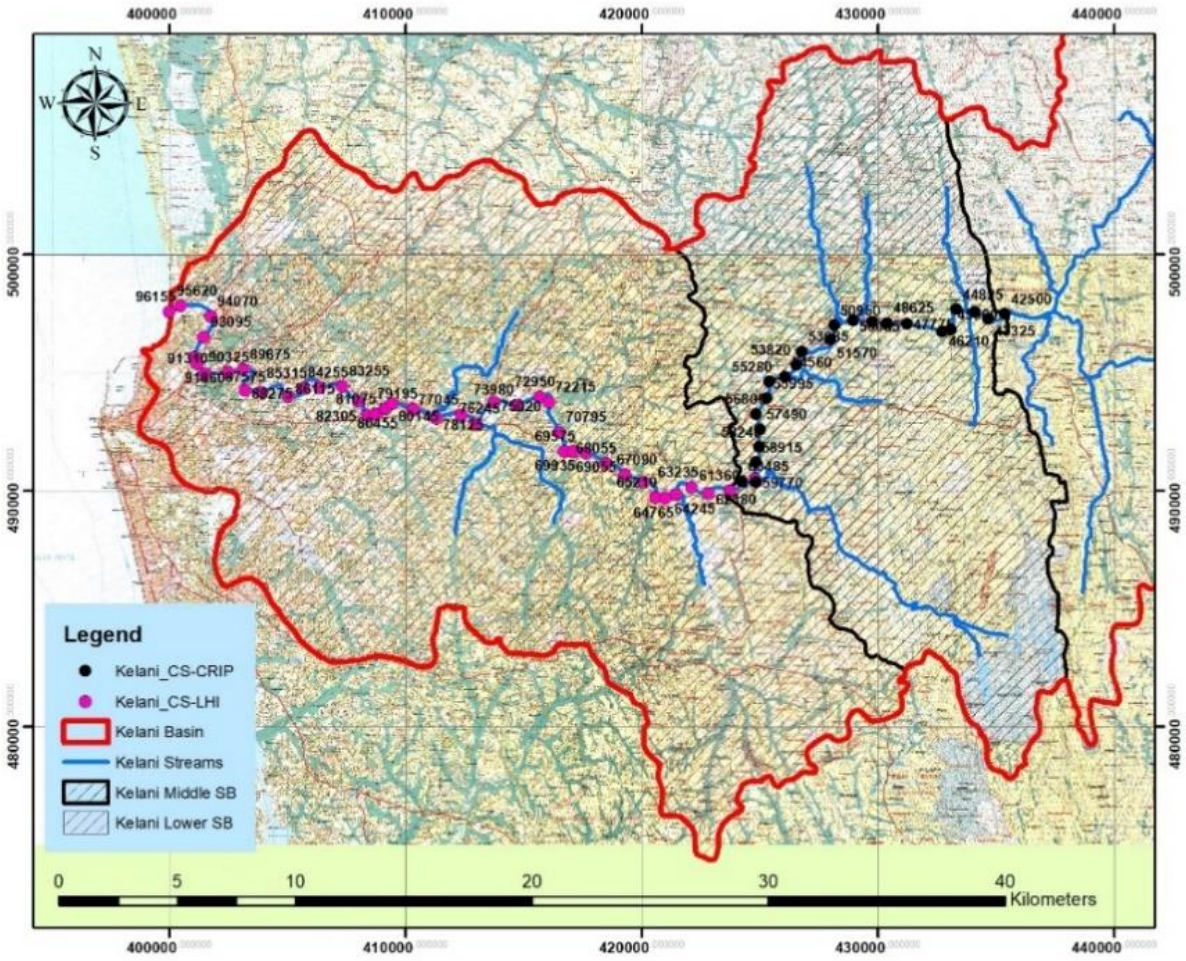

Figure 4-3: Kelani River Cross Sections measurement Locations

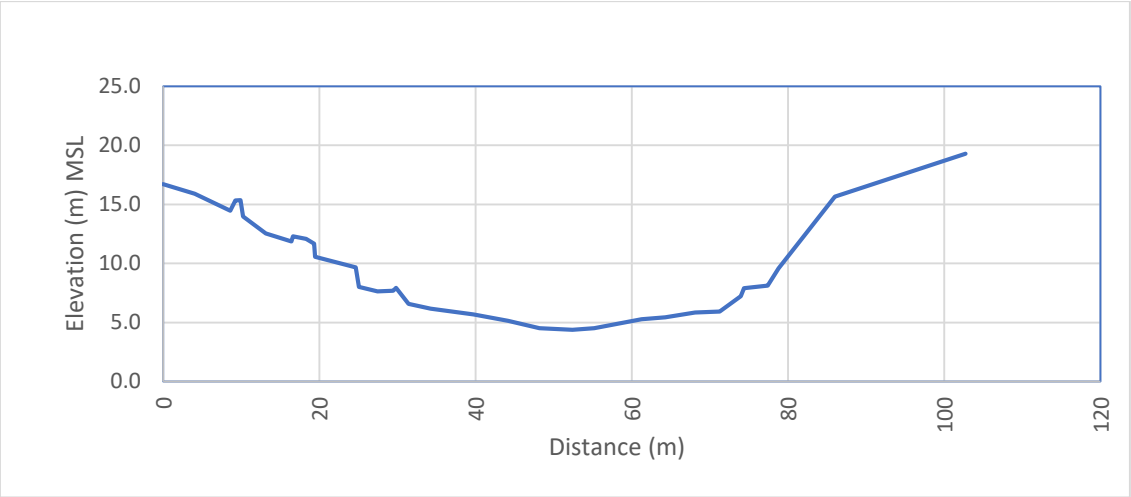

Figure 4-4: Sample Cross Section (CS) profile at 43+325 Chainage

4.2.1.3 Kelani Basin Land Use

A land use map is a map that shows how land is being used in a particular area. It was used to identify different land use types, such as agriculture, forestry, urban areas, and water bodies as well as define the SCS curve numbers in Hydrological modelling and define Manning's N roughness coefficient in flood modelling. The data were collected in Vector GIS format.

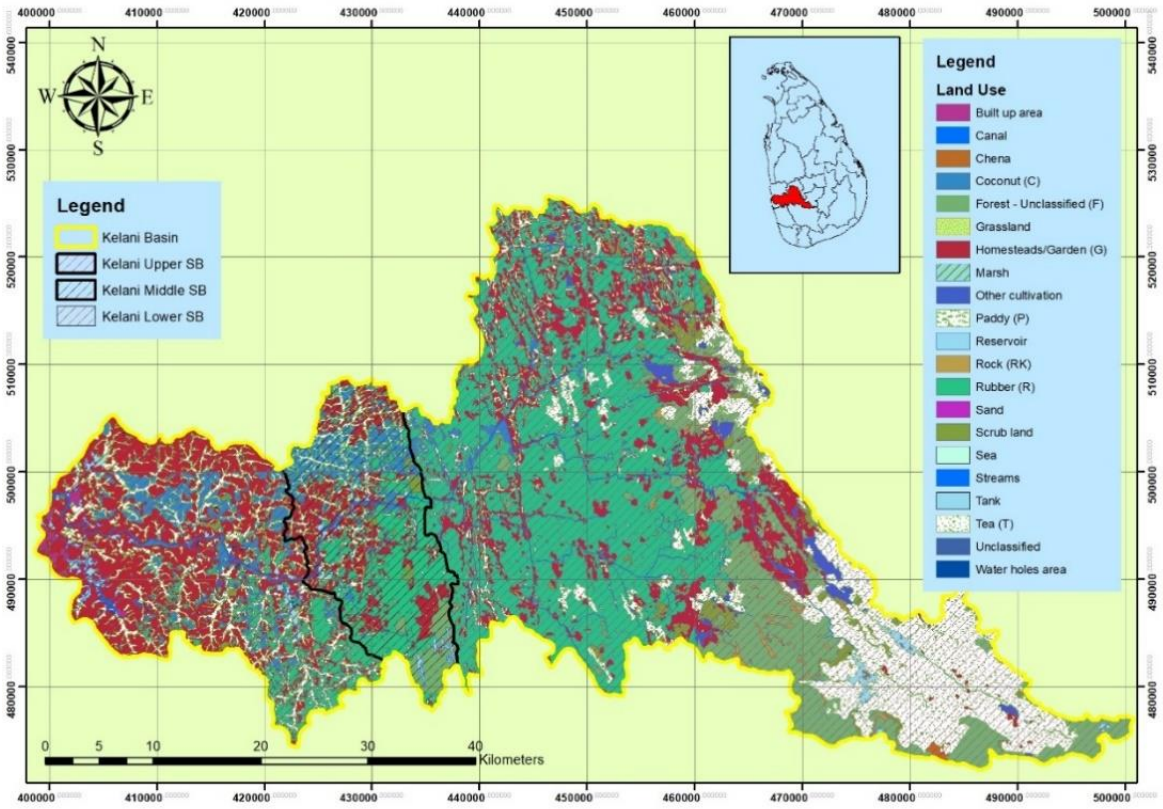

Figure 4-5: Kelani Basin Land Use Map

4.2.1.4 Kelani Basin Soil Map

The soil map of the Kelani River Basin represented the distribution of different soil types in an area consisting of soil properties, such as texture, depth, and fertility. This data was used in defining the SCS Curve numbers in hydrological modelling. The Soil Type data were collected in Vector GIS format.

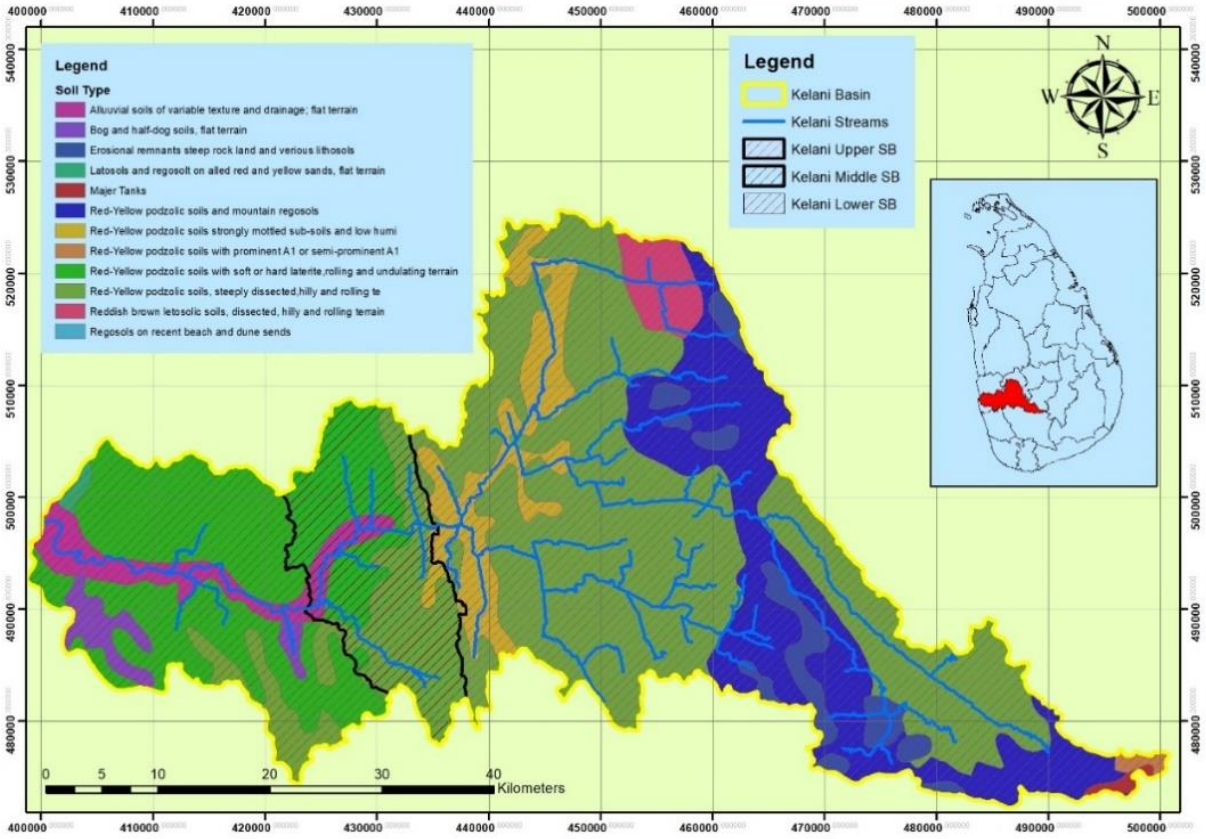

Figure 4-6: Kelani Basin Soil Map

4.2.2 Meteorological Data

Rainfall data were collected from weather stations established inside the Kelani basin based on the selected flood events such that the 2016 May event for model calibration and the 2017 May event for model calibration, as hourly temporal resolution. As well recently published IDF equations are collected for the same rainfall stations for design flood event simulations.

4.2.2.1 Rainfall Data

The Rainfall data were collected from Colombo, Hanwella, Glencourse, Deraniyagala, Kithulgala and Norwood stations. The Holombuwa Rainfall data was not collected due to the unavailability of hourly data for selected flood events. Colombo Station Rainfall data were collected from the Department of Meteorological while other stations data were collected from the Department of Irrigation. The Geographical locations and elevations of selected rainfall stations are presented in Table 4-2.

Table 4-2: Geographical Coordinates of Selected Rain Gauge Locations

Station	Latitude (WGS84)	Longitude (WGS84)	Easting (SLD99)	Northing(SLD99)	Elevation (m) MSL
Colombo	6.939	79.858	398803.73	493312.97	6.17
Hanwella	6.910	80.082	423520.17	489984.24	10.17
Glencourse	6.978	80.203	436944.34	497523.07	17.26
Deraniyagala	6.925	80.339	452008.67	491668.39	70.18
Kithulagala	6.991	80.420	460867.86	498955.23	62.75
Norwood	6.836	80.615	482419.38	481739.21	1,108.21

2016 May Flood Event

The 2016 May flood event was identified as the most devastating recent flood event in Kelani Basin. Most of the vulnerable areas of the Lower Kelani basin were inundated resulting in massive flood damages. This 2016 May flood event was selected for model calibration.

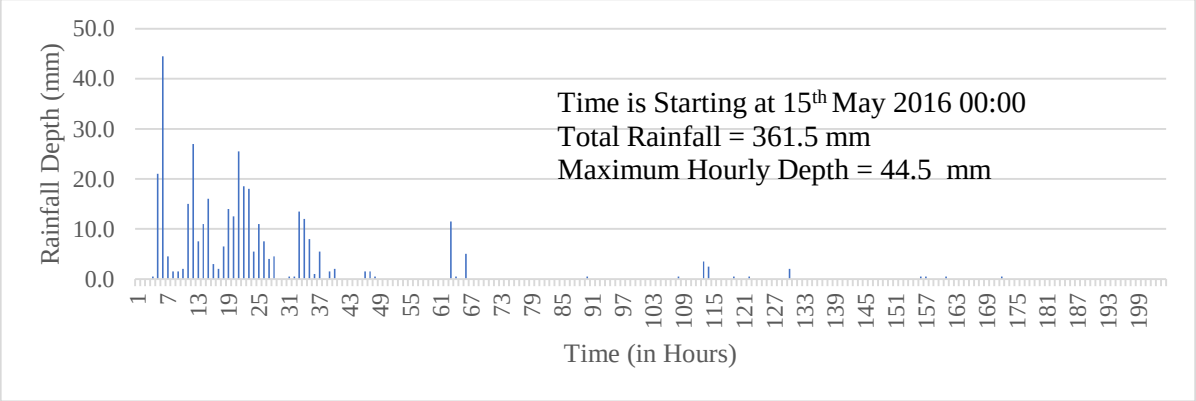

Figure 4-7: 2016 May Hourly Rainfall Data - Colombo Station

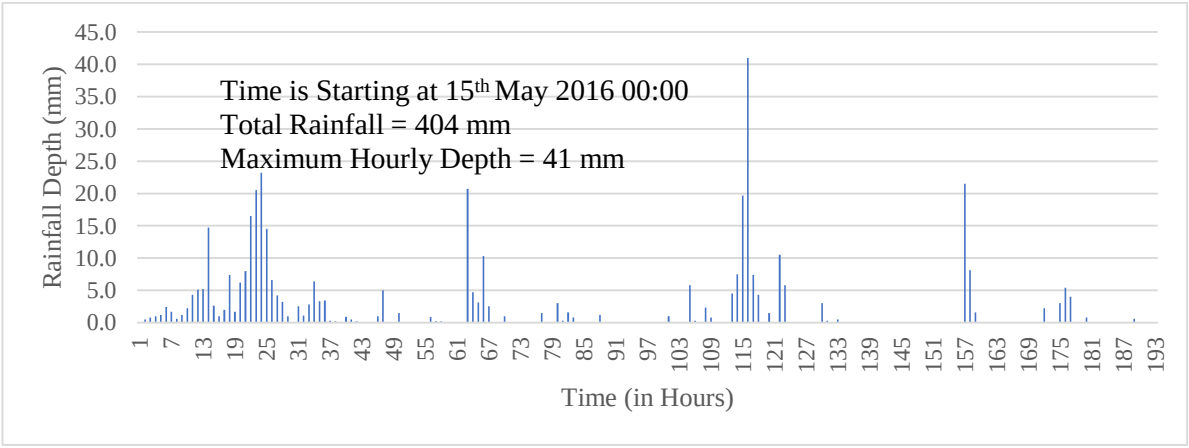

Figure 4-8: 2016 May Hourly Rainfall Data - Hanwella Station

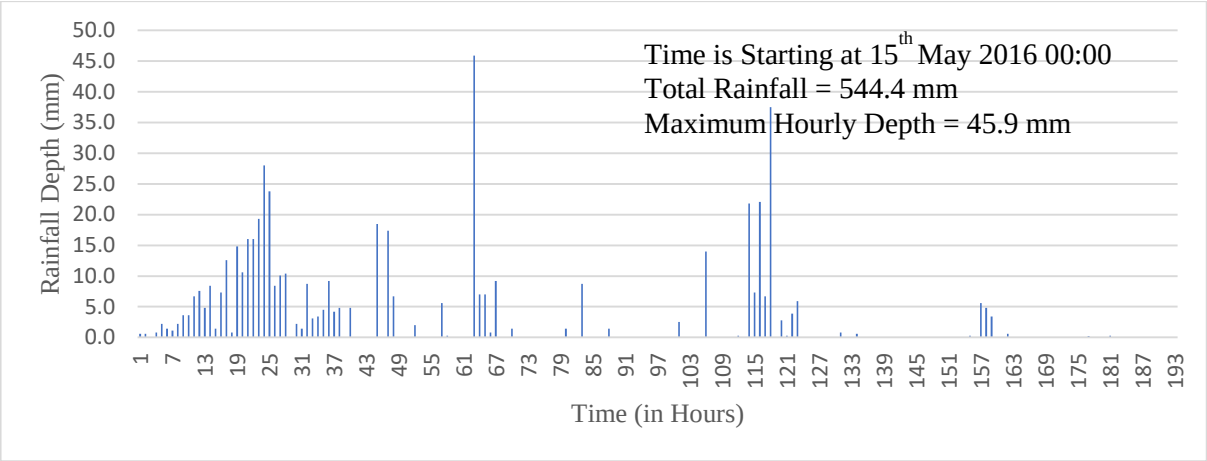

Figure 4-9: 2016 May Hourly Rainfall Data - Glencourse Station

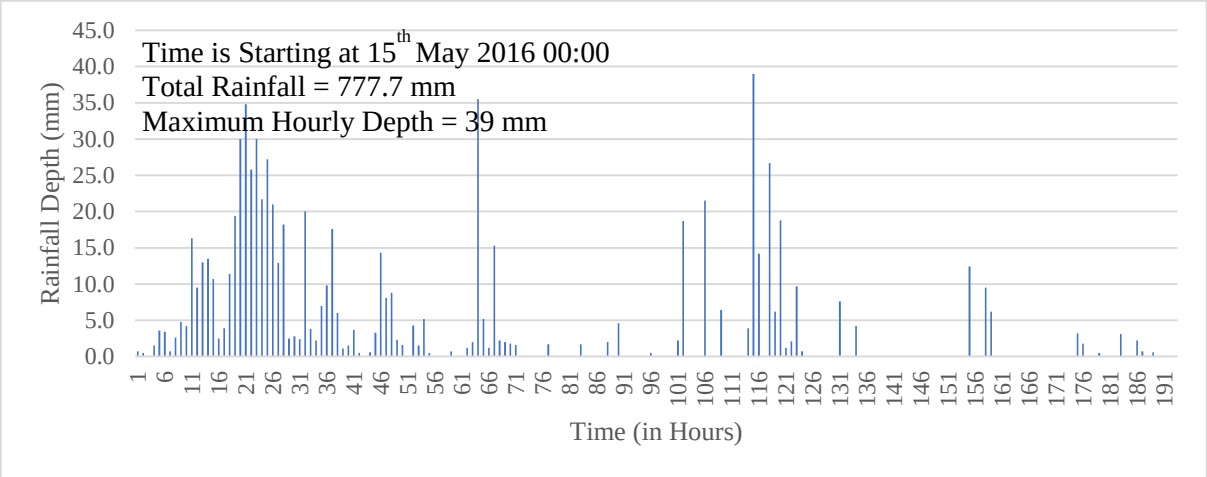

Figure 4-10: 2016 May Hourly Rainfall Data - Deraniyagala Station

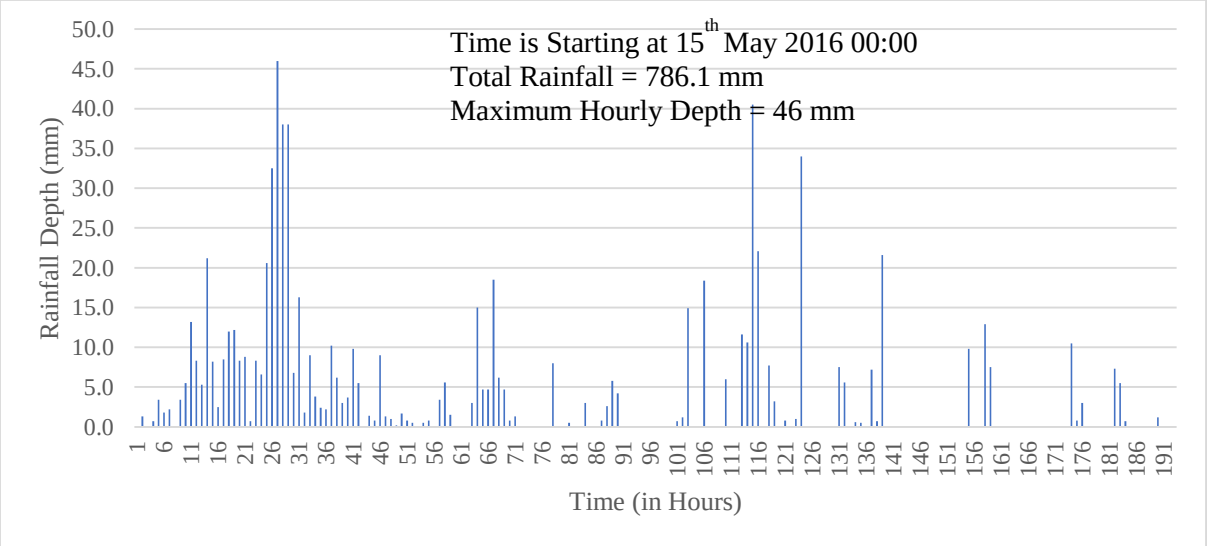

Figure 4-11: 2016 May Hourly Rainfall Data - Kithulgala Station

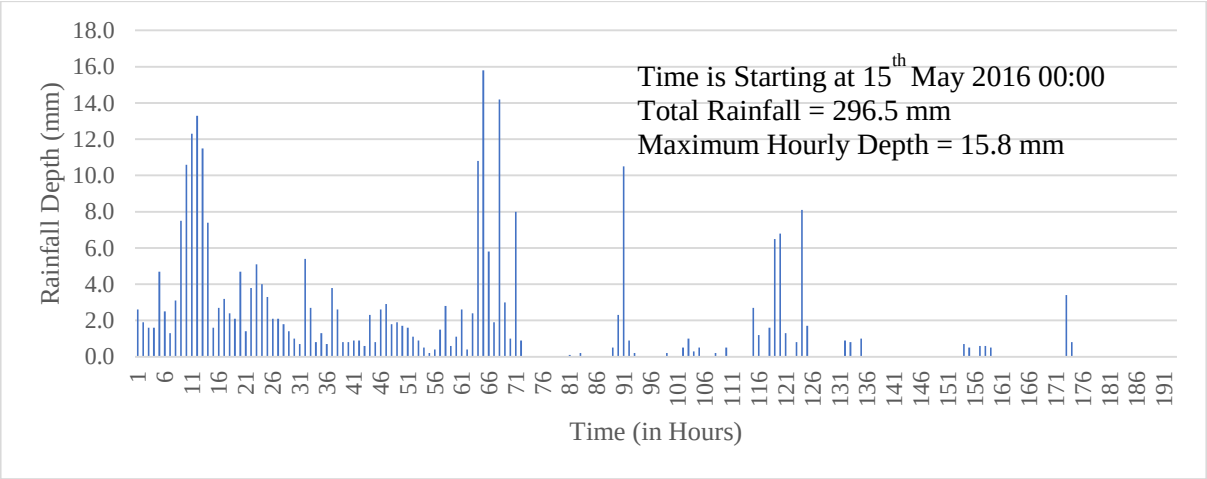

Figure 4-12: 2016 May Hourly Rainfall Data - Norwood Station

The Basin Average Rainfall is developed using Thiessen Polygon Method. The Thiessen weights for each station were calculated with the aid of GIS as presented in Table 4-3 as well as the developed data series presented in Figure 4-13.

Table 4-3: Kelani Basin Average Thiessen weights

No.	Station	Area (km²)	Thiessen Weight
1	Colombo	202.64	0.09
2	Deraniyagala	288.76	0.12
3	Glencourse	502.51	0.22
4	Hanwella	445.57	0.19
5	Kithulagala	541.70	0.23
6	Norwood	340.78	0.15

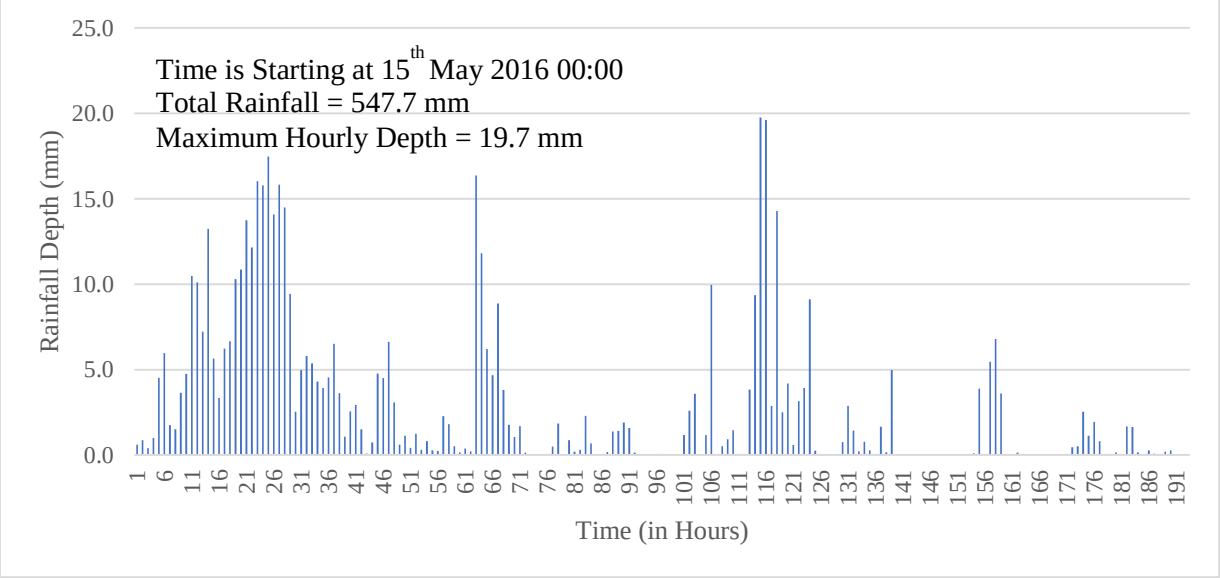

Figure 4-13: 2016 May Hourly Rainfall Data - Basin Average

Single Mass Curve

The single mass curve is a graphical representation of the cumulative distribution of precipitation created by plotting the cumulative values of the rainfall depth on the y-axis and the time periods on the x-axis. Single mass curves can be used to identify trends in rainfall in selected periods, such as increasing or decreasing. Figure 4-14 is representing the single mass curves of selected rainfall stations and Thiessen averaged rainfall.

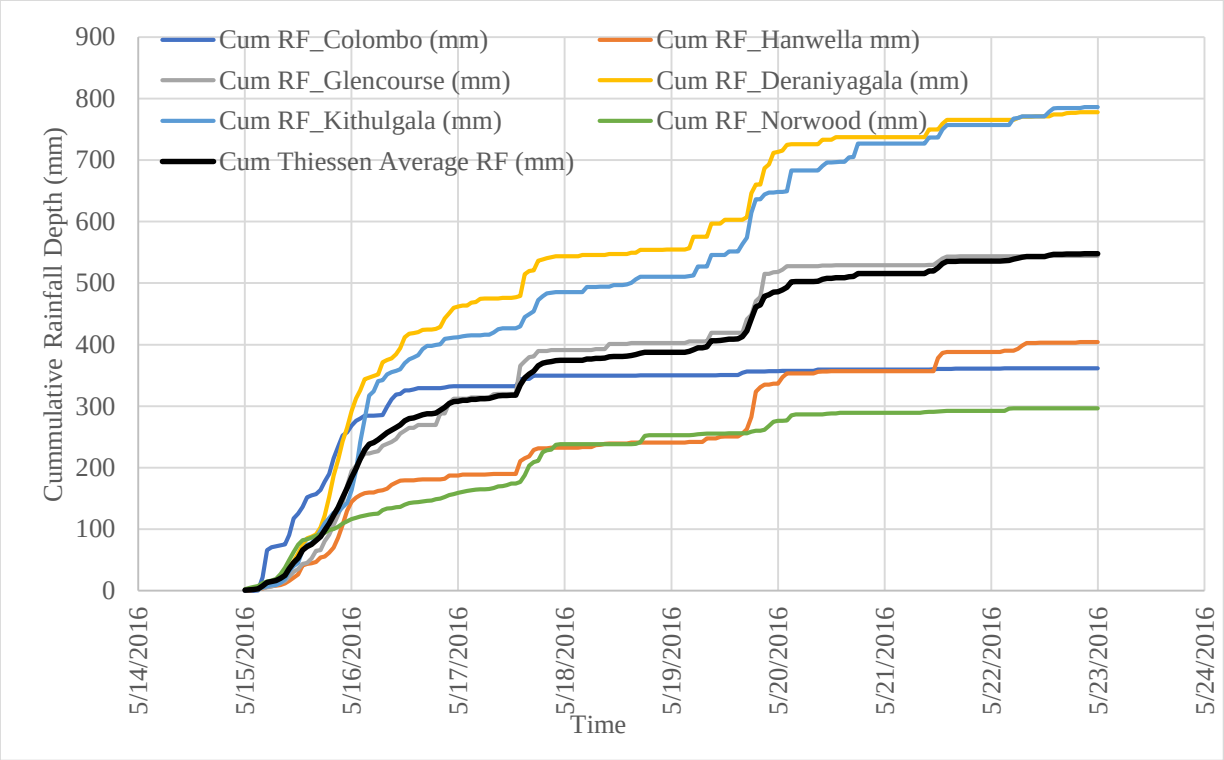

Figure 4-14: 2016 May Event Single Mass Curve

Double Mass Curve

The double mass curve is a graphical method used to evaluate the consistency of rainfall data. It was created by plotting the cumulative rainfall depths of Thiessen averaged rainfall against the cumulative rainfall depths of other rainfall stations. Figure 4-15 is representing the double mass curves of selected rainfall stations.

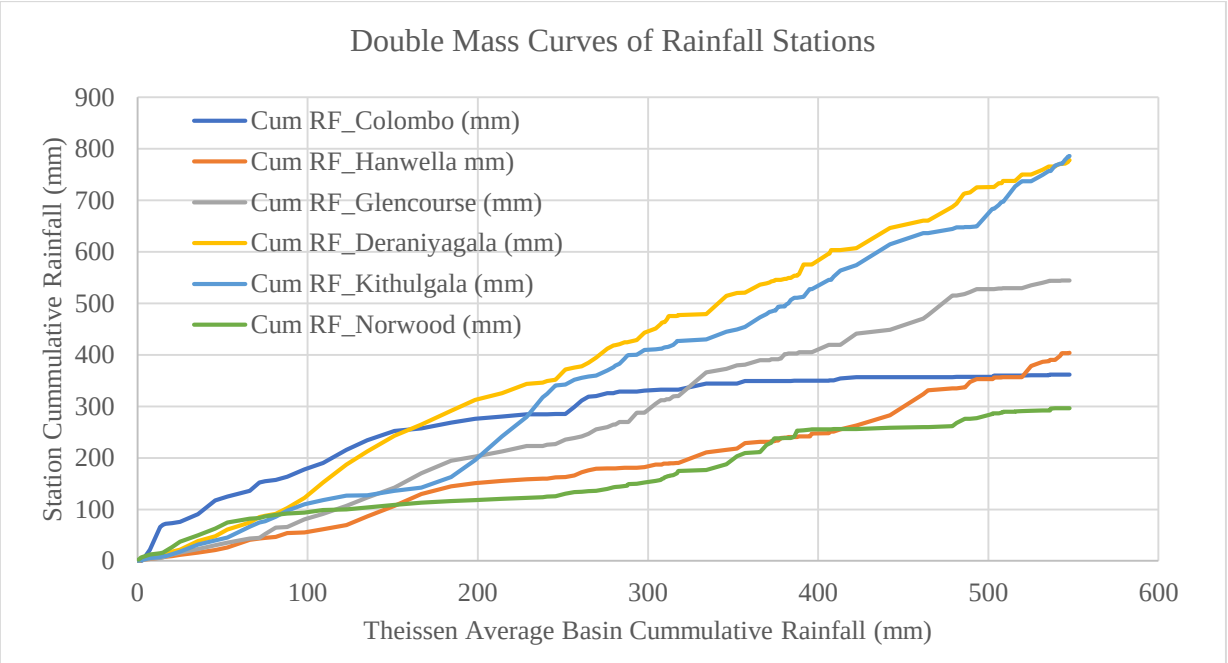

Figure 4-15: 2016 May Event Double Mass Curve

2017 May Flood Event

The 2017 May Flood event data was used to validate the model in this study. This flood event was a significant event, as it caused flooding in the Lower Kelani basin that was comparable to the 2016 flood event. Hourly rainfall data was collected for selected rainfall stations during the time period of interest. Figure 4-16 to Figure 4-21 presents the collected Rainfall Data for the 2017 May event from May 24th to 29th.

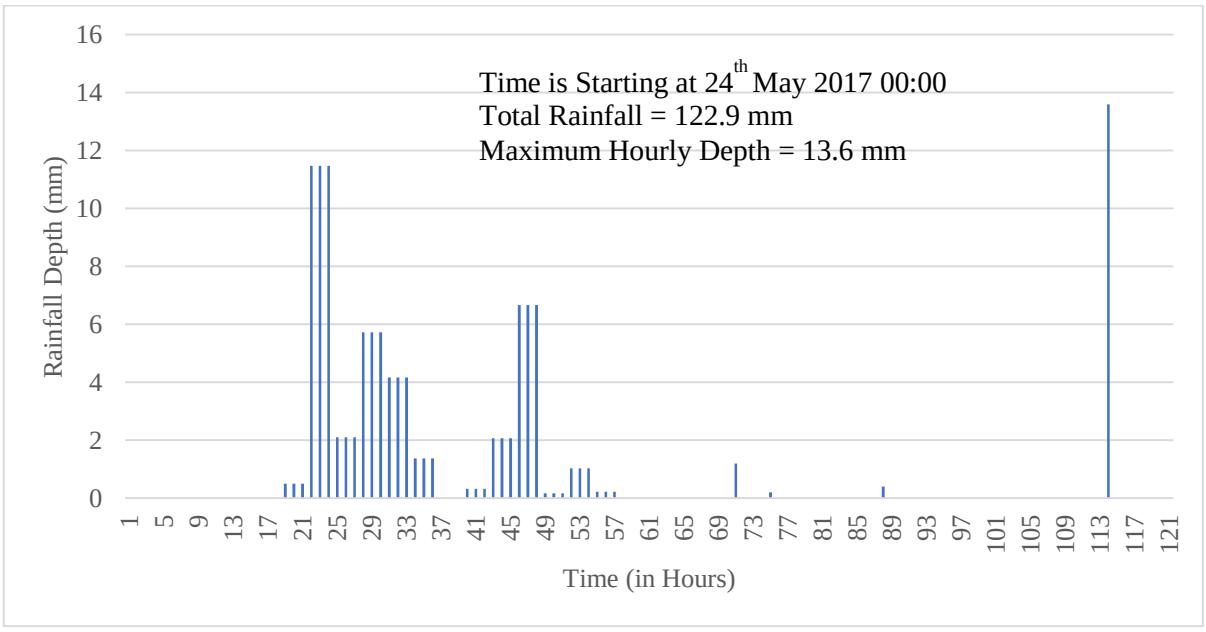

Figure 4-16: 2017 May Hourly Rainfall Data - Colombo Station

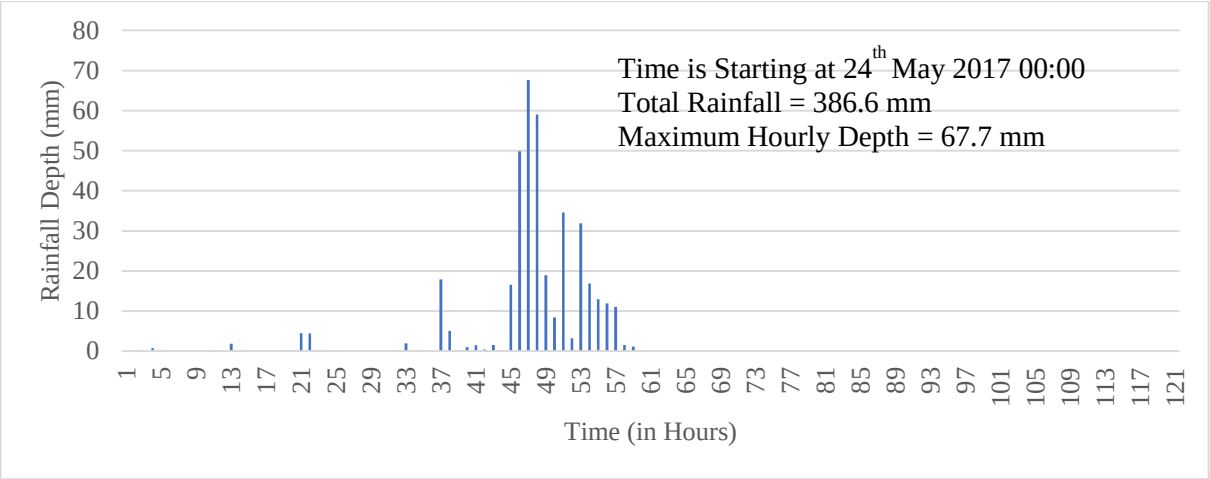

Figure 4-17: 2017 May Hourly Rainfall Data - Hanwella Station

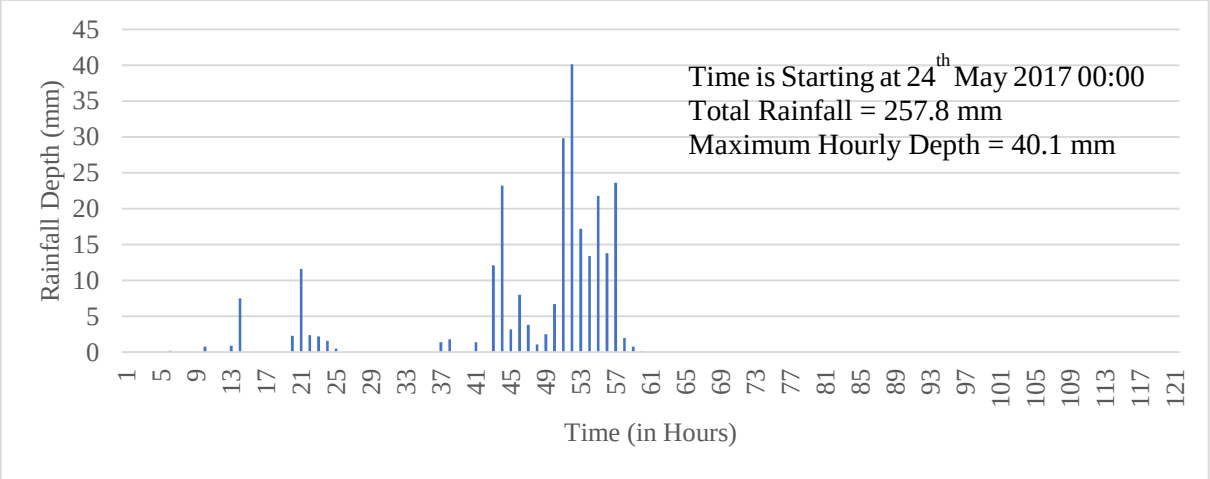

Figure 4-18: 2017 May Hourly Rainfall Data - Glencourse Station

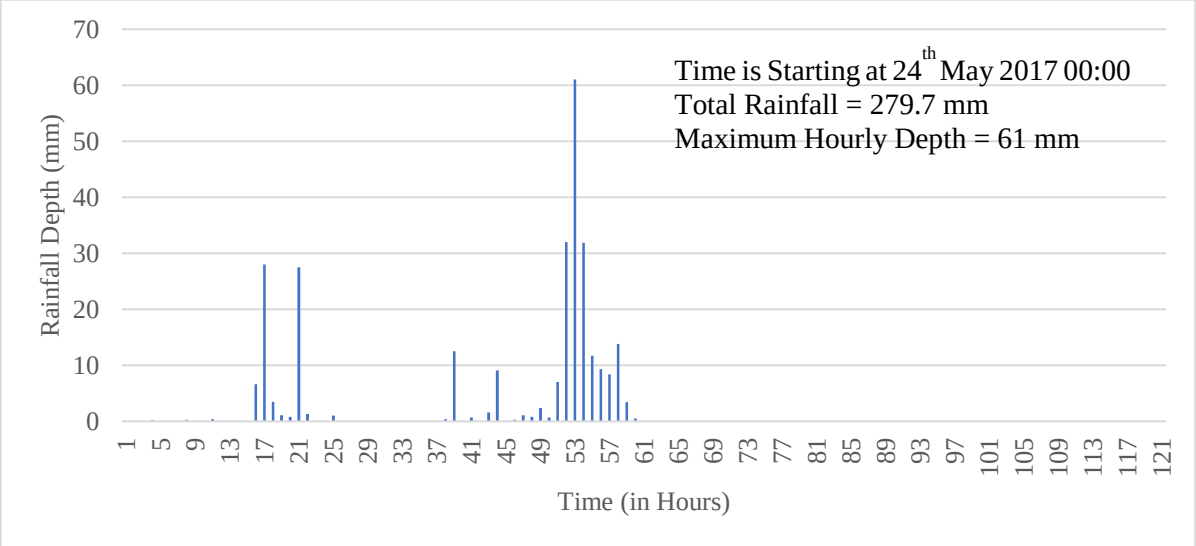

Figure 4-19: 2017 May Hourly Rainfall Data - Deraniyagala Station

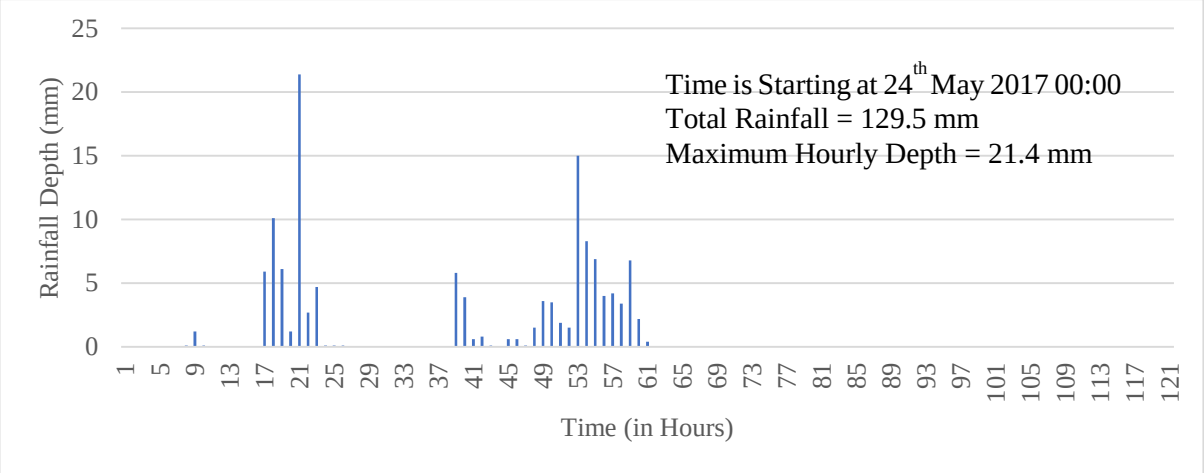

Figure 4-20: 2017 May Hourly Rainfall Data - Kithulgala Station

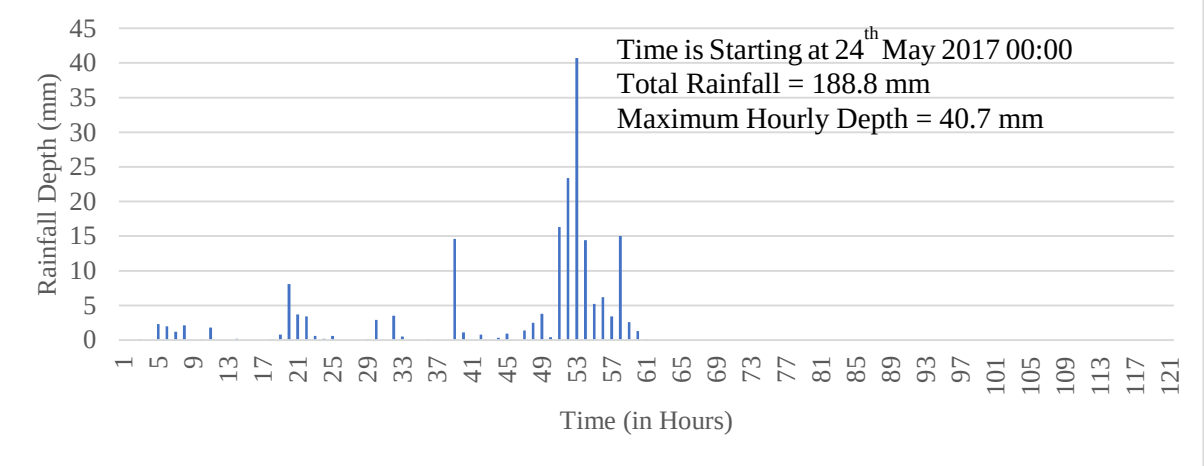

Figure 4-21: 2017 May Hourly Rainfall Data - Norwood Station

Basin Thiessen Average Rainfall

The basin average rainfall was developed using the Thiessen polygon method, with the same Thiessen weights as those presented in Table 4-3.

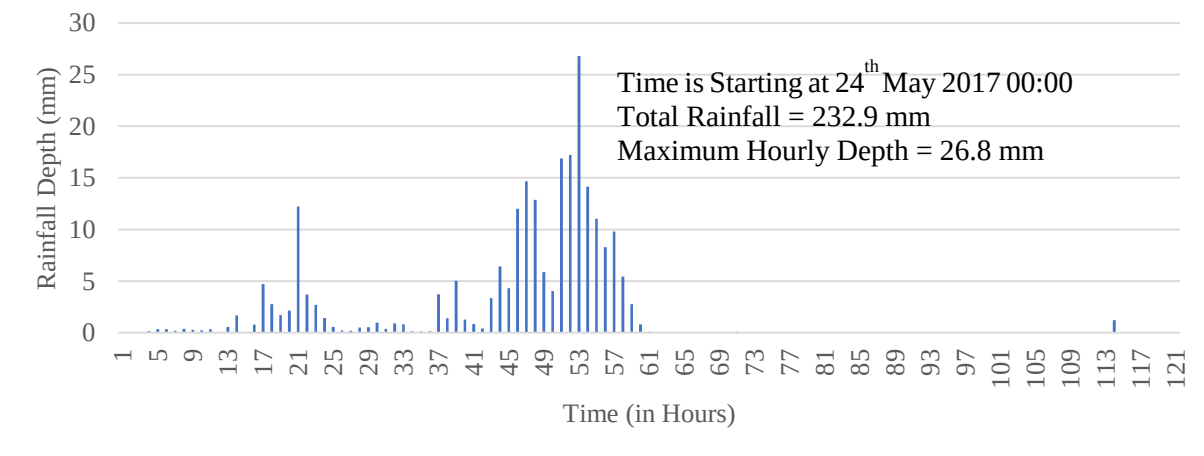

Figure 4-22: 2017 May Hourly Rainfall Data - Basin Average

Single Mass Curve

Figure 4-23 represents the single mass curves of selected rainfall stations and Thiessen averaged rainfall for the 2017 May flood event.

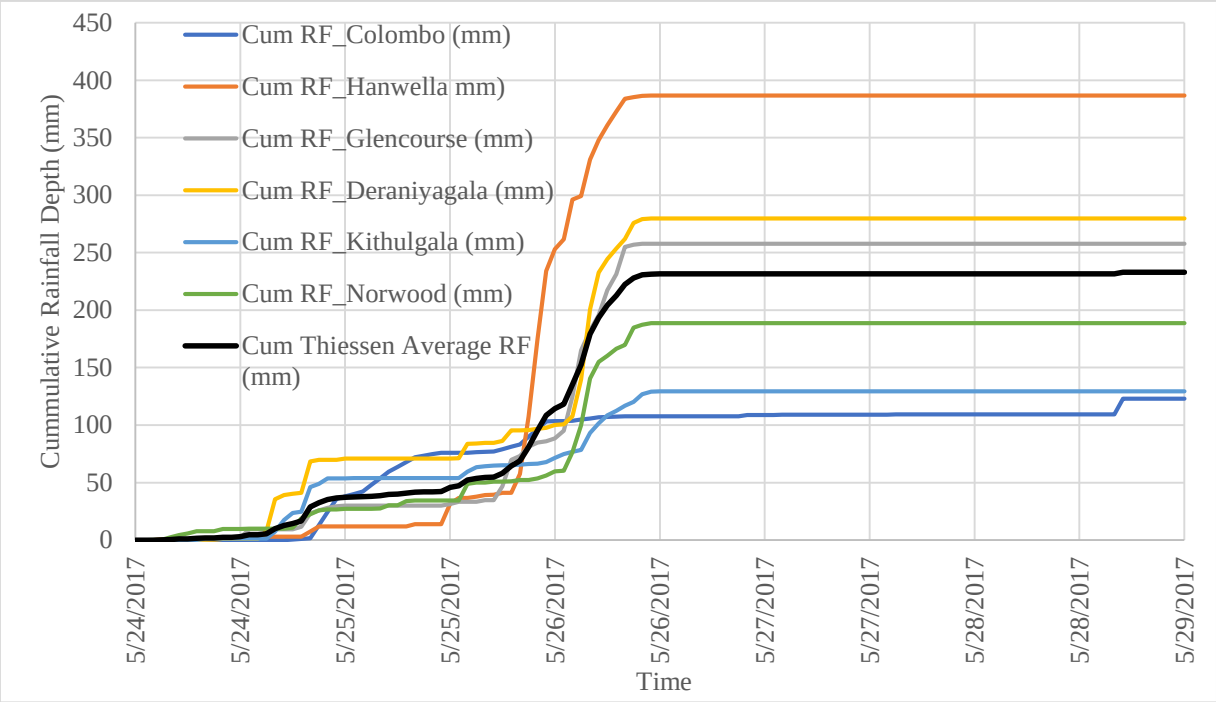

Figure 4-23: 2017 May Hourly Single Mass Curve

Double Mass Curve

Figure 4-24 is representing the double mass curves of selected rainfall stations for the 2017 May flood event.

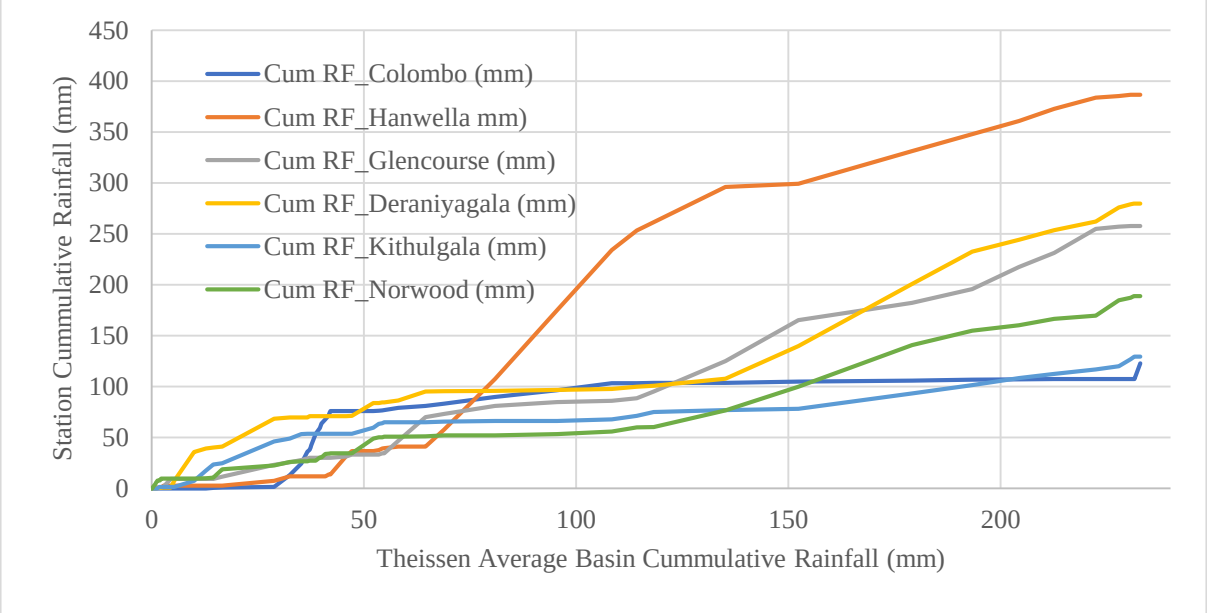

Figure 4-24: 2017 May Hourly Double Mass Curve

4.2.2.2 IDF Data

Intensity-Duration-Frequency (IDF) relationships such that IDF curves and IDF equations were extracted from recent publications for selected rainfall stations. The Colombo IDF equation is extracted from the "IDF Curves" report published by the Hydrology Division of Irrigation Department, 2019 October (Irrigation, 2019) while other data were extracted from "Environmental Impact Assessment for Alterations to the Salinity Barrier at Ambathale in Kelani River – Annex 9: Flood Modelling" report published by Irrigation Department, 2022 January (Irrigation, 2022). Figure 4-25 to Figure 4-30 represent the IDF data for selected Rainfall stations used for the present study during design flood event simulations.

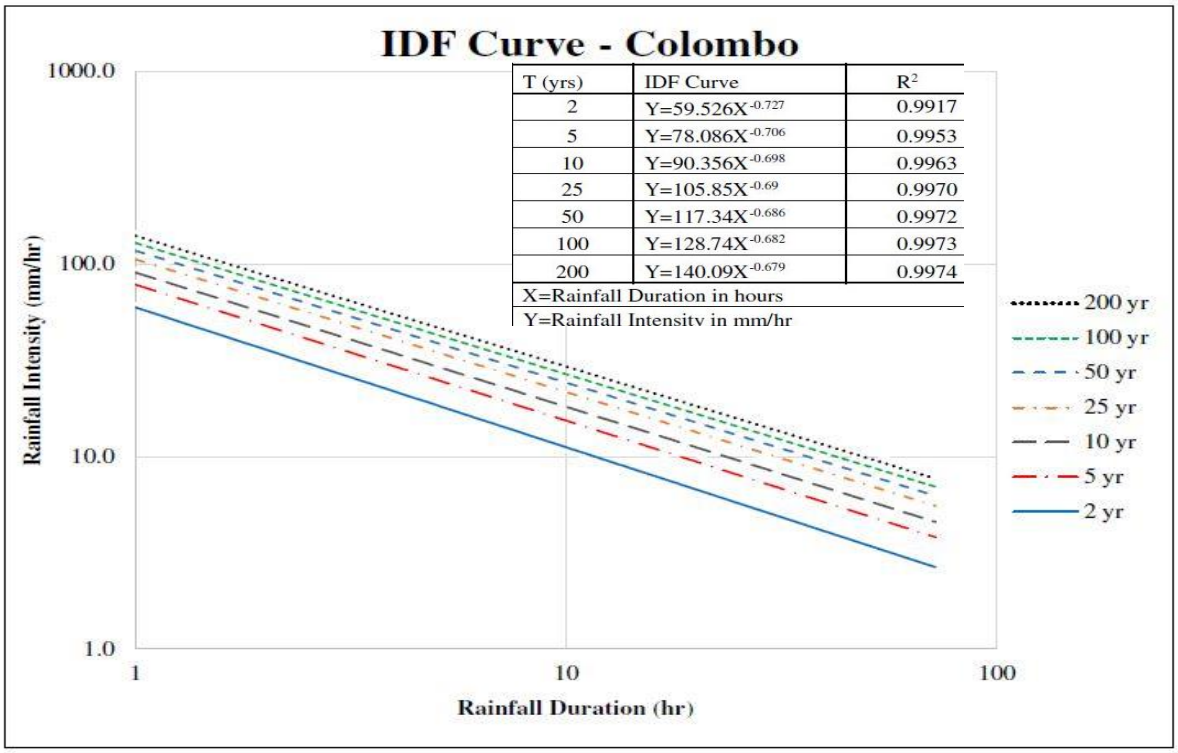

Figure 4-25: Published IDF curves for Colombo Station

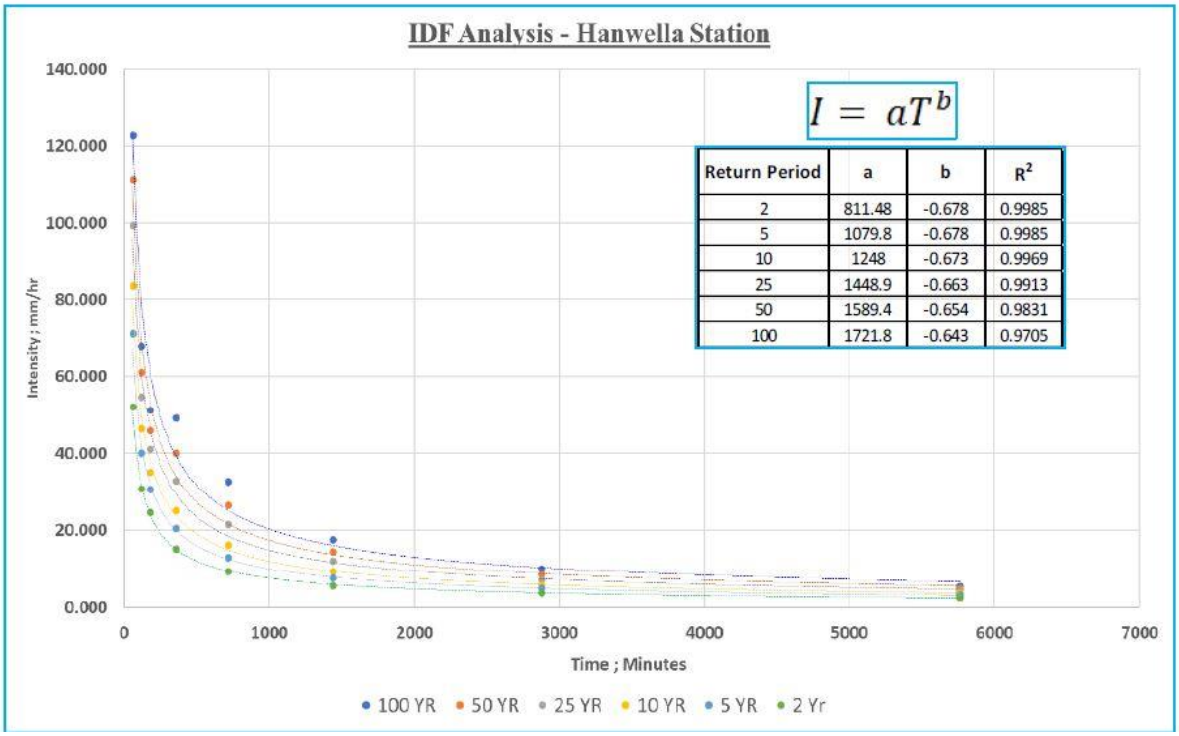

Figure 4-26: Published IDF curves for Hanwella Station

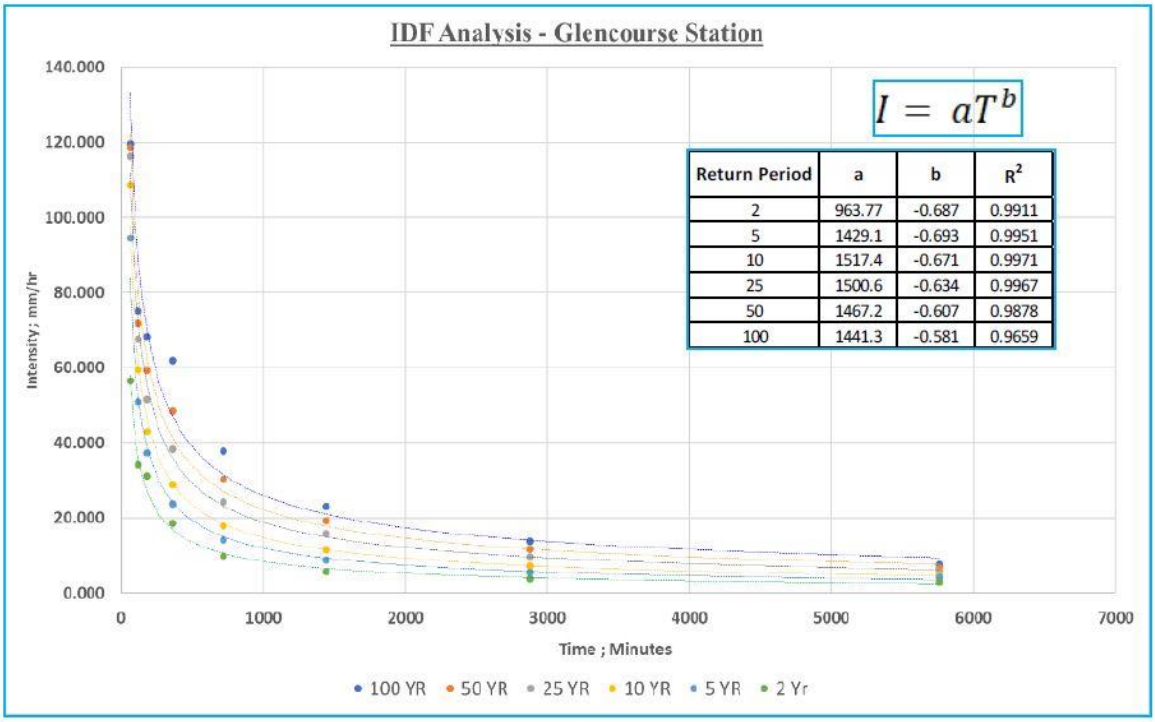

Figure 4-27: Published IDF curves for Glencourse Station

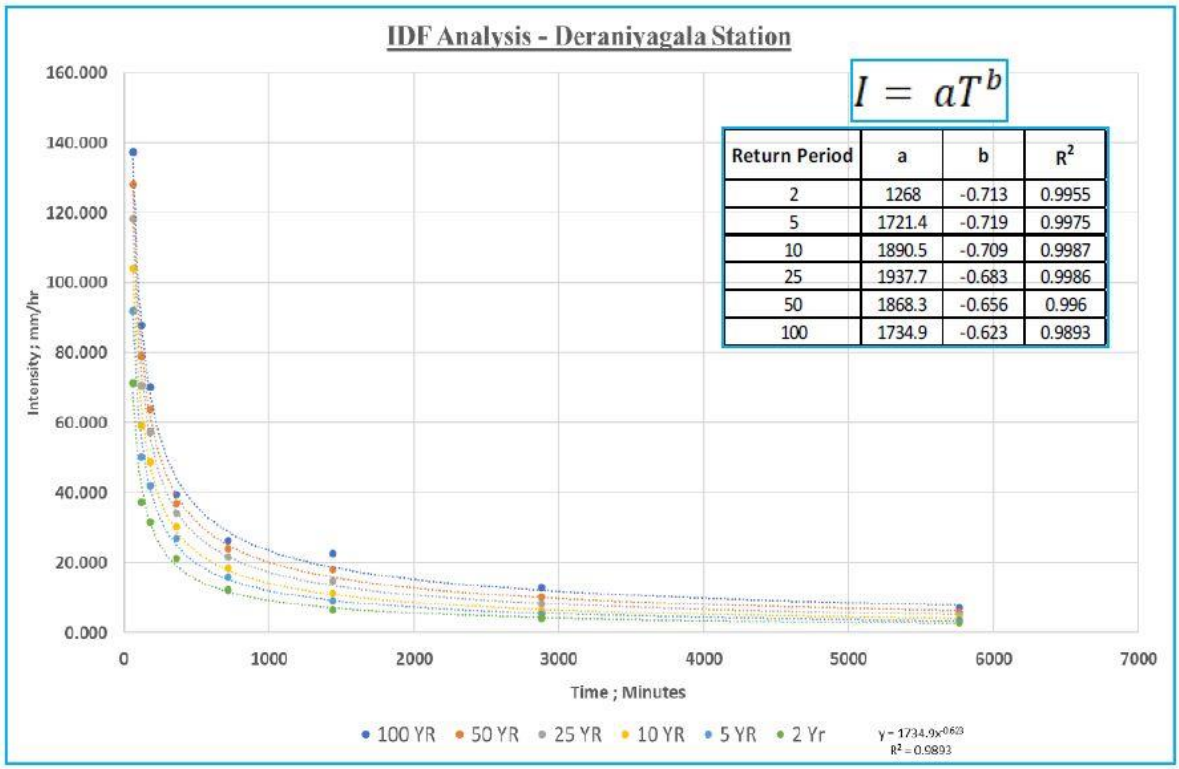

Figure 4-28: Published IDF curves for Deraniyagala Station

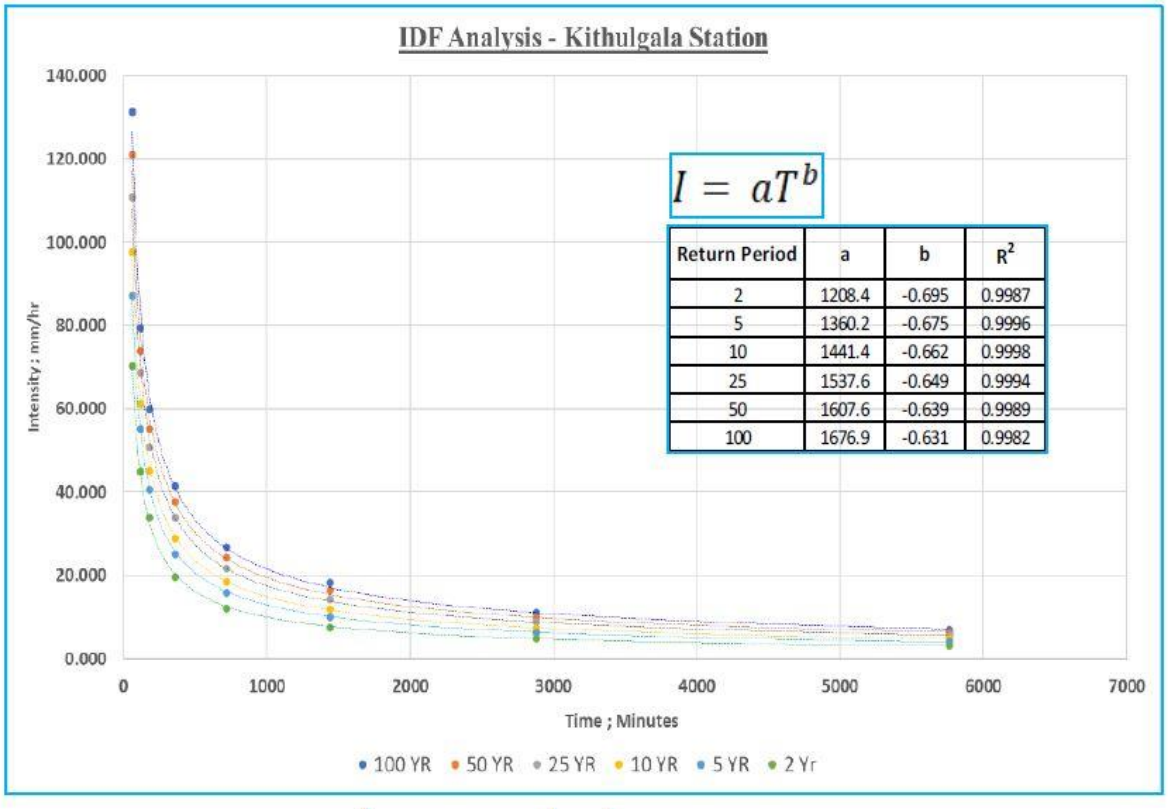

Figure 4-29: Published IDF curves for Kithulgala Station

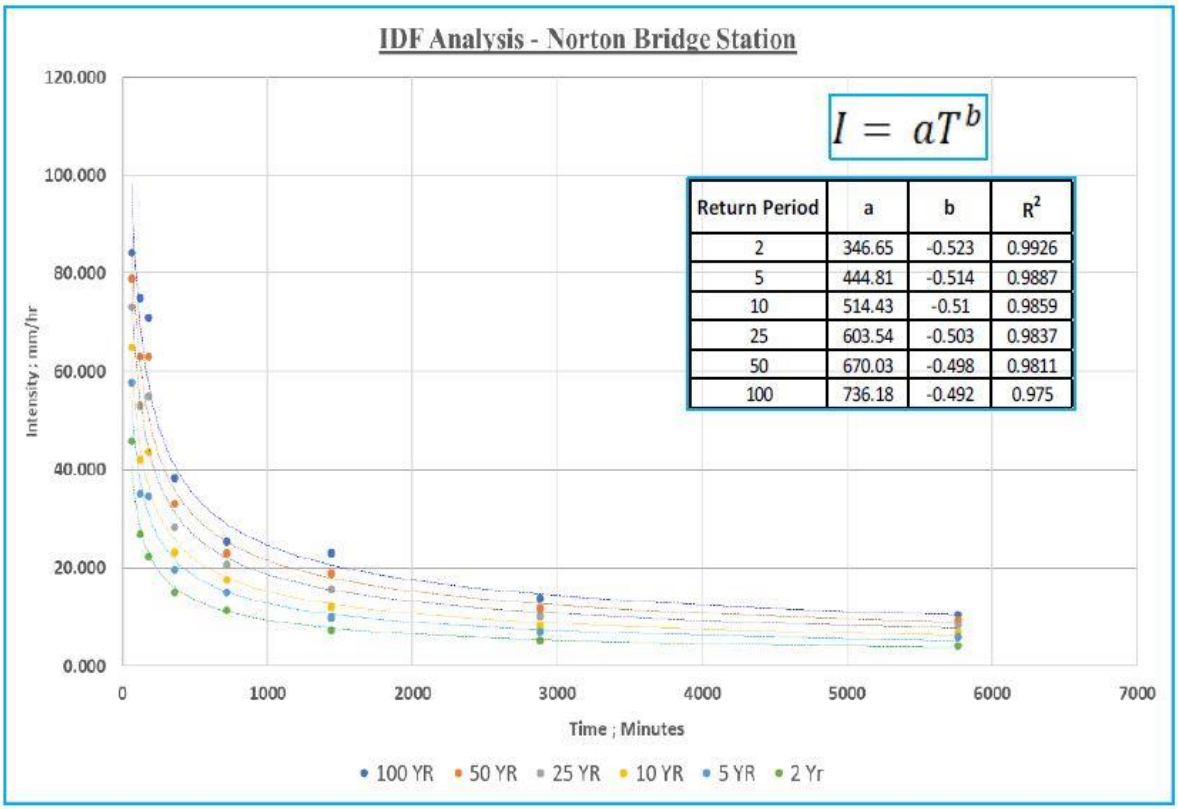

Figure 4-30: Published IDF curves for Norwood Station

4.2.3 Hydrological Data

Observed time series water levels and discharges were collected from available hydrological gauging stations along the Kelani River, owned by the Irrigation Department, for the 2016 May and 2017 May events. Hourly data were collected from Glencourse, Hanwella, and Nagalagama Street for selected time durations during the aforementioned flood events, in order to calibrate and validate the model.

4.2.3.1 Discharge Data

Hourly Discharge (in m^3/s unit), data from Glencourse, Hanwella and Nagalagama Street gauging stations were collected in tabulated format.

2016 May Flood Event

Discharge Data from 15th May 2016 to 23rd May 2016 were collected for the 2016 May flood event which were used for the model calibration. This data is represented in Figure 4-31.

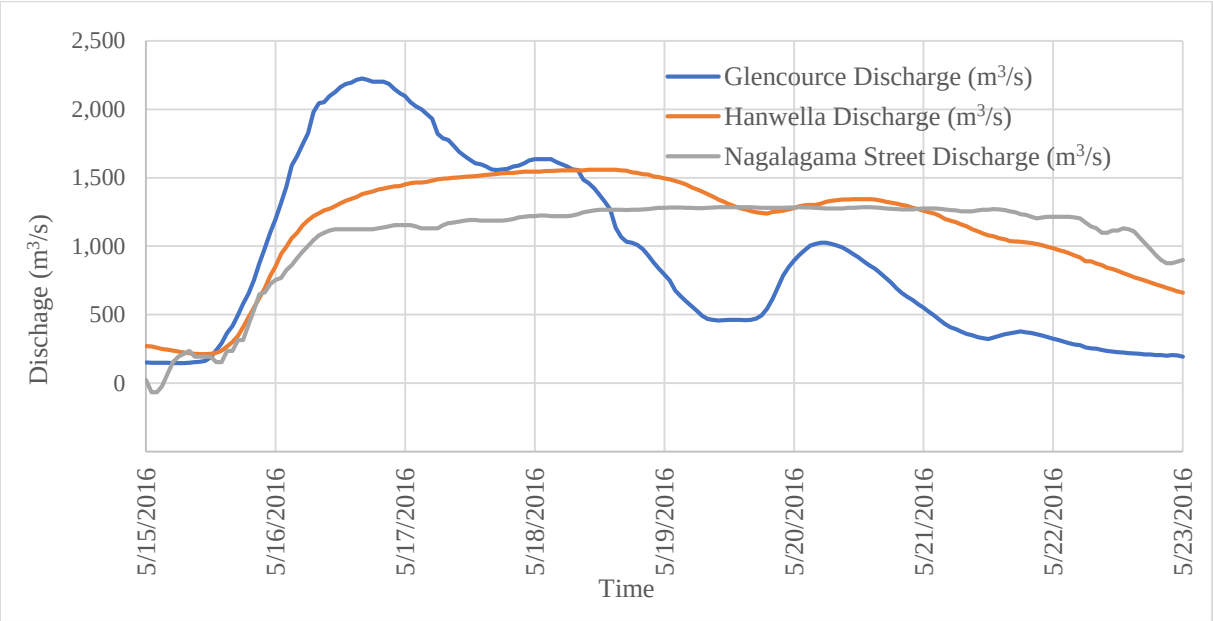

Figure 4-31: 2016 May Observed Discharge Data

2017 May Flood Event

Discharge Data from 24th May 2017 to 29th May 2017 were collected for the 2017 May flood event which were used for the model validation. This data is represented in Figure 4-32.

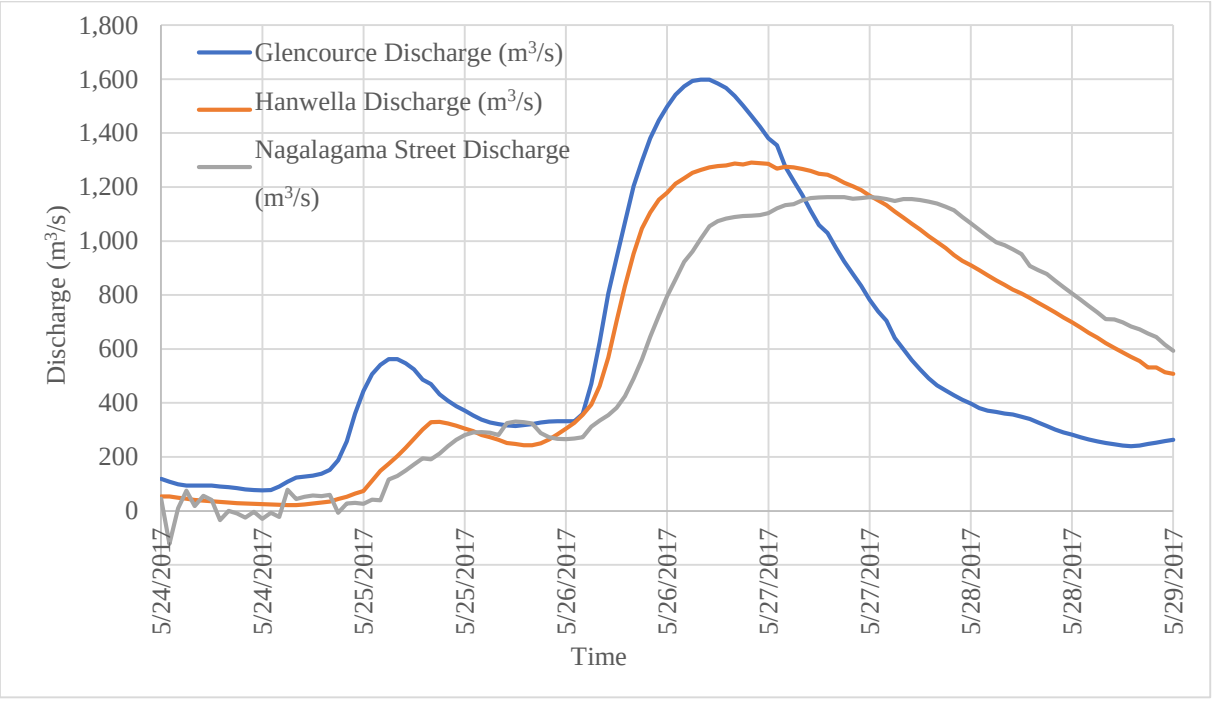

Figure 4-32: 2017 May Observed Discharge Data

4.2.3.2 Water Level Data

Hourly Water Level (in m MSL – meters Mean Sea Level), data from Glencourse, Hanwella and Nagalagama Street gauging stations were collected in tabulated format.

2016 May Flood Event

Water Level Data from 15th May 2016 to 23rd May 2016 were collected for the 2016 May flood event which were used for the model calibration. This data is represented in Figure 4-33.

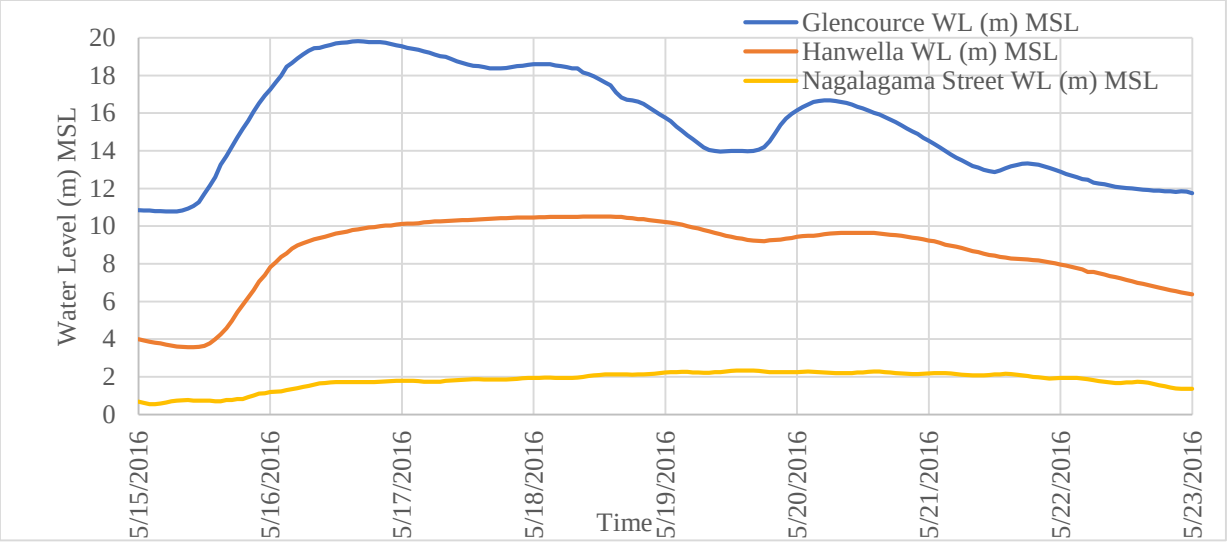

Figure 4-33: 2016 May Observed Water Level Data

2017 May Flood Event

Water Level Data from 24th May 2017 to 29th May 2017 were collected for the 2017 May flood event which were used for the model validation. This data is represented in Figure 4-34.

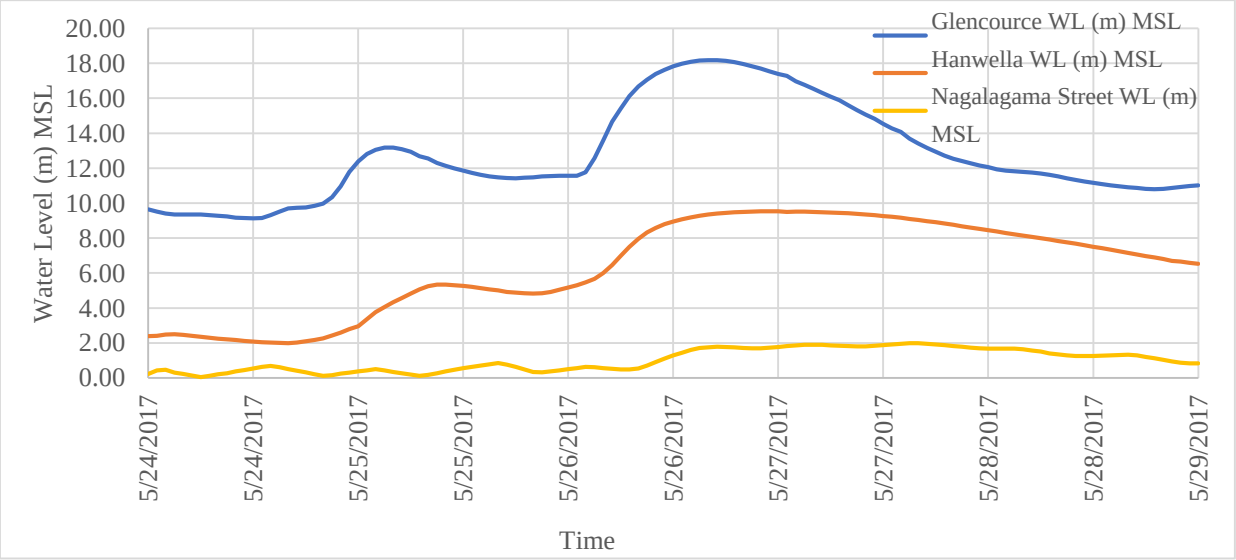

Figure 4-34: 2017 May Observed Water Level Data

4.2.3.3 Sea Levels

Observed Sea level (in m MSL) data (tide level) were collected for the 2016 May Flood Event and 2017 May Flood events. This data was used for downstream boundary conditions of Flood models during model calibration and model validation.

2016 May Observed Sea Levels

Sea Level Data from 15th May 2016 to 23rd May 2016 were collected for the 2016 May flood event which is represented in Figure 4-35.

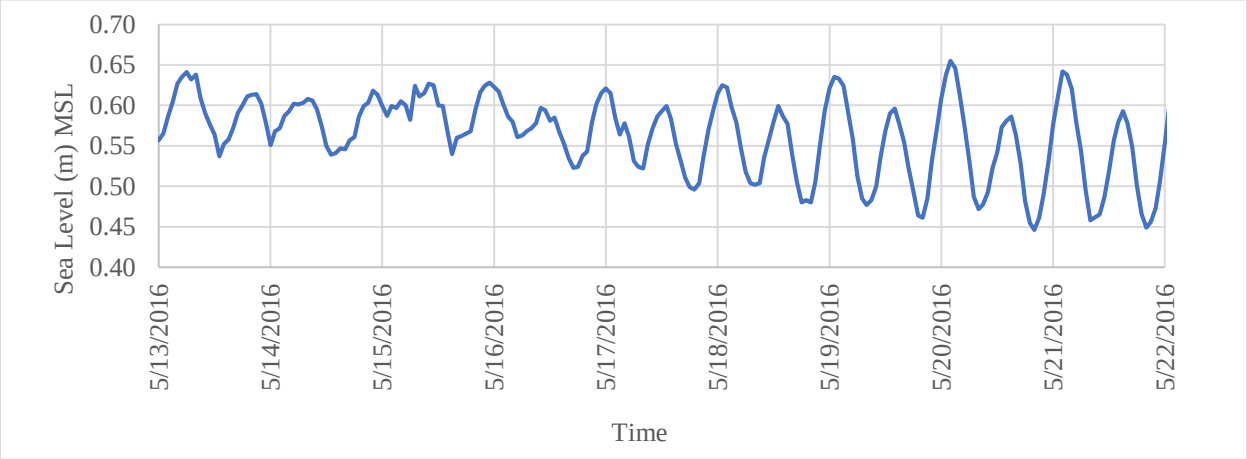

Figure 4-35: 2016 May Observed Sea Level Data

2017 May Observed Sea Levels

Sea Level Data from 24th May 2017 to 29th May 2017 were collected for the 2017 May flood event which is represented in Figure 4-36.

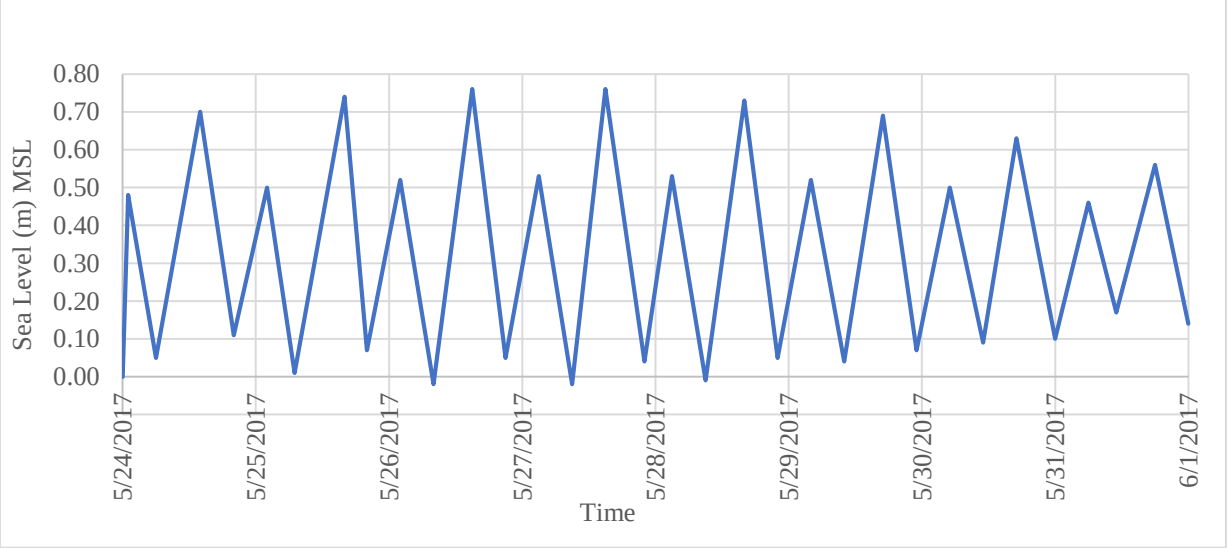

Figure 4-36: 2017 May Observed Sea Level Data

4.2.3.4 Observed Flood Maps

Published flood extent maps prepared from observed flood inundation were collected for the 2016 May and 2017 May flood events.

2016 May – Irrigation Department Flood Map

The flood extent map for the 2016 May event which was prepared by the Irrigation Department covering the whole Kelani Basin was collected as represented in Figure 4-37.

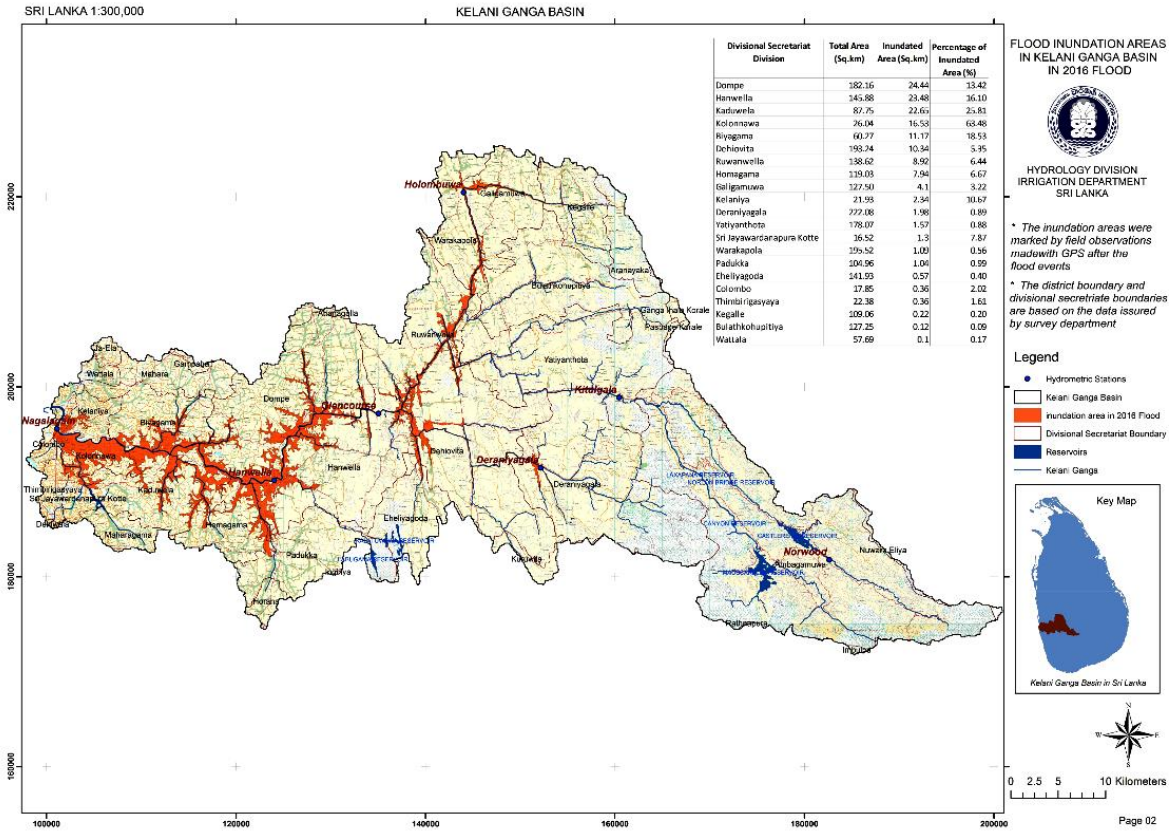

Figure 4-37: Published 2016 May observed Flood Map (Source: Irrigation Department)

2016 May – Survey Department Flood Map

As well, the Flood Extent map for the 2016 May event which was prepared by the Survey Department covering Lower Kelani Basin was collected as represented in Figure 4-38.

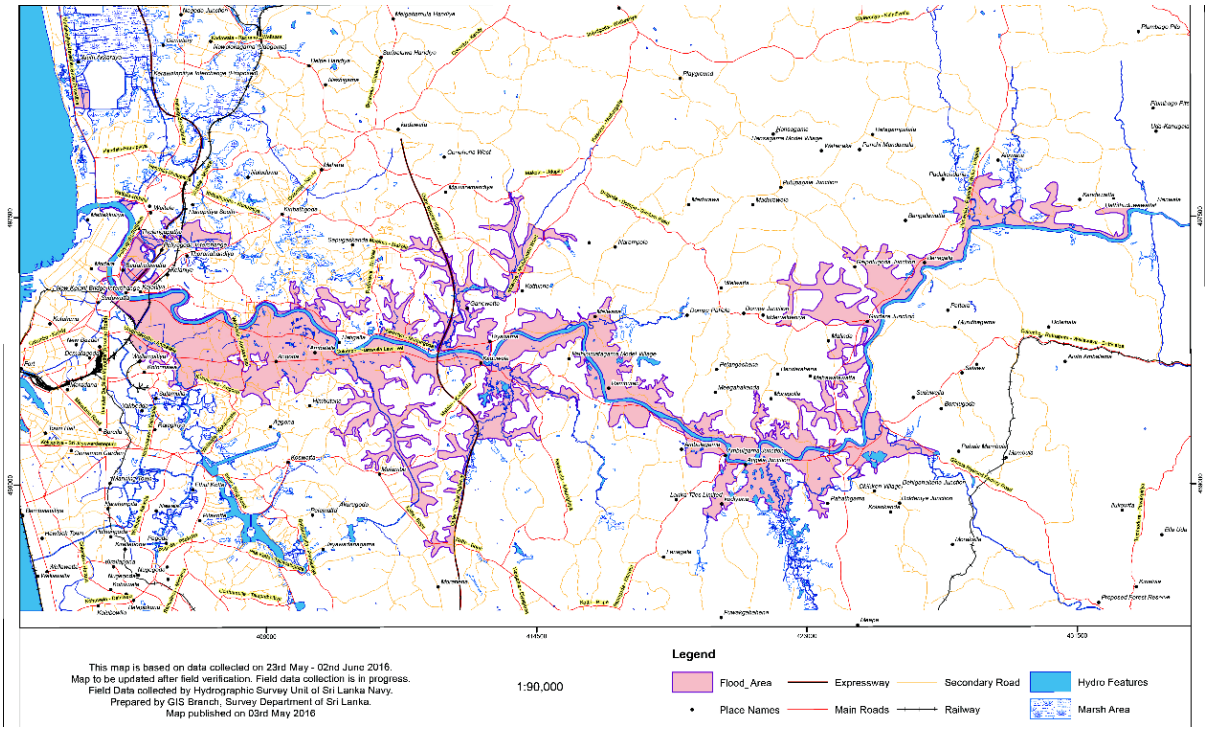

Figure 4-38: Published 2016 May Observed Flood Map (Source: Survey Department)

2017 May – Survey Department Flood Map

The flood extent map for the 2017 May event which was prepared by the Survey Department covering the Lower Kelani Basin was collected as represented in Figure 4-39.

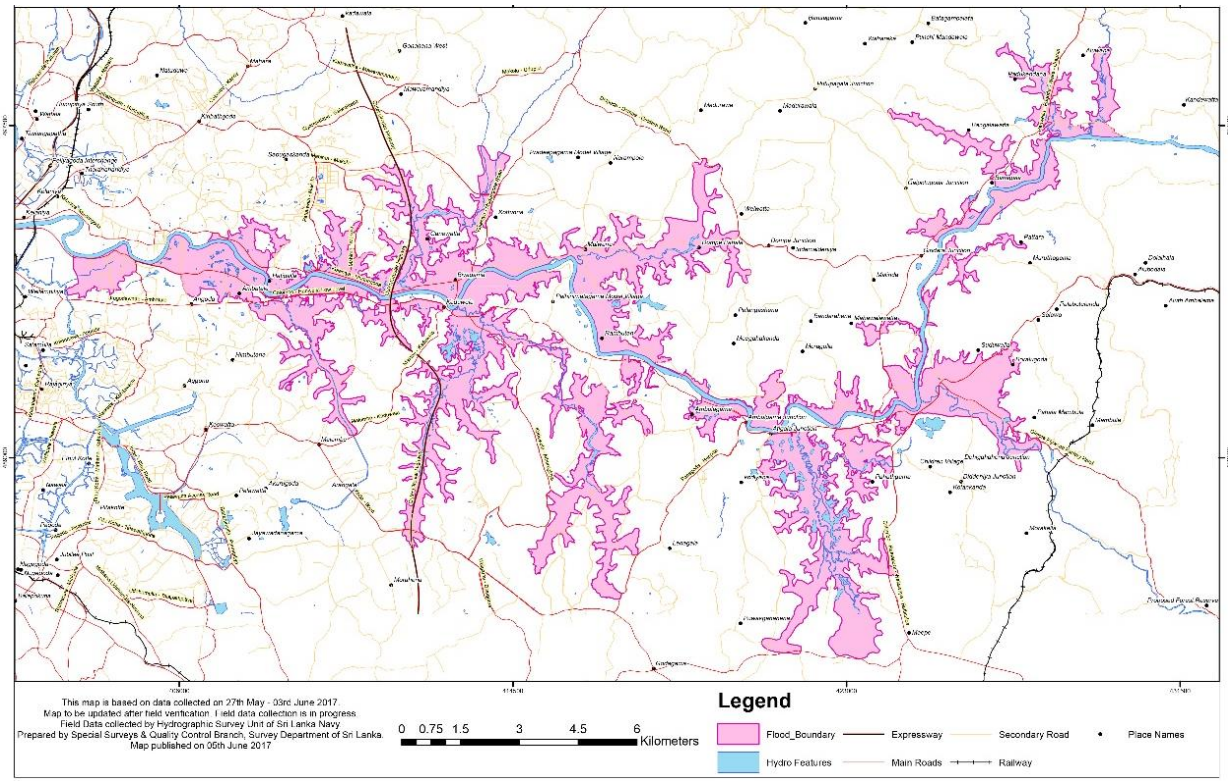

Figure 4-39: Published 2017 May Observed Flood Map (Source: Survey Department)

4.3 Data Processing

Design rainfall hyetograph development for selected Rainfall stations based on collected IDF equations using the Alternative Block Method (ABM) is explained in this section. The alternating block method is a simple and effective way to create synthetic hyetographs. It is often used in hydrologic modelling and design applications.

4.3.1 Design Rainfall Developed by the Alternative Block Method

The alternating block method is a technique used to create a synthetic hyetograph, which is a graphical representation of rainfall intensity over time. The alternating block method works by first dividing the storm duration into equal time intervals. Then, the rainfall intensities for each time interval are determined using a depth-duration-frequency (IDF) curve. Once the rainfall intensities for each time interval are known, they are arranged in an alternating pattern, with the largest intensity in the middle and the smaller intensities on either side.

Further to the literature review, a 50-year scale was selected for the design return period and a 3-day storm duration was selected.

Sample calculation of 3-day, 50-year return period design rainfall development for the Colombo Station is presented in Annex 1.

$I = 117.34\ T^{-0.686}$; $R^2 = 0.9972$

Here, I - Rainfall Intensity (mm/hr), T - Rainfall Duration (hr) and R^2 - Coefficient of determination

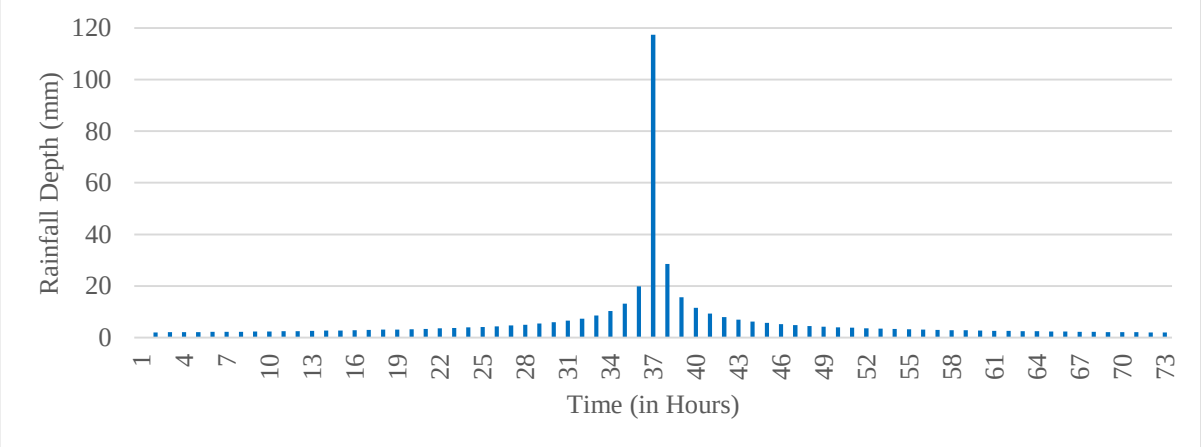

Figure 4-40: 50-year 3-day Design Rainfall of Colombo Station

The IDF equations and Coefficient of Determination of Other Selected Rainfall Stations which were used for Design Rainfall Development are presented in Table 4-4.

Table 4-4: Published IDF Equations for selected Rain gauges

Rainfall Station	IDF Equation	R^2
Hanwella	$I = 1589.4\ T^{-0.654}$	0.9831
Glencourse	$I = 1467.2\ T^{-0.607}$	0.9878
Deraniyagala	$I = 1868.3\ T^{-0.656}$	0.996
Kithulgala	$I = 1607.6\ T^{-0.639}$	0.9989
Norwood	$I = 670.03\ T^{-0.498}$	0.9811

I = Rainfall Intensity (mm/hr), T = Rainfall Duration (min), R^2 = Coefficient of determination

Developed rainfall events using the Alternative Block Method (ABM) are presented in Figure 4-41 to Figure 4-45.

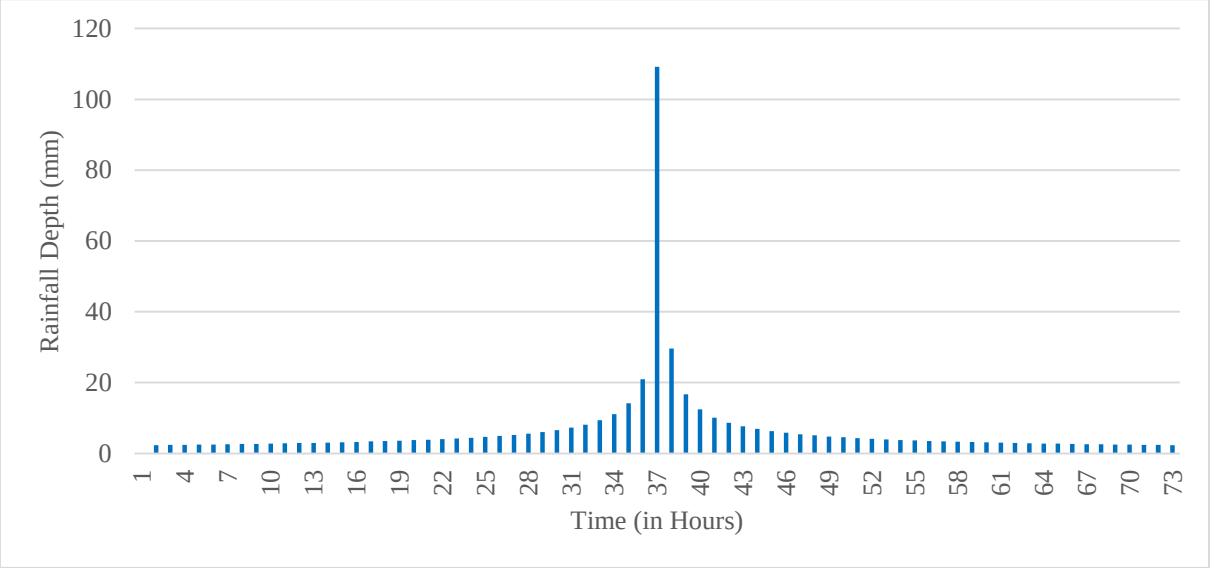

Figure 4-41: 50-year 3-day Design Rainfall of Hanwella Station

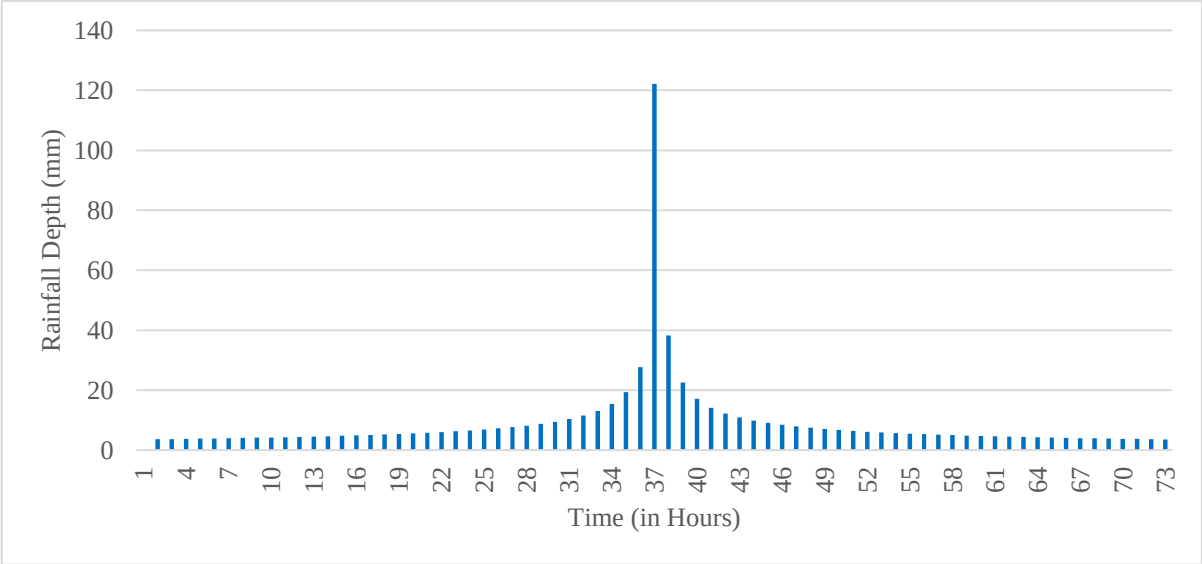

Figure 4-42: 50-year 3-day Design Rainfall of Glencourse Station

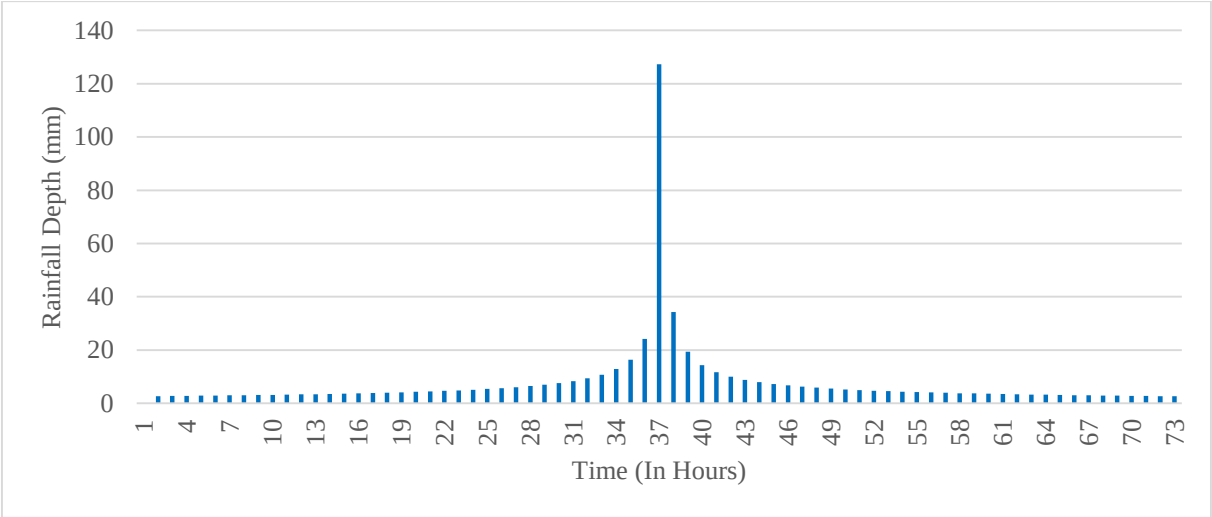

Figure 4-43: 50-year 3-day Design Rainfall of Deraniyagala Station

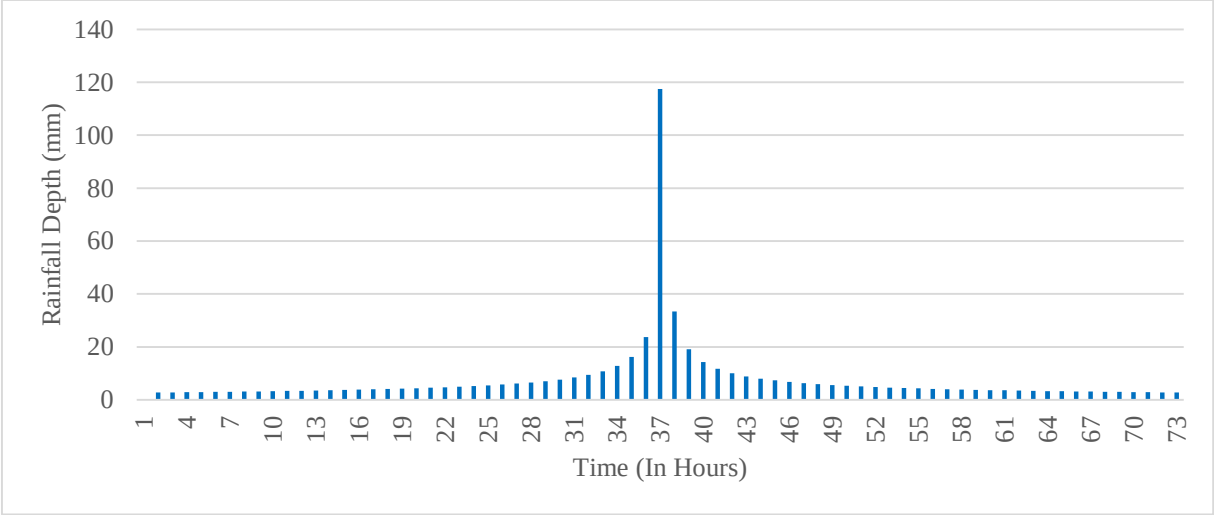

Figure 4-44: 50-year 3-day Design Rainfall of Kithulgala Station

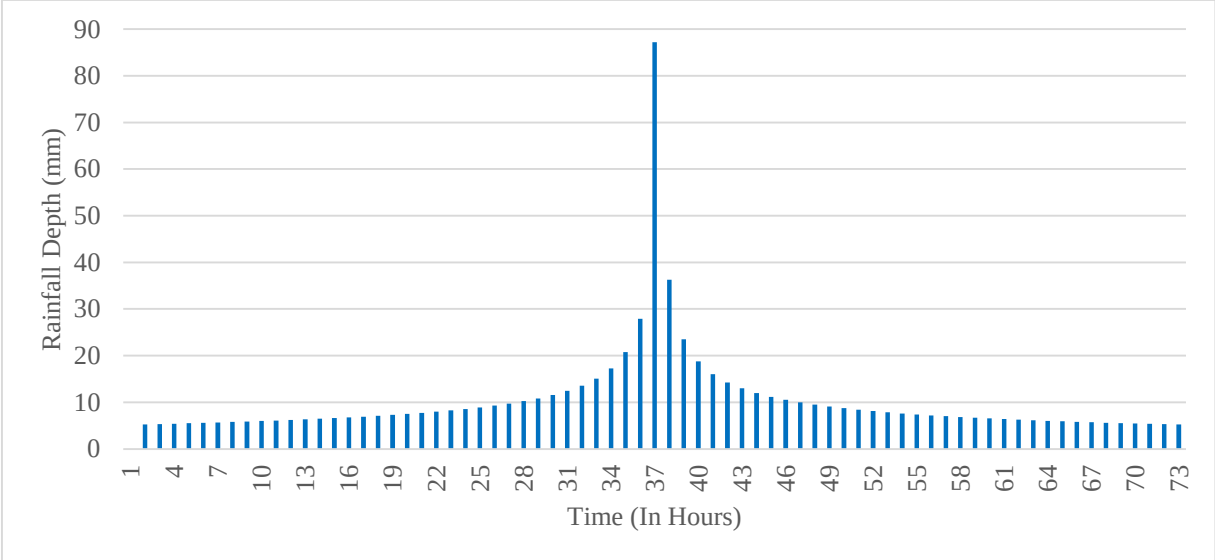

Figure 4-45: 50-year 3-day Design Rainfall of Norwood Station

CHAPTER 5

5 MODEL DEVELOPMENT AND APPLICATIONS

This chapter describes model development and its applications to achieve specific objectives and the main objective. Modelling includes hydrological model development using HEC-HMS and flood model development using HEC-RAS. Additionally, each model development includes initial model parameter estimation using basic principles, parameter sensitivity analysis, model calibration, model validation, and design rain event simulations with and without climate change projections.

5.1 Hydrological Model Development by HEC HMS

As mentioned in Chapter 3, hydrological model development was done using the Engineering Centre Hydrologic Modelling System (HEC-HMS). HEC-HMS is a software package developed by the U.S. Army Corps of Engineers' Hydrologic Engineering Centre (HEC) for simulating hydrologic processes. During the study, three HEC-HMS models were developed based on input availability and output requirements: Kelani Upper, Kelani Middle, and Kelani Lower. These HEC-HMS models generated discharges for the Kelani River and its sub-catchments at interested locations. They were then used as inputs to the HEC-RAS model.

Based on the outputs of the Literature Review and the availability of data, the Subbasin elements were defined using the SCS Curve Number for the Loss Method, the Clark Unit Hydrograph for the Transform Method, and the Recession Method for the Baseflow Method in Basin Models. Similarly, for the Reach elements, the Muskingum method was employed as the Routing method in Basin Models.

5.1.1 Parameter Estimation

The number of parameters available for each method under each element in the HEC-HMS model setup is presented in Table 5-1.

Table 5-1: HEC-HMS Parameters for each Model Elements

Element	Method	Parameters
Subbasin	Loss Method: SCS Curve Number	Initial Abstraction (mm)
		Curve Number
		Impervious (%)
	Transform Method: Clark Unit Hydrograph	Time of Concentration (Hr)
		Storage Coefficient (Hr)
	Baseflow Method: Recession	Initial Discharge (m^3/s)
		Recession Constant
		Ratio to Peak
Reach	Routing Method: Muskingum	Muskingum *K* (Hr)
		Muskingum *X*

The SCS Curve Number and Time of concentration were calculated using the basic principles as described in Chapter 3.

SCS Curve Number Estimation

The SCS curve number is a dimensionless number that is used to estimate the amount of runoff from a watershed based on the land use, soil type, and antecedent moisture conditions of the watershed. The SCS curve number ranges from 0 to 100, with 0 representing a completely pervious surface and 100 representing a completely saturated surface which generates the highest runoff.

In reference to Annex 2: CN Table by Ven. T Chow in Applied Hydrology (Chow et al., 1988), the SCS Curve Number categories were defined for Land Use types and, then the Curve Number Value was defined for each Land Use category. Here, it was assumed that the Type B Hydrological Soil Group (HSG) and Type II Antecedent Moisture Condition (AMC). Basin average curve number value is calculated based on the area percentage of each land use type within each sub-basin. The Basin average CN calculation is presented in Annexure 3. Calculated Basin average SCS Curve Number values are presented in Table 5-2.

Table 5-2: Estimated SCS Curve Numbers for each Sub-Basins

Sub-Basin	Area (km^2)	SCS Curve Number (CN)
Upper	1,524.29	62.87
Middle	291.10	63.68
Lower	506.57	65.12
Kelani Basin	2,321.97	63.46

Gunathilake et al. (2019) reported that the SCS CN value for the Seethawaka Ganga Sub-basin, obtained through the HEC-HMS model, was 60. Similarly, Senadhinatha (2020) listed the computed SCS CNs for 20 sub-basins ranging from 73 to 80. In the current study, the

initially estimated SCS CN values ranged from approximately 63 to 65, which fell between the range of 60 to 73 observed in the previous study. However, it is important to note that these initial estimated SCS CN values serve as a starting point, and the optimal values are determined through model calibration.

Time of Concentration

The time of concentration (*Tc*) represents the duration required for water to travel from the farthest location in a watershed to the outlet. It depends on various factors, including the topography, geology, and land usage within the watershed. The calculation of the time of concentration employed the travel time method, which estimates the travel times for different types of flows, namely Sheet Flow, Shallow Concentrated Flow, and Channel Flow. In this particular study, the literature outputs were used to assume the sheet flow time, while the velocities of the channel flows were determined based on the slope of each river segment. The Time of concentration is presented in Table 5.3.

Table 5-3: Time of Concentration (*Tc*) Calculation for each Sub-Basins using Travel Time Method

Type of Flow		**Basin**	**Upper-SB**	**Middle-SB**	**Lower-SB**
Sheet Flow	Travel Time - T1 (Assume) (min)	15	15	15.0	15.0
Shallow Concentrated	Longest Flow Path (km)	7.12168	7.12168	3.80742	4.22225
	Longest Flow Path (ft)	23365.09	23365.09	12491.54	13852.53
	Highest EL (m) MSL	2312.4	2312.4	398.9	189.1
	Lowest EL (m) MSL	1594.8	1594.8	47.9	10.5
	Slope (%)	10.08	10.08	9.22	4.23
	CN	63.5	62.9	63.7	65.1
	Lag Time (min)	197.4	200.4	124.4	192.1
	Travel Time - T2 (min)	329.6	334.7	207.7	320.8
Stream Flow	Stream Length (km)	24.6612	24.6612	9.64643	13.0853
	Flow Velocity (Assume) m/s	2	2	1.5	1.5
	Travel Time - T3 (min)	205.5	205.5	107.2	145.4
River Flow	River Length (km)	115.006	62.0218	16.8897	31.4732
	Flow Velocity (Assume) m/s	1	1.5	1	1
	Travel Time - T4 (min)	1916.8	689.1	281.5	524.6
Total Flow	Tc = T1+T2+T3+T4 (min)	2466.9	1244.3	611.3	1005.7
	Tc (Hr)	41.11	20.74	10.19	16.76

Based on the findings of De Silva et al. (2014), the Time of Concentration (*T*c) value calculated for the Kelani Upper basin from Hanwella was reported to be 28 hours. In the present study, the calculated *T*c up to Hanwella was found to be 25.5 hours, indicating a reasonably close similarity between the two values. According to Rajkumar et al. (2021), the optimal *Tc* value for the Hanwella upper basin, determined through model calibration and validation, was reported as 13 hours. This value was significantly lower than the calculated *Tc* value in the current study. However, this initial estimation of *Tc* serves as a starting point, and the optimal value is determined through model calibration.

Assumed Parameters

The estimation of other HEC-HMS parameters was derived from relevant literature sources and also from observed discharge data.De Silva et al. (2014) calculated a storage coefficient value of 40 hours for the Kelani Upper basin from Hanwella. Similarly, Rajkumar et al. (2021) reported a storage coefficient value of 39 hours. Taking these values into consideration, an initial value of 40 hours was assumed for the storage coefficient in this study. Gunathilake et al. (2019) found that the initial abstraction value was 5 mm based on their study. Senadhinatha (2020) provided a range of computed initial abstraction values for 20 sub-basins, varying from 12.7 mm to 18.7 mm. Considering these values, an initial value of 5 mm was assumed for the initial abstraction in this study. Additionally, Senadhinatha (2020) listed the computed per cent impervious values for 20 sub-basins, ranging from 0.0% to 4.25%. Therefore, a per cent impervious value of 5% was assumed for the current study. The initial discharge associated with the baseflow method was determined using the initially observed discharge at Glencourse, which was assumed to be 150 m3/s. The study by De Silva et al. (2014) reported a recession constant of 0.54 and a ratio to peak of 0.4. Senadhinatha (2020) provided a range of ratio to peak values for 20 sub-basins, varying from 0.21 to 0.76. Additionally, Rajkumar et al. (2021) reported a recession constant value of 0.8. Based on these reference values from the literature, the initial recession constant and ratio to peak were assumed to be 0.5 each.

Gunathilake et al. (2019) employed the Muskingum method for flood modeling, utilizing Muskingum *K* and Muskingum *X* parameters. The study reported that the Muskingum *X* values ranged from 0.30 to 0.40, while the Muskingum *K* values varied from 2 hours to 3 hours across different reaches. However, upon comparing the reach lengths between their study and the current study, it was observed that the reach lengths in the current study were significantly larger. Taking this into consideration, initial estimates of 20 hours for Muskingum *K* and 0.5 for Muskingum *X* were assumed in the present study. It is important to note that these initial values are starting points, and the optimal values will be determined through model calibration.

The parameters were determined based on a thorough literature review and careful examination of the available data, as outlined in Table 5-4.

Table 5-4: Assumed Parameters in HEC-HMS Models

Model	Method	Parameter	Value	Unit
Loss	CSC Curve Number	Initial Abstraction	5	mm
		Impervious	5	%
Transform	Clark Unit Hydrograph	Storage Coefficient	40	Hr
Baseflow	Recession	Initial Discharge	150	m^3/s
		Recession Constant	0.5	
		Ratio to Peak	0.5	
Reach - Routing	Muskingum	Muskingum *K*	20	Hr
		Muskingum *X*	0.05	

5.1.2 Hydrological Model Parameter Sensitivity Analysis

Model parameter sensitivity analysis is a technique used to assess the influence of different parameters on the model's output or performance which helps in understanding the sensitivity and importance of individual parameters in representing the hydrological processes within the model. In the present study, the estimated parameter values were systematically varied within a predefined parameter range as presented in Table 5-5 and Table 5-6 such that one parameter at a time while keeping the other parameters constant, and observing the resulting changes in the model's output. This analysis helped to identify which parameters have a significant impact on the model's behaviour and which ones have a relatively minor effect further to Model calibration. For analysis of the parameters in the subbasin element, the Kelani Upper Model was used and the Parameter Ranges are presented in Table 5-5.

Table 5-5: Parameters Values Used for Sensitivity Analysis - Sub-Basin Element in HEC-HMS

Method	Scenario No.										
	1	**2**	**3**	**4**	**5**	**6**	**7**	**8**	**9**	**10**	**11**
Loss	**SCS Curve Number**										
Curve Number	35	45	50	55	60	**65**	70	75	80	85	95
Initial Abstraction (mm)	0	1	2	3	4	**5**	6	7	8	9	10
Transform	**Clark Unit Hydrograph**										
Time Of Concentration (HR)	5	8	11	14	17	**20**	23	26	29	32	35
Storage Coefficient (HR)	10	15	20	25	30	**40**	40	45	50	55	60
Baseflow	**Recession**										
Recession Constant	0.01	0.1	0.2	0.3	0.4	**0.5**	0.6	0.7	0.8	0.9	1
Ratio	0	0.1	0.2	0.3	0.4	**0.5**	0.6	0.7	0.8	0.9	1

For analysis of the parameters in the reach element the Kelani Middle Model removing the subbasin element, was used and the Parameter Ranges are presented in Table 5-6.

Table 5-6: Parameters Values Used for Sensitivity Analysis - Reach Element in HEC-HMS

Method	**Scenario No.**										
	1	**2**	**3**	**4**	**5**	**6**	**7**	**8**	**9**	**10**	**11**
Reach	**Muskingum**										
Muskingum - *K* (Hr)	0.001	1	5	10	15	**20**	25	30	35	40	50
Muskingum - *X*	0.001	0.01	0.02	0.03	0.04	**0.05**	0.1	0.2	0.3	0.4	0.5

The Kelani Upper HEC-HMS model was constructed as a one subbasin element, encompassing the Kelani Upper Basin. Within this basin, there were a total of four (4) rain gauges strategically positioned. To obtain the basin-averaged rainfall, the Thiessen average method was employed. The Thiessen weights associated with each rain gauge are provided in Table 5-7.

Table 5-7: Thiessen Weights for Rain Gauges of Kelani Upper Basin

Station	**Area (km^2)**	**Thiessen Weight**
Deraniyagala	288.76	0.19
Glencourse	353.05	0.23
Kithulagala	541.70	0.36
Norwood	340.78	0.22

Based on the Thiessen weights presented in Table 5-7, Thiessen weighted 2016 May Rainfall for Upper Basin was developed as meteorological model time series input of Kelani Upper model as presented in Figure 5-1.

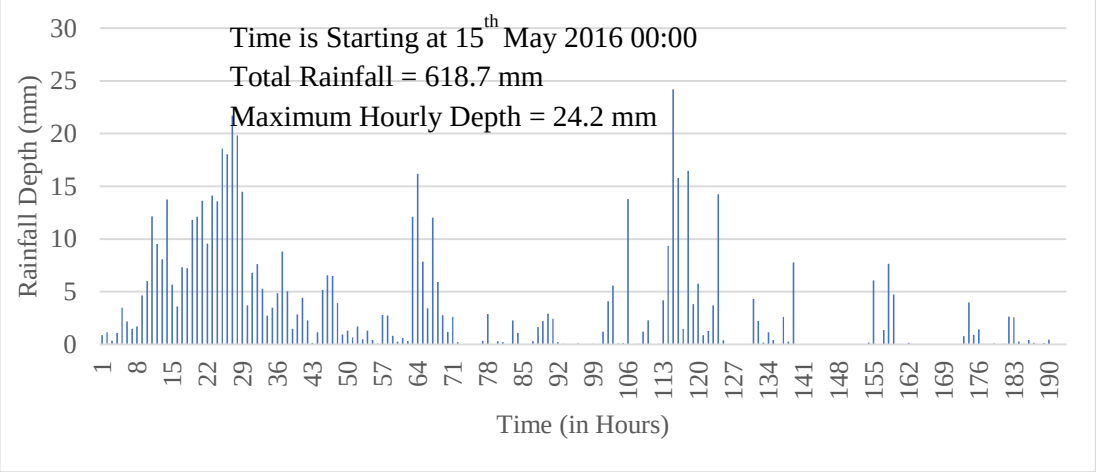

Figure 5-1: 2016 May Thiessen Averaged Hourly Rainfall Data - Kelani Upper Basin

Figure 5-2 presents the snapshot of the HEC-HMS model setup of the Kelani Upper Model used for subbasin model sensitivity analysis. Here, the Calculation point is included in the Upper Subbasin element, to evaluate the model performance using the Nash efficiency and Coefficient of determination (R^2).

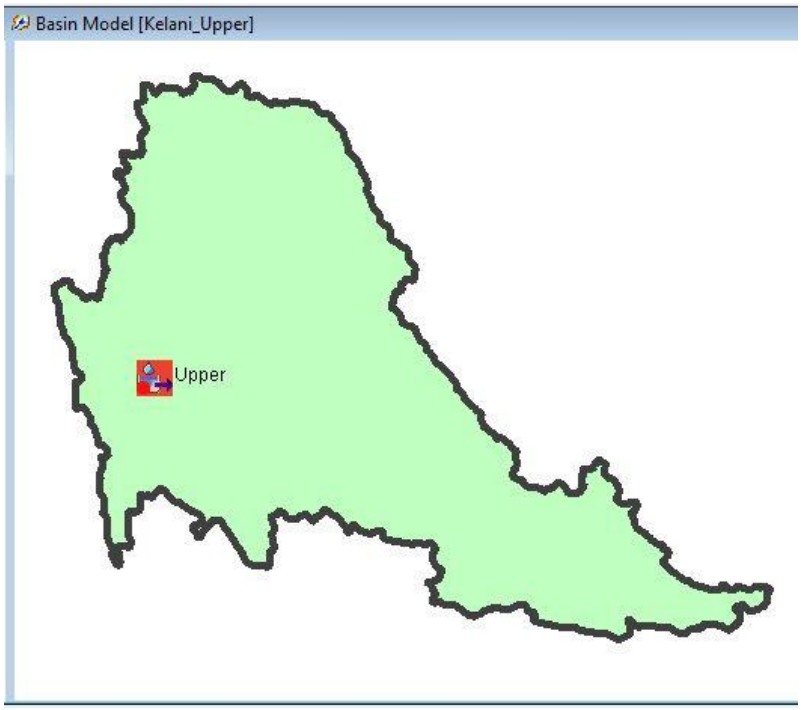

Figure 5-2: Basin Model of Kelani Upper HEC-HMS Model used for Sensitivity Analysis

Table 5-8 describes the HEC-HMS model setup of the Kelani Upper Model used for subbasin model sensitivity analysis.

Table 5-8: HEC-HMS Model Setup of Kelani Upper for Parameter Sensitivity Analysis

Model	Kelani-Upper	
Elements	Subbasin: Upper	
Input Data	Rainfall	2016 May Thiessen Weighted
	Discharge	2016 May Observed Glencourse Flow
Control Specification	Start Date	15th May 2016
	Start Time	00:00
	End Date	23rd May 2016
	End Time	00:00
Computation Method	Simulation Run	
Outputs	Simulated Time Series Discharge at Basin Outflow	
	Peak Discharge	
	Nash Coefficient and R^2	

Figure 5-3 presents the snapshot of the HEC-HMS model setup of Kelani Middle Model used for reach element sensitivity analysis. Here, the Calculation point is included in Junction 1 representing Hanwella discharge, for evaluating the model performance using the Nash efficiency and Coefficient of determination (R^2).

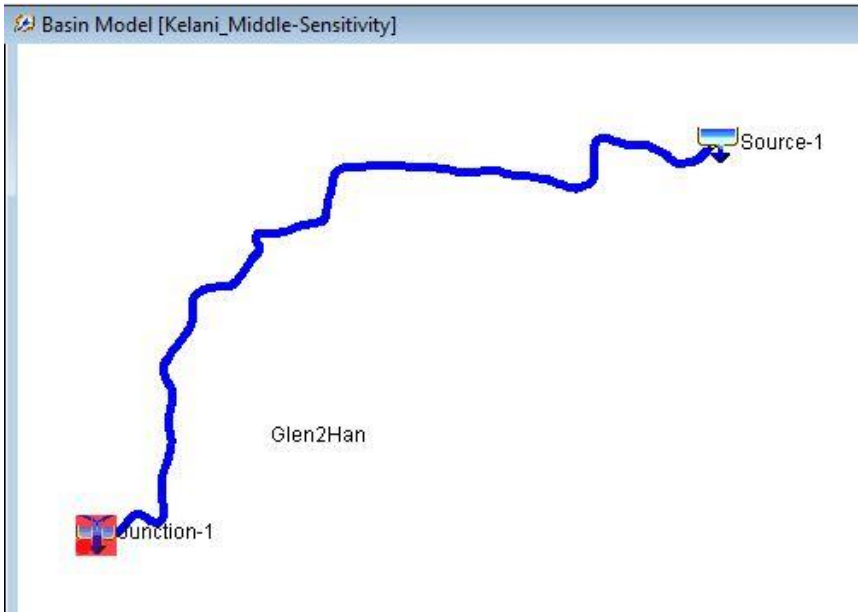

Figure 5-3: Basin Model of Kelani Middle HEC-HMS Model used for Sensitivity Analysis

Table 5-9 describes the HEC-HMS model setup of the Kelani Middle Model used for reach element parameter sensitivity analysis.

Table 5-9: HEC-HMS Model Setup of Kelani Middle for Parameter Sensitivity Analysis

Model	Kelani-Middle	
Elements	Source: For Inserting Inflow at Glencourse	
	Reach: For Representing Kelani River Portion from Glencourse to Hanwella	
	Junction: For Representing Outflow at Hanwella	
Input Data	Discharge	2016 May Observed Glencourse Flow
		2016 May Observed Hanwella Flow
Control Specification	Start Date	15th May 2016
	Start Time	00:00
	End Date	23rd May 2016
	End Time	00:00
Computation Method	Simulation Run	
Outputs	Simulated Time Series Discharge at Junction (Hanwella)	
	Peak Discharge	
	Nash Coefficient and R^2	

5.1.3 Hydrological Model Calibration

Hydrological model calibration is the process of adjusting model parameters to improve the agreement between simulated model outputs and observed hydrological data. The aim is to ensure that the model adequately represents the hydrological processes and accurately predicts the behaviour of the system being modelled.

The 2016 May Flood event from 15th May 2016 to 23rd May 2016 was used for the model calibration with the aid of identified most sensitive parameters resulting from parameter sensitivity analysis.

As previously mentioned, Table 5-10 presents the Thiessen weights for the Kelani Upper model and the following Table 5-10 presents the Thiessen weights for Kelani Middle and Kelani Lower Models.

Table 5-10 : Thiessen weights for Kelani Middle and Lower Basins

Sub-Basin	Station	Area (km^2)	Thiessen Weight
Middle	Glencourse	149.46	0.51
	Hanwella	141.64	0.49
Lower	Colombo	202.64	0.40
	Hanwella	303.92	0.60

Using the Thiessen weights assigned to the Kelani Middle and Kelani Lower basins, the rainfall time series for the May 2016 event was computed using the Thiessen average method. The resulting Thiessen averaged rainfall data for the event are depicted in Figure 5-4 and Figure 5-5.

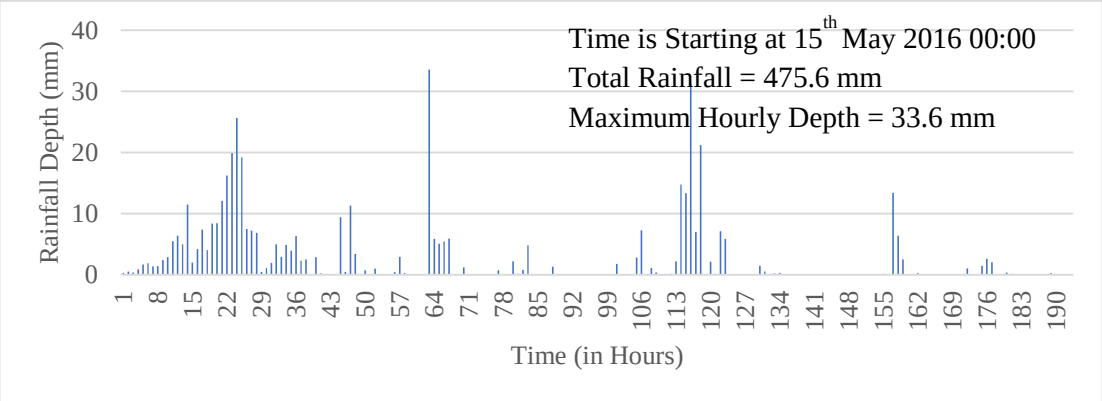

Figure 5-4: 2016 May Thiessen Averaged Hourly Rainfall Data for Kelani Middle Basin

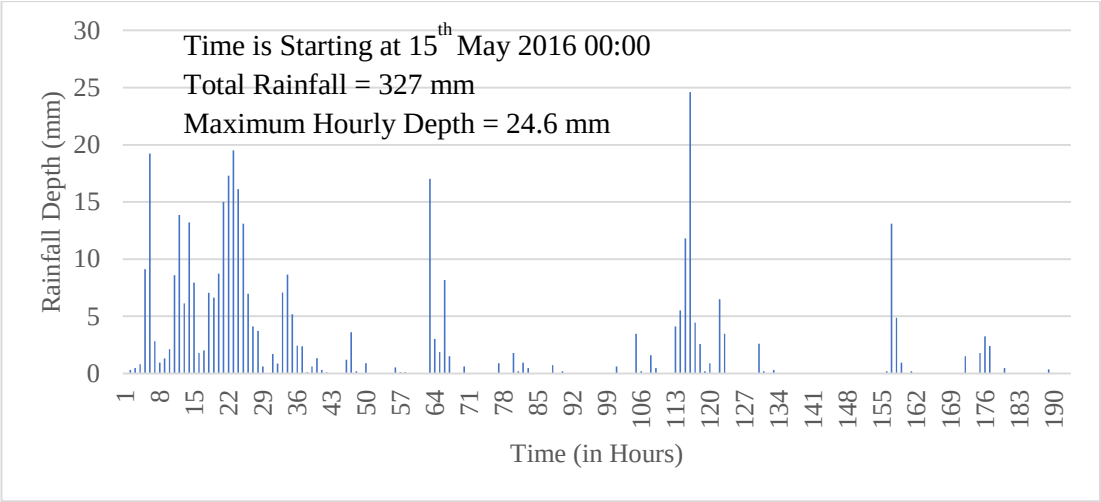

Figure 5-5: 2016 May Thiessen Averaged Hourly Rainfall Data for Kelani Lower Basin

Figure 5-6 presents the snapshot of the HEC-HMS model setups of the Kelani Upper (a), Kelani Middle (b) and Kelani Lower (c) Models used for calibration. Here, Calculation points were included in the Upper subbasin (representing Glencourse discharge) Junction 1 (representing Hanwella discharge) and Junction 2 (representing discharge at sea outfall) to evaluate the model performance using the Nash efficiency and Coefficient of determination (R^2).

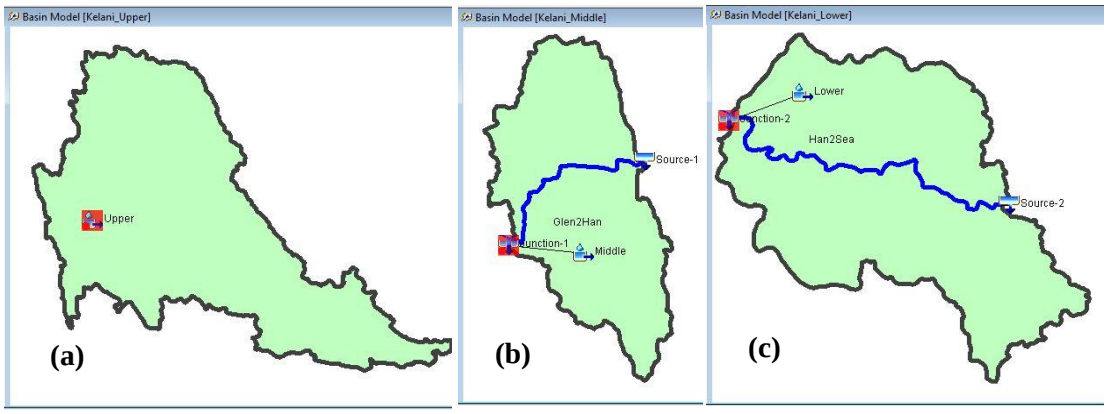

Figure 5-6: Basin Models of HEC-HMS models (a) Kelani Upper, (b) Kelani Middle and (c) Kelani Lower

Table 5-11 describes the HEC-HMS model setups of the Kelani Upper, Kelani Middle and Kelani Lower Models used for calibration. Optimization Trial computation method having parameter auto calibration is used during the calibration process. This was an iterative process for optimizing the parameters observing Nash Coefficient and R^2 as well the Time Series graphs of Observed and Simulated Flow.

Table 5-11:HEC-HMS Model setups for Calibration

Model	Kelani-Upper	Kelani-Middle	Kelani-Lower
Elements	Subbasin: Kelani Upper SB	Source-1: Glencource Inflow	Source-2: Hanwella Inflow
		Reach (Glen2Han):Glencourse to Hanwella Kelani River	Reach (Han2Sea):Hanwella to Sea Kelani River
		Subbasin (Middle): Kelani Middle SB	Subbasin (Lower): Kelani Lower SB
		Junction-1:Hanwella Outflow	Junction-2:Sea Outflow
Input Data	Rainfall: 2016 May Thiessen Weighted		
	Discharge: 2016 May Observed Glencourse, Hanwella and Nagalagama Street Flow		
Control Specification	Start Date: 15th May 2016		
	Start Time: 00:00		
	End Date: 23rd May 2016		
	End Time: 00:00		
Computation Method	Optimization Trial		
Optimize Objective Function	Peak Weighted Root Mean Square Error		
Outputs	Optimized Parameters		
	Time Series graph of Observed and Simulated Flow		
	Nash Coefficient and R^2		

5.1.4 Model Validation

Hydrological model validation is the process of assessing the accuracy and reliability of a hydrological model by comparing its simulated outputs with independent observed data. During the validation process, the model is tested against datasets that were not used in the model calibration. The purpose of model validation is to evaluate the model's ability to accurately represent real-world hydrological processes and to ensure that it can provide reliable predictions under various conditions.

In the present study, the model validation was conducted using the observed data of the 2017 May flood event, which spanned from 24th May 2017 to 29th May 2017. The Kelani Upper, Kelani Middle, and Kelani Lower models, which had been calibrated with appropriate

parameter values, were simulated using the observed data from May 2017. The performance of these models was then evaluated.

To construct the Thiessen averaged rainfall series for the Kelani Upper, Kelani Middle, and Kelani Lower models, the Thiessen weights provided in Table 5-7 and Table 5-10 were employed. The resulting rainfall graphs for the 2017 May event are displayed in Figure 5-7, Figure 5-8, and Figure 5-9.

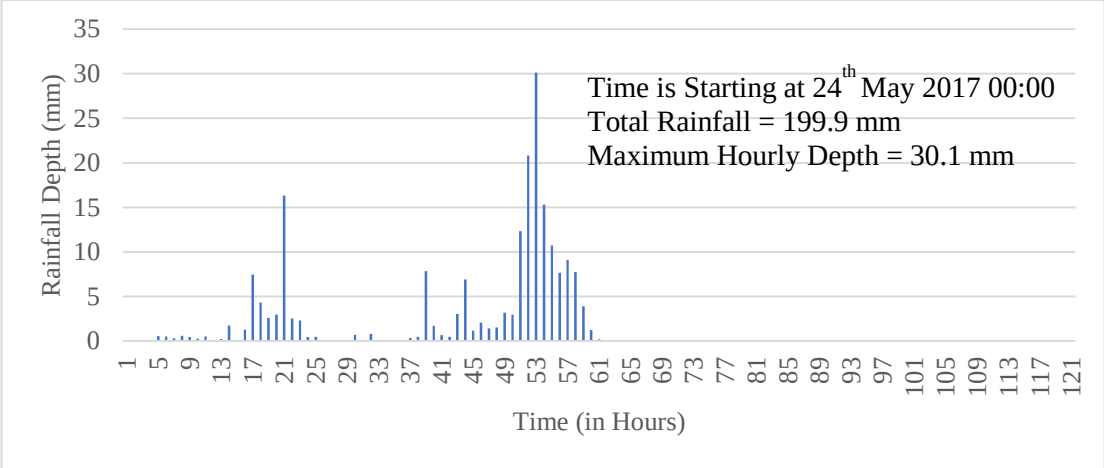

Figure 5-7: 2017 May Thiessen Averaged Hourly Rainfall Data for Kelani Upper Basin

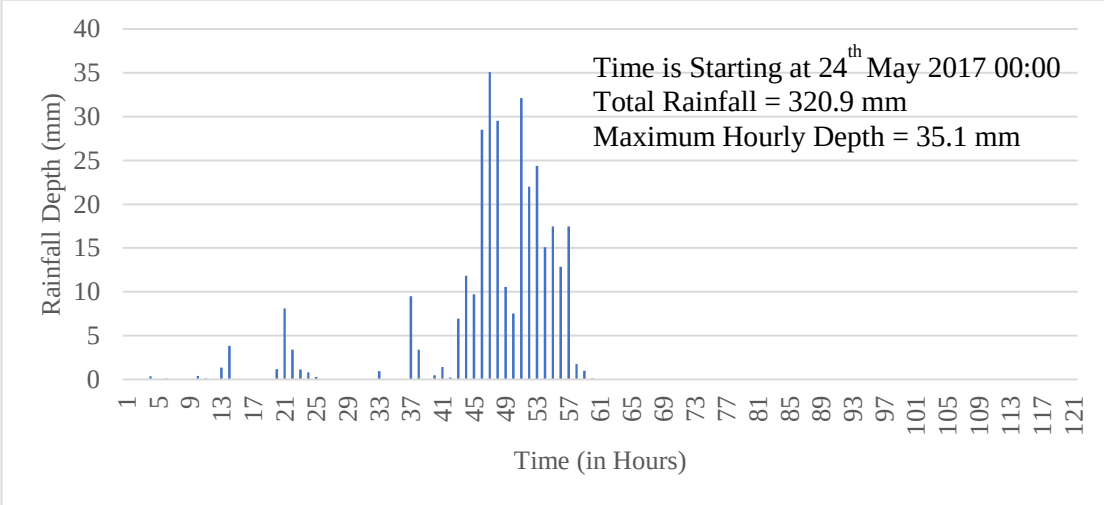

Figure 5-8: 2017 May Thiessen Averaged Hourly Rainfall Data for Kelani Middle Basin

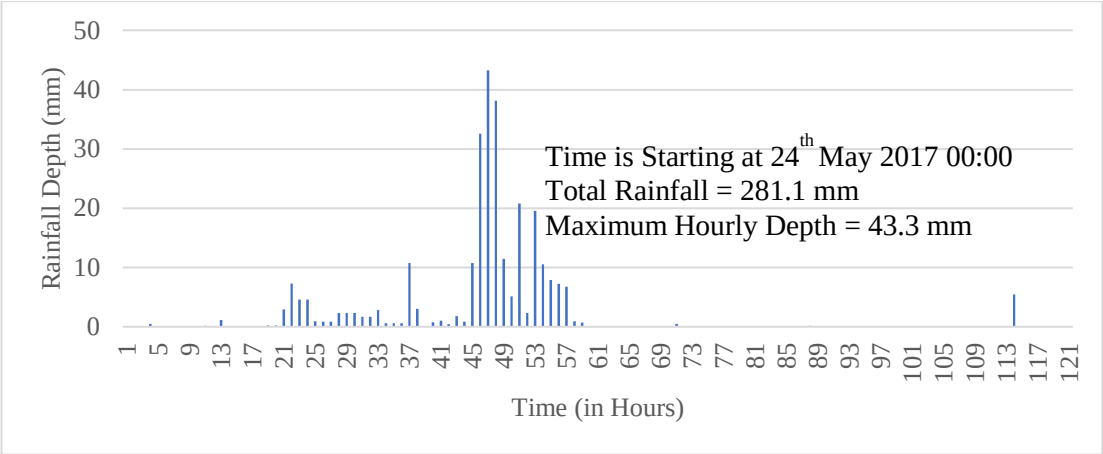

Figure 5-9: 2017 May Thiessen Averaged Hourly Rainfall Data for Kelani Lower Basin

Table 5-12 provides a description of the HEC-HMS model setups utilized for validation, including the Kelani Upper, Kelani Middle, and Kelani Lower Models. The validation process employed the Simulation Run computation method, which yielded evaluation metrics such as the Nash Coefficient and R^2. Additionally, the Time Series graph comparing the Observed and Simulated Flow was generated to further assess the model's performance.

Table 5-12: HEC-HMS Model Setups for Validation

<table>
<tr><td>Model</td><td>Kelani-Upper</td><td>Kelani-Middle</td><td>Kelani-Lower</td></tr>
<tr><td rowspan="4">Elements</td><td rowspan="4">Subbasin: Kelani Upper SB</td><td>Source-1: Glencource Inflow</td><td>Source-2: Hanwella Inflow</td></tr>
<tr><td>Reach (Glen2Han): Glencourse to Hanwella Kelani River</td><td>Reach (Han2Sea): Hanwella to Sea Kelani River</td></tr>
<tr><td>Subbasin (Middle): Kelani Middle SB</td><td>Subbasin (Lower): Kelani Lower SB</td></tr>
<tr><td>Junction-1:Hanwella Outflow</td><td>Junction-2:Sea Outflow</td></tr>
<tr><td rowspan="2">Input Data</td><td colspan="3">Rainfall: 2017 May Thiessen Weighted</td></tr>
<tr><td colspan="3">Discharge: 2017 May Observed Glencourse, Hanwella and Nagalagama Street Flow</td></tr>
<tr><td rowspan="4">Control Specification</td><td colspan="3">Start Date: 24th May 2017</td></tr>
<tr><td colspan="3">Start Time: 00:00</td></tr>
<tr><td colspan="3">End Date: 29th May 2017</td></tr>
<tr><td colspan="3">End Time: 00:00</td></tr>
<tr><td>Computation Method</td><td colspan="3">Simulation Run</td></tr>
<tr><td rowspan="2">Outputs</td><td colspan="3">Nash Coefficient and R^2</td></tr>
<tr><td colspan="3">Time Series graph of Observed and Simulated Flow</td></tr>
</table>

5.1.5 Hydrological Model Simulation for Statistical Rain Event

For the statistical simulation of rain events in the hydrological model, 3-day design rainfall values were employed. These values were derived using IDF (Intensity-Duration-Frequency) equations for selected rainfall stations, considering a 50-year return period. To construct the Thiessen weighted 50-year return period 3-day rainfall series for each sub-basin, the Thiessen weights from Table 5-7 and Table 5-10 were utilized. Areal reduction factors, as specified in Annex 4 of "Applied Hydrology" by Ven T. Chow (Chow et al., 1988) were applied for correcting the rainfall series. The specific Areal Reduction Factors used in this study are presented in Table 5-13.

Table 5-13: Areal Reduction factors applied for Rainfall correction

Sub-Basin	Area (km^2)	Areal Reduction Factor
Upper SB	1,524.29	0.65
Middle SB	291.103	0.70
Lower SB	506.572	0.70

The developed rainfall series for Upper Basin, Middle Basin and Lower Basin are presented in Figure 5-10, Figure 5-11 and Figure 5-12.

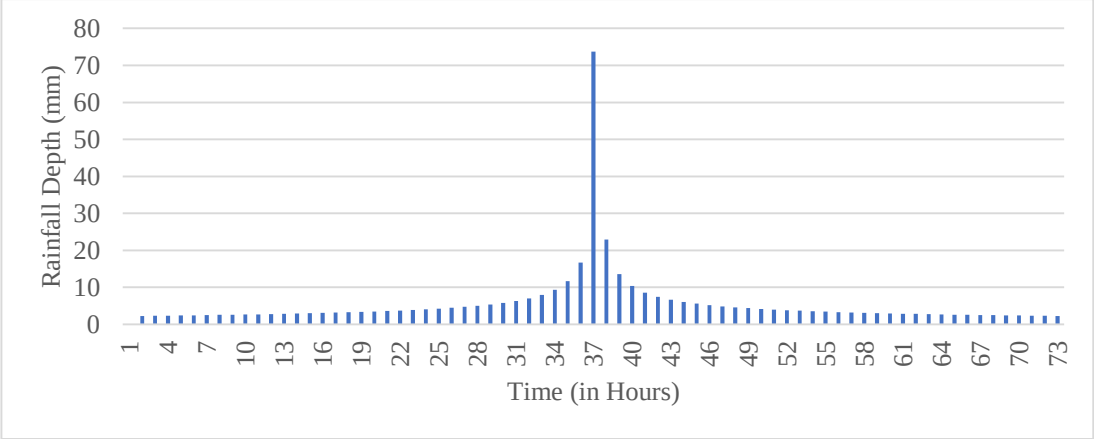

Figure 5-10: 50-year 3-day Thiessen Averaged Design Rainfall with ARF Applied for Kelani Upper Basin

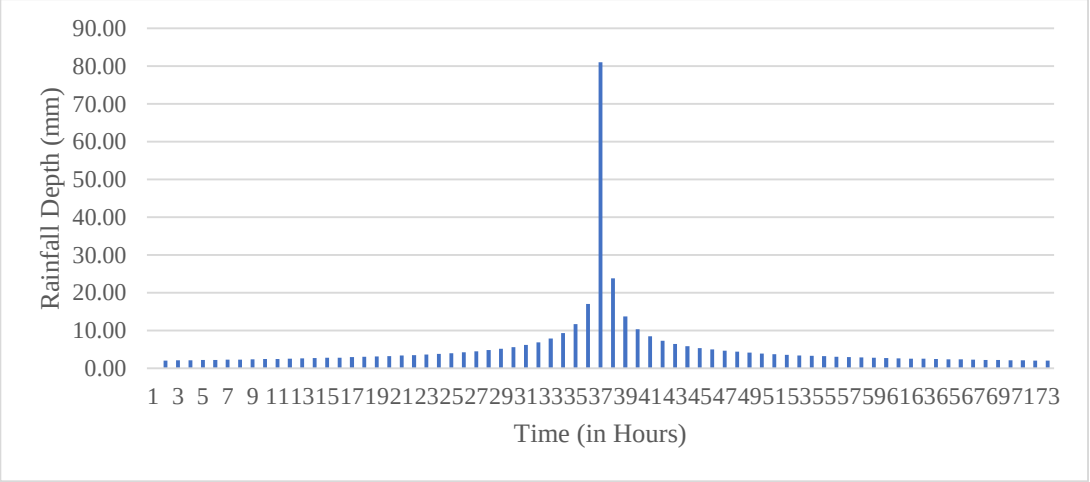

Figure 5-11: 50-year 3-day Thiessen Averaged Design Rainfall with ARF Applied for Kelani Middle Basin

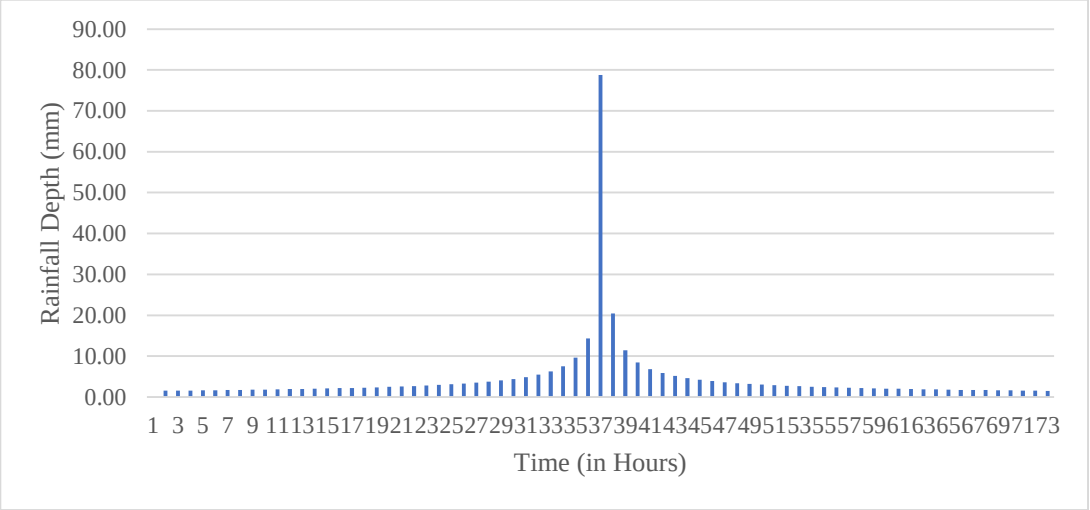

Figure 5-12: 50-year 3-day Thiessen Averaged Design Rainfall with ARF Applied for Kelani Lower Basin

Design Rainfall Temporal distribution check with observed Rainfall Temporal distribution

The design rainfalls created using the alternative block method exhibit a nearly symmetrical and bell-shaped distribution. It is essential to validate this temporal distribution by comparing it with observed rainfall data used for model calibration and validation. Specifically, for the calibration event in May 2016, the rainfall can be divided into two portions: the first portion from the 15th to the 18th and the second portion from the 18th to the 21st. These two three-day events were analyzed separately to assess the actual distribution of rainfall. Similarly, for the validation event in May 2017, the three-day rainfall event from the 24th to the 27th was

examined to verify the shape of the actual rainfall distribution. These three rainfall events, spanning three days each, were compared with the three-day design rainfall for the Kelani Upper, Kelani Middle, and Kelani Lower sub-basins using Thiessen-averaged rainfall. The cumulative rainfall distribution percentages for the Kelani Upper, Kelani Middle, and Kelani Lower sub-basins were presented in Figure 5-13, Figure 5-14, and Figure 5-15, respectively.

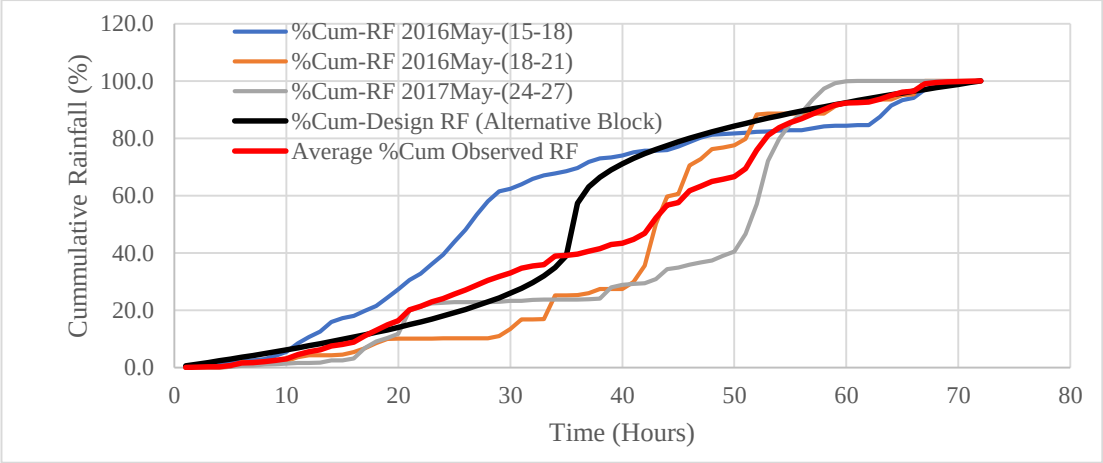

Figure 5-13: Comparison of % Cumulative Rainfall of Kelani Upper Model

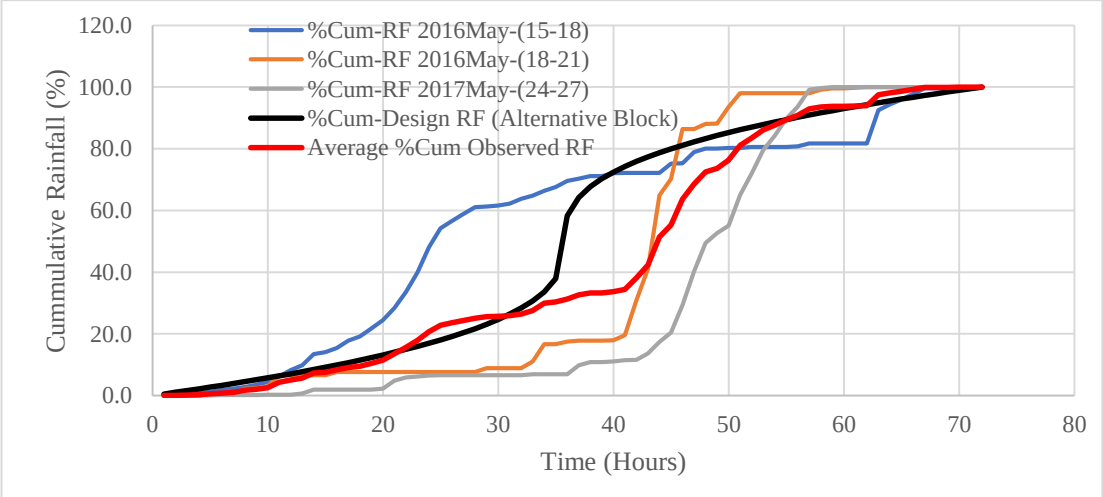

Figure 5-14: Comparison of % Cumulative Rainfall of Kelani Middle Model

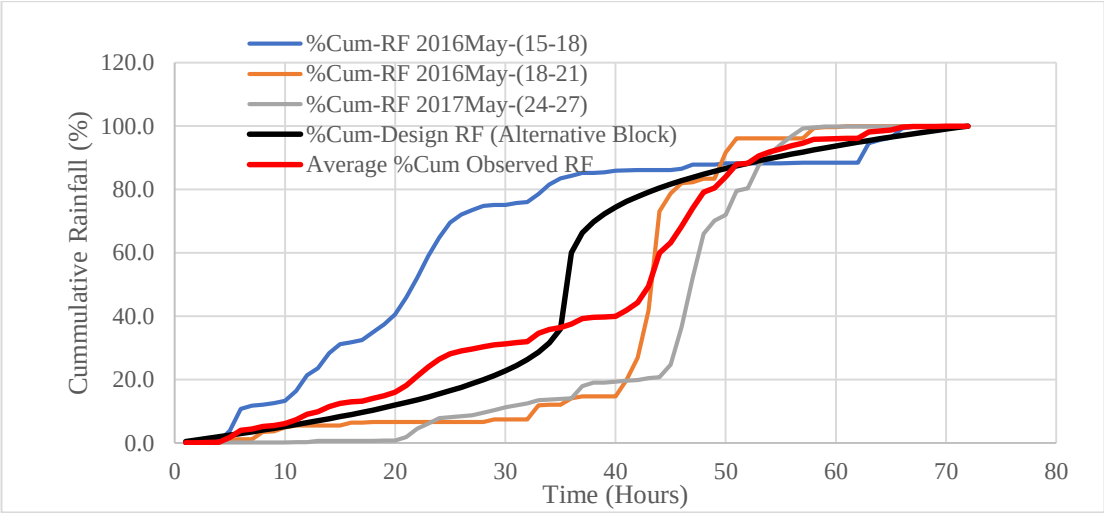

Figure 5-15: Comparison of % Cumulative Rainfall of Kelani Lower Model

Upon comparing the graphs shown in Figure 5-13, Figure 5-14, and Figure 5-15, it was observed that the percentage cumulative rainfall of the design rainfall falls between the graphs representing the first portion of the May 2016 rainfall and the May 2017 rainfall for all sub-basins. Consequently, average percentage cumulative rainfall graphs were plotted on the same graphs. It was noticed that the observed distribution and the design rainfall distribution did not exhibit a similar shape. Furthermore, the average percentage cumulative rainfall graphs for the three sub-basins were plotted alongside the design rainfall distribution, as illustrated in Figure 5-16.

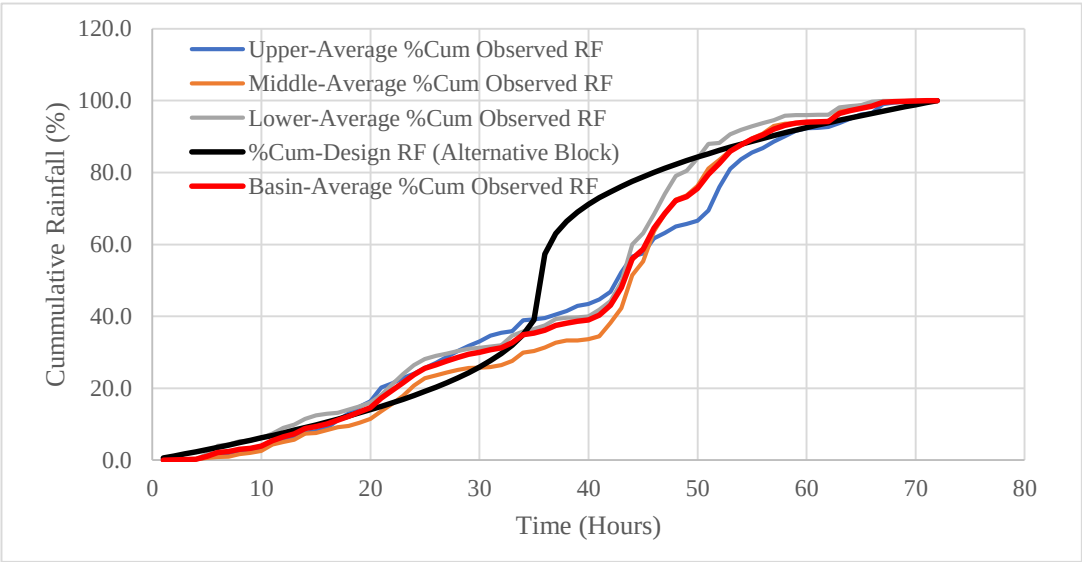

Figure 5-16: Comparison of sub-basin average cumulative Rainfall with Design Rainfall

According to Figure 5-16, it was observed that the actual rainfall distribution in the sub-basins appears to be approximately similar. Consequently, a graph depicting the basin average actual rainfall distribution was plotted on the same graph. Upon comparing this basin average percentage cumulative rainfall with the percentage cumulative rainfall of the design rainfall constructed using the alternative block method, it is evident that the actual rainfall exhibited a back-loaded shape. As a result, the peak of the design rainfall was adjusted to align with the shape of the actual rainfall distribution. This adjustment process was conducted as a trial, shifting the design rainfall peak by 4 hours, 8 hours, and 12 hours. The graphical representation of the design rainfall shifting is presented in Figure 5-17.

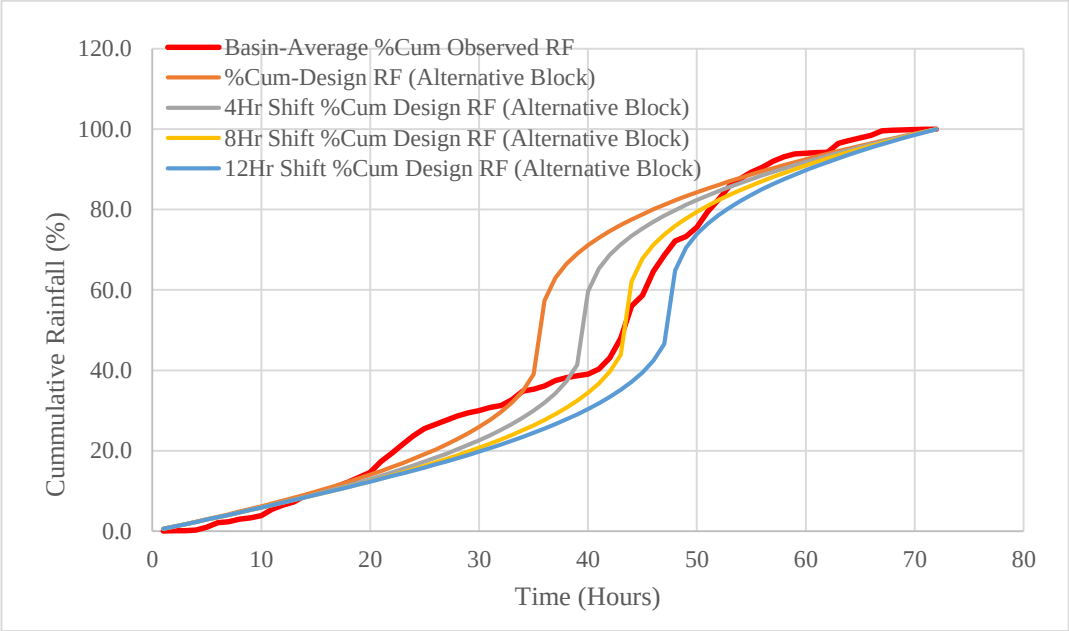

Figure 5-17: Comparison of Design Rainfall Shifting with Observed Rainfall

Upon analyzing Figure 5-17, it was observed that the design rainfall series with an 8-hour peak backward shift closely matched the actual rainfall distribution. Therefore, this 8-hour shifted 3-day 50-year return period design rainfall was selected for statistical rainfall simulations. The 8-hour shifted design rainfalls for Kelani Upper, Kelani Middle, and Kelani Lower are depicted in Figure 5-18, Figure 5-19, and Figure 5-20, respectively.

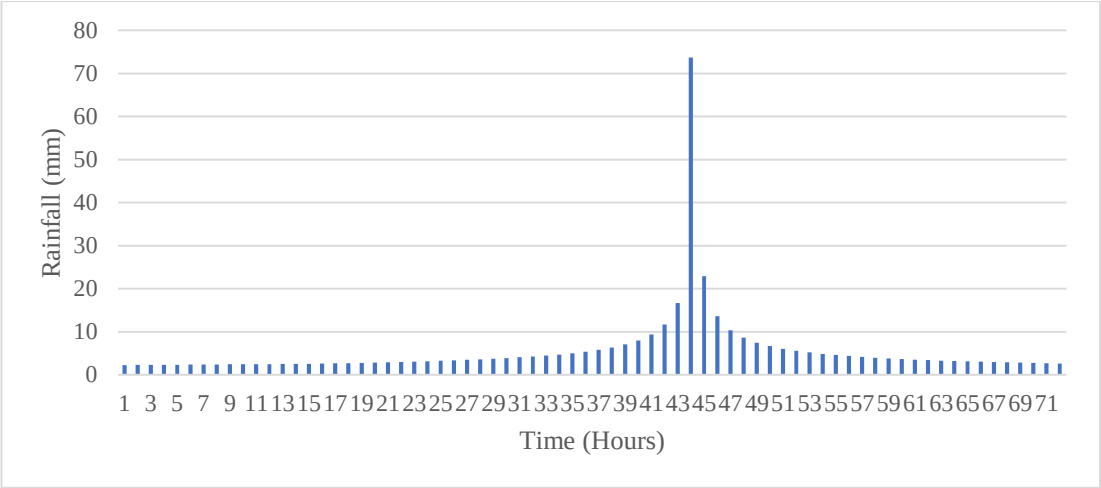

Figure 5-18: 8 Hours Shifted Design Rainfall for Kelani Upper

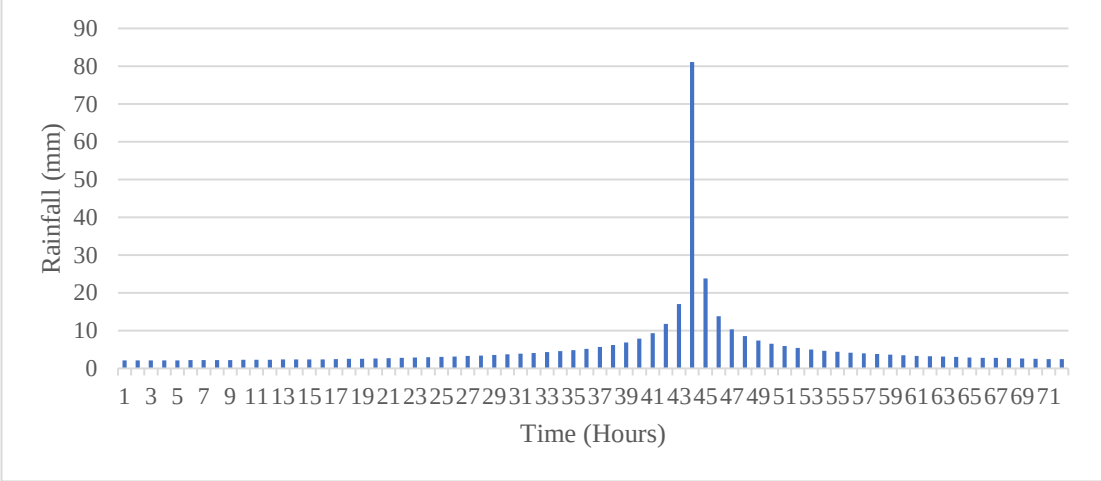

Figure 5-19: 8 Hours Shifted Design Rainfall for Kelani Middle

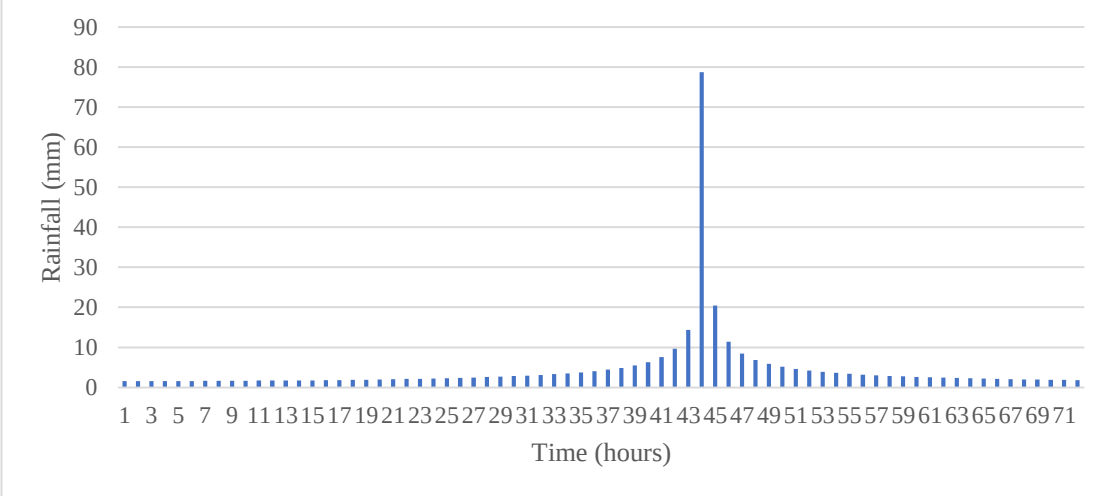

Figure 5-20: 8 Hours Shifted Design Rainfall for Kelani Lower

Table 5-14 presents a detailed description of the HEC-HMS model setups utilized for conducting design rainfall simulations in the Kelani Upper, Kelani Middle, and Kelani Lower Models. The design rainfall simulations employed the Simulation Run computation method, which provided forecasted time series discharges at Glencourse from the Kelani Upper Basin, sub basin runoff from Glencourse to Hanwella from the Kelani Middle model, and sub basin runoff from Hanwella to the sea from the Kelani Lower Model. These discharge outputs were subsequently utilized as inputs for the Flood model.

Table 5-14: HEC-HMS Model Setup for Design Rainfall Simulations

<table>
<tr><td>Model</td><td>Kelani-Upper</td><td>Kelani-Middle</td><td>Kelani-Lower</td></tr>
<tr><td rowspan="4">Elements</td><td rowspan="4">Subbasin: Kelani Upper SB</td><td>Source-1: Glencource Inflow</td><td>Source-2: Hanwella Inflow</td></tr>
<tr><td>Reach (Glen2Han):Glencourse to Hanwella Kelani River</td><td>Reach (Han2Sea):Hanwella to Sea Kelani River</td></tr>
<tr><td>Subbasin (Middle): Kelani Middle SB</td><td>Subbasin (Lower): Kelani Lower SB</td></tr>
<tr><td>Junction-1:Hanwella Outflow</td><td>Junction-2:Sea Outflow</td></tr>
<tr><td>Input Data</td><td colspan="3">Rainfall: Thiessen Weighted 50-year Design Rainfall with Areal Reduction Factor applied - For Upper Basin, Middle Basin and Lower Basin</td></tr>
<tr><td rowspan="4">Control Specification (Arbitrary 5 Day Simulation)</td><td colspan="3">Start Date: 01st Jan 2050</td></tr>
<tr><td colspan="3">Start Time: 00:00</td></tr>
<tr><td colspan="3">End Date: 06th Jan 2050</td></tr>
<tr><td colspan="3">End Time: 00:00</td></tr>
<tr><td>Computation Method</td><td colspan="3">Simulation Run</td></tr>
<tr><td>Outputs</td><td colspan="3">Time Series Simulated discharge of Glencourse (Kelai-Upper), Sub Basin Discharge of Middle Basin (Kelani-Middle), and Sub Basin Discharge of Lower Basin (Kelani-Lower)</td></tr>
</table>

5.1.6 Hydrological Model Simulations Considering Climate Change Projections

The climate change data available for the Kelani River Basin, as described in Chapter 2 of the literature review and presented in Figure 5-13 and Figure 5-14, were utilized to define the climate change scenario for the study. In this study, the flood modelling in the Kelani Basin was evaluated using three selected projections: RCP4.5, RCP6.0, and RCP8.5. These scenarios, which are representative concentration pathways (RCPs), serve to project future climate change based on varying levels of greenhouse gas emissions. RCP4.5 represents a

future where greenhouse gas emissions peak around 2040 and then decline, resulting in moderate mitigation of climate change. RCP6.0 assumes emissions peak around 2080 and gradually decreases, indicating a moderately higher level of emissions compared to RCP4.5. On the other hand, RCP8.5 represents a high-emission scenario with continuous increases throughout the 21st century, leading to more severe climate change impacts.

In the study conducted by Dorji et al. (2017), the authors examined the seasonal and monthly variations of temperature and precipitation using the SDSM and TDNN models. They analyzed the data from 1961 to 1990 and calculated the seasonal and monthly biases for both models, presenting them in graphical form. The study also included an average box plot to illustrate the seasonal variation. Additionally, Dorji et al. (2017) provided future climate change projections based on the median values for SDSM and TDNN models, considering the RCP4.5 and RDC8.5 scenarios for the 2020s, 2050s, and 2080s. However, the precipitation increasing factors shown in Figure 5-13 were not specified for specific seasons or months; instead, they were defined for annual projections. Consequently, the analysis of seasonal variation was not taken into account when applying the climate change rainfall increasing factors for design rainfall.

Variable	RCP	Models	2020's	2050's	2080's
Av. temp. (°C)	4.5	SDSM	0.14	0.91	1.24
		TDNN	0.15	0.99	1.39
	8.5	SDSM	0.14	1.39	2.83
		TDNN	0.14	1.54	3.03
Rainfall (%)	4.5	SDSM	0.7	10	13
		TDNN	0.3	20	29
	8.5	SDSM	5	14	33
		TDNN	4	11	63

Figure 5-21: Temperature and Rainfall Projections with Climate Change, Source: Dorji et al. (2017)

Return period	Pessimistic	Average	Optimistic
2YR	1.086	1.067	1.020
	RCP6_IPSL_CM5A_MR	RCP8.5_IPSL_CM5A_MR	RCP6_MIROC5
5YR	1.100	1.075	1.020
	RCP6_IPSL_CM5A_MR	RCP6_CSIRO_MK3_6_0	RCP6_MIROC5
10YR	1.108	1.076	1.020
	RCP6_IPSL_CM5A_MR	RCP6_CSIRO_MK3_6_0	RCP6_MIROC5
25YR	1.116	1.074	1.022
	RCP6_IPSL_CM5A_MR	RCP8.5_FIO_ESM	RCP6_MIROC5
50YR	1.122	1.079	1.024
	RCP6_IPSL_CM5A_MR	RCP6_CSIRO_MK3_6_0	RCP6_MIROC5
100YR	1.126	1.080	1.025
	RCP6_IPSL_CM5A_MR	RCP6_CSIRO_MK3_6_0	RCP6_MIROC5
200YR	1.130	1.081	1.026
	RCP6_IPSL_CM5A_MR	RCP6_CSIRO_MK3_6_0	RCP6_MIROC5

Figure 5-22: Rainfall Projections with Climate Change, Source: CRIP (2019)

The Rainfall Depth Increasing factors for various climate change projections were determined based on the data provided in Figure 5-13 and Figure 5-14. These factors represent the expected increase in rainfall depth under different scenarios. The specific details of these factors for each climate change projection can be found in Table 5-15.

Table 5-15: Selected Climate Change Projections and Rainfall Increasing Factors

Projection	**Rainfall Depth Increase Factor**	**Reference**	**Scenario**
RCP 4.5	1.100	Dorji et al. (2017)	2050-SDSM
RCP 6.0	1.122	CRIP (2019)	Pessimistic (50-year)
RCP 8.5	1.140	Dorji et al. (2017)	2050-TDNN

The Rainfall Depth Increasing factors, derived from different climate change projections, were employed to construct the 3-day 50-year return period design rainfall time series. These rainfall series were specifically developed for each sub-basin to facilitate design rainfall simulations considering the impact of climate change. Graphical representations of the constructed rainfall series can be observed in Figure 5-23, Figure 5-24, and Figure 5-25.

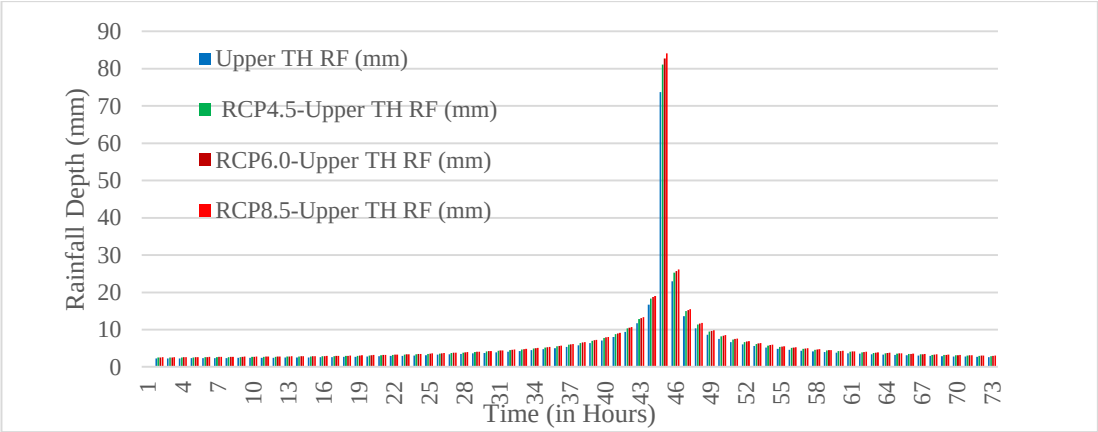

Figure 5-23: Comparison of 50-year 3-day Design Rainfall for CC Projections - Kelani Upper

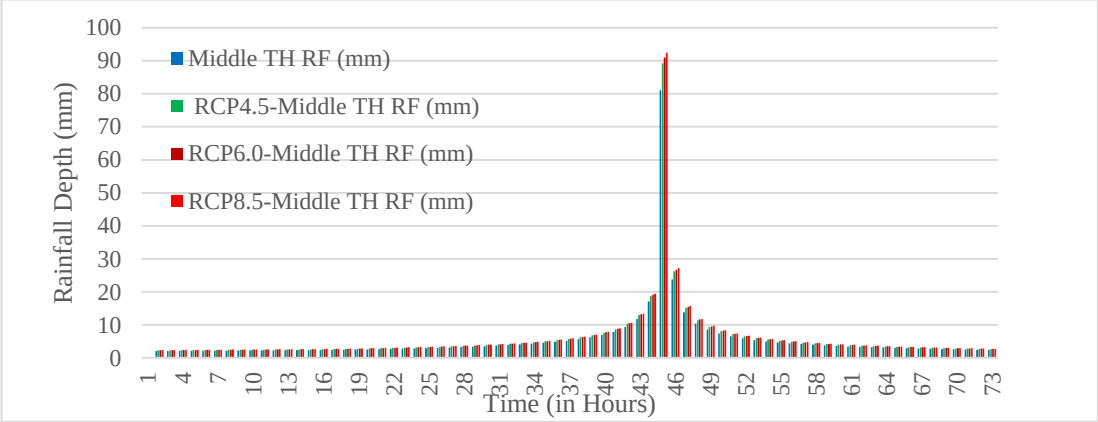

Figure 5-24: Comparison of 50-year 3-day Design Rainfall for CC Projections - Kelani Middle

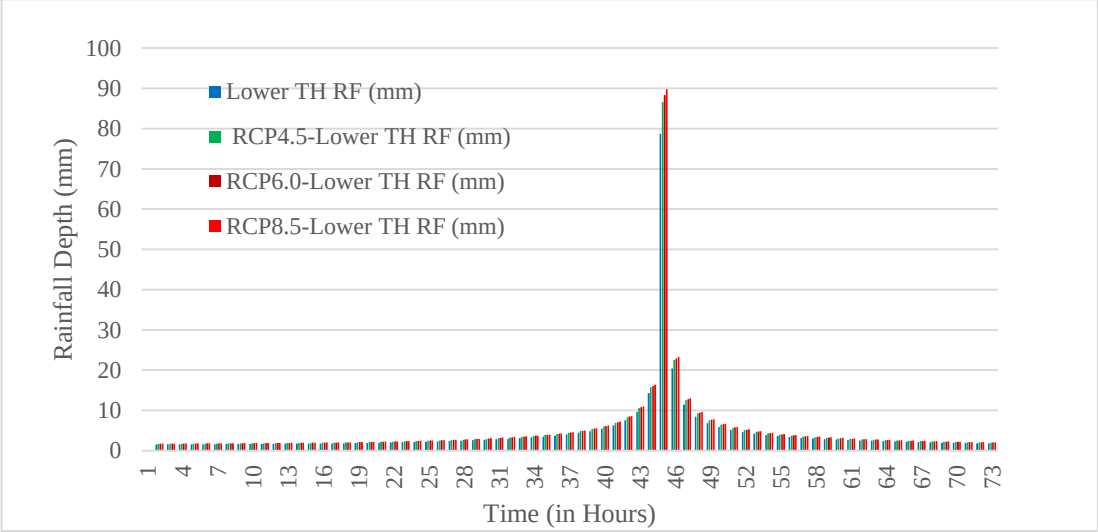

Figure 5-25: Comparison of 50-year 3-day Design Rainfall for CC Projections - Kelani Lower

Table 5-16 provides a comprehensive description of the HEC-HMS model setups used for design rainfall simulations, taking into account the climate change projections for the Kelani Upper, Kelani Middle, and Kelani Lower Models. These simulations employed the Simulation Run computation method to generate specific discharge outputs. These discharge outputs were then utilized as inputs for conducting Flood model simulations that incorporated the projected impacts of climate change.

Table 5-16: HEC-HMS model setups for Design Rainfall simulations with CC Projections

Model	Kelani-Upper	Kelani-Middle	Kelani-Lower
Elements	Subbasin: Kelani Upper SB	Source-1: Glencource Inflow	Source-2: Hanwella Inflow
		Reach (Glen2Han): Glencourse to Hanwella Kelani River	Reach (Han2Sea): Hanwella to Sea Kelani River
		Subbasin (Middle): Kelani Middle SB	Subbasin (Lower): Kelani Lower SB
		Junction-1:Hanwella Outflow	Junction-2:Sea Outflow
Input Data	Rainfall: RCP 2.6, RCP 6.0, and RCP 8.5 Climate Change Projected Thiessen Weighted 50-year Design Rainfall with Areal Reduction Factor applied - For Upper Basin, Middle Basin, and Lower Basin		
Control Specification (Arbitrary 5 Day Simulation)	Start Date: 01st Jan 2050		
	Start Time: 00:00		
	End Date: 06th Jan 2050		
	End Time: 00:00		
Computation Method	Simulation Run		
Outputs	Time Series Simulated discharge of Glencourse (Kelai-Upper), Sub Basin Discharge of Middle Basin (Kelani-Middle), and Sub Basin Discharge of Lower Basin (Kelani-Lower) for RCP 2.6, RCP 6.0, and RCP 8.5 Climate Change Projections		

5.2 Flood Model Development

HEC-RAS (Hydrologic Engineering Centers River Analysis System) is a widely used hydraulic modelling software developed by the U.S. Army Corps of Engineers. The 2D capabilities of HEC-RAS allow for a more accurate representation of flood flows and water movement, taking into account complex factors such as channel geometry, topography, and flow velocities. It enables the visualization and analysis of flood extents, depths, velocities,

and other flood-related parameters, aiding in flood risk assessment, floodplain mapping, and the development of effective flood management strategies.

5.2.1 HEC-RAS Model

Figure 5-26 depicts the 2D flow areas of the HEC-RAS 2D flood model, encompassing the Lower Kelani basin up to Glencourse. The model utilized 10 m resolution terrain raster data, generated from 1 m terrain data that included river bathymetry derived from surveyed river cross sections. A 100 m grid resolution was defined for the 2D perimeter mesh grid, while a 30 m grid resolution was applied to the River Flow area as refinement regions and flow separating boundaries. This allowed for more precise modelling by incorporating bunds, roads, and other brake lines. Additionally, a 10 m resolution Land Cover raster data was employed, which included Manning's N values for different land use types. Boundary conditions were defined to incorporate time series Discharge boundary conditions and water level conditions. This standardized model setup described in Table 5-17 was utilized for all flood model simulations, with adjustments made to the boundary conditions to account for different model scenarios.

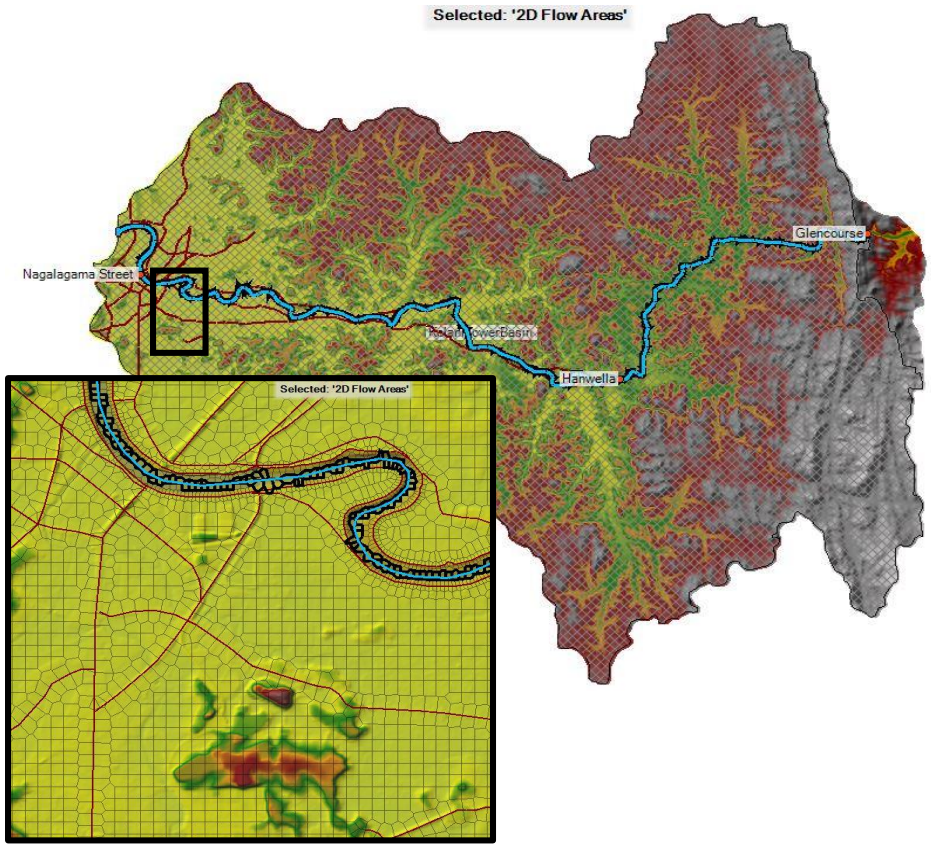

Figure 5-26: 2D Flow Area Grid of HEC-RAS Flood Model

Table 5-17: HEC-RAS Flood Model General Setup

Geometry (2D Flow Area)	Perimeters	Kelani Sub Basin Lower to Glencourse ; 100 m Grid	
	Refinement Regions	Kelani River Glencourse to Sea ; 30 m Grids	
	Breaklines	Kelani River Bunds, Roads, Barriers ; 30 m Grids	
Geometry Association	Terrain	DEM with Kelani River Bathymetry; 10 m Resolution	
	Land Cover	Manning's n associated Land Use Raster; 10 m Resolution	
Unsteady Flow (Boundary Conditions)	Inflow	Glencourse	Observed or HMS Simulated Discharge (Kelai Upper)
	Lateral Inflow	Glencourse to Hanwella	HMS Simulated Sub Basin Discharge (Kelani Middle)
		Hanwella to Sea	HMS Simulated Sub Basin Discharge (Kelani Lower)
	Outfall	Sea Outlet	Observed or Projected Sea Level (Stage Hydrograph)
Simulation (Plan)	Start Date	Past Flood events and Projected Simulations	
	Start Time		
	End Date		
	End Time		
Outputs	Time Series Flood Maps		
	Maximum Flood Depth and Water Surface Elevation Map		
	Simulated Discharge Hydrograph at Hanwella		
	Simulated Water Level Hydrograph at Hanwella and Nagalagama Street		

5.2.2 Parameter Sensitivity Analysis by HEC RAS

In reference to Annex 2 extracted from "Applied Hydrology" by Ven. T Chow (Chow et al., 1988), Manning's N roughness coefficients were assigned to different Land Use types. These coefficients provide a measure of the resistance to flow within each Land Use category. By defining specific Manning's N roughness values for each Land Use category, the hydrological model can more accurately simulate the flow behaviour. The Manning's N roughness values for each Land Use type are presented in Table 5-18.

Table 5-18: Estimated Manning's N Roughness values for Land Use types

Land Cover Type	Category	Manning's N Category	Manning's N
Coconut (C)	Agricultural Crops	Field Crops	0.04
Chena	Agricultural Crops	Field Crops	0.04
Other cultivation	Agricultural Crops	Field Crops	0.04
Rubber (R)	Agricultural Crops	Field Crops	0.04
Tea (T)	Agricultural Crops	Field Crops	0.04
Built up area	Built up area	Gravel Bottom / Riprap	0.035
Rock (RK)	Built up area	Gravel Bottom / Riprap	0.035
Forest - Unclassified (F)	Forest	Dense Trees	0.1
Scrub land	Forest	Dense Trees	0.1
Homesteads/Garden (G)	Garden	Light brush / Weeds	0.05
Sand	Garden	Light brush / Weeds	0.05
Marsh	Marsh	Winding with weeds and pools	0.05
Paddy (P)	Paddy	Dense Brush	0.07
Canal	Water Bodies	Clean straight Streams	0.03
Reservoir	Water Bodies	Clean straight Streams	0.03
Sea	Water Bodies	Clean straight Streams	0.03
Streams	Water Bodies	Clean straight Streams	0.03
Tank	Water Bodies	Clean straight Streams	0.03
Water holes area	Water Bodies	Clean straight Streams	0.03

After assessing Manning's N values for each Land Use category, referred to as baseline values, the sensitivity of the Flood model was evaluated through parameter sensitivity analysis simulations. In this process, systematic adjustment factors were applied to the baseline values to generate Manning's N value matrices used for the sensitivity analysis. These adjusted values are presented in Table 5-19. By examining the variations in Manning's N values, the sensitivity analysis helps to understand the impact of different parameter settings on the model's performance and provides insights into the sensitivity of the Flood model to changes in Manning's N values for different Land Use categories.

Table 5-19: Manning's N values used for Flood Model Parameter Sensitivity Analysis

Land Cover Category	**Manning's N**							
	n x (-50%)	**n x (-25%)**	**n**	**n x (+25 %)**	**n x (+50 %)**	**n x (+75 %)**	**n x (+100 %)**	**n x (+200 %)**
No Data	0.020	0.030	**0.040**	0.050	0.060	0.07	0.08	0.120
Built up area	0.018	0.026	**0.035**	0.044	0.053	0.06	0.07	0.105
Agricultural Crops	0.020	0.030	**0.040**	0.050	0.060	0.07	0.08	0.120
Water Bodies	0.015	0.023	**0.030**	0.038	0.045	0.05	0.06	0.090
Forest	0.050	0.075	**0.100**	0.125	0.150	0.18	0.2	0.300
Garden	0.025	0.038	**0.050**	0.063	0.075	0.09	0.1	0.150
Marsh	0.025	0.038	**0.050**	0.063	0.075	0.09	0.1	0.150
Paddy	0.035	0.053	**0.070**	0.088	0.105	0.12	0.14	0.210

Table 5-20 provides a comprehensive description of the Flood model setup used to assess the effect of Manning's N values on model sensitivity. The sensitivity of the model was evaluated through various metrics, including the Nash Coefficient, R^2 comparison for Hanwella Discharge, water levels at Hanwella and Nagalagama Street, and a comparison of observed and simulated hydrograph and water level graphs.

Table 5-20: HEC-RAS flood model setup used for Parameter Sensitivity Analysis

Land Cover	Manning's N Table was varied as Table 5-19		
Unsteady Flow (Boundary Conditions)	Inflow	Glencourse	2016 May Observed Glencourse discharge
	Lateral Inflow	Glencourse to Hanwella	2016 May HMS (Calibrated) Simulated Kelani-Middle Discharge
		Hanwella to Sea	2016 May HMS (Calibrated) Simulated Kelani-Lower Discharge
	Outfall	Sea Outlet	2016 May Observed Sea Level (Stage Hydrograph)
Simulation (Plan)	Start Date	13th May 2016	
	Start Time	00:00	
	End Date	23rd May 2016	
	End Time	00:00	
Model Outputs	2016 May Simulated Discharge Hydrograph at Hanwella		
	2016 May Simulated Water Level Hydrograph at Hanwella and Nagalagama Street		
Results	Nash Coefficient, R^2 Comparison for Hanwella Discharge, Water Levels of Hanwella and Nagalagama Street		
	Comparison of Observed and Simulated Hydrograph and Water Level Graphs		

5.2.3 Model Calibration

The Model sensitivity analysis identified Optimum Manning's N value column in Table 5-19, considering the Nash coefficient and R^2 values. These specific Manning's N values were chosen for the Flood Model Calibration process. The calibration utilized the observed and simulated discharge hydrograph at Hanwella, as well as the water level hydrograph at both Hanwella and Nagalagama Street, specifically focusing on the 2016 May Flood event. Table 5-21 provides a comprehensive description of the Flood model setup employed for the calibration process, including all the relevant details necessary for conducting the calibration accurately.

Table 5-21: HEC-RAS flood model setup used for Calibration

Land Cover	Selected Manning's N value column in Table 5-20 based on sensitivity analysis the Nash coefficient and R^2		
Unsteady Flow (Boundary Conditions)	Inflow	Glencourse	2016 May Observed Glencourse discharge
	Lateral Inflow	Glencourse to Hanwella	2016 May HMS (Calibrated) Simulated Kelani-Middle Discharge
		Hanwella to Sea	2016 May HMS (Calibrated) Simulated Kelani-Lower Discharge
	Outfall	Sea Outlet	2016 May Observed Sea Level (Stage Hydrograph)
Simulation (Plan)	Start Date	13th May 2016	
	Start Time	00:00	
	End Date	23rd May 2016	
	End Time	00:00	
Model Outputs	2016 May Simulated Maximum Flood Depth Map		
	2016 May Simulated Hydrograph at Hanwella, Water Level Hydrograph at Hanwella and Nagalagama Street		
Results	Nash Coefficient and R^2 for Hanwella Discharge, Water Levels of Hanwella and Nagalagama Street		
	Comparison of Observed and Simulated Hydrograph and Water Level Graphs		

5.2.4 Model Validation

The data from the 2017 May Flood event were utilized for the validation of the Flood model, as same as the Hydrological models. The Flood model, equipped with calibrated Manning's N values, was employed to simulate this specific flood event. As a result, the Nash Coefficient

and R^2 values for the Hanwella Discharge, as well as the water levels at Hanwella and Nagalagama Street, were obtained. These performance metrics serve as indicators of the model's accuracy and ability to capture the dynamics of the flood event. Table 5-22 provides a comprehensive description of the Flood model setup employed for the validation.

Table 5-22: HEC-RAS flood model setup used for Validation

Land Cover	Optimized Manning's n Table		
Unsteady Flow (Boundary Conditions)	Inflow	Glencourse	2017 May Observed Glencourse discharge
	Lateral Inflow	Glencourse to Hanwella	2017 May HMS (Calibrated) Simulated Kelani-Middle Discharge
		Hanwella to Sea	2017 May HMS (Calibrated) Simulated Kelani-Lower Discharge
	Outfall	Sea Outlet	2017 May Observed Sea Level (Stage Hydrograph)
Simulation (Plan)	Start Date	22nd May 2017	
	Start Time	00:00	
	End Date	29th May 2017	
	End Time	00:00	
Model Outputs	2017 May Simulated Maximum Flood Depth Map		
	2017 May Simulated Hydrograph at Hanwella, Water Level Hydrograph at Hanwella and Nagalagama Street		
Results	Nash Coefficient and R^2 for Hanwella Discharge, Water Levels of Hanwella and Nagalagama Street		
	Comparison of Observed and Simulated Hydrograph and Water Level Graphs		

5.2.5 Flood Model Simulation for Statistical Rain Event and Climate Change Projections

The Flood risk assessment study conducted as part of the Metro Colombo Urban Development Project focused on determining the design sea tide level necessary for simulating design flood events in the Flood modelling process. The findings of this study were utilized as the sea level boundary condition for the HEC-RAS model employed in this research, as shown in Figure 5-19.

The Intergovernmental Panel on Climate Change (IPCC) provided sea level rise forecasts for various climate change projections. Table 5-23 includes the sea level rise projections adopted in this study to adjust the sea level boundary conditions for the flood model. The resulting time series tide level graphs are presented in Figure 5-27.

Table 5-23: Sea Level Rising Factors for selected Climate Change Projections

Climate Change Projection	Sea Level Rising (m)
RCP 4.5	0.47
RCP 6.0	0.48
RCP 8.5	0.63

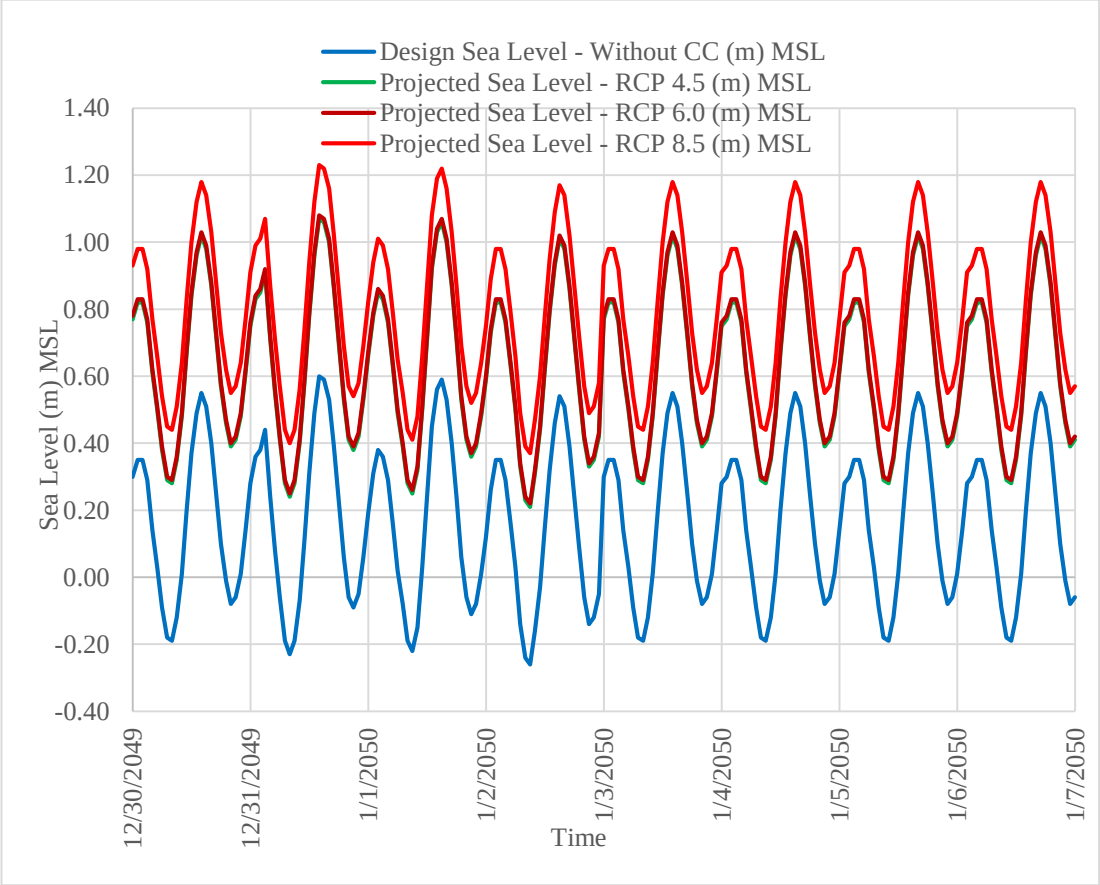

Figure 5-27: Design Sea Levels used for Design Rain event simulations as HEC-RAS Model Downstream Boundary Conditions

Table 5-24 presents a detailed overview of the Flood model setup utilized for simulating design rainfall events both without climate change projections and with climate change projections for selected scenarios. The simulations generated hydrographs for Hanwella, water level hydrographs for Hanwella and Nagalagama Street, as well as simulated maximum flood depth maps. These results provide valuable insights into the behaviour of the flood system under different rainfall conditions and climate change scenarios, aiding in the understanding of potential flood risks and informing effective mitigation strategies.

Table 5-24: HEC-RAS flood model setup used for Design Rainfall simulations with and without CC Projections

Land Cover	Optimized Manning's n Table		
Simulations	50-year. Design Rain without CC Projection, and with CC Projection for RCP 2.6, RCP 6.0, and RCP 8.5		
Unsteady Flow (Boundary Conditions)	Inflow	Glencourse	HMS (Calibrated) Simulated Glencourse discharge
	Lateral Inflow	Glencourse to Hanwella	HMS (Calibrated) Simulated Kelani-Middle Discharge
		Hanwella to Sea	HMS (Calibrated) Simulated Kelani-Lower Discharge
	Outfall	Sea Outlet	Projected Sea Level associated with CC Projections as presented in Table 5-23.
Simulation (Plan)	Start Date	30th Dec 2049	
	Start Time	00:00	
	End Date	06th Jan 2050	
	End Time	00:00	
Model Outputs	Simulated Maximum Flood Depth Maps		
	Hydrographs at Hanwella, Water Level Hydrographs at Hanwella and Nagalagama Street		

CHAPTER 6

6 RESULTS

This chapter presents the results of the hydrological modelling and flood modelling, encompassing various aspects such as model parameter sensitivity analysis, model calibration, model validation, and design rainfall event simulations conducted both with and without climate change projections. These results provide valuable insights into the behaviour and performance of the models, shedding light on their accuracy and reliability in simulating hydrological processes and flood events. By evaluating the sensitivity of model parameters, calibrating the models, validating their performance, and conducting design rainfall simulations, a comprehensive understanding of the hydrological and flood characteristics is achieved, aiding in effective flood risk management and mitigation strategies.

6.1 Hydrological Model Results

This section provides a description of the results obtained from the HEC HMS model for the three developed models, namely Kelani Upper, Kelani Middle, and Kelani Lower. The findings highlight the performance and outcomes of these models in simulating the hydrological processes within the respective areas.

6.1.1 Hydrological Model Parameter Sensitivity Analysis Results

Loss Method – SCS Curve Number: Curve Number

Table 6-1 illustrates the fluctuations in simulated peak discharge, Nash efficiency, and coefficient of determination (R^2) as they relate to the SCS Curve Number. Furthermore, Figure 6-1 visually represents the tabulated values, offering a graphical depiction of the relationship between the SCS Curve Number and the simulated peak discharge, Nash efficiency, and R^2. Additionally, Figure 6-2 provides a comprehensive comparison between the observed discharge and the behaviour of the entire simulated discharges, aiding in the evaluation and assessment of the model's performance.

Table 6-1: HEC-HMS Parameter Sensitivity Analysis Results - SCS Curve Number

Simulation No.	**1**	**2**	**3**	**4**	**5**	**6**	**7**	**8**	**9**	**10**	**11**
Curve Number	35	45	50	55	60	**65**	70	75	80	85	95
Peak Discharge (m^3/s)	1083	1221	1315	1415	1513	**1608**	1701	1791	1878	1962	2117
Nash	0.06	0.20	0.25	0.29	0.32	**0.34**	0.36	0.37	0.38	0.38	0.39
R^2	0.16	0.23	0.26	0.29	0.33	**0.36**	0.40	0.43	0.47	0.50	0.58

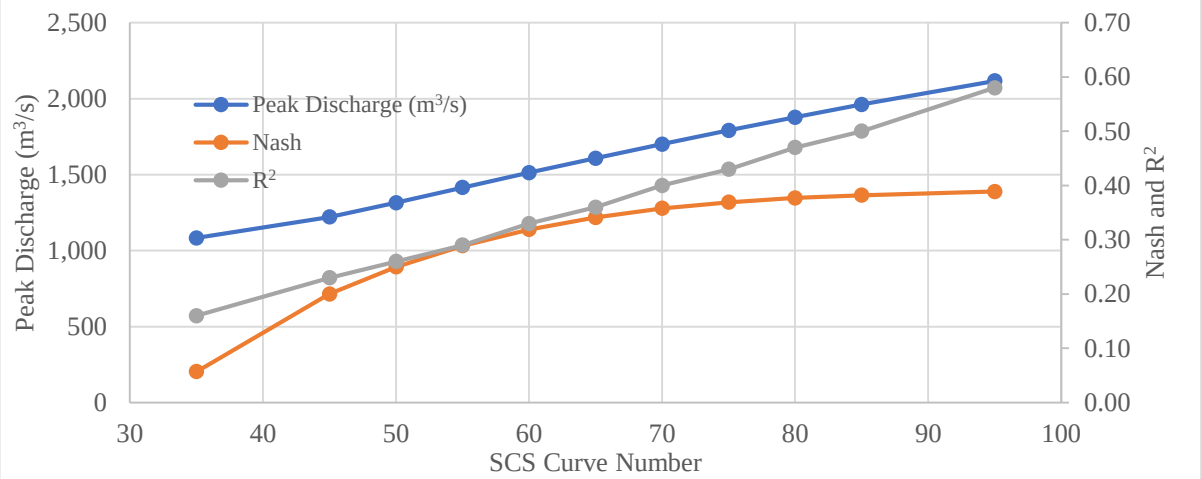

Figure 6-1: Comparison of Peak Discharge, Nash and R^2 with SCS Curve Number

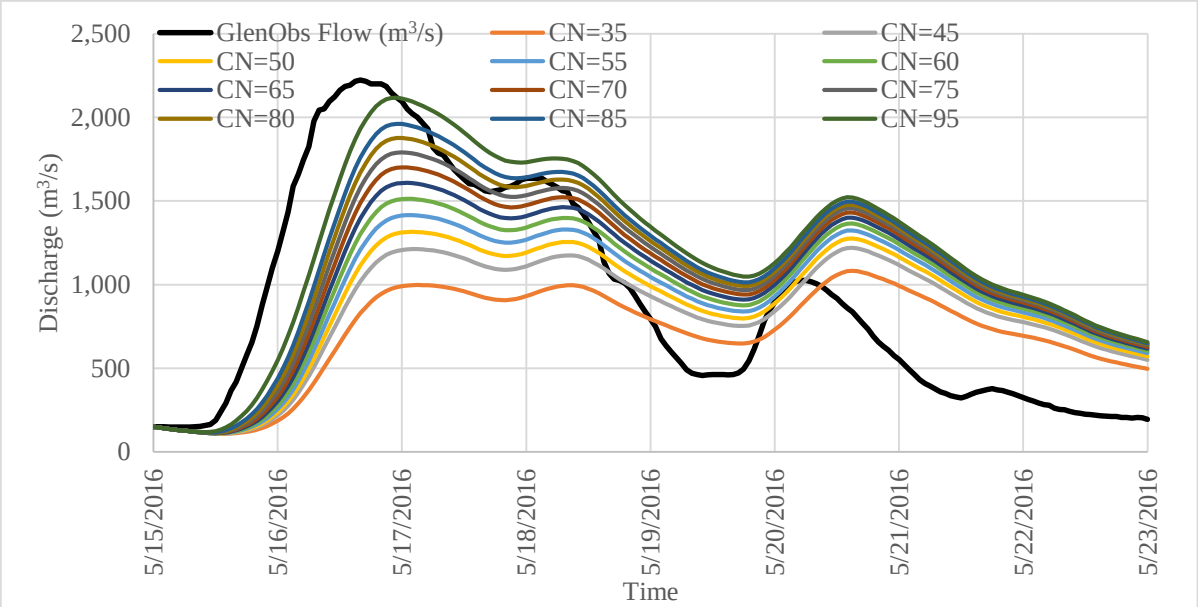

Figure 6-2: Observed Discharges comparison with Simulated discharges varies with SCS Curve Number

Based on the obtained results, it has been determined that the SCS curve number is the most sensitive parameter that significantly impacts the peak discharge, Nash efficiency, and coefficient of determination (R^2). Thus, the SCS curve number emerges as a critical parameter to consider and calibrate in hydrological modelling.

Loss Method – SCS Curve Number: Initial Abstraction

Table 6-2 presents the variations in simulated peak discharge, Nash efficiency, and coefficient of determination (R^2) with respect to the Initial Abstraction. The graphical representation of these values is depicted in Figure 6-3, providing a visual understanding of the correlation between the Initial Abstraction and the simulated peak discharge, Nash efficiency, and R^2. Furthermore, Figure 6-4 offers a comprehensive comparison between the observed discharge and the overall behaviour of the simulated discharges, facilitating a thorough evaluation and assessment of the model's performance.

Table 6-2: HEC-HMS Parameter Sensitivity Analysis Results - Initial Abstraction

Simulation No	**1**	**2**	**3**	**4**	**5**	**6**	**7**	**8**	**9**	**10**	**11**
Initial Abstraction (mm)	0	1	2	3	4	**5**	6	7	8	9	10
Peak Discharge (m^3/s)	1634	1629	1624	1618	1613	**1608**	1603	1598	1593	1588	1583
Nash	0.36	0.35	0.35	0.35	0.34	**0.34**	0.34	0.34	0.33	0.33	0.33
R^2	0.38	0.38	0.37	0.37	0.37	**0.36**	0.36	0.35	0.35	0.35	0.34

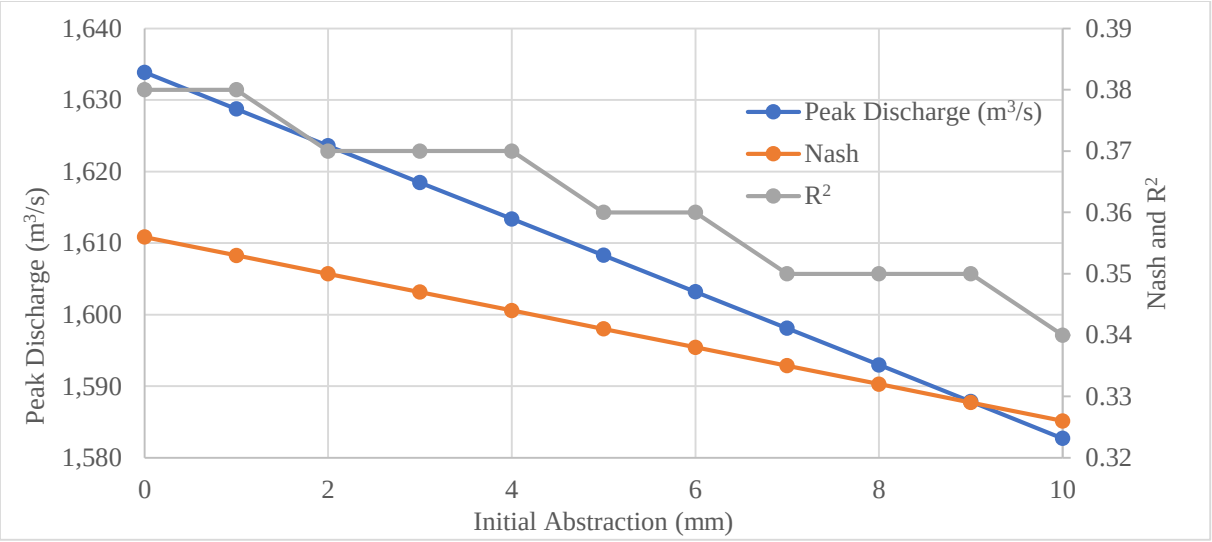

Figure 6-3: Comparison of Peak Discharge, Nash and R^2 with Initial Abstraction

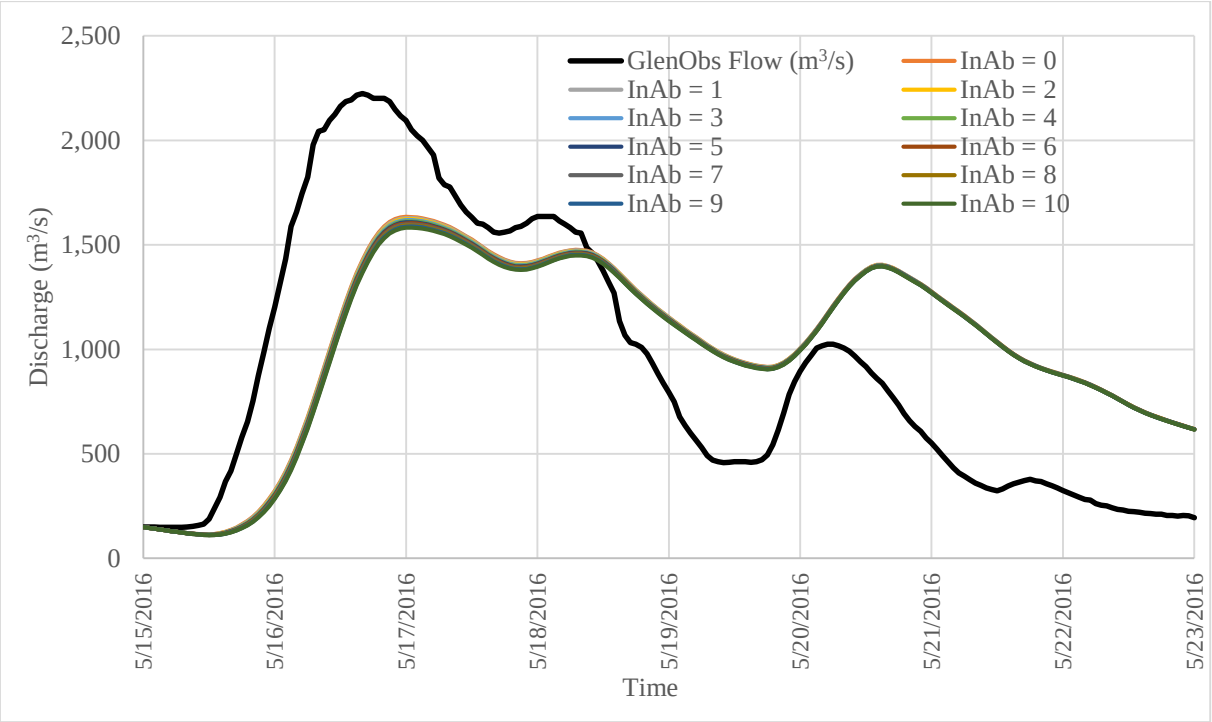

Figure 6-4: Observed Discharges comparison with Simulated discharges varies with Initial Abstraction

Based on the results obtained, it has been concluded that the Initial Abstraction is not a sensitive parameter and does not have a significant impact on the peak discharge, Nash efficiency, and coefficient of determination (R^2).

Transform Method – Clark Unit Hydrograph: Time of Concentration (*Tc*)

Table 6-3 displays the variations in simulated peak discharge, Nash efficiency, and coefficient of determination (R^2) in relation to the time of concentration (*Tc*). To provide a visual representation of these variations, Figure 6-5 presents the graphical depiction of the correlation between *Tc* and the simulated peak discharge, Nash efficiency, and R^2. Additionally, Figure 6-6 provides a comprehensive comparison between the observed discharge and the overall behaviour of the simulated discharges.

Table 6-3: HEC-HMS Parameter Sensitivity Analysis Results - Time of Concentration (*Tc*)

Simulation No.	**1**	**2**	**3**	**4**	**5**	**6**	**7**	**8**	**9**	**10**	**11**
Tc (HR)	5	8	11	14	17	**20**	23	26	29	32	35
Peak Discharge (m^3/s)	1651	1641	1634	1626	1616	**1608**	1601	1591	1577	1561	1544
Nash	0.62	0.58	0.53	0.48	0.41	**0.34**	0.27	0.19	0.11	0.04	-0.04
R^2	0.67	0.62	0.56	0.50	0.43	**0.36**	0.30	0.24	0.18	0.14	0.10

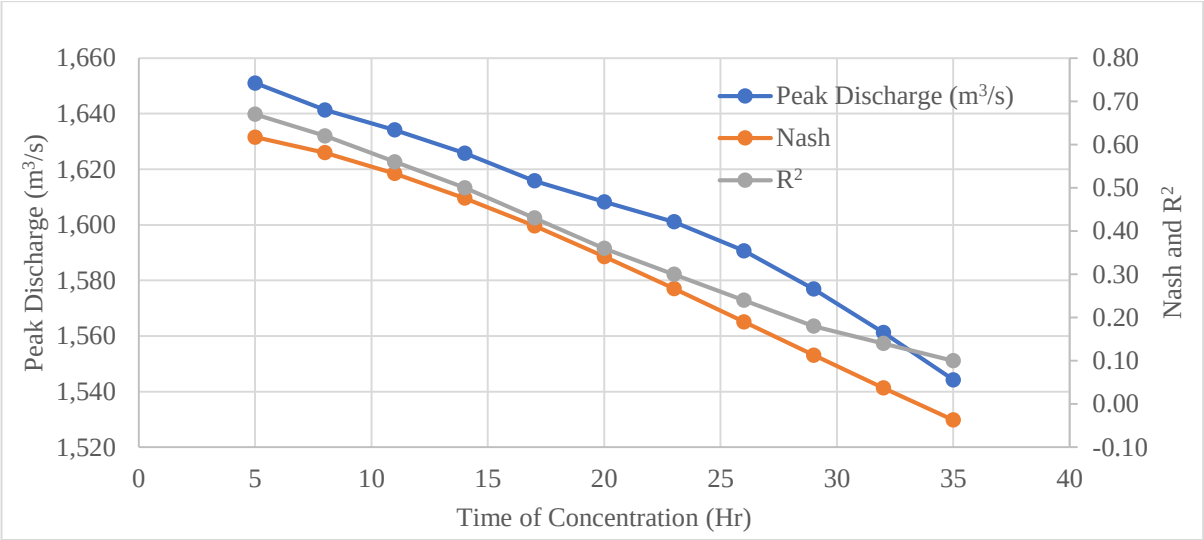

Figure 6-5: Comparison of Peak Discharge, Nash and R^2 with Time of Concentration (*Tc*)

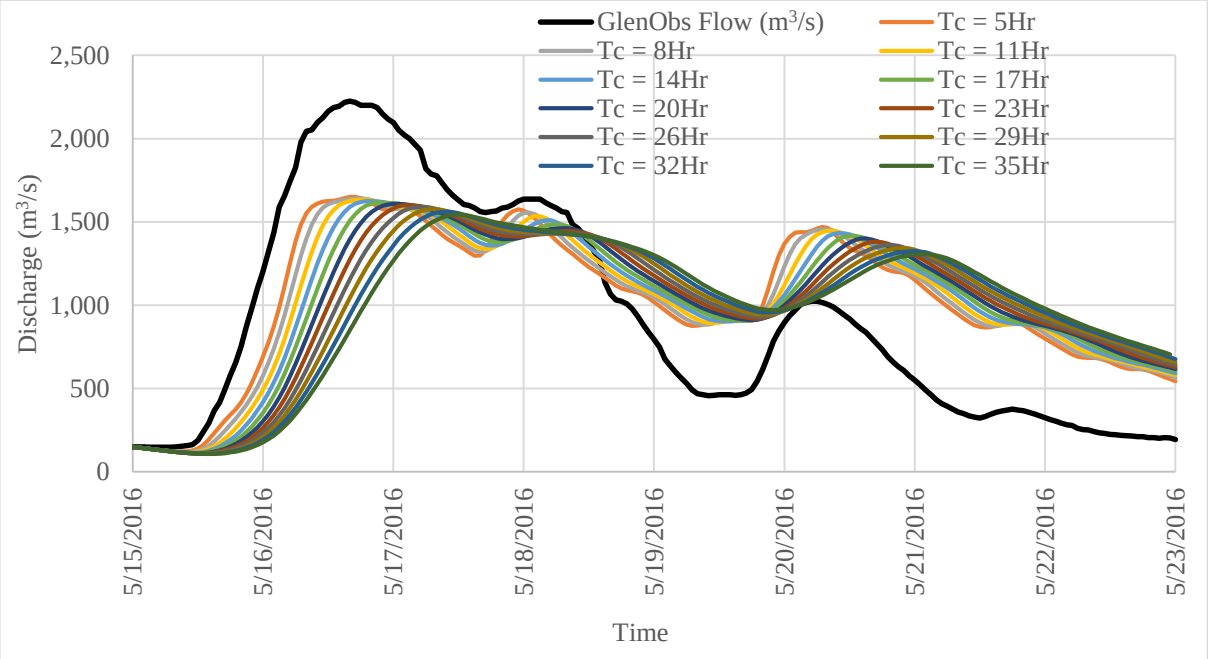

Figure 6-6: Observed Discharges comparison with Simulated discharges varies with Time of Concentration

The obtained results reveal that the time of concentration (*Tc*) is a highly sensitive parameter that has a significant impact on the peak discharge, Nash efficiency, and coefficient of determination (R^2). This finding emphasizes the importance of considering and calibrating the *Tc* parameter in hydrological modelling.

Transform Method – Clark Unit Hydrograph: Storage Coefficient

Table 6-4 provides a comprehensive overview of the fluctuations in simulated peak discharge, Nash efficiency, and coefficient of determination (R^2) with respect to the Storage Coefficient. To better visualize these variations, Figure 6-7 presents a graphical representation illustrating the relationship between the Storage Coefficient and the simulated peak discharge, Nash efficiency, and R^2. Furthermore, Figure 6-8 offers a comprehensive comparison between the observed discharge and the overall behaviour of the simulated discharges, allowing for a thorough evaluation and assessment of the model's performance.

Table 6-4: HEC-HMS Parameter Sensitivity Analysis Results - Storage Coefficient

Simulation No.	**1**	**2**	**3**	**4**	**5**	**6**	**7**	**8**	**9**	**10**	**11**
Storage Coefficient (HR)	10	16	22	28	34	**40**	46	52	58	64	70
Peak Discharge (m^3/s)	3252	2703	2307	2012	1786	**1608**	1466	1350	1283	1246	1210
Nash	0.30	0.57	0.61	0.53	0.44	**0.34**	0.25	0.18	0.11	0.05	-0.01
R^2	0.70	0.72	0.68	0.58	0.47	**0.36**	0.27	0.20	0.14	0.10	0.06

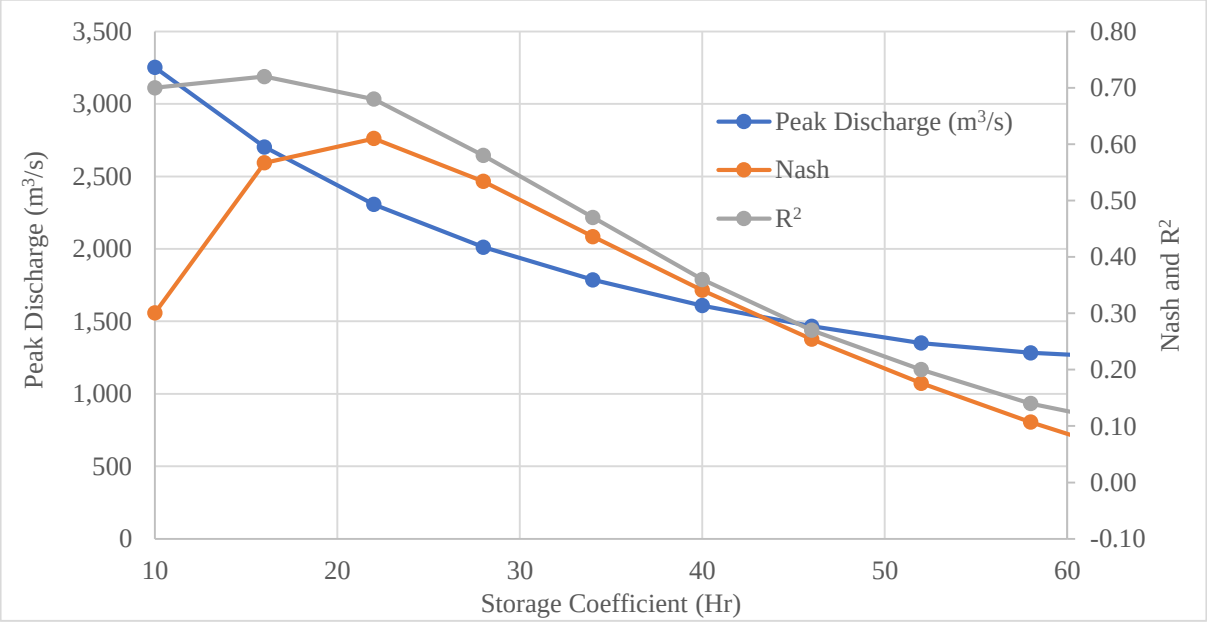

Figure 6-7: Comparison of Peak Discharge, Nash and R^2 with Storage Coefficient

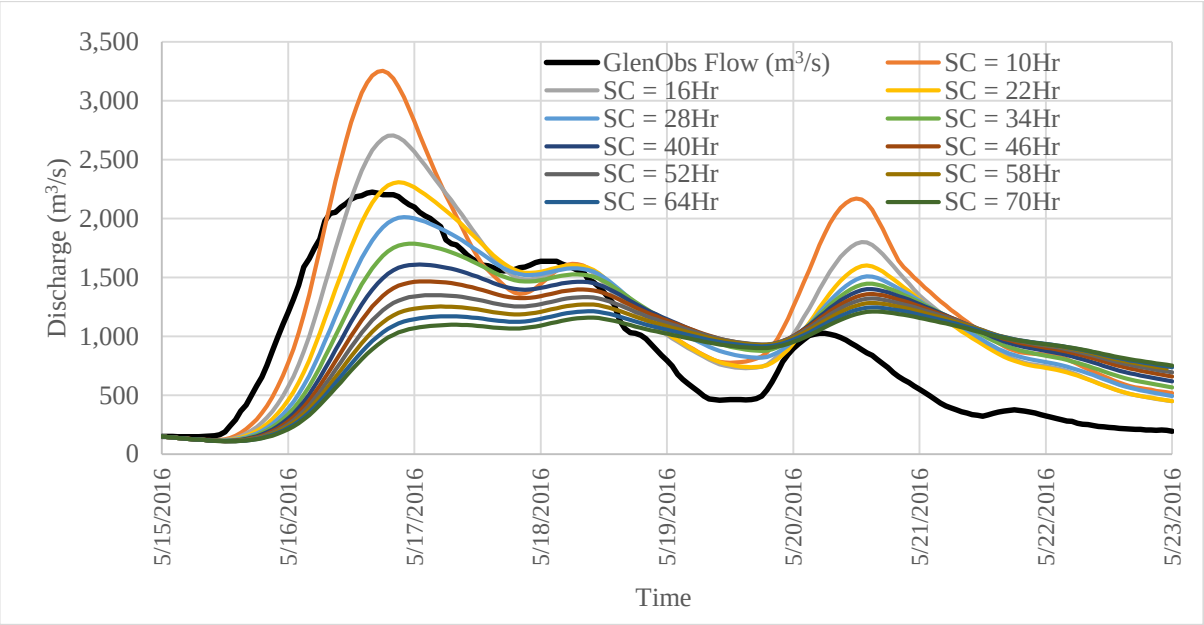

Figure 6-8: Observed Discharges comparison with Simulated discharges varies with Storage Coefficient

Based on the obtained results, it is evident that the Storage Coefficient is a critical and highly influential parameter that significantly affects the peak discharge, Nash efficiency, and coefficient of determination (R^2). These findings underscore the importance of carefully considering and accurately calibrating the Storage Coefficient in hydrological modelling.

Base Flow Method – Recession: Recession Constant

Table 6-5 offers a comprehensive overview of the variations observed in simulated peak discharge, Nash efficiency, and coefficient of determination (R^2) in relation to the Recession Constant. To provide a more visual understanding of these fluctuations, Figure 6-9 presents a graphical representation that showcases the correlation between the Recession Constant and the simulated peak discharge, Nash efficiency, and R^2. Additionally, Figure 6-10 enables a comprehensive comparison between the observed discharge and the overall behaviour of the simulated discharges, facilitating a thorough evaluation and assessment of the model's performance.

Table 6-5: HEC-HMS Parameter Sensitivity Analysis Results - Recession Constant

Simulation No.	**1**	**2**	**3**	**4**	**5**	**6**	**7**	**8**	**9**	**10**	**11**
Recession Constant	0.01	0.1	0.2	0.3	0.4	**0.5**	0.6	0.7	0.8	0.9	1
Peak Discharge (m^3/s)	1572	1573	1577	1585	1595	**1608**	1625	1644	1667	1693	1722
Nash	0.30	0.30	0.31	0.32	0.33	**0.34**	0.35	0.35	0.32	0.28	0.19
R^2	0.32	0.33	0.33	0.34	0.35	**0.36**	0.37	0.38	0.37	0.35	0.31

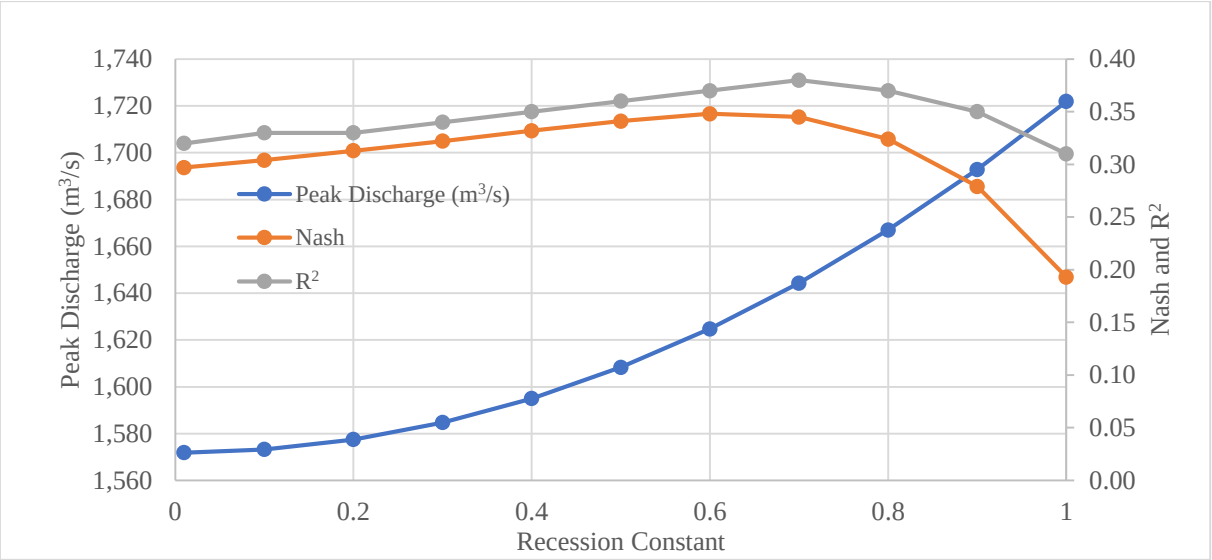

Figure 6-9: Comparison of Peak Discharge, Nash and R^2 with Recession Constant

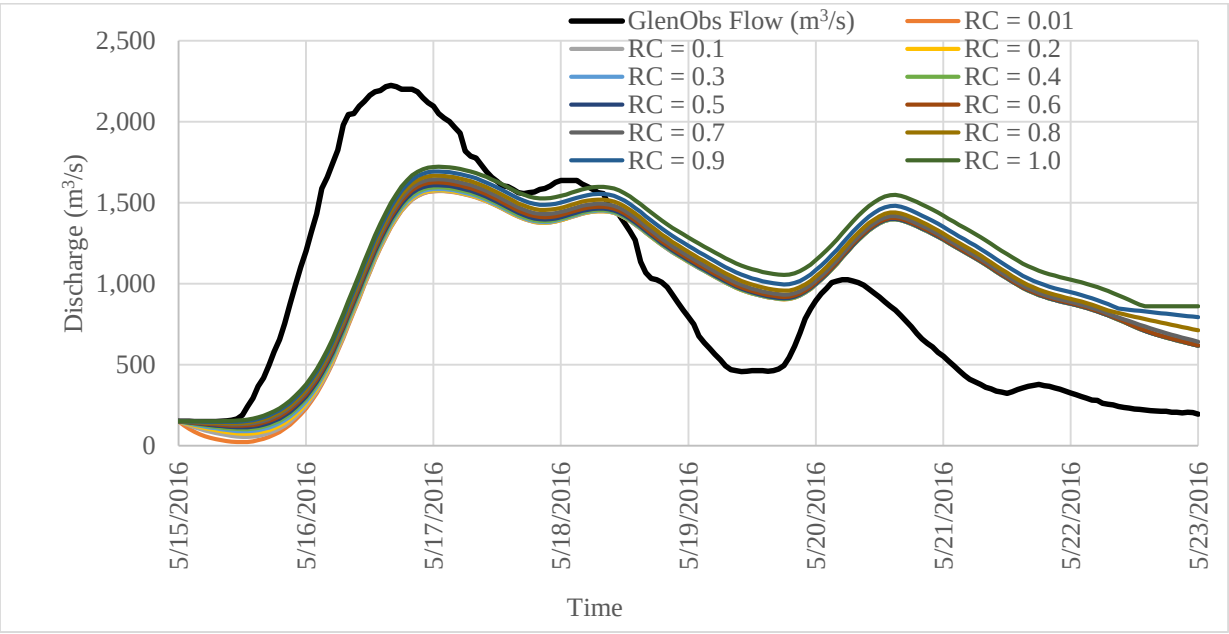

Figure 6-10: Observed Discharges comparison with Simulated discharges varies with Recession Constant

Based on the results obtained, it is evident that the Recession Constant is a parameter with relatively minor influence that does not significantly impact the peak discharge, Nash efficiency, and coefficient of determination (R^2).

Base Flow Method – Recession: Ratio to Peak

Table 6-6 provides a comprehensive overview of the observed variations in simulated peak discharge, Nash efficiency, and coefficient of determination (R^2) with respect to the Ratio to Peak. To enhance the visual understanding of these fluctuations, Figure 6-11 presents a graphical representation that illustrates the relationship between the Ratio to Peak and the simulated peak discharge, Nash efficiency, and R^2.

Furthermore, Figure 6-12 allows for a comprehensive comparison between the observed discharge and the overall behaviour of the simulated discharges, enabling a thorough evaluation and assessment of the model's performance.

Table 6-6: HEC-HMS Parameter Sensitivity Analysis Results - Ratio to Peak

Simulation No.	**1**	**2**	**3**	**4**	**5**	**6**	**7**	**8**	**9**	**10**	**11**
Ratio	0	0.1	0.2	0.3	0.4	**0.5**	0.6	0.7	0.8	0.9	1
Peak Discharge (m^3/s)	1608	1608	1608	1608	1608	**1608**	1608	1608	1608	1608	1608
Nash	0.34	0.34	0.34	0.34	0.34	**0.34**	0.34	0.34	0.34	0.34	0.34
R^2	0.36	0.36	0.36	0.36	0.36	**0.36**	0.36	0.36	0.36	0.36	0.36

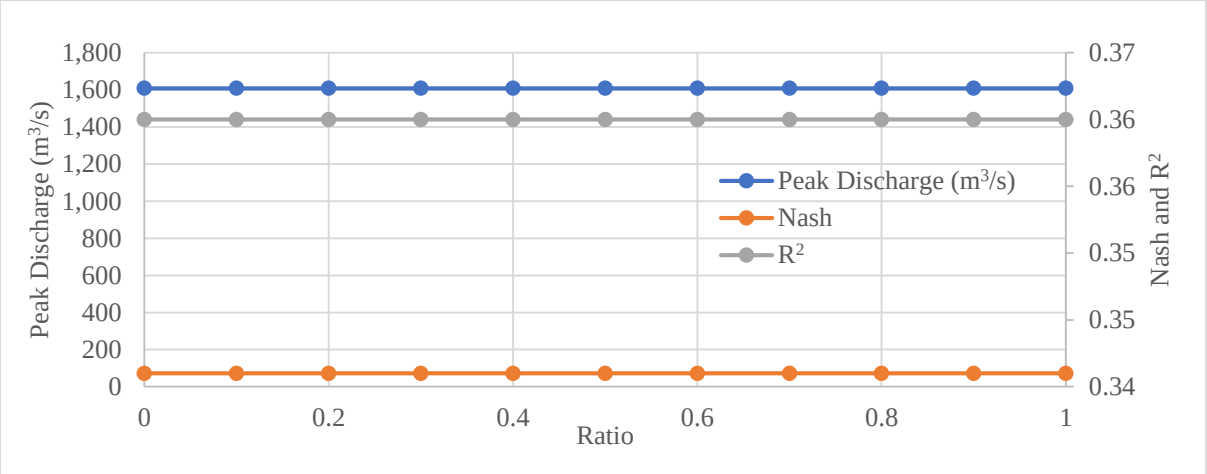

Figure 6-11: Comparison of Peak Discharge, Nash and R^2 with Ratio to Peak

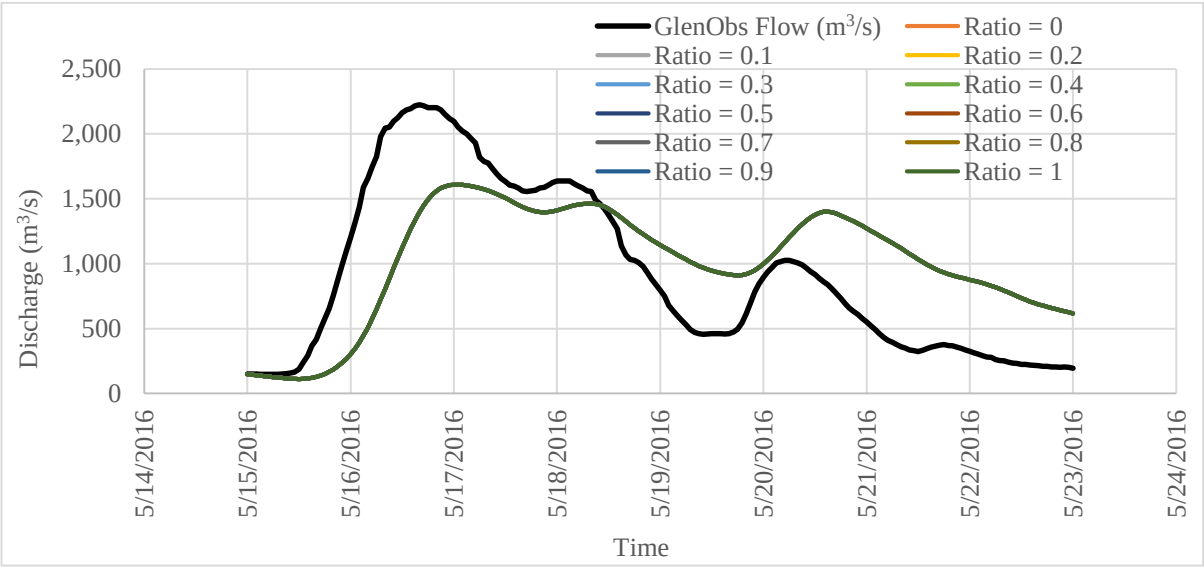

Figure 6-12:Observed Discharges comparison with Simulated discharges varies with Ratio to Peak

The results obtained from the analysis lead to the conclusion that the Ratio to Peak is not a sensitive parameter and does not exert a significant influence on the peak discharge, Nash efficiency, and coefficient of determination (R^2).

Reach Routing Method – Muskingum *K*

The observed variations in simulated peak discharge, Nash efficiency, and coefficient of determination (R^2) in relation to the Muskingum *K* are comprehensively presented in Table 6-7. To further enhance the understanding of these fluctuations, Figure 6-13 visually depicts the correlation between the Muskingum *K* and the simulated peak discharge, Nash efficiency, and R^2. Moreover, Figure 6-14 enables a comprehensive comparison between the observed discharge and the overall behaviour of the simulated discharges, facilitating a thorough evaluation and assessment of the model's performance.

Table 6-7: HEC-HMS Parameter Sensitivity Analysis Results - Muskingum K

Simulation No.	**1**	**2**	**3**	**4**	**5**	**6**	**7**	**8**	**9**	**10**	**11**
Muskingum - *K* (Hr)	0.1	1	5	10	15	**20**	25	30	35	40	50
Peak Discharge (m^3/s)	2225	2218	2156	2003	1852	**1711**	1600	1545	1487	1431	1328
Nash	-1.02	-0.94	-0.58	-0.20	0.07	**0.23**	0.32	0.35	0.33	0.27	0.10
R^2	0.40	0.43	0.55	0.66	0.74	**0.80**	0.83	0.85	0.84	0.83	0.77

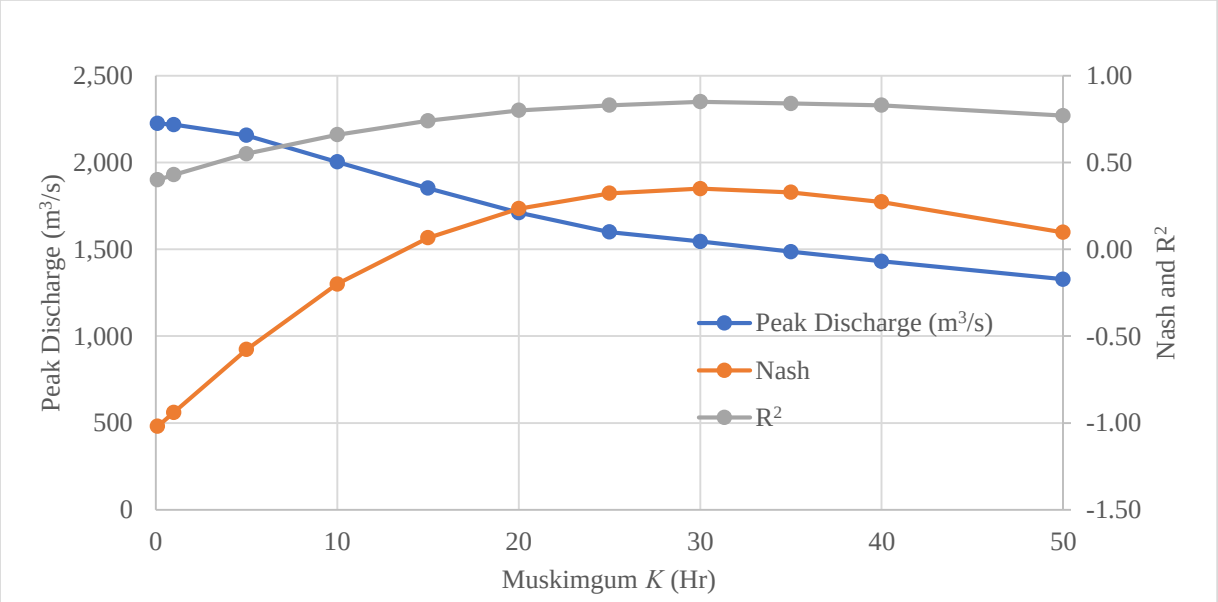

Figure 6-13: Comparison of Peak Discharge, Nash and R^2 with Muskingum *K*

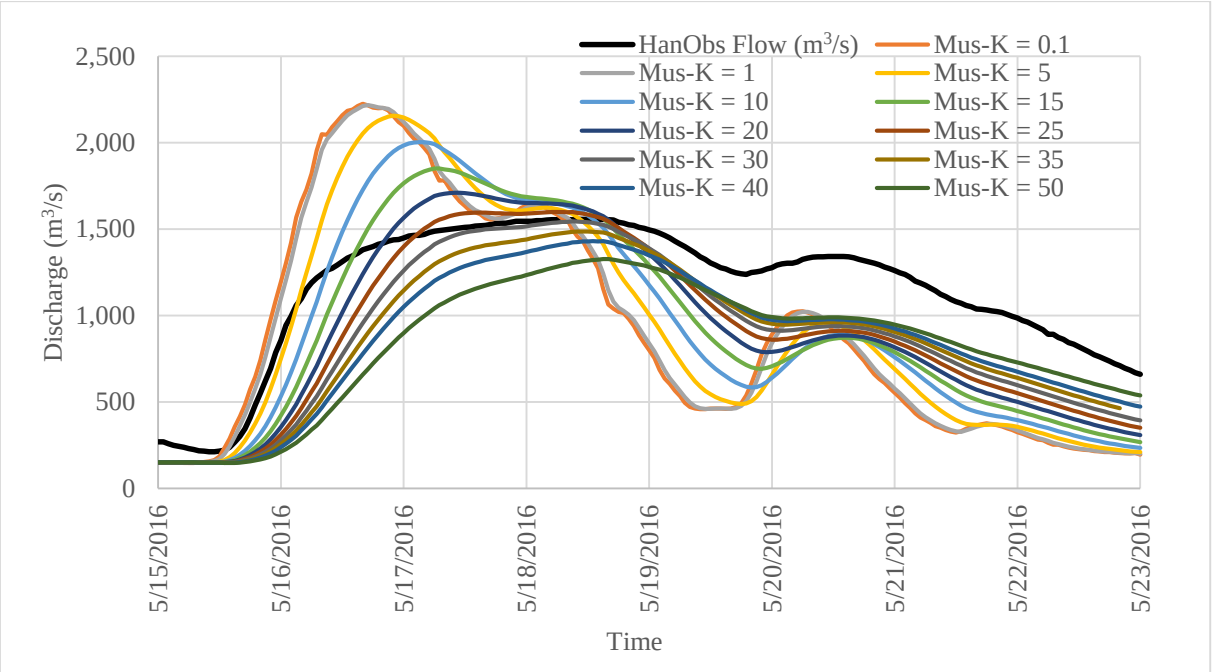

Figure 6-14: Observed Discharges comparison with Simulated discharges varies with Muskingum *K*

The results obtained clearly demonstrate the critical and highly influential role of the Muskingum *K* parameter in hydrological modelling. It is evident that the Muskingum *K* has a significant impact on the peak discharge, Nash efficiency, and coefficient of determination (R^2).

Reach Routing Method – Muskingum *X*

Table 6-8 provides a comprehensive presentation of the observed variations in simulated peak discharge, Nash efficiency, and coefficient of determination (R^2) with respect to the Muskingum *X* parameter. To enhance the understanding of these fluctuations, Figure 6-15 visually illustrates the relationship between the Muskingum *X* and the simulated peak discharge, Nash efficiency, and R^2. Additionally, Figure 6-16 allows for a comprehensive comparison between the observed discharge and the overall behaviour of the simulated discharges, enabling a thorough evaluation and assessment of the model's performance.

Table 6-8: HEC-HMS Parameter Sensitivity Analysis Results - Muskingum *X*

Simulation No.	**1**	**2**	**3**	**4**	**5**	**6**	**7**	**8**	**9**	**10**	**11**
Muskingum - *X*	0.001	0.01	0.02	0.03	0.04	**0.05**	0.1	0.2	0.3	0.4	0.5
Peak Discharge (m^3/s)	1685	1689	1695	1700	1706	**1711**	1741	1811	1896	1997	2125
Nash	0.26	0.26	0.25	0.25	0.24	**0.23**	0.20	0.11	-0.03	-0.22	-0.44
R^2	0.80	0.80	0.80	0.80	0.80	**0.80**	0.79	0.76	0.74	0.70	0.67

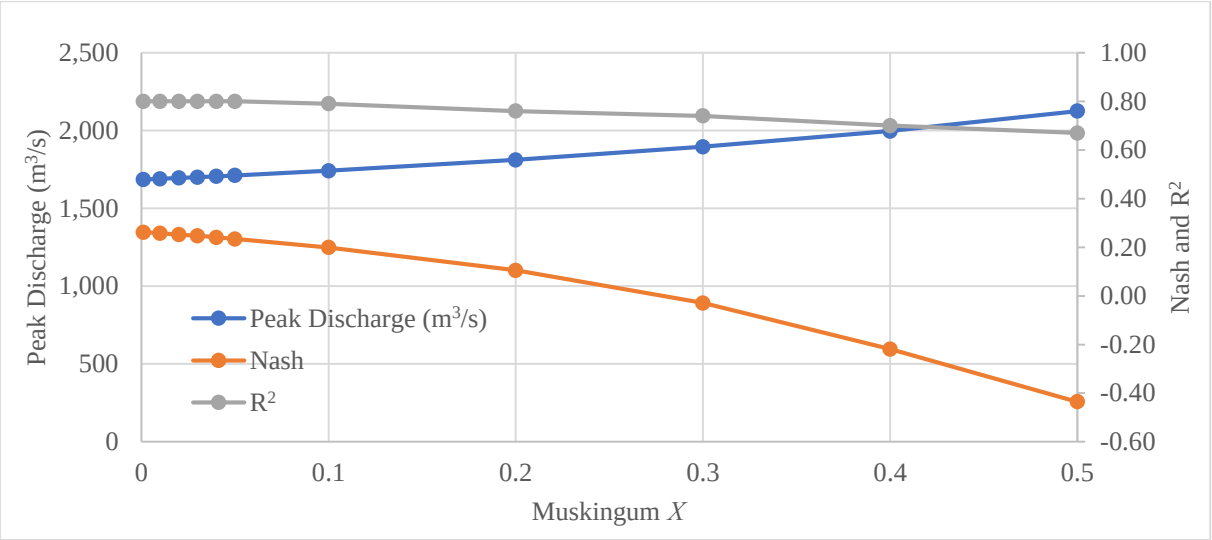

Figure 6-15: Comparison of Peak Discharge, Nash and R^2 with Muskingum *X*

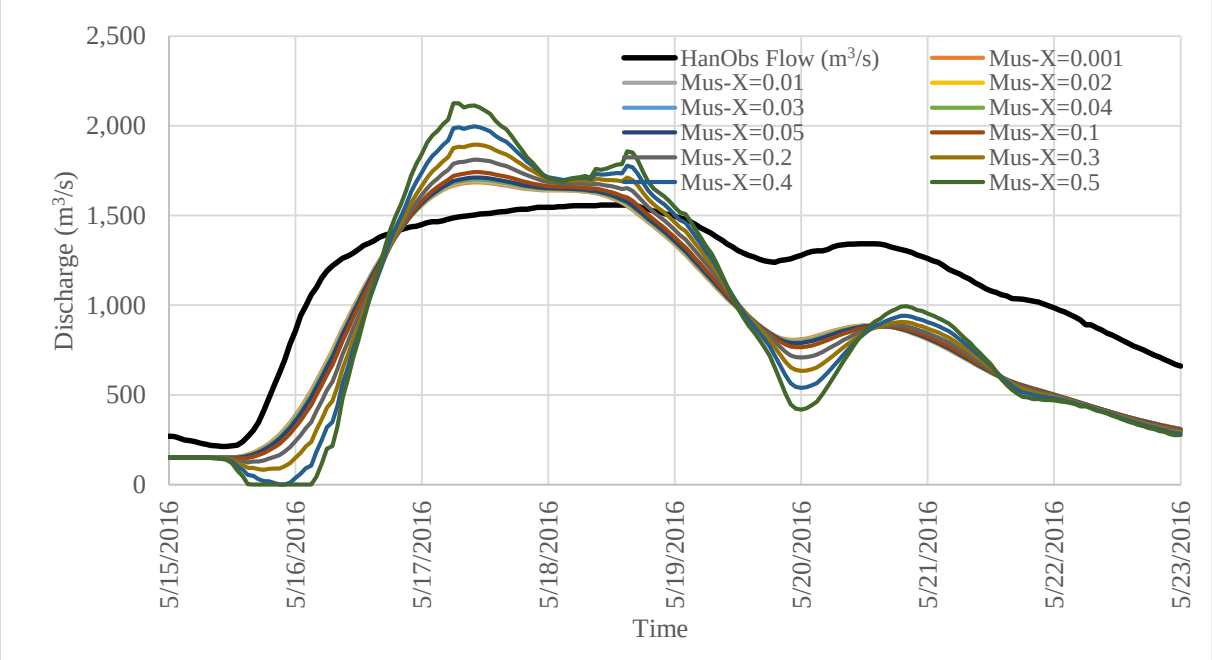

Figure 6-16: Observed Discharges comparison with Simulated discharges varies with Muskingum *X*

The results obtained provide clear evidence of the critical and highly influential role of the Muskingum *K* parameter in hydrological modelling. It is evident that the Muskingum *K* parameter exerts a significant impact on key performance indicators such as peak discharge, Nash efficiency, and coefficient of determination (R^2).

6.1.2 Hydrological Model Calibration and Validation Results

Table 6-9 provides an overview of the calibrated HEC-HMS model parameters for each specific element in three model setups: Kelani Upper, Kelani Middle, and Kelani Lower models.

Table 6-9: Calibrated Parameter Values of HEC-HMS Models

Element	Optimized Parameter Values	Model		
		Kelani-Upper	**Kelani-Middle**	**Kelani-Lower**
Subbasin	**Loss : SCS Curve Number**			
	Initial Abstraction (mm)	0.109	0.136	0.201
	Curve Number	54.8	75.0	72.8
	Impervious (%)	5	10	15
	Transform : Clark Unit Hydrograph			
	Time of Concentration (Hr)	12.00	5.71	13.02
	Storage Coefficient	18.45	13.33	26.21
	Baseflow : Recession			
	Initial Discharge (m^3/s)	150	116	50
	Recession Constant	0.623	0.828	0.500
	Ratio to Peak	0.108	0.374	0.200
Reach	**Routing : Muskingum**			
	Muskingum *K* (Hr)		42.06	72.77
	Muskingum *X*		0.0011	0.0012

Table 6-10 presents the performance of model calibration and validation, assessed through metrics such as Nash efficiency and coefficient of determination. The results indicate that all three models performed well during the calibration phase. Moreover, both the Kelani Upper and Kelani Middle models demonstrated strong performance during the validation process. However, the Kelani Lower basin exhibited lower Nash efficiency, indicating some room for improvement. Nonetheless, the coefficient of determination demonstrated satisfactory performance, suggesting that the model adequately captures the observed data.

Table 6-10: HEC-HMS Models performance Evaluation results for Calibration and Validation

Model	Objective Function			
	Calibration		Validation	
	Nash	**R^2**	**Nash**	**R^2**
Kelani-Upper	0.79	0.82	0.871	0.94
Kelani-Middle	0.95	0.95	0.853	0.95
Kelani-Lower	0.85	0.85	0.251	0.89

Figure 6-17 illustrates the graphical outputs of the HEC-HMS results for various scenarios. Subfigure (a1) represents the calibration results for the Kelani Upper model, while subfigure (a2) showcases the validation results for the same model. Similarly, subfigures (b1) and (b2) correspond to the calibration and validation results, respectively, for the Kelani Middle model. Lastly, subfigures (c1) and (c2) display the calibration and validation results, respectively, for the Kelani Lower model.

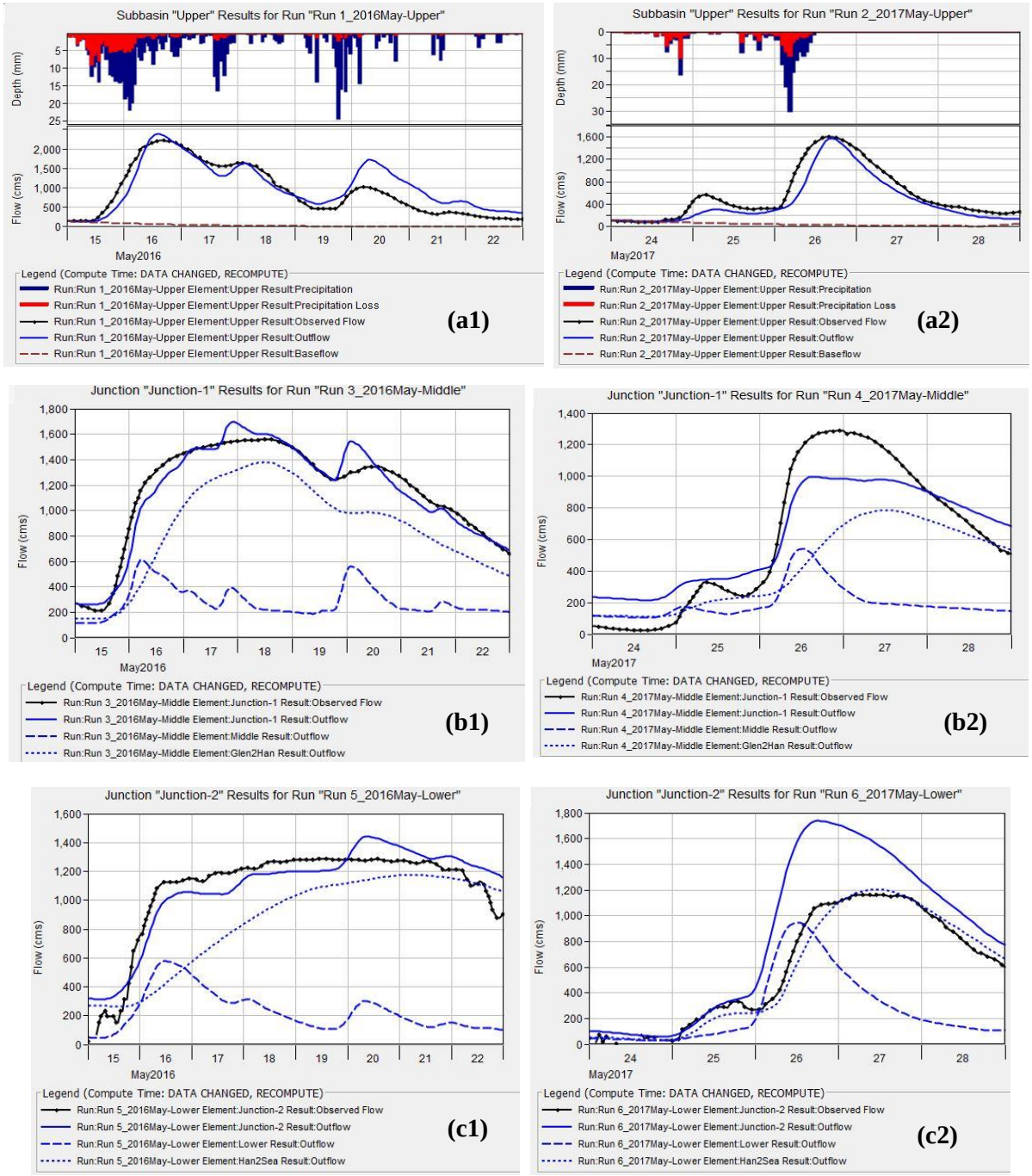

Figure 6-17: HEC-HMS Results (Graphs) generated by Calibration and Validation

6.1.3 Hydrological Model Simulation for Statistical Rain Event and Climate Change Projections Results

Figure 6-18 displays the simulated Glencourse discharges obtained from the 3-days 50-year. return period design rainfall simulations conducted using the calibrated Kelani Upper HEC-HMS model. The simulations were performed both without considering climate change projections and with selected climate change projections. The figure provides a visual representation of the discharge results for comparison and evaluation.

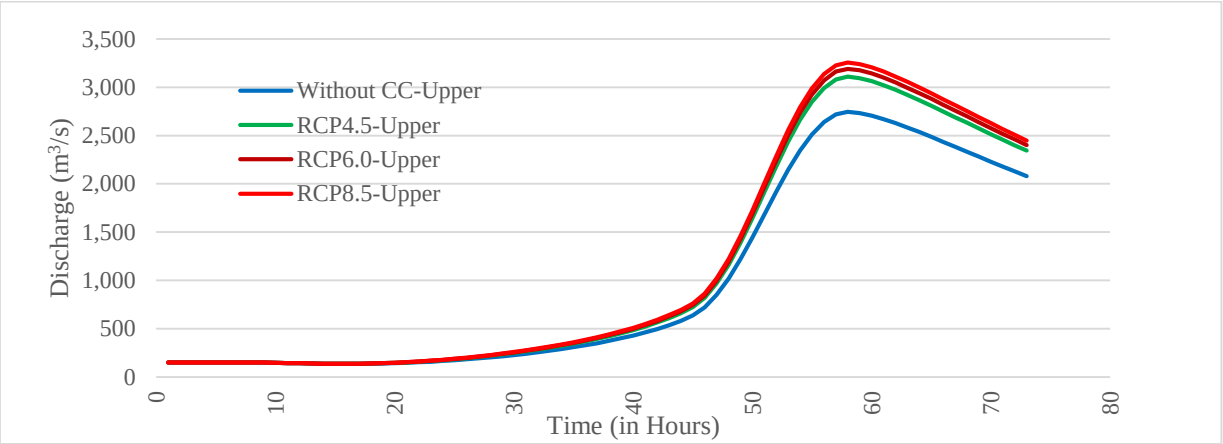

Figure 6-18:Comparison HEC-HMS Results considering CC Projections - generated from Kelani Upper Sub-basin

Figure 6-19 illustrates the simulated discharge of the Kelani Middle sub-basin resulting from the 3-day, 50-year return period design rainfall simulations conducted using the calibrated Kelani Upper HEC-HMS model. These simulations were carried out with and without considering climate change projections.

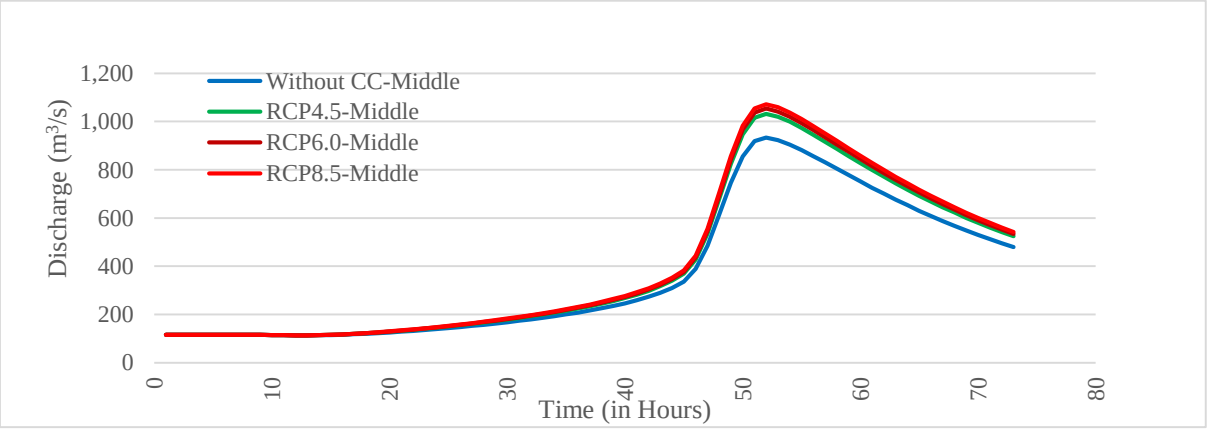

Figure 6-19: Comparison HEC-HMS Results considering CC Projections - generated from Kelani Middle Sub-basin

Figure 6-20 presents the simulated discharge of the Kelani Lower sub-basin obtained from the 3-day, 50-year return period design rainfall simulations performed using the calibrated Kelani Upper HEC-

HMS model. The simulations were conducted both with and without considering climate change projections.

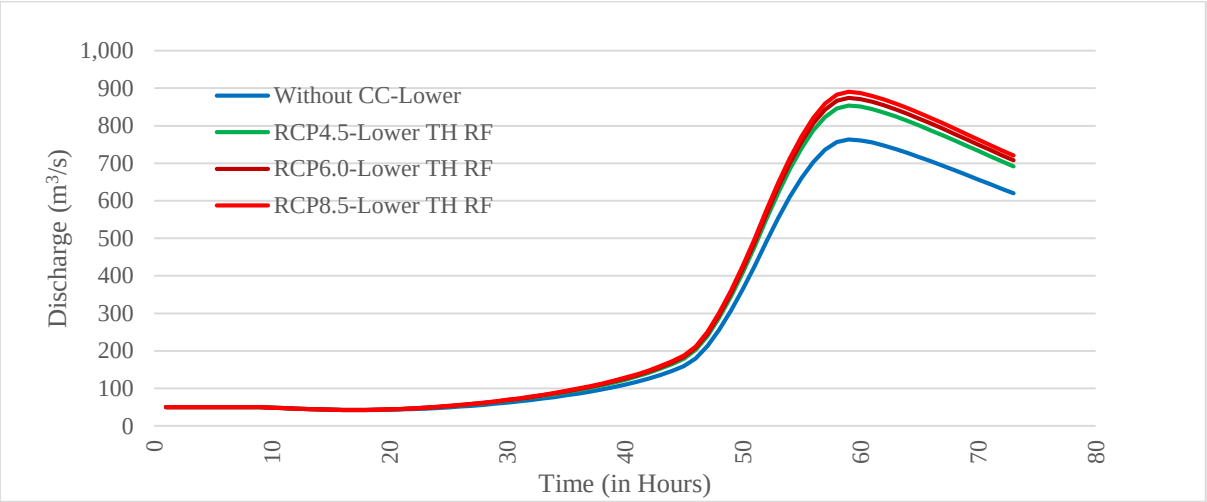

Figure 6-20: Comparison HEC-HMS Results considering CC Projections - generated from Kelani Lower Sub-basin

6.2 Flood Model Results

This section presents the results obtained from the HEC RAS model for the Lower Kelani basin to Glencourse, focusing on the performance and outcomes of these models in simulating the hydrodynamic processes in the respective areas. The findings provide a comprehensive description of the model's performance and its ability to accurately simulate the dynamic behaviour of water flow in the Lower Kelani basin to Glencourse region.

6.2.1 Flood Model Parameter Sensitivity Analysis Results

Hanwella Discharge

Table 6-11 shows the variations in simulated discharges at Hanwella compared to observed values, along with the corresponding Nash efficiency and coefficient of determination (R^2) based on Manning's N values according to land use type. These fluctuations provide insights into the performance of the model for different land use categories. Figure 6-21 provides a comprehensive comparison between the observed discharge and the behaviour of the entire simulated discharges. This aids in the evaluation and assessment of the model's performance.

Table 6-11: HEC-RAS Flood Model Sensitivity Analysis for Hanwella Discharge

Scenario	0.5n	0.25n	n	1.25n	1.5n	1.75n	2n	3n
Nash	-1.01	-0.59	-0.04	0.41	0.57	0.60	0.51	-0.26
R^2	0.45	0.52	0.60	0.68	0.75	0.79	0.83	0.87

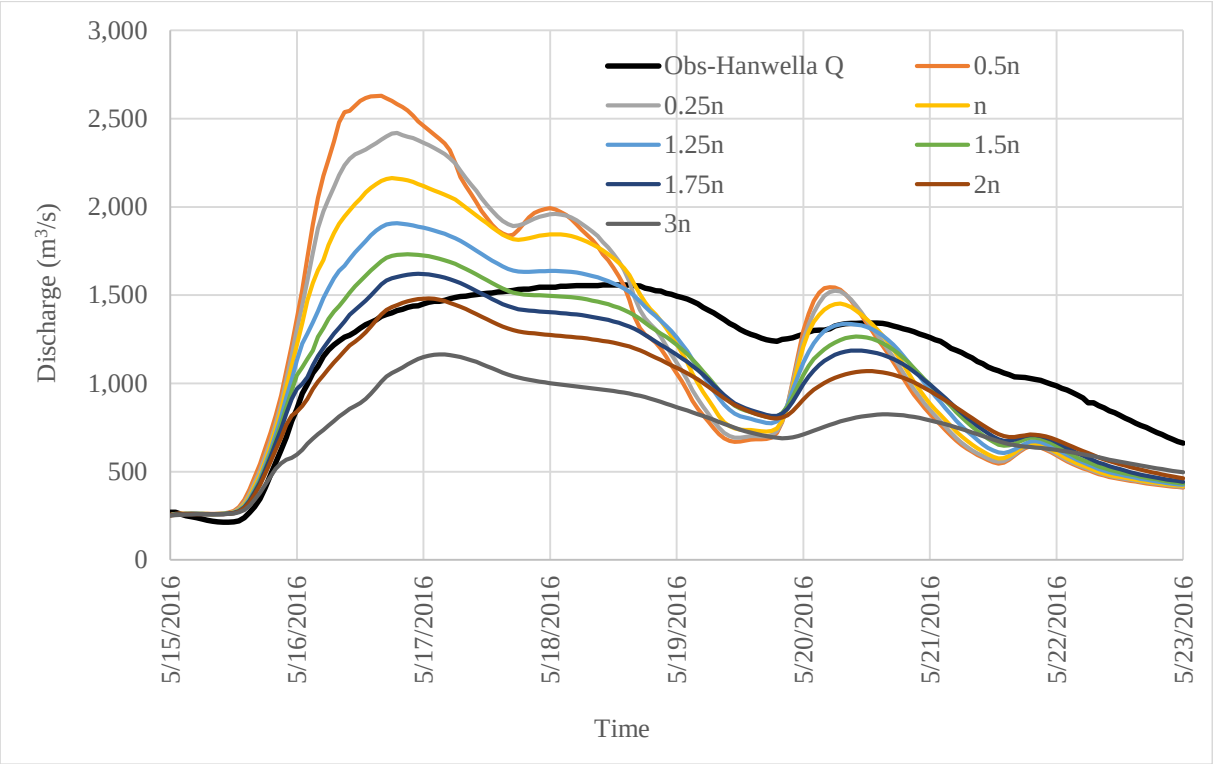

Figure 6-21:Observed and Simulated Hanwella Discharge comparison varies with Manning's N

Hanwella Water Level

Table 6-12 presents the fluctuations in simulated water levels at Hanwella in comparison to observed values, accompanied by the corresponding Nash efficiency and coefficient of determination (R^2), which are determined based on Manning's N values. Additionally, Figure 6-22 facilitates a comprehensive comparison between the observed water levels and the overall behaviour of the simulated water levels.

Table 6-12: HEC-RAS Flood Model Sensitivity Analysis for Hanwella Water Levels

Scenario	**0.5n**	**0.25n**	**n**	**1.25n**	**1.5n**	**1.75n**	**2n**	**3n**
Nash	-0.66	0.57	0.91	0.94	0.83	0.67	0.42	-0.53
R^2	0.78	0.88	0.94	0.97	0.99	0.99	0.97	0.89

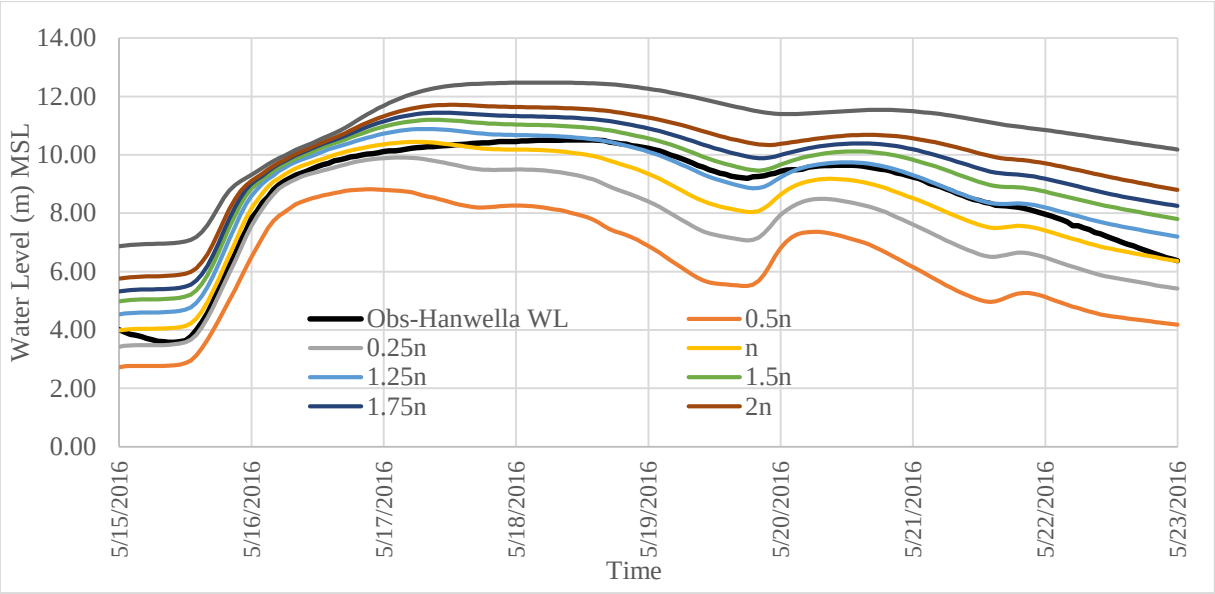

Figure 6-22: Observed and Simulated Hanwella Water Level comparison varies with Manning's N

Nagalagama Street Water Level

Table 6-13 showcases the variations in simulated water levels at Nagalagama Street, comparing them with the corresponding observed values. The table also includes the Nash efficiency and coefficient of determination (R^2), which are calculated using Manning's N values. Furthermore, Figure 6-23 aids in conducting a comprehensive comparison between the observed water levels and the overall behaviour of the simulated water levels.

Table 6-13: HEC-RAS Flood Model Sensitivity Analysis for Nagalagama Street Water Levels

Scenario	**0.5n**	**0.25n**	**n**	**1.25n**	**1.5n**	**1.75n**	**2n**	**3n**
Nash	-13.75	-5.47	-1.30	-0.30	-1.87	-4.10	-9.15	-25.85
R^2	0.00	0.11	0.34	0.61	0.72	0.72	0.65	0.40

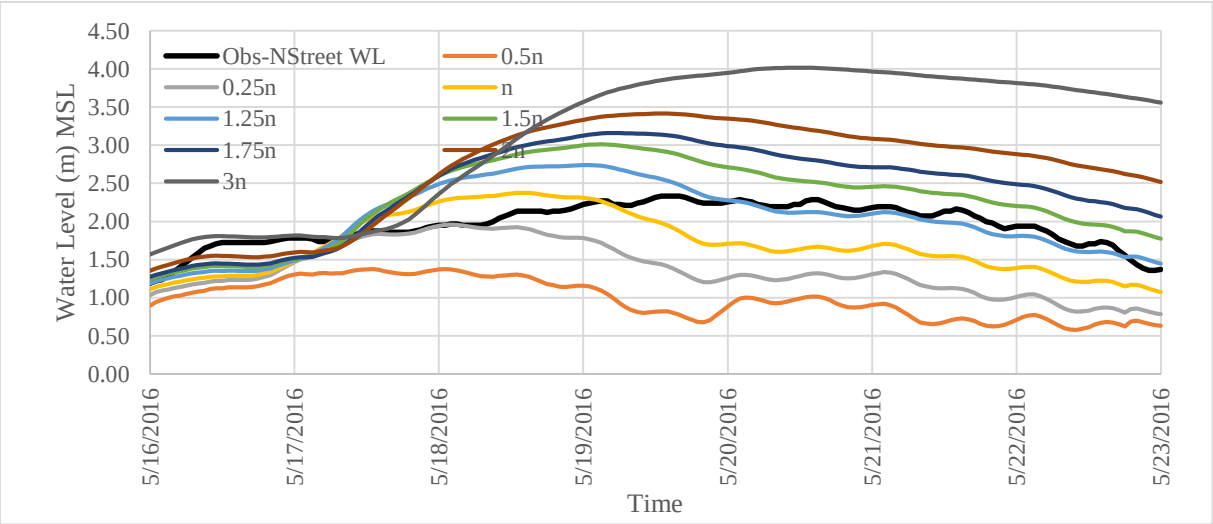

Figure 6-23: Observed and Simulated Nagalagama Street Water Level comparison varies with Manning's N

6.2.2 Flood Model Calibration and Validation Results

Based on the results of the flood model sensitivity analysis, which considered the discharges at Hanwella, water levels at Hanwella, and Nagalagama Street, the Manning's N value set generated by multiplying the calculated N value by 1.5 was selected as the baseline. The calibration process involved conducting multiple manual calibration runs and assessing the Nash efficiency and coefficient of determination at the specified locations. Table 6-14 presents the optimized Manning's N values for each land category, obtained through the calibration of the HEC-RAS model using data from the May 2016 flood event.

Table 6-14: Optimized Manning's N values for Land use Category of HEC-RAS Flood Model

Land Cover Category	Optimized Manning's N
No Data	0.1
Built up area	0.1
Agricultural Crops	0.14
Water Bodies	0.033
Forest	0.2
Garden	0.14
Marsh	0.18
Paddy	0.16

Table 6-15 presents the evaluation of the model's performance during both calibration and validation stages, assessed using Nash efficiency and coefficient of determination. The evaluation was conducted for Hanwella, considering both discharges and water levels, as well as for Nagalagama Street. The table provides an overview of the model's performance at these locations.

Table 6-15: HEC-RAS Flood model Performance evaluation results for Calibration and Validation

Observation	Objective Function			
	Calibration		Validation	
	Nash	R^2	Nash	R^2
Hanwella Discharge	0.57	0.75	0.80	0.85
Hanwella Water Level	0.56	0.99	0.57	0.99
Nagalagama Street Water Level	0.52	0.81	0.53	0.72

Figure 6-24 presents a graphical comparison of the hydrographs obtained from the observed data and the simulated data at the Hanwella gauging station. The figure provides a visual representation that allows for a direct comparison between the observed and simulated hydrographs, aiding in the assessment of the model's accuracy.

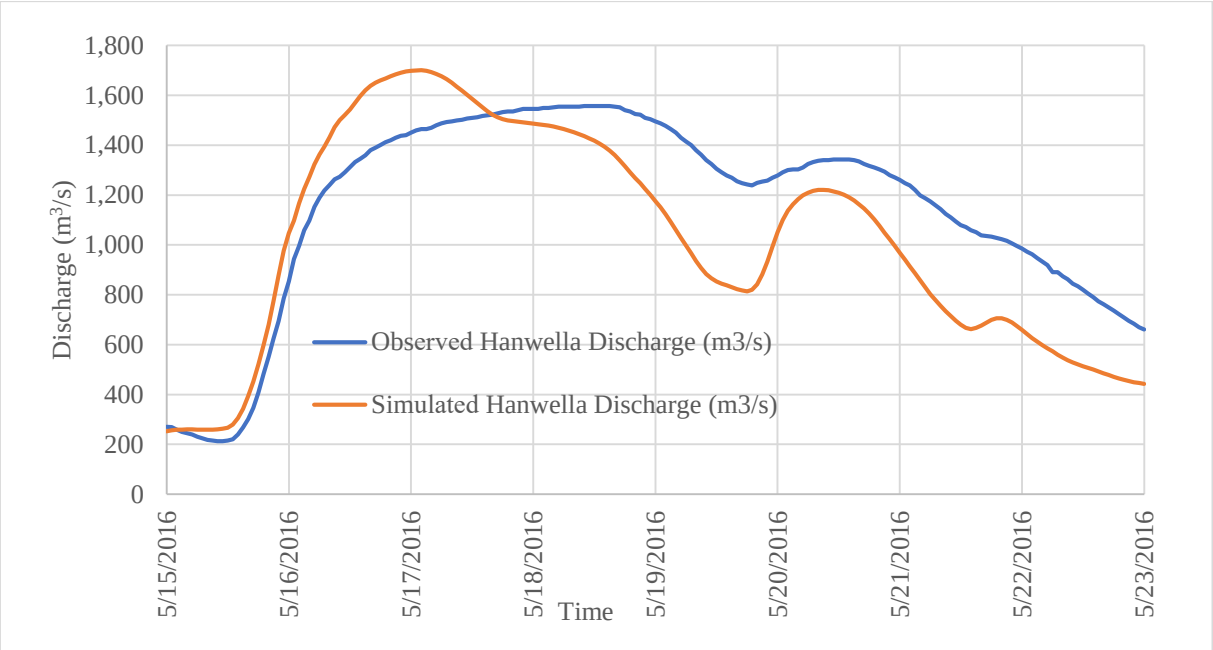

Figure 6-24: Comparison of Observed and Simulated Hanwella Discharge of HEC-RAS Calibration

Figure 6-25 displays a graphical comparison of the time series of water levels obtained from both observed and simulated data at the Hanwella gauging station which provides a visual representation that allows for a direct comparison between the observed water levels and the simulated water levels.

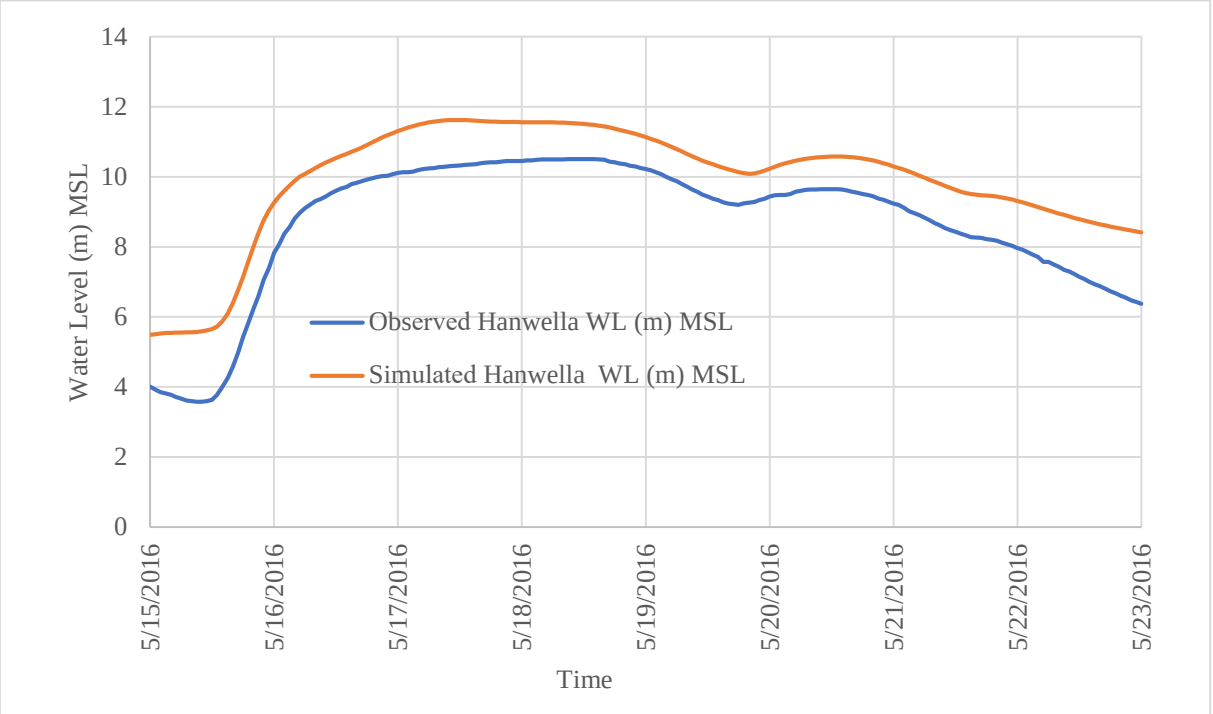

Figure 6-25: Comparison of Observed and Simulated Hanwella Water Level of HEC-RAS Calibration

Figure 6-26 presents a graphical comparison of the time series of water levels obtained from both observed and simulated data at the Nagalagama Street gauging station. It allows for a comprehensive assessment of the model's performance and accuracy in capturing the dynamics of water levels at the Nagalagama Street location.

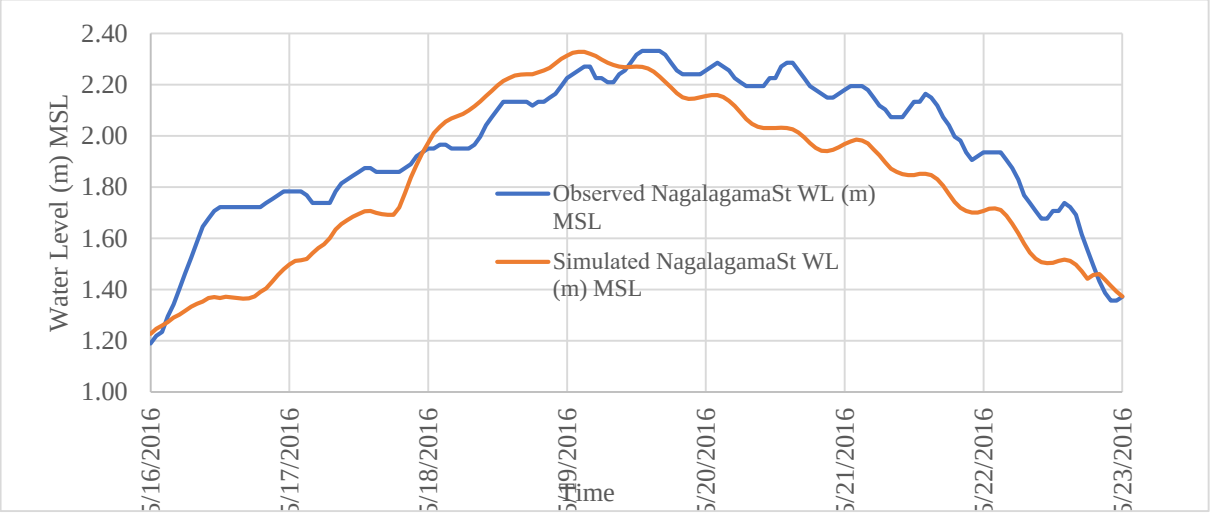

Figure 6-26: Comparison of Observed and Simulated Nagalagama Street Water Level of HEC-RAS Calibration

Figure 6-27 presents the simulated flood map of the 2016 May flood event generated through HEC-RAS calibration. Additionally, Figure 6-28 and Figure 6-29 provide a comparison between the simulated flood and the observed flood maps published by the Department of Survey and the Department of Irrigation, respectively.

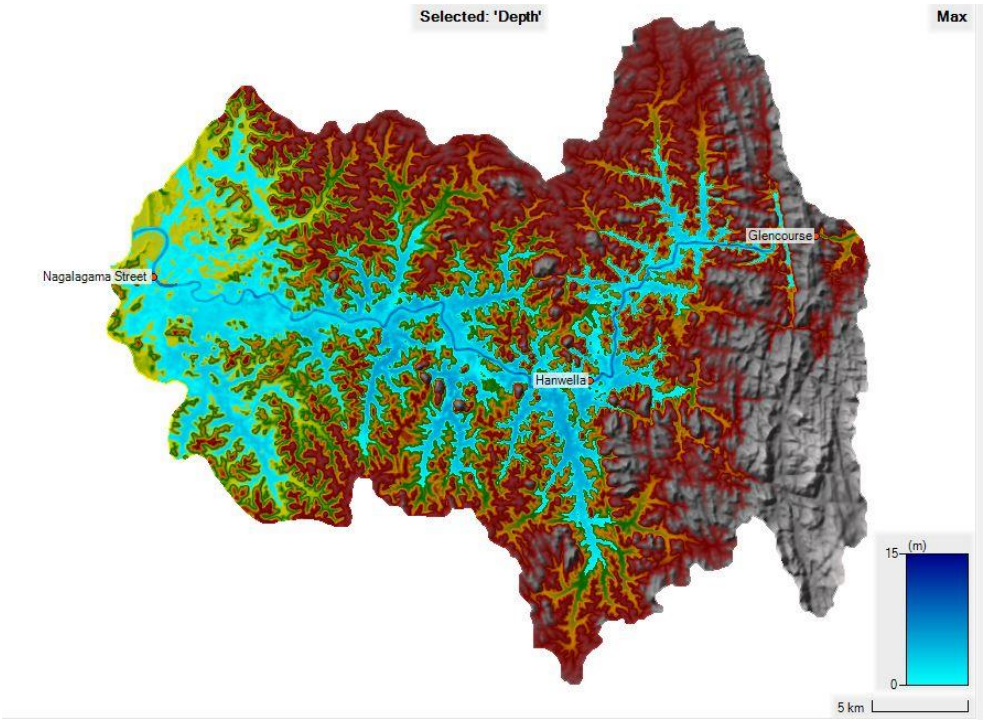

Figure 6-27: Simulated Flood inundation map by HEC-RAS Calibration

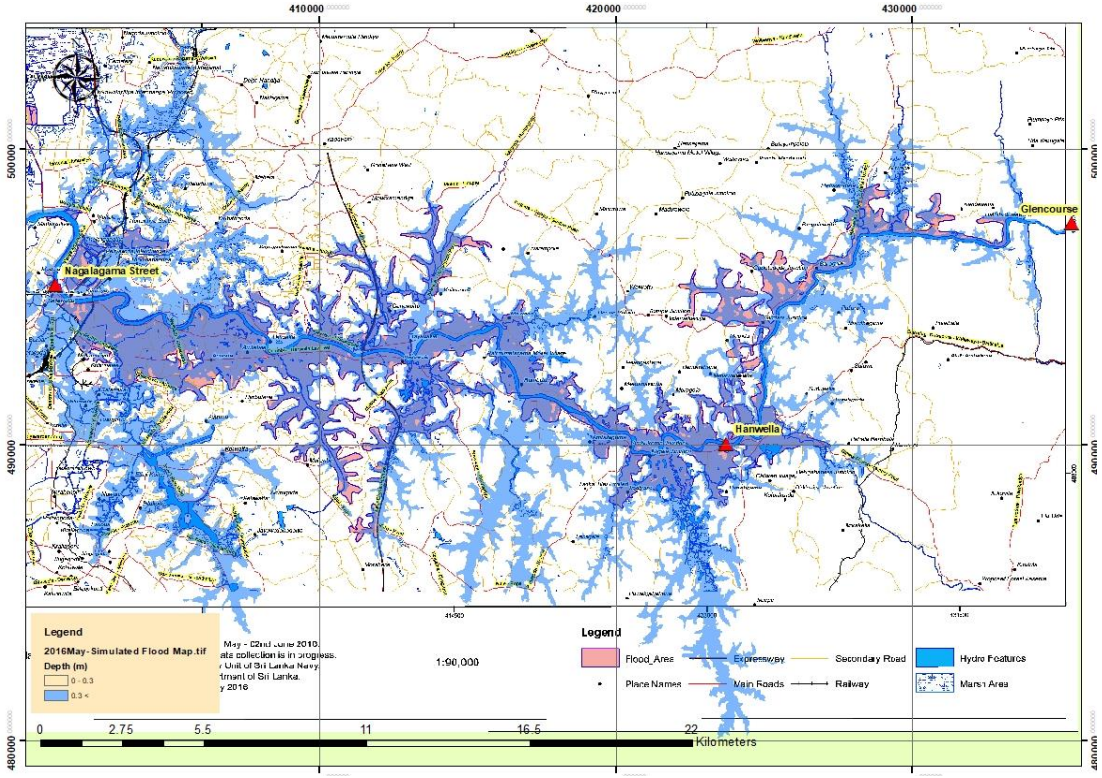

Figure 6-28: Comparison of observed (Survey Department) and simulated flood maps for 2016 May event

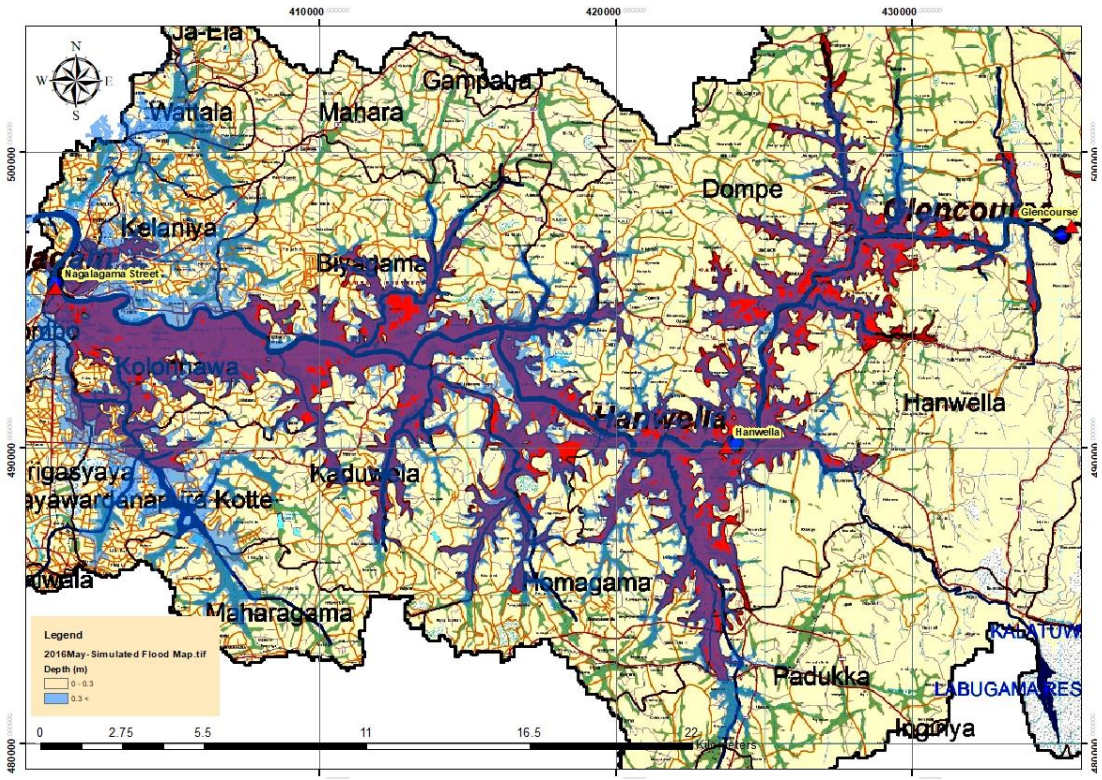

Figure 6-29: Comparison of observed (Irrigation Department) and simulated flood maps for 2016 May event

Figure 6-30 illustrates a graphical comparison between the observed and simulated hydrographs at the Hanwella gauging station for HEC-RAS validation, based on the 2017 May Flood event.

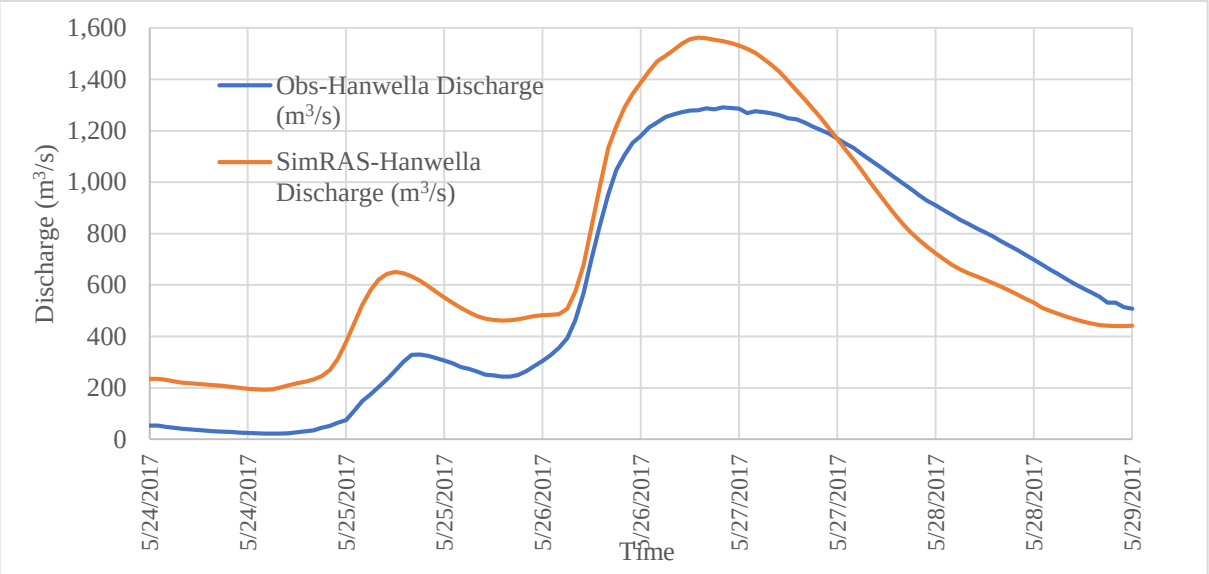

Figure 6-30: Comparison of Observed and Simulated Hanwella Discharge of HEC-RAS Validation

Figure 6-31 presents a graphical comparison of the observed and simulated water levels at the Hanwella gauging station during the HEC-RAS validation process, focusing on the specific 2017 May Flood event.

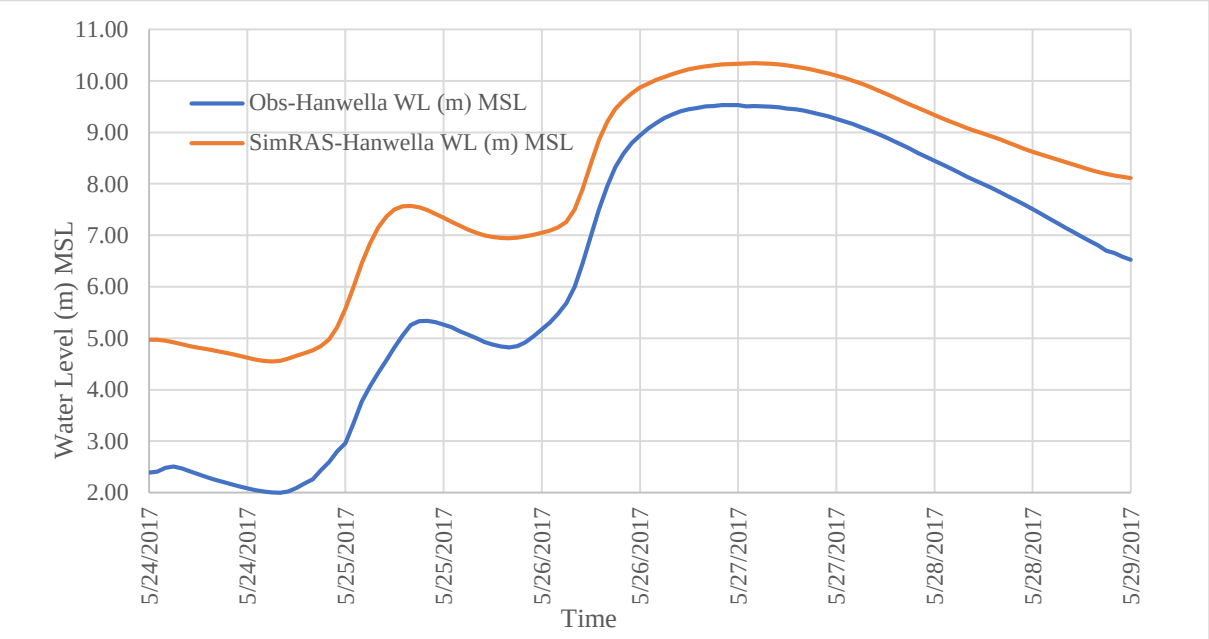

Figure 6-31: Comparison of Observed and Simulated Hanwella Water Level of HEC-RAS Validation

Figure 6-32 displays a graphical comparison of the observed and simulated water levels at the Nagalagama Street gauging station as part of the HEC-RAS validation process, with a specific focus on the 2017 May Flood event.

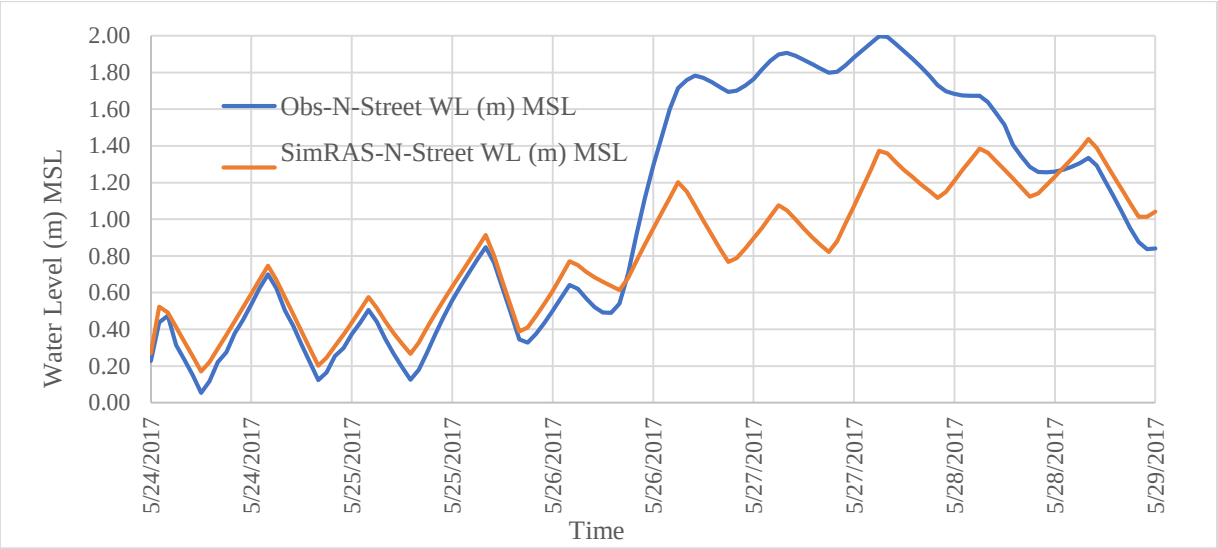

Figure 6-32: Comparison of Observed and Simulated Nagalagama Street Water Level of HEC-RAS Validation

Figure 6-33 displays the simulated flood map of the 2017 May flood event generated through HEC-RAS validation. Furthermore, Figure 6-34 offers a comparison between the simulated flood and the observed flood maps published by the Department of Survey.

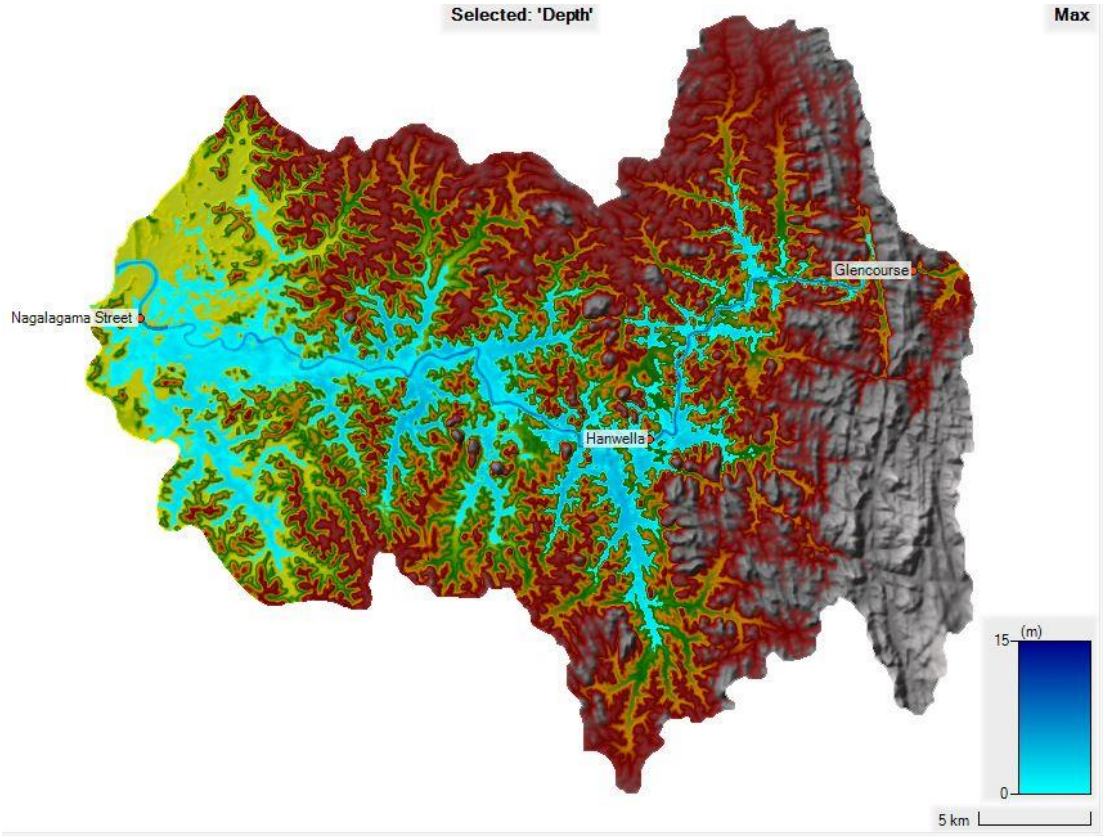

Figure 6-33: Simulated Flood inundation map by HEC-RAS Validation

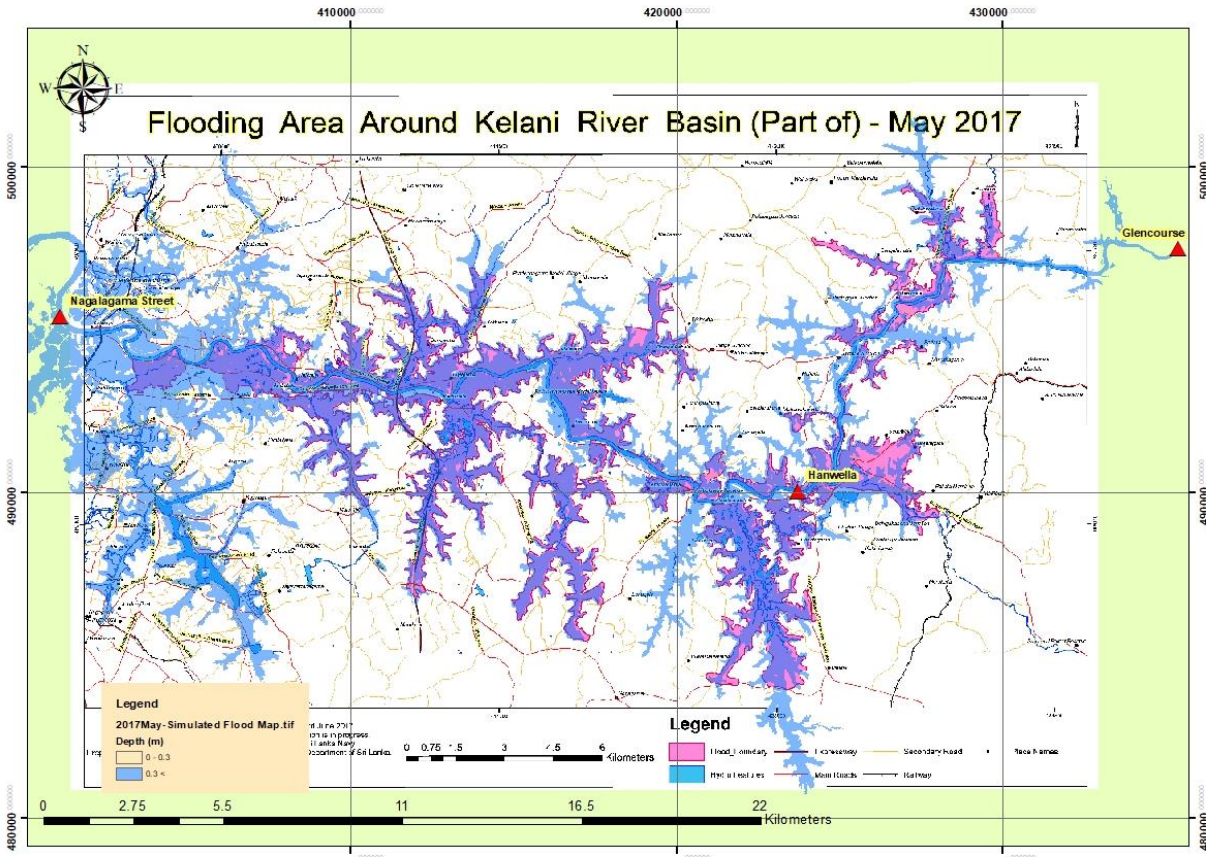

Figure 6-34: Comparison of observed (Survey Department) and simulated flood maps for 2017 May event

6.2.3 Flood Model Simulation for Statistical Rain Event and Climate Change Projections Results

Figure 6.35 presents the simulated Hanwella discharges resulting from the 3-day, 50-year return period design rainfall simulations conducted using the calibrated HEC-RAS model. These simulations were carried out under two scenarios: one without considering climate change projections and the other with selected climate change projections. The figure provides a visual representation of the simulated discharges, allowing for a comparison between the scenarios and an assessment of the potential impacts of climate change on the Hanwella discharges.

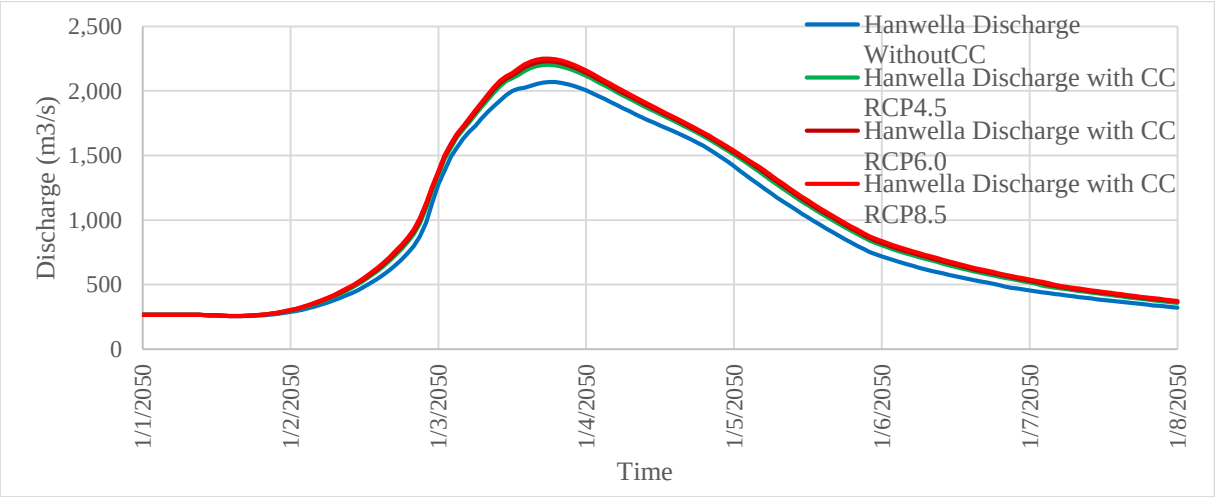

Figure 6-35: Comparison of Hanwella Discharge considering Climate Change Projections

Figure 6-36 displays the simulated Hanwella water levels obtained from the 3-day, 50-year return period design rainfall simulations conducted using the calibrated HEC-RAS model. The simulations were performed under two scenarios: one scenario did not consider climate change projections, while the other scenario incorporated selected climate change projections.

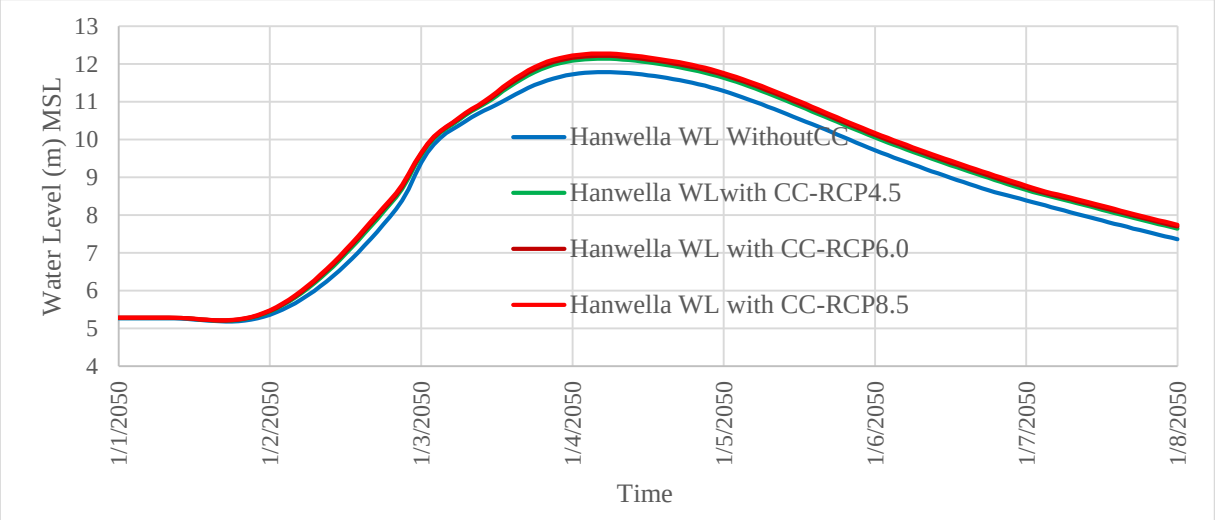

Figure 6-36: Comparison of Hanwella Water Level considering Climate Change Projections

Figure 6-37 presents the simulated water levels at Nagalagama Street obtained from the 3-day, 50-year return period design rainfall simulations conducted using the calibrated HEC-RAS model. These simulations were carried out under two scenarios: one without considering climate change projections and the other with selected climate change projections.

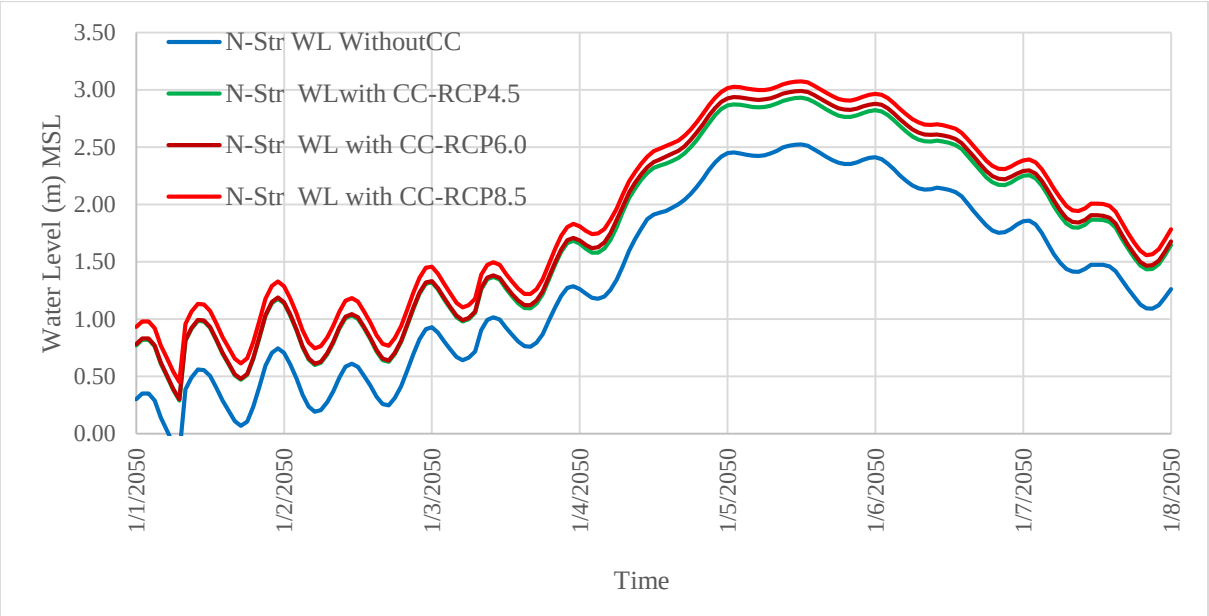

Figure 6-37: Comparison of Nagalagama Street Water Level considering Climate Change Projections

CHAPTER 7

7 DISCUSSION

This chapter presents a comprehensive discussion on the activities conducted in the previous chapters. It establishes connections between each task and provides justifications for the chosen approaches. Furthermore, this chapter delves into a detailed analysis of the study outputs and outcomes, aligning them with the specific objectives and overarching main objective. The aim is to provide a thorough understanding of the work undertaken and its relevance to the overall research goals.

7.1 Data Collection

Data collection was focused on the Hydrological and Flood Models development, Models calibration and Validation and Design Rainfall simulations with climate change projections.

Digital Elevation Models (DEMs) were collected for basin and sub-basin delineation in hydrological modelling and also used as the terrain grid in flood modelling. While the 2 m DEM did not cover the entire Kelani Basin, the 30 m SRTM DEM was utilized to fill in the data gaps. However, neither of these DEMs included the elevation profile of the submerged areas of the Kelani River, known as bathymetry data. To address this, measured cross-sections data were utilized to construct the bathymetry profile of the Kelani River. The DEM developed using these cross-sections data was then merged with the aforementioned DEMs to create a fully detailed DEM that would serve as a foundation for further model development.

Land Use data was extracted from 1:50,000 data sheets as shapefiles and merged, followed by clipping based on the boundaries of the Kelani Basin. This process resulted in the creation of a comprehensive Land Use Data set specific to the Kelani Basin. In total, 21 distinct Land Use categories were identified. After conducting a thorough analysis of the attributes associated with each land use type within this dataset, they were assigned into seven categories: Agricultural Crops, Built-Up areas, Forest, Garden, Marsh, Paddy, and Water Bodies. These Land Use categories played a crucial role in assigning SCS Curve numbers for hydrological modelling and Manning's N values for flood modelling during the initial estimation of model parameters. Additionally, a Soil map was obtained for the Kelani Basin, revealing the presence of various soil types within the basin. However, for the purposes of initial parameter estimation, it was assumed that the entire basin consisted of 'Hydrological Soil Group Type B'.

The selection of flood events for this study was based on factors such as flood event magnitude, data availability, and recency. Specifically, the flood events that occurred in May 2016 and May 2017 were chosen. Hourly time series rainfall data were collected for these events, with the dataset from the 2016 May flood event used for model calibration and the dataset from the 2017 May flood event used for model validation. Geographical coordinates of rain gauges within the Kelani Basin were obtained, including Colombo (owned by the Meteorological Department) and Hanwella, Glencourse, Deraniyagala, Kithulgala, Noorwood, and Holombuwa (owned by the Irrigation Department). However, hourly rainfall data for Holombuwa was not available for these events, so it was excluded from the analysis. Using the geographical coordinates, Thiessen polygons were constructed, assuming that the rainfall within each polygon area was evenly distributed.

The collected rainfall data series were visually analysed to examine the spatial and temporal variation of rainfall for both events. Basin average rainfall data series were created using the previously constructed Thiessen polygons (Thiessen weights) to analyse the variation in rainfall at each station using the Single Mass Curve and Double Mass Curve techniques. The graphical representation of these analyses revealed that the data from the Colombo station exhibited some deviations compared to the other stations for both flood events.

The IDF equations for the selected rainfall stations were obtained from two recent publications by the Department of Irrigation. These equations were used to formulate the design hyetograph using the alternative block method. Based on the literature, a design return period of 50-years and a rainfall duration of 3-days were selected.

Hydrological data were collected from river gauging stations located along the Kelani River in the Lower Kelani Basin, specifically Glencourse, Hanwella, and Nagalagama Street. Hourly data series of both discharge and water levels were obtained for the 2016 May and 2017 May flood events at these gauging stations. Additionally, sea level data were collected to serve as downstream boundary conditions for the flood model. These data were carefully analysed and visually examined to ensure accuracy and consistency. Subsequently, the collected data were used for the calibration and validation of both the hydrological and flood models.

Furthermore, published flood maps depicting the observed flood extent for the 2016 May and 2017 May flood events were obtained from the Department of Survey and the Department of Irrigation. These maps were used to compare and evaluate the simulated flood extent maps generated by the flood model.

7.2 Modelling Tools Selection

When selecting the modelling tools (software) for this study, several factors were taken into consideration. The availability of the tools, particularly as freely downloadable options, was considered important. Additionally, the suitability of the tools for similar applications, particularly those related to

the Kelani Basin, played a role in the selection process. The availability of necessary data and the ability of the tools to produce the desired outputs were also key considerations. Based on these factors, the HEC-HMS was chosen for hydrological modelling for entire Kelani Basin and HEC-RAS for Lower Kelani Basin (Downstream to Glencourse) was selected for flood modelling as they fulfilled the aforementioned requirements. HEC-HMS tool was selected for Hydrological modelling for whole Kelani basin producing discharges from rainfall inputs. This simulated discharges were defined as boundary conditions of HEC-RAS model.

7.3 Models Parameter Sensitivity Analysis

During the parameter sensitivity analysis of the Kelani Upper Model using the HEC-HMS, several key parameters were examined. The sensitivity of the SCS Curve Number (CN), which falls under the Loss Method, was analysed in relation to peak discharges, Nash efficiency, and coefficient of determination. The results showed that the SCS Curve Number had a significant impact on all aspects. Graphical representations illustrated that increasing the CN led to higher peak discharges, as well as improved Nash efficiency and coefficient of determination. Similarly, the Initial Abstraction, also belonging to the Loss Method, was evaluated but found to be less sensitive. The graphs demonstrated that Nash efficiency and coefficient of determination decreased with an increase in Initial Abstraction. The Time of Concentration (*Tc*), analysed using the Clark Unit Hydrograph in the Transform Method, was found to be a highly sensitive parameter across all evaluators. The graphs indicated that Nash efficiency and coefficient of determination decreased as *Tc* increased. The Storage Coefficient, belonging to the Clark Unit Hydrograph in the Transform Method, was also identified as a highly sensitive parameter. Graphical analysis revealed that peak discharge decreased with an increase in Storage Coefficient, while Nash efficiency and coefficient of determination initially increased up to an optimum value before decreasing with further increases in Storage Coefficient. The Recession Constant, evaluated using the Recession Baseflow method, was found to be less sensitive. Similarly, the Ratio to Peak, assessed using the same method, was determined to be an insensitive parameter.

During the parameter sensitivity analysis of the Kelani Middle HEC-HMS model for Reach elements, two parameters, Muskingum *K* and Muskingum *X*, were found to be highly sensitive in relation to the aforementioned three parameters. Graphical analysis revealed that increasing Muskingum *K* resulted in a decrease in peak discharge, while Nash efficiency and coefficient of determination increased up to an optimal value and then decreased with further increases in Muskingum *K*. On the other hand, the graphs related to Muskingum *X* showed that peak discharge increased with an increase in Muskingum *X*, while Nash efficiency and coefficient of determination decreased. The qualitative sensitivity and behaviour of the resulting hydrographs were used for the calibration of the HEC-HMS model, both through auto-calibration and manual fine-tuning.

During the sensitivity analysis of the Flood model, the assigned Manning's N values for each land use type were evaluated in relation to Nash efficiency, coefficient of determination, peak discharges, and peak water levels for Hanwella Discharges, Hanwella Water Levels, and Nagalagama Street Water Levels. The results consistently showed that Manning's N value has a high sensitivity to Nash efficiency, coefficient of determination, peak discharges, and peak water levels. For Hanwella Discharges, it was observed that Nash efficiency increased up to an optimum value and then decreased with increasing Manning's N value, while coefficient of determination increased with Manning's N value. Similarly, for Hanwella Water Levels, both Nash efficiency and coefficient of determination increased up to an optimum value and then decreased with increasing Manning's N value. In the case of Nagalagama Street Water Levels, Nash efficiency increased up to an optimum value and then decreased, whereas coefficient of determination continued to increase with increasing Manning's N value. The qualitative sensitivity and behaviour of the results were utilized to calibrate the HEC-RAS model and fine-tune the Manning's N value.

7.4 Models Calibration and Validation

The performance of the HEC-HMS model during calibration and validation is presented in Table 6-10. The Nash efficiency values for calibration ranged from 0.79 to 0.85, indicating that the model performed well in replicating observed data. Similarly, the coefficient of determination values for calibration ranged from 0.82 to 0.95, further confirming the good performance of the model. In terms of validation, the Nash efficiency values for Kelani Upper and Kelani Middle models were 0.87 and 0.85, respectively, indicating a strong agreement with the observed data. However, the Nash efficiency for the Kelani Lower model was 0.25, indicating a poorer performance in replicating the observed data. Nevertheless, when considering the coefficient of determination, all models showed values ranging from 0.89 to 0.95, demonstrating overall strong model performance. According to De Silva et al. (2014), the study reported Nash-Sutcliffe efficiencies of 0.91 for event-based simulations and 0.88 for continuous simulations. Similarly, Senadhinatha (2020) found Nash-Sutcliffe Coefficients (NASH) of 0.80 for calibration and 0.89 for validation, while the coefficient of determination (R^2) was 0.83 for calibration and 0.90 for validation. Comparing these values, the obtained results demonstrate that the models perform well.

The Flood model efficiency evaluation for Hanwella discharge, Hanwella Water Level, and Nagalagama Street Water levels are presented in Table 6-15. The Nash Efficiency values for calibration ranged from 0.52 to 0.57, indicating good performance of the model. Similarly, the coefficient of determination values ranged from 0.75 to 0.99, further confirming the satisfactory performance of the model. In terms of validation, the Nash Efficiency values ranged from 0.53 to 0.80, demonstrating a good fit between the model and observed data. Additionally, the coefficient of determination values ranged from 0.72 to 0.99, indicating a strong performance of the model.

In the study conducted by Moriasi et al. (2007), the performance ratings of objective functions for hydrological modelling were examined. The study established performance ratings, including Very Good, Good, Satisfactory, and Unsatisfactory, based on the value ranges of Coefficient of Determination (R^2), Nash Efficiency (NSE), Root Mean Square Error-observations standard deviation ratio (RSR), and Percent Bias. For daily and weekly time steps, the performance ratings for both Nash and Coefficient of Determination (R^2) were defined as Very Good (0.65-1.00), Good (0.55-0.65), Satisfactory (0.40-0.55), and Unsatisfactory (below 0.4). The performance rating values for monthly time steps were slightly lower than those for daily and weekly time steps. Consequently, it can be assumed that the performance ratings for hourly time steps should be slightly lower than those for daily and weekly time steps. Based on this, the hydrological and flood models used in this study can be considered to be performing well.

7.5 Hydrological and Flood Models Outputs for Design Rainfall Event Simulations Considering Climate Change Projection

The impact of climate change on flood events, specifically the increase in discharges and water levels, is summarized in Table 7-1. These findings are based on the model results presented in Chapter 6.

Table 7-1: Discharges and Water Levels increasing of Climate Change projections for 50-year. Return Period

Model	Location and Measurement	Without CC Projection	With CC Projection		% Increase
HEC-HMS (Kelani Upper)	Glencourse Peak Discharge (m^3/s)	2745	RCP 4.5	3109	13.3
			RCP 6.0	3191	16.2
			RCP 8.5	3256	18.6
HEC-RAS	Hanwella Peak Discharge (m^3/s)	2069	RCP 4.5	2201	6.4
			RCP 6.0	2229	7.7
			RCP 8.5	2251	8.8
HEC-RAS	Hanwella Maximum Water Level (m MSL)	11.78	RCP 4.5	12.14	3.1
			RCP 6.0	12.21	3.7
			RCP 8.5	12.27	4.2
HEC-RAS	Nagalagama Street Maximum Water Level (m MSL)	2.53	RCP 4.5	2.94	16.2
			RCP 6.0	2.97	17.4
			RCP 8.5	3.08	21.7

Referring to the values presented in Table 7-1, it is observed that the Glencourse Peak Discharge is expected to increase by approximately 13.3% to 16.2% under climate change Projections. Similarly, for Hanwella, the peak discharge is projected to increase by approximately 6.4% to 8.8%, while the maximum water level is expected to rise by approximately 3.1% to 4.2% with climate change Projections. Furthermore, the maximum water level at Nagalagama Street is likely to experience an increase of around 16.2% to 21.7% under climate change Projections.

CHAPTER 8

8 CONCLUSIONS

1. The three HEC-HMS models, namely Kelani Upper, Kelani Middle, and Kelani Lower, underwent successful calibration using hourly data for the 2016 May event and were subsequently validated for the 2017 May event. The statistical analyses revealed a strong correlation between the simulated values and the measured flow for all three HEC-HMS models. The Nash Efficiency values during calibration were 0.79, 0.95, and 0.85 for Kelani Upper, Kelani Middle, and Kelani Lower models, respectively. During validation, the corresponding Nash Efficiency values were 0.87, 0.85, and 0.25.

2. The HEC-RAS Flood model for the Lower Kelani Basin, located downstream from Glencourse, underwent successful calibration for the 2016 May event and subsequent validation for the 2017 May event using hourly data. The statistical analyses demonstrated a strong correlation between the simulated values and the measured discharges at Hanwella, as well as the water levels at Hanwella and Nagalagama Street. The Nash Efficiency values during calibration were 0.57, 0.56, and 0.52, respectively, and during validation, the corresponding values were 0.80, 0.57, and 0.53.

3. The study utilized a 50-year design rainfall dataset with a duration of 3 days, employing published Intensity Duration Frequency (IDF) equations from selected rain gauge locations. climate change Projections (RCP4.5, RCP6.0, and RCP8.5) were applied to the dataset. Rainfall depth increasing factors of 1.100, 1.122, and 1.140 were implemented for the RCP4.5, RCP6.0, and RCP8.5 scenarios, respectively. Furthermore, sea level rise values of 0.47m, 0.48m, and 0.63m were incorporated into the simulations corresponding to the respective climate change projection scenarios.

4. For the Glencourse location, the projected peak discharge is expected to increase by 13.3%, 16.2%, and 18.6% for the RCP4.5, RCP6.0, and RCP8.5 climate change projection scenarios, respectively. Similarly, at the Hanwella location, the peak discharge is projected to increase by 6.4%, 7.7%, and 8.8% for the respective climate change scenarios. Additionally, the maximum water level at Hanwella is anticipated to rise by 3.1%, 3.7%, and 4.2% for the RCP4.5, RCP6.0, and RCP8.5 scenarios, respectively. Furthermore, the maximum water level at Nagalagama Street is projected to increase by 3.1%, 3.7%, and 4.2% for the RCP4.5, RCP6.0, and RCP8.5 scenarios, respectively.

CHAPTER 9

9 RECOMMENDATIONS

1. It is recommended to utilize the verified HEC-HMS models, namely Kelani Upper, Kelani Middle, and Kelani Lower, in conjunction with the HEC-RAS Lower Kelani Model for future flood forecasting and infrastructure design in the Kelani River Basin, Sri Lanka.
2. To enhance the model setup, it is suggested to incorporate the Holombuwa Rainfall Data.
3. Improving the model setup should include the utilization of flood extent and flood depth data during the calibration and validation process.
4. Additionally, it is advisable to assess the model's performance using temporal data lower than hourly intervals, such as 15 minutes, for real-time flood operations.
5. Furthermore, it is recommended to evaluate the model's performance using alternative rain gauge locations, specifically those managed by the Sri Lanka Land Development Corporation (SLLDC) and/or the National Building Research Organization (NBRO), as well as water level gauge location data.

BIBLIOGRAPHY

Abeysingha, N. (2022). A Review of Recent Changes in Rainfall Trend in Sri Lanka. *Tropical Agricultural Research and Extension*, 25(1).

Alahacoon, N., & Edirisinghe, M. (2021). Spatial variability of rainfall trends in Sri Lanka from 1989 to 2019 as an indication of climate change. *ISPRS International Journal of Geo-Information*, 10(2), 84.

Alahacoon, N., Pani, P., Matheswaran, K., Samansiri, S., Amarnath, G., Balasubramanya, S., & Horbulyk, T. (2016). Rapid emergency response mapping for the 2016 floods in Kelani river basin, Sri Lanka. *International Eater management Institude (IWMI)*.

Anuruddhika, M., Perera, K., Premarathna, L., Hansameenu, W., & Weerasinghe, V. (2022). Forecasting flood inundation areas of Attanagalu Oya. *Ceylon Journal of Science*, 51(3), 217-227.

Bandara, W., Dinelka, K., & Neluwala, N. (2022). Discharge Observations Assimilation to Improve Flood Prediction Skills. *ICSBE 2020* (pp. pp. 143-150). Singapore: Springer.

Chathuranika, I., Gunathilake, M., Azamathulla, H., & Rathnayake, U. (2022). Evaluation of Future Streamflow in the Upper Part of the Nilwala River Basin (Sri Lanka) under Climate Change. *Hydrology*, 9(3), 48.

Chow, V., Maidment, D., & Mays, L. (1988). *Applied hydrology*. McGraw-hill.

Chunderlik, J., & Simonovic, S. (2004). Calibration, verification and sensitivity analysis of the HEC-HMS hydrologic mode. *Water Resources Research Report No. 048; Facility for Intelligent Decision Support, Department of Civil and Environmental Engineering, London, Ontario, Canada*.

Climate Resilience Improvement Project (CRIP). (2019). *Flood and Drought Risk Assessment for the Kelani Ganga Basin, Volume I : Main Report.*

Dammalage, T. L., & Jayasinghe, N. T. (2019). Land-use change and its impact on urban flooding: A case study on Colombo district flood on May 2016. *Engineering, Technology & Applied Science Research, 9(2),* 3887-3891.

Dammalage, T., & Jayasinghe, N. (2019). Land-use change and its impact on urban flooding: A case study on Colombo district flood on May 2016. *Engineering, Technology & Applied Science Research*, 9(2), 3887-3891.

Darshika, T., & Jayawardane, S. (2017). Future climate projections for annual and seasonal rainfall in Sri Lanka using CMIP5 models. *International Conference on Climate Change*, (pp. 79-85, Vol. 1).

De Silva, C. (2006). Impacts of climate change on water resources in Sri Lanka.

De Silva, C. (2007). Impacts of climate change on rainfall runoff and water security in Sri Lanka-Predictions for 2050s. Water Resources Research in Sri Lanka. *Water Professionals Day, Postgraduate Institute of Agriculture, University of Peradeniya*, (pp. 183-196).

De Silva, M., Weerakoon, S., & Herath, S. (2014). Modeling of event and continuous flow hydrographs with HEC–HMS: Case study in the Kelani River Basin, Sri Lanka. *Journal of Hydrologic Engineering*, 19(4), 800-806.

De Silva, M., Weerakoon, S., Herath, S., Ratnayake, U., & Mahanama, S. (2012). Flood inundation mapping along the lower reach of Kelani river basin under the impact of climatic change. *Engineer, 45(02)*, 23-29.

Disaster Management Center, S. L. (2016). *Sri Lanka Post Disaster Needs Assessment: Floods and Landslides May 2016.*

Disaster Management Center, S. L. (2017). *Sri Lanka Post Disaster Needs Assessment: Floods and Landslides May 2017.*

Dissanayaka, K., & Rajapakse, R. (2019). Long-term precipitation trends and climate extremes in the Kelani River basin, Sri Lanka, and their impact on streamflow variability under climate change. *Paddy and Water Environment*, 17(2), 281-289.

Dorji, S., Herath, S., & Mishra, B. (2017). Future Climate of Colombo Downscaled with SDSM-Neural Network. *Climate*, 5, 24.

Dushyantha, C., & Ptuhina, I. (2020). Flood risk assessment of river "Kelani Ganga" exceeding its threshold water level. *E3S Web of Conferences* (pp. 02006, Vol. 157). EDP Sciences.

Erena, S., & Worku, H. (2018). Flood risk analysis: causes and landscape based mitigation strategies in Dire Dawa city, Ethiopia. *Geoenvironmental Disasters*, 5(1), 1-19.

Fowze, J., Gunasekara, I., Liyanage, P., Hazarika, M., & Samarakoon, L. (2008). Flood hazard mapping in lower reach of Kelani River, Sri Lanka. *Proceedings of the 29th Asian Conference on Remote Sensing–ACRS.*

Green, A., & Stephenson, D. (1986). Criteria for comparison of single event models. *Hydrological Sciences -Journal -Des Sciences Hydrologiques*, 313(9).

Guinot, V., Cappelaere, B., Delenne, C., & Ruelland, D. (2011). Towards improved criteria for hydrological model calibration: theoretical analysis of distance- and weak form-based functions. *Journal of Hydrology*, 401(1–2), 1–13.

Gunasekara, I. (2008). Flood hazard mapping in lower reach of Kelani river.

Gunathilake , M., Panditharathne, P., Gunathilake, A., & Warakagoda, N. (2019). Application of HEC-HMS Model on Event-Based Simulations in the Seethawaka Ganga River, Sri Lanka. *Sch. J. Appl. Sci. Res*, 2, 32-40.

Gupta, H., Kling, H., Yilmaz, K., & Martinez, G. (2009). Decomposition of the mean squared error and NSE performance criteria: Implications for improving hydrological modelling. *Journal of Hydrology*, 377(1–2), 80–91. 3.

Halwatura, D., & Najim, M. (2013). Application of the HEC-HMS model for runoff simulation in a tropical catchment. *Environmental modelling & software*, 46, 155-162.

Herath , S., & Ratnayake, U. (2004). Monitoring rainfall trends to predict adverse impacts—a case study from Sri Lanka (1964–1993). *Global Environmental Change*, 14, 71-79.

Herath, H., Dayananda, R., & Weerakoon, S. (2015). Climate change impact prediction in upper Mahaweli Basin. *International Conference on Structural Engineering and Construction Management*, 148–152.

Herath, M., & Wijesekera, N. (2021). Evaluation of HEC-HMS model for water resources management in Maha Oya Basin in Sri Lanka. *ENGINEER*, 54(02), 45-53.

IPCC. (2007). Climate Change 2007. In S. Solomon, D. Qin, M. Manning, Z. Chen, M. Marquis, K. Averyt, . . . H. Miller, *The Physical Science Basis. Contribution of Working Group I to the Fourth Assessment Report of the Intergovernmental Panel on Climate Change.* Cambridge, United Kingdom and New York, NY, USA: Cambridge University Press.

IPCC. (2014). Climate Change 2014: Synthesis Report. In R. Pachauri, & L. Meyer, *Contribution of Working Groups I, II and III to the Fifth Assessment Report of the Intergovernmental Panel on Climate Change* (p. 151). Geneva, Switzerland: IPCC.

Irrigation, D. (2019). *IDF Curves, 75% Probability Rainfall, Evapotranspiration.*

Irrigation, D. (2022). *Environmental Impact Assessment for Alterations to the Salinity Barrier at Ambatale in Kelani River*.Ministry of Irrigation.

Iturbide, M., Gutiérrez, J., Alves, L., Bedia, J., Cerezo-Mota, R., Cimadevilla, E., & Vera, C. (2020). An update of IPCC climate reference regions for subcontinental analysis of climate model data: definition and aggregated datasets. *Earth System Science Data*, 12(4), 2959-2970.

Januriyadi, N., Kazama, S., Moe, I., & Kure, S. (2018). Evaluation of future flood risk in Asian megacities: a case study of Jakarta. *Hydrological Research Letters*, 12(3), 14-22.

Jayadeera, P. (2016). Development of a rainfall runoff model for Kalu ganga basin of Sri Lanka using HEC-HMS model. *Retrieved from http://dl.lib.mrt.ac.lk/handle/123/12800*.

Jayawardene, H., Sonnadara, D., & Jayewardene, D. (2005). Trends of rainfall in Sri Lanka over the last century. *Sri Lankan Journal of Physics*, 6.

Kamran , M., & Rajapakse, R. (2018). Effect of watershed subdivision and antecedent moisture condition on HEC-HMS model performance in the Maha Oya basin, sri Lanka. *International Journal of Engineering Technology and Sciences*, 5(2), 22-37.

Kay, A., Crooks, S., Pall, P., & Stone, D. (2011). Attribution of Autumn/Winter 2000 flood risk in England to anthropogenic climate change: a catchment-based study. *Journal of Hydrology*, 406(1-2), 97-112.

Klein, R., & Nicholls, R. (1999). Assessment of coastal vulnerability to climate change. *Ambio*, 182-187.

Komolafe, A., Herath, S., & Avtar, R. (2018a). Methodology to Assess Potential Flood Damages in Urban Areas under the Influence of Climate Change. *Natural Hazards Review*,, 19(2), 05018001.

Komolafe, A., Herath, S., Avtar, R., & Vuillaume, J. (2019). Comparative analyses of flood damage models in three Asian countries: Towards a regional flood risk modelling. *Environment Systems and Decisions*, 39(2), 229–246.

Krause, P., Boyle, D., & Base, F. (2005). Comparison of different efficiency criteria for hydrological model assessment. *Advances in Geosciences*, 5, 89–97.

Kundzewicz, Z., Pińskwar, I., & Brakenridge, G. (2013). Large floods in Europe, 1985–2009. *Hydrological Sciences Journal*, 58(1), 1-7.

Legates, D., & Mccabe, G. (1999). Evaluating the use of "goodness-of-fit" Measures in hydrologic and hydroclimatic model validation. *Water Resources Research*, 35(1), 233–241.

Madhushankha, J., & Wijesekera, N. (2021). Application of HEC-HMS Model to Estimate Daily Streamflow in Badddegama Watershed of Gin Ganga Basin Sri Lanka. *ENGINEER*, 54(01), 89-97.

Mahenthiran, B., & Rajapakse, L. (2021). Water Resources Availability and Low Flow Discharge Analysis of Two Selected River Basins in the Dry Zone Under Changing Climate Conditions. *2021 Moratuwa Engineering Research Conference (MERCon)* (pp. 504-509). IEEE.

Manawadu, L., & Fernando, N. (2008). Climate Change in Sri Lanka. *Journal of Hydrology*.

Moriasi, D., Arnold, J., Van Liew, M., Bingner, R., Harmel, R., & Veith, T. (2007). Model evaluation guidelines for systematic quantification of accuracy in watershed simulations. *Transactions of the ASABE*, 50(3), 885-900.

Moufar, M., & Perera, E. (2018). Floods and Countermeasures Impact Assessment for the Metro Colombo Canal System, Sri Lanka. *Hydrology*, 5(1), 11.

Mullan, B., Porteous, A., Wratt, D., & Hollis, M. (2005). *Changes in drought risk with climate change. Prepared for Ministry for the Environment (NZ Climate Change Office) and Ministry of Agriculture and Forestry. NIWA Client Report:WLG2005–23.* Wellington: National Institute of Water and Atmospheric Research.

Muthuwaththa , L., & Liyanage, P. (2013). Impact of rainfall change on the agro-ecological regions of Sri Lanka. *International conference on climate change impacts and adaptations for food and environment security sustaining agriculture under changing climate*, (pp. 59-66).

Nandalal, H., & Ratnayake, U. (2010). Event based modeling of a watershed using HEC-HMS. *J Inst Eng Sri Lanka* , xxxxiii(2):28–37.

Nanseer, N., & Rajkumar, S. (2006). Kelani Ganga Conservation Barrage and Results of Model Studies. *ENGINEER*, Vol. XXXIX, No. 02, 42-49.

Naveendrakumar, G., Vithanage, M., Kwon, H. H., Iqbal, M., Pathmarajah, S., & Obeysekera, J. (2018). Five decadal trends in averages and extremes of rainfall and temperature in Sri Lanka. *Advances in Meteorology*.

Niroshinie, M., Babel, M., & Herath, S. (2011). A methodology to analyze extreme flooding under future climate change scenarios for Colombo.

O'Brien, G., O'keefe, P., Rose, J., & Wisner, B. (2006). Climate change and disaster management. *Disasters*, 30(1), 64-80.

Papaioannou, G., Loukas, A., Vasiliades, L., & Aronica, G. (2016). Flood inundation mapping sensitivity to riverine spatial resolution and modelling approach. *Natural Hazards*, 83(S1), 117–132.

Patabendige, C., Kazama, S., & Komori, D. (2016). Near future climatic impact on seasonal runoff in Sri Lanka. *In Proceedings of water in the past, water in the present and water for the future: 20th Congress of the Asia Pacific Division of the International Association for Hydro Environment Engineering & Research* , (p. Vol. 20).

Pattnayak, K., Kar, S., Dalal, M., & Pattnayak, R. (2017). Projections of annual rainfall and surface temperature from CMIP5 models over the BIMSTEC countries. *Global and Planetary Change*, 152, 152-166.

Premalal, K. (2009). Climate Change in Sri Lanka. *Global Climate Change and its Impacts on Agriculture, Forestry and Water in the Tropics*, 21.

Punsara, C., & Rajapakse, L. (2021). Water Resources Availability and Low Flow Discharge Analysis of Kelani River Basin in Wet Zone under Changing Climate Conditions. *Moratuwa Engineering Research Conference (MERCon)* (pp. pp. 516-521). IEEE.

Rajkumar, S., Mishra, S., & Singh, R. (2021). Application of hydrologic modelling system (HEC-HMS) for flood assessment; case study of Kelani River Basin, Sri Lanka. *Hydrological extremes* (pp. pp. 3-18). Cham: Springer.

Rathnayake, U., Sachindra, D., & Nandalal, K. (2010). Rainfall forecasting for flood prediction in the Nilwala basin. *the International Symposium on Coastal Zones and Climate Change: Assessing the Impacts and Developing Adaptation Strategies.* Melbourne, Australia: Monash University.

Ritter, A., & Muñoz-Carpena, R. (2013). Performance evaluation of hydrological models: Statistical significance for reducing subjectivity in goodness-of-fit assessments. *Journal of Hydrology*, 480, 33–45.

Samarasinghe, J., Basnayaka, V., Gunathilake, M., Azamathulla, H., & Rathnayake, U. (2022). Comparing Combined 1D/2D and 2D Hydraulic Simulations Using High-Resolution

Topographic Data: Examples from Sri Lanka - Lower Kelani River Basin. *Hydrology*, 9(2), 39.

Samarasinghe, J., Perera, E., Teo, F., Chan, A., & Ghosh, S. (2021). Flood inundations and risk mapping in a tidal river: a case study for the Kelani River basin, Sri Lanka.

Sampath, D., Weerakoon, S., & Herath, S. (2015). HEC-HMS model for runoff simulation in a tropical catchment with intra-basin diversions—case study of the Deduru Oya River Basin, Sri Lanka. *J Inst Eng Sri Lanka*, XLVIII(1):1–9.

Selvarajah, H., Koike, T., Rasmy, M., Tamakawa, K., Yamamoto, A., Kitsuregawa, M., & Zhou, L. (2021). Development of an integrated approach for the assessment of climate change impacts on the hydro-meteorological characteristics of the Mahaweli river basin, Sri Lanka. *Water*, 13(9), 1218.

Senadhinatha, N. (2020). *Flood forecasting model using HEC-HMS for Nagalagam Street hydrometric station with relative impact of antecedent rainfall in Kelani river basin (Doctoral dissertation).*

Shantha, W., & Jayasundara, J. (2005). Study on changes of rainfall in the Mahaweli upper watershed in Sri Lanka due to climatic changes and develop a correction model for global warming. *International Symposium on the Stabilisation of Greenhouse Gas Concentrations* (p. Vol. 114). Exeter, UK: Hadley Centre, Met Office.

Siddiqui, M., Haider, S., Gabriel, H., & Shahzad, A. (2018). Rainfall–runoff, flood inundation and sensitivity analysis of the 2014 Pakistan flood in the Jhelum and Chenab river basin. *Hydrological Sciences Journal*, 63(13-14), 1976-1997.

Sirisena, T., Maskey, S., Bamunawala, J., Coppola, E., & Ranasinghe, R. (2021). Projected streamflow and sediment supply under changing climate to the coast of the Kalu river basin in tropical Sri Lanka over the 21st century. *Water*, 13(21), 3031.

Siriwardena, K., Widanapathirana, S., & Pannala, P. (2021). Evaluation of the Impacts of the Salinity Barrage in Kelani Ganga Using 1D-2D Hydraulic Model in Terms of Flooding. In Multi-Hazard Early Warning and Disaster Risks . *Springer*, (pp. pp. 349-362). Cham.

Sudeshika, P., & Rajapakse, L. (2021).). Impact of Digital Elevation Model on Rainfall-Runoff-Inundation modelling-A Case Study of Lower Kelani River Basin. *Moratuwa Engineering Research Conference (MERCon)* (pp. pp. 528-533). IEEE.

Suja , A., & Rajapakse, R. (2020). Evaluation of topographic data sources for 2D flood modelling: case study of Kelani basin, Sri Lanka. *IOP Conference Series: Earth and Environmental Science* (pp. 012043, Vol. 612, No. 1). IOP Publishing.

Tanaka, T., Tachikawa, Y., Ichikawa, Y., & Yorozu, K. (2019). An automatic domain updating method for fast 2-dimensional flood-inundation modelling. *Environmental Modelling & Software*, 116, 110–118.

Teng, J., Jakeman, A., Vaze, J., Croke, B., Dutta, D., & Kim, S. (2017). Flood inundation modelling: A review of methods, recent advances and uncertainty analysis. *Environmental Modelling & Software*, 90, 201–216.

UNFCCC. (2013). *Reporting and accounting of LULUCF activities under the Kyoto Protoco.* Bonn, Germany: United Nations Framework Convention on Climatic Change.

Vuillaume, J., Dorji, S., Komolafe, A., & Herath, S. (2018). Sub-seasonal extreme rainfall prediction in the Kelani River basin of Sri Lanka by using self-organizing map classification. *Natural Hazards*, 94(1), 385-404.

Wagenaar, D., Dahm, R., Diermanse, F., Dias, W., Dissanayake, D., Vajja, H., & Bouwer, L. (2019). Evaluating adaptation measures for reducing flood risk: A case study in the city of Colombo, Sri Lanka. *International Journal of Disaster Risk Reduction*, 37, 101162.

Wijekoon, T., & Rajapakse, L. (2022). Climate Elasticity of Runoff in Kalu and Kelani River Basins in the Wet Zone of Sri Lanka. *In 2022 Moratuwa Engineering Research Conference (MERCon)* (pp. pp. 1-6). IEEE.

Wijesekera, N. (2000). Parameter Estimation in Watershed Model : A Case Study Using Gin Ganga Watershed. *The Institution of Engineers, Sri Lanka*, 1, 26–32.

Wijesekera, N., & Abeynayake, J. (2003). Watershed similarity conditions for peakflow transposition-a study of river basins in the wet zone of Sri Lanka.

Willmott, C., Ackleson, S., Davis, R., Feddema, J., Klink, K., Legates, D., & Rowe, C. (1985). Statistics for the evaluation and comparison of models . *Journal of Geophysical Research-Oceans*, 90(NC5), 8995–9005.

World Meteorological Organization. (1982). WMO project for the intercomparison of conceptual models of snowmelt runoff. *In Hydrological Aspects of Alpine and High-Mountain Areas*, (pp. 193–202).

Wu, Y., & Liu, S. (2014). A suggestion for computing objective function in model calibration. *Ecological Informatics*, 24, 107–111.

Yu, D., Yin, J., & Liu, M. (2016). Validating city-scale surface water flood modelling using crowd-sourced data. *Environmental Research Letters*, 11(12), 124011.

Zheng, H., Chiew, F., Charles, S., & Podger, G. (2018). Future climate and runoff projections across South Asia from CMIP5 global climate models and hydrological modelling. *Journal of Hydrology: Regional Studies*, 18, 92-109.

Zubair, L., & Agalawatte, P. (2014). Climate Change Projections for Sri Lanka for the mid-twentieth Century from CMIP5 Simulations under a High Emissions Scenario. *AGU Fall Meeting Abstracts*, (pp. GC23D-0664, Vol. 2014).

ANNEXURE 1

SAMPLE CALCULATION OF 3 DAY, 50-YEAR RETURN PERIOD DESIGN RAINFALL DEVELOPMENT FOR COLOMBO STATION

$I = 117.34\ T^{-0.686}$; $R^2 = 0.9972$

I = Rainfall Intensity (mm/hr), T = Rainfall Duration (hr), R^2 = Coefficient of determination

No	Time (min)	Rainfall intensity (mm/hr)	Rainfall depth (mm)	Hyetograph ordinates (mm)	Rank
1	0			0	
2	60	117.3	117.3	2.0	71
3	120	72.9	28.5	2.0	69
4	180	55.2	19.8	2.1	67
5	240	45.3	15.7	2.1	65
6	300	38.9	13.2	2.2	63
7	360	34.3	11.5	2.2	61
8	420	30.9	10.2	2.3	59
9	480	28.2	9.3	2.3	57
10	540	26.0	8.5	2.4	55
11	600	24.2	7.9	2.4	53
12	660	22.6	7.3	2.5	51
13	720	21.3	6.9	2.6	49
14	780	20.2	6.5	2.6	47
15	840	19.2	6.2	2.7	45
16	900	18.3	5.9	2.8	43
17	960	17.5	5.6	2.9	41
18	1020	16.8	5.4	3.0	39
19	1080	16.2	5.2	3.1	37
20	1140	15.6	5.0	3.2	35
21	1200	15.0	4.8	3.4	33
22	1260	14.5	4.6	3.5	31
23	1320	14.1	4.5	3.7	29
24	1380	13.7	4.4	3.9	27
25	1440	13.3	4.2	4.1	25
26	1500	12.9	4.1	4.4	23
27	1560	12.6	4.0	4.6	21
28	1620	12.2	3.9	5.0	19
29	1680	11.9	3.8	5.4	17

30	1740	11.6	3.7	5.9	15
31	1800	11.4	3.6	6.5	13
32	1860	11.1	3.5	7.3	11
33	1920	10.9	3.5	8.5	9
34	1980	10.7	3.4	10.2	7
35	2040	10.4	3.3	13.2	5
36	2100	10.2	3.2	19.8	3
37	2160	10.0	3.2	117.3	1
38	2220	9.9	3.1	28.5	2
39	2280	9.7	3.1	15.7	4
40	2340	9.5	3.0	11.5	6
41	2400	9.3	3.0	9.3	8
42	2460	9.2	2.9	7.9	10
43	2520	9.0	2.9	6.9	12
44	2580	8.9	2.8	6.2	14
45	2640	8.8	2.8	5.6	16
46	2700	8.6	2.7	5.2	18
47	2760	8.5	2.7	4.8	20
48	2820	8.4	2.6	4.5	22
49	2880	8.2	2.6	4.2	24
50	2940	8.1	2.6	4.0	26
51	3000	8.0	2.5	3.8	28
52	3060	7.9	2.5	3.6	30
53	3120	7.8	2.5	3.5	32
54	3180	7.7	2.4	3.3	34
55	3240	7.6	2.4	3.2	36
56	3300	7.5	2.4	3.1	38
57	3360	7.4	2.3	3.0	40
58	3420	7.3	2.3	2.9	42
59	3480	7.2	2.3	2.8	44
60	3540	7.2	2.3	2.7	46
61	3600	7.1	2.2	2.6	48
62	3660	7.0	2.2	2.5	50
63	3720	6.9	2.2	2.5	52
64	3780	6.8	2.2	2.4	54
65	3840	6.8	2.1	2.3	56
66	3900	6.7	2.1	2.3	58
67	3960	6.6	2.1	2.2	60
68	4020	6.6	2.1	2.2	62
69	4080	6.5	2.0	2.1	64
70	4140	6.4	2.0	2.1	66
71	4200	6.4	2.0	2.0	68
72	4260	6.3	2.0	2.0	70
73	4320	6.2	2.0	2.0	72

ANNEXURE 2

SCS CURVE NUMBER TABLE

Source: Applied Hydrology, (Chow et al., 1988).

TABLE 5.5.2
Runoff curve numbers for selected agricultural, suburban, and urban land uses (antecedent moisture condition II, $I_a = 0.2S$)

Land Use Description		Hydrologic Soil Group			
		A	B	C	D
Cultivated land[1]: without conservation treatment		72	81	88	91
with conservation treatment		62	71	78	81
Pasture or range land: poor condition		68	79	86	89
good condition		39	61	74	80
Meadow: good condition		30	58	71	78
Wood or forest land: thin stand, poor cover, no mulch		45	66	77	83
good cover[2]		25	55	70	77
Open Spaces, lawns, parks, golf courses, cemeteries, etc.					
good condition: grass cover on 75% or more of the area		39	61	74	80
fair condition: grass cover on 50% to 75% of the area		49	69	79	84
Commercial and business areas (85% impervious)		89	92	94	95
Industrial districts (72% impervious)		81	88	91	93
Residential[3]:					
Average lot size	Average % impervious[4]				
1/8 acre or less	65	77	85	90	92
1/4 acre	38	61	75	83	87
1/3 acre	30	57	72	81	86
1/2 acre	25	54	70	80	85
1 acre	20	51	68	79	84
Paved parking lots, roofs, driveways, etc.[5]		98	98	98	98
Streets and roads:					
paved with curbs and storm sewers[5]		98	98	98	98
gravel		76	85	89	91
dirt		72	82	87	89

[1]For a more detailed description of agricultural land use curve numbers, refer to Soil Conservation Service, 1972, Chap. 9

[2]Good cover is protected from grazing and litter and brush cover soil.

[3]Curve numbers are computed assuming the runoff from the house and driveway is directed towards the street with a minimum of roof water directed to lawns where additional infiltration could occur.

[4]The remaining pervious areas (lawn) are considered to be in good pasture condition for these curve numbers.

[5]In some warmer climates of the country a curve number of 95 may be used.

ANNEXURE 3

AVERAGE CN CALCULATIONS FOR THE KELANI BASIN AND SUB-BASINS

SB Name	Land Use Type	Category	SCS CN Category	CN	Area (km^2)	SB CN
Upper	Coconut (C)	Agricultural Crops	Wood or Forest - Poor Cover	64	15.5	**62.87**
	Chena	Agricultural Crops	Wood or Forest - Poor Cover	64	1.8	
	Forest - Unclassified (F)	Forest	Wood or Forest - Good Cover	51	213.0	
	Homesteads/Garden (G)	Garden	Open Space / Fair Condition	67	245.1	
	Marsh	Marsh	Meadow	54	0.7	
	Other cultivation	Agricultural Crops	Wood or Forest - Poor Cover	64	23.2	
	Paddy (P)	Paddy	Pasture / Good Condition	60	51.6	
	Rubber (R)	Agricultural Crops	Wood or Forest - Poor Cover	64	613.9	
	Rock (RK)	Built up area	Paved / Gravel	84	16.0	
	Reservoir	Water Bodies	Water Bodies	94	7.5	
	Scrub land	Forest	Wood or Forest - Good Cover	51	44.2	
	Streams	Water Bodies	Water Bodies	94	18.4	
	Tea (T)	Agricultural Crops	Wood or Forest - Poor Cover	64	273.1	
	Coconut (C)	Agricultural Crops	Wood or Forest - Poor Cover	64	43.3	
	Forest - Unclassified (F)	Forest	Wood or Forest - Good Cover	51	21.3	
	Homesteads/Garden (G)	Garden	Open Space / Fair Condition	67	82.4	
	Marsh	Marsh	Meadow	54	2.5	
Middle	Paddy (P)	Paddy	Pasture / Good Condition	60	35.4	**63.68**

SB Name	Land Use Type	Category	SCS CN Category	CN	Area (km^2)	SB CN
	Rubber (R)	Agricultural Crops	Wood or Forest - Poor Cover	64	95.5	
	Rock (RK)	Built up area	Paved / Gravel	84	0.2	
	Reservoir	Water Bodies	Water Bodies	94	2.1	
	Scrub land	Forest	Wood or Forest - Good Cover	51	5.0	
	Streams	Water Bodies	Water Bodies	94	3.3	
	Built up area	Built up area	Commercial (85% Impervious)	92	5.1	
	Coconut (C)	Agricultural Crops	Wood or Forest - Poor Cover	64	54.6	
	Chena	Agricultural Crops	Wood or Forest - Poor Cover	64	0.3	
	Canal	Water Bodies	Water Bodies	94	0.2	
	Homesteads/Garden (G)	Garden	Open Space / Fair Condition	67	250.0	
	Marsh	Marsh	Meadow	54	13.6	
Lower	Other cultivation	Agricultural Crops	Wood or Forest - Poor Cover	64	3.0	**65.12**
	Paddy (P)	Paddy	Pasture / Good Condition	60	92.2	
	Rubber (R)	Agricultural Crops	Wood or Forest - Poor Cover	64	75.1	
	Sand	Garden	Open Space / Fair Condition	67	0.5	
	Scrub land	Forest	Wood or Forest - Good Cover	51	4.0	
	Streams	Water Bodies	Water Bodies	94	6.3	
	Tank	Water Bodies	Water Bodies	94	0.3	
	Tea (T)	Agricultural Crops	Wood or Forest - Poor Cover	64	0.2	
	Water holes area	Water Bodies	Water Bodies	94	0.8	
	Water holes area	Water Bodies	Water Bodies	94	0.8	
	Water holes area	Water Bodies	Water Bodies	94	0.8	
	Water holes area	Water Bodies	Water Bodies	94	0.8	
Kelani Basin						**63.46**

ANNEXURE 4

AREAL REDUCTION FACTORS

Source: Applied Hydrology, (Chow et al., 1988).

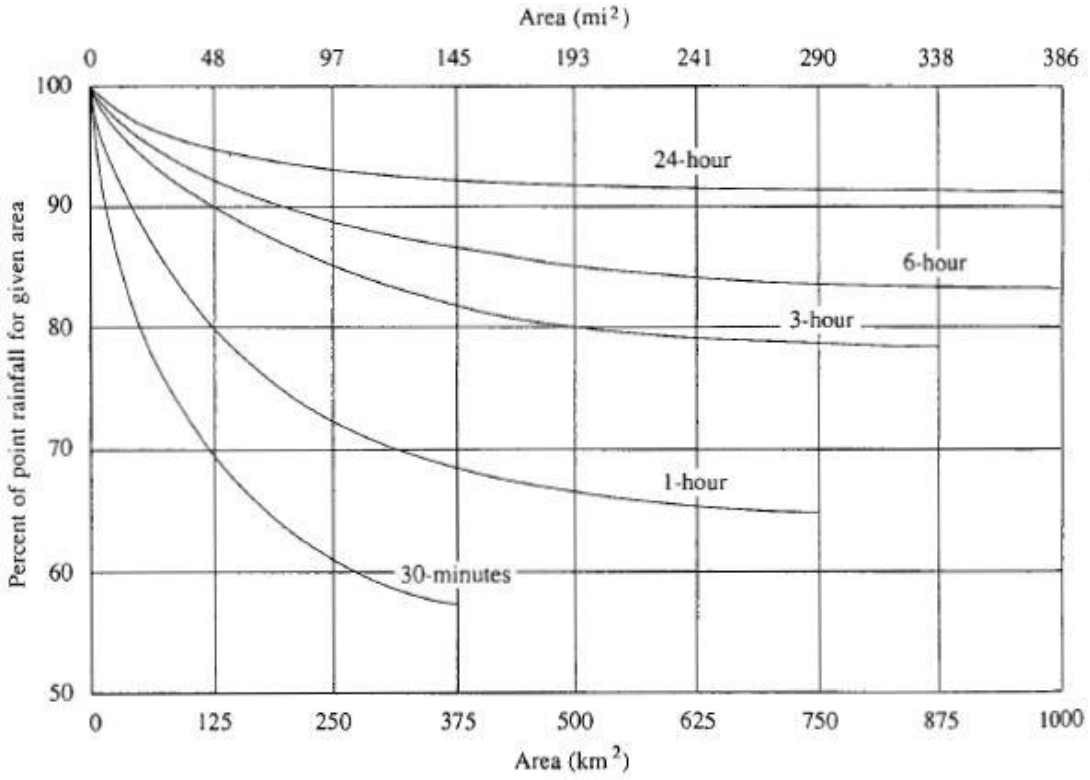

FIGURE 14.1.3
Depth-area curves for reducing point rainfall to obtain areal average values. (*Source*: World Meteorological Organization, 1983; originally published in Technical Paper 29, U. S. Weather Bureau, 1958.)

ANNEXURE 5

MANNING'S N ROUGHNESS VALUES

Source: Applied Hydrology, (Chow et al., 1988).

TABLE 2.5.1
Manning roughness coefficients for various open channel surfaces

Material		Typical Manning roughness coefficient
Concrete		0.012
Gravel bottom with sides	— concrete	0.020
	— mortared stone	0.023
	— riprap	0.033
Natural stream channels		
Clean, straight stream		0.030
Clean, winding stream		0.040
Winding with weeds and pools		0.050
With heavy brush and timber		0.100
Flood Plains		
Pasture		0.035
Field crops		0.040
Light brush and weeds		0.050
Dense brush		0.070
Dense trees		0.100

Source: Chow, 1959.